

**UNIVERSITÀ DEGLI STUDI DI NAPOLI  
“FEDERICO II”**



**PHD PROGRAM  
IN  
EARTH, ENVIRONMENT AND RESOURCES SCIENCES  
XXIX CYCLE**

**Hydrological monitoring and  
modeling of pyroclastic soil covers for  
assessing debris flows hazard in  
volcanic and peri-volcanic areas of  
Campania region (southern Italy)**

**PHD CANDIDATE:  
DR. FRANCESCO FUSCO**

**ADVISOR:  
PROF. DOMENICO CALCATERRA**

**CO-ADVISOR:  
PROF. PANTALEONE DE VITA**

**PHD COORDINATOR:  
PROF. MAURIZIO FEDI**

**ACADEMIC YEAR: 2015/2016**



# Index

---

<b>CHAPTER 1 .....</b>	<b>7</b>
<b>Introduction.....</b>	<b>7</b>
<b>1.1. Relevance of debris flows in the peri-volcanic areas of the Campania ...</b>	<b>7</b>
<b>1.2. Scope of the research.....</b>	<b>9</b>
<b>1.3. Structure of the manuscript .....</b>	<b>10</b>
 <b>CHAPTER 2 .....</b>	 <b>12</b>
<b>Geological and geomorphological settings of the study areas .....</b>	<b>12</b>
<b>2.1. Quaternary volcanic activity in the Campania region.....</b>	<b>12</b>
2.1.1. Volcanological history of the Somma-Vesuvius .....	13
<i>The Sarno or Basal Pumice eruption (17 k-years B.P.).....</i>	<i>14</i>
<i>The Ottaviano or Mercato Pumice eruption (8 k-years B.P.).....</i>	<i>15</i>
<i>The Avellino eruption (3.7 k-years B.P.).....</i>	<i>15</i>
<i>The 79 A.D. eruption or Pompeii eruption.....</i>	<i>15</i>
<i>The 472 A.D. eruption or Pollena eruption .....</i>	<i>16</i>
<i>The 1631 A.D. eruption .....</i>	<i>16</i>
2.1.2. Volcanological history of the Phlegraean Fields .....	18
<i>The 1<sup>st</sup> cycle (60 ÷ 39 k-years B.P.) .....</i>	<i>18</i>
<i>The 2<sup>nd</sup> cycle (39 ÷ 15 k-years B.P.).....</i>	<i>18</i>
<i>The 3<sup>rd</sup> cycle (Neapolitan Yellow Tuff eruption) .....</i>	<i>19</i>
<i>The 4<sup>th</sup> cycle (15 k-years B.P. ÷ 1538 A.D.).....</i>	<i>19</i>
<b>2.2. Sarno Mountains Range .....</b>	<b>20</b>
2.2.1. Pre-Quaternary geological features .....	20
2.2.2. Stratigraphic characterization of ash-fall pyroclastic deposits mantling Sarno Mountains slopes .....	22
<b>2.3. The Camaldoli hill.....</b>	<b>28</b>
2.3.1. Geological features of the Phlegraean area .....	28
2.3.2. Stratigraphic characterization of the Camaldoli hillslopes.....	30
 <b>CHAPTER 3 .....</b>	 <b>32</b>

<b>Hydrological processes and shallow slope instability.....</b>	<b>32</b>
<b>3.1. Hydrological slope processes .....</b>	<b>32</b>
3.1.1 Infiltration.....	32
3.1.2 Runoff, sub-surficial (throughflow) and deep percolation flows .....	35
<b>3.2. Stability of soil-mantled slopes.....</b>	<b>39</b>
3.2.1. Predisposing and triggering factors to shallow landsliding.....	41
3.2.2. Landslide classifications.....	43
<i>Pierson and Costa's classification (1987)</i> .....	44
<i>Hutchinson's classification (1988)</i> .....	46
<i>Sassa's classification (1989)</i> .....	48
<i>Cruden and Varnes's classification (1996)</i> .....	50
<i>Hungr et al. (2014) classification</i> .....	51
3.2.3. Hydrological threshold conditions leading to landslide triggering .....	53
 <b>CHAPTER 4 .....</b>	 <b>57</b>
<b>Landslide involving ash-fall pyroclastic soil mantled slopes of the peri-Vesuvian and Phlegraean areas.....</b>	<b>57</b>
<b>4.1 Principal case histories.....</b>	<b>58</b>
<b>4.2. Landslide kinematics and rheological behavior .....</b>	<b>63</b>
<b>4.3. The role of geomorphological factors to landslide susceptibility.....</b>	<b>66</b>
<b>4.4. Hydraulic and geotechnical properties of pyroclastic soils mantling peri-Vesuvian and Phlegraean Fields slopes .....</b>	<b>76</b>
4.4.1 Geotechnical properties of pyroclastic soils in peri-Vesuvian and Phlegraean areas .....	77
4.4.2 Saturated and unsaturated hydraulical properties of pyroclastic soils in peri-Vesuvian and Phlegraean areas .....	81
<b>4.6 The role of hydrological conditions to landslide triggering.....</b>	<b>84</b>
 <b>CHAPTER 5 .....</b>	 <b>89</b>
<b>Data and methods for engineering-geological characterization, hydrological monitoring and modelling of test areas.....</b>	<b>89</b>
<b>5.1. The Sarno Mountains test area .....</b>	<b>90</b>

5.1.1. Reconstruction of the engineering-geological model .....	91
5.1.2. Setting up of the hydrological monitoring station .....	94
<b>5.2. Camaldoli hill test area .....</b>	<b>100</b>
5.2.1. Reconstruction of the engineering-geological model .....	101
5.2.2. Setting up of the hydrological monitoring station .....	105
<b>5.3 Local scale hydrological and slope stability modelling for deterministic rainfall thresholds estimation .....</b>	<b>106</b>
5.3.1 Overview of VS2DTI code .....	106
5.3.2. Short-term and long-term hydrological modelling for Sarno tests area.....	111
5.3.2.1. Estimation of daily evapotranspiration rate .....	111
5.3.2.2. Model calibration (short-period) and long-period hydrological modelling .....	114
5.3.3. Short-term and long-term hydrological modeling for the Camaldoli test area.....	117
5.3.4 Estimation of I-D rainfall thresholds for the Sarno Mountains sample areas using a deterministic approach .....	120
<b>5.4. Distributed scale hydrological and slope stability modelling for hazard maps definition .....</b>	<b>126</b>
5.4.1. Overview of the TRIGRS model .....	127
5.4.2. Setting up of the distributed modelling for the Sarno Mountains .....	129
<b>CHAPTER 6 .....</b>	<b>135</b>
<b>Results.....</b>	<b>135</b>
<b>6.1 Hydrological monitoring and modeling for the Sarno Mountains test area .....</b>	<b>135</b>
6.1.1 Hydrological regime of ash-fall pyroclastic soil mantle.....	135
6.1.2. Intensity-Duration deterministic rainfall threshold .....	140
6.1.3. Distributed hazard map.....	148
<b>6.2 Hydrological monitoring and modeling results for Camaldoli hill test area .....</b>	<b>161</b>
6.2.1. Pressure head regime of pyroclastic soils covering Camaldoli hill slopes .....	161

6.1.2. Short and long-term hydrological modelling results .....	164
<b>CHAPTER 7 .....</b>	<b>168</b>
<b>Discussion.....</b>	<b>168</b>
<b>7.1. Interpretation and comparison of results in the framework of scientific literature .....</b>	<b>168</b>
7.1.1. The Sarno Mountains test area .....	168
7.1.2. The Camaldoli hill test area.....	173
<b>CHAPTER 8 .....</b>	<b>176</b>
<b>Conclusions .....</b>	<b>176</b>
<b>REFERENCES .....</b>	<b>180</b>
<b>ATTACHMENTS.....</b>	<b>198</b>

# Chapter 1

---

## Introduction

### 1.1. Relevance of debris flows in the peri-volcanic areas of the Campania

Flow-type landslides involving ash-fall pyroclastic deposits, which mantle mountainous and hilly slopes surrounding volcanic structures, are typically triggered by high intensity/duration rainfall events. Such geohazard represent one of the principal geological risks of the Campania region (southern Italy), particularly in the area surrounding the Mount Somma-Vesuvius and Phlegraean Fields. In the last century, flow-type landslides in this region have led to hundreds of casualties with both single and areal events. Among the largest and most widespread landslide areal events, there are the two massive ones occurred in the Salerno and Lattari Mountains respectively in October 1910 and October 1954, leading to 468 deaths, and in the Sarno Mountains in May 1998, which led to 160 deaths. After this last catastrophic debris flow event, several studies were focused on the comprehension of the landslide triggering mechanisms. As a result, there have been relevant advances in understanding the geomorphological aspects predisposing to landslide onset (Del Prete et al., 1998; Calcaterra et al., 1999; Guadagno et al., 2005; Di Crescenzo and Santo, 2005; Cascini et al., 2008; Palma et al., 2009; De Vita et al., 2013) and hydrological triggering factors (Cascini, 2003; Cascini et al., 2008; Cascini et al., 2010; De Vita et al., 2013, Napolitano et al., 2015, 2016; Tufano et al., 2016).

The shallow flow-type landslides involving ash-fall pyroclastic soils covering peri-Vesuvian and Phlegraean slopes can be defined as debris flows triggered by initial small landslides, namely “*debris-slide-triggered debris flows*” as defined by Jakob and Hungr (2005) and are characterized by a complex style (Cruden and Varnes, 1996) due to their different evolutionary stages: (1) an initial sliding stage, that involves very limited volumes of pyroclastic deposits (from some tens to few thousands cubic meters) and approximately the uppermost pedogenized part of the ash-fall

volcaniclastic series, up to a depth limited to about 2 m, (2) an intermediate avalanche phase, where the landslide increases its volume by the entrainment of other material along the slope, and (3) a final debris flow stage, when the avalanche flow is channelized into the drainage network. Although typical slope failures in the region all involve the first phase, the last two phases are not always present, because they strongly depend on slope morphology and cover thickness involved.

The cause-effect relationship between these shallow landslides and intense/prolonged rainfall events is commonly recognized. However, considering the recurrency of these events especially in the case of peri-Vesuvian slopes, the scientific community has focused the research specifically on the assessment of rainfall conditions that trigger areal landsliding, because they represent a fundamental reference for the developing landslide early warning systems (Baum and Godt, 2010). Empirical approaches for developing rainfall thresholds are the most used in the scientific literature (Guadagno, 1991; Calcaterra et al., 2000; Chirico et al., 2000; De Vita, 2000; De Vita and Piscopo, 2002; Crosta and Dal Negro, 2003; Fiorillo and Wilson, 2004; Godt et al. 2005; Chleborad et al. 2006), which are based on statistical analyses of rainfall data recorded in conjunction with debris flow events. For example, after the areal landslide event occurred in the Sarno mountains in May '98, the "Basin Authority of Central Campania" adopted the FLAIR (Forecasting of Landslides Induced by Rainfall; Sirangelo and Versace, 1992) early warning system, based on two modules: Rainfall-Landslide (RL) and Rainfall-Forecasting (RF). In detail, RL considers the relation between the rainfall event and the landslide occurrence probability, the latter being a function of the potential rainfall infiltrated in a slope, while RF gives a probabilistic forecasting of a rainfall, deriving from both stochastic modeling and local weather forecasting data. Finally, the evaluation of the landslide occurrence probability derives from the forecasted rainfall event (RF) and RL.

However, due to the limits of empirical rainfall thresholds, more recently deterministic approaches based on physically-based numerical modelling of hydrological and stability processes have been implemented (De Vita et al., 2013; Papa et al., 2013; Napolitano et al., 2015; 2016; Tufano et al., 2016). Results of these researches demonstrated that ash-fall pyroclastic coverings have peculiar hydrological and geotechnical properties, which make them very different from common regolith deposits. Among the most important, the following features were recognized: complex stratigraphic settings, with alternating high-permeability pumiceous lapilli horizons

and low-permeability paleosols; high water retention properties, which allow retaining water as a finer non-pyroclastic soil; relevant shear strength values in comparison with soils of the same grain size; important effects on shear strength of capillary water (soil suction); low dry unit weight, which is not much higher than that of water. These differences can be inferred to control values of Intensity-Duration rainfall thresholds, which were recognized as being higher than those found in different parts of the world for shallow landslides involving common regolith mantles. Despite the peculiarity of these soils, it is important to advance studies on stability of ash-fall pyroclastic soil-mantled slopes due to their existence in many areas of the world.

## 1.2. Scope of the research

Starting from known results in the scientific literature and from a collaboration with the USGS' Landslide Hazard Program in Golden (CO, USA), this research project was focused on the aspects described below.

- 1) Analysis of the hydrological behavior of the pyroclastic soils, mantling peri-Vesuvian and Phlegraeian slopes, and of the processes controlling the onset of initial slides triggering debris flows. Analyses were based on hydrological field monitoring (Fusco et al., 2013; Fusco and De Vita, 2015, Fusco et al., 2016a; 2016c) of pyroclastic cover, including pressure head of soil water and other basic climatic data;
- 2) Numerical modeling of hydrological and slope stability processes in landslide source areas (De Vita et al., 2013; Napolitano et al., 2015; 2016; Fusco et al., 2016c; Tufano et al., 2016), using the VS2DTI code (Hsieh et al., 2000), and then the definition of deterministic rainfall thresholds, starting from physically-based slope models. In detail, the approach is based on detailed process-based models of the initial phase of landslide initiations, reconstructed by detailed in situ surveys in different test areas that were considered representative of typical geomorphological conditions. Slope models were calibrated considering hydro-mechanical properties (De Vita et al., 2013) and field monitoring results (Fusco et al., 2013; Fusco and De Vita, 2015, Fusco et al., 2016a; 2016c);

- 3) Extension of site-specific findings to a distributed scale by modelling variable saturation and stability conditions of the ash-fall pyroclastic covers over large areas. This approach used TRIGRS code (Baum et al., 2010) to produce maps of susceptibility (Fusco et al., 2016b) of the initial failure stage (debris slide). These maps accounted for both spatial and temporal probabilities by considering morphological factors, variable thickness of ash-fall pyroclastic soil deposits, different antecedent (seasonal) conditions of the soil cover (pressure-head) and variable triggering rainfall, according to different return times or probability. The implementation of the last three factors (variable deposit thickness, initial soil suction, and rainfall) in the TRIGRS model has not been attempted previously for the ash-fall pyroclastic soil-mantled slopes of the area that surrounds the Somma-Vesuvius volcano.

### **1.3. Structure of the manuscript**

The shallow landsliding involving pyroclastic coverings mantling peri-Vesuvian and Phlegraean slopes represent a challenging theme which can be analyzed through different approaches. These landslides are characterized by a series of processes whose triggering mechanisms are affected by geological, geomorphological and hydrological factors.

Due to the aim of this research project, this manuscript was organized considering results of the research activities carried out for two sample areas of the Campania region, which are affected by the same type of geohazard.

Different geological settings and similar geomorphological features which characterize Phlegraean and peri-Vesuvian slopes were described, shifting attention mostly about the origin of the pyroclastic soils involved by slope instabilities. In particular, volcano-tectonic activity occurred in the Campanian Plain was described, analyzing the evolutionary phases of two main volcanic districts of the area: the Somma-Vesuvius volcano and Phlegraean Fields volcanic district.

After this introduction, hydrological and slope stability processes were described to define the predisposing and triggering features of rainfall-induced flow-type landslides, as well as their rheology and kinematics. For these reasons, a detailed description of the hydrological slope processes, related to rainfall events, and hydro-

mechanical properties of the involved materials were described. In addition, following the different landslide classifications, these slope instabilities were described. Finally, to underline the relevance of this geohazard, which strongly affect the urban settlements located at the foothill of peri-Vesuvian mountains and Phlegraean slopes, main documented historical and recent cases of landslide events were shown.

The main section of this manuscript is represented by the description of the methods and results of the hydrological monitoring and numerical modeling activities. In detail, settings of field monitoring stations, located in the two sample areas, and the reconstruction of physically-based models, used for the hydrological modeling at slope and regional scale, were described. As a final result, rainfall thresholds, by using a deterministic approach, and landslide susceptibility maps were estimated. Finally, results were analyzed and then discussed by comparison with results from prior literature.

# Chapter 2

## Geological and geomorphological settings of the study areas

### 2.1. Quaternary volcanic activity in the Campania region

The Campanian Plain (Fig. 2.1), interposed between the volcanic districts of Somma-Vesuvius and Phlegraean Fields and the surrounding mountain ranges, is an extended flat area originated by the Quaternary filling of this regional semi-graben structure. The deposits filling the structural depression are of alluvial, marine and chiefly pyroclastic origin. The latter derived by eruptions since about 200 k-years, until historical times, related to different eruptive centers of the “*Campanian volcanic district*” (Ischia, Roccamonfina, Phlegraean Fields and Somma-Vesuvius). This volcanic activity is related to the Apennine orogenic phases, in particular to the subduction of the Tyrrhenian Plate below the Euro-Asiatic Plate.

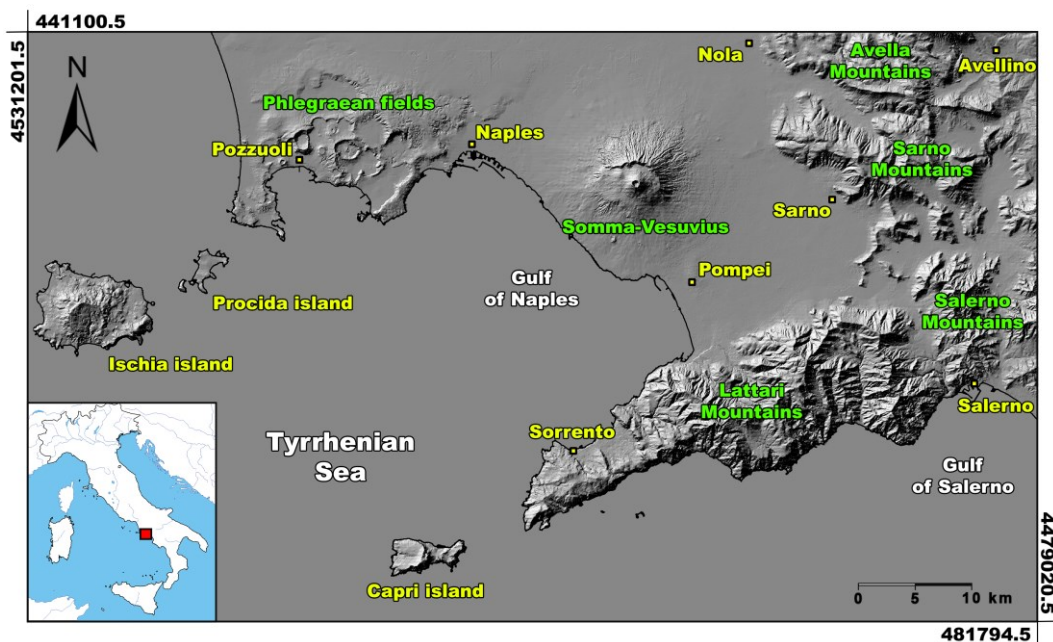


**Figure 2.1.** Geographical setting of the Campanian plain including mountain ranges around the Somma-Vesuvius volcano and Phlegraean Fields.

For this reason, ash-fall and pyroclastic flow deposits filled the plain and covered irregularly the mountain slopes surrounding the Campanian Plain, such as the Phlegraean slopes directly linked to the formation of the volcanic center. In detail, a larger part of the volcanoclastic series, often incomplete along slopes due to denudational processes, mantling the carbonate mountain ridges came from the deposition of ash-fall deposits erupted by the youngest Somma-Vesuvius volcano (Rolandi et al., 2000 and references therein). They are characterized by complex depositional settings, due to the alternation of unweathered pyroclastic deposits to paleosols, which were formed during stages between consecutive eruptions.

The entire volcanic activity in the plain can be divided in two pyroclastic complexes (Rolandi et al., 2000): 1) the “*Ancient Pyroclastic Complex*” (APC), deriving from Plegraean Fields and Ischia island volcanic activity; 2) the “*Recent Pyroclastic Complex*” (RPC), deriving from the Somma-Vesuvius volcanic district.

### 2.1.1. Volcanological history of the Somma-Vesuvius

The Somma-Vesuvius is a strato-volcano characterized by the Mt. Somma, the remaining structure of the older volcano, which was calderized several times, and by the Vesuvius cone grown inside the caldera in historical times and that represent the actual higher peak (1281 m a.s.l.) (Fig. 2.2).



**Figure 2.2.** Geographical setting of the Mt. Somma-Vesuvius volcanic district surrounded by an almost continuous urbanized area.

However, deepest drilling, down to 1125 m, carried out close to the volcano shown the presence of an oldest volcanic structure, dated back to 400 k-years B.P., located below the Phlegraean CI deposits (Campanian Ignimbrite - 39 kys B.P - Rolandi, 2001). After this huge eruptive event, the Somma volcano grew up to 2000 m a.s.l., with a diameter of about 16 km (Rolandi, 2001). Several eruption events, effusive and/or explosive, characterized the complex history of this famous volcano (Rolandi et al., 2006 - Fig. 2.3), but only some main Plinian events strongly affected the morphology of the Somma-Vesuvius volcanic district (Fig. 2.4).

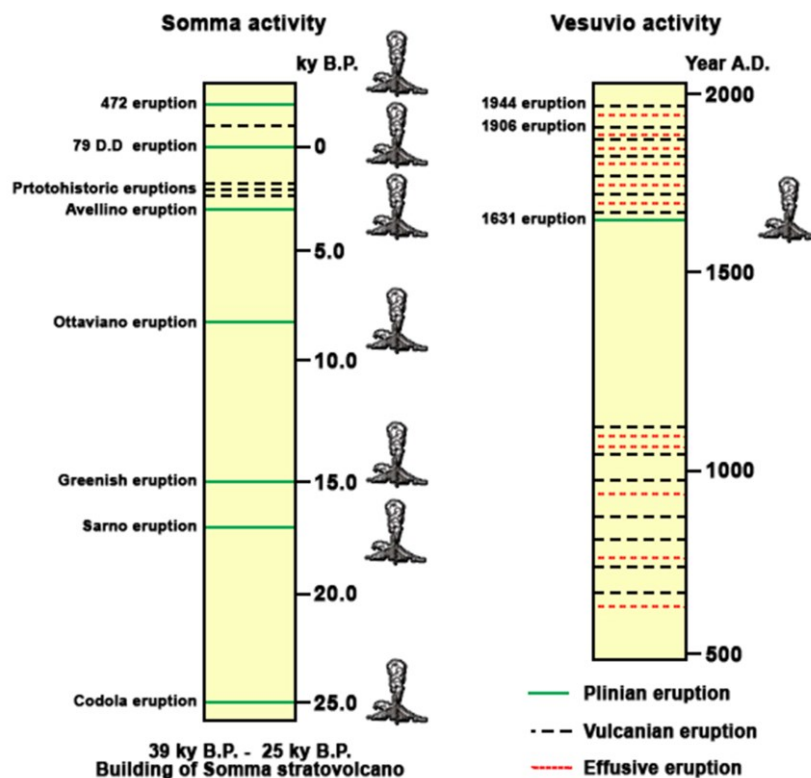


**Figure 2.3.** Recognized principal volcanic eruptions of Somma-Vesuvius volcanic district (modified from Rolandi, 2000).

### The Sarno or Basal Pumice eruption (17 k-years B.P.).

This volcanic event represents one of the most catastrophic Plinian eruptions of the Somma volcano, which caused the partial collapse of the western part of the volcanic structure (Fig. 2.4A). Fall-out and surge deposits derived from this eruption was characterized by intense freatomagmatic activity (Rolandi et al., 2000). The Plinian eruptive column was about 20 km high, with a dispersion axis E-NE oriented, and a

deposits volume of about 4.0 km<sup>3</sup> (Bertagnini et al., 1998), estimated using the Pyle (1989) method. Plinian fall-out deposits are characterized by white pumice (trachytic composition - 63.0% of SiO<sub>2</sub>) and dark scoriae (latite composition - 53.7% of SiO<sub>2</sub>), that shown a magmatic chamber zonation before the volcanic event. The freatomagmatic and the calderization phases occurred concurrently as shown by the presence of hypo-abysal rock fragments in the deposits (Bertagnini et al., 1998).

### **The Ottaviano or Mercato Pumice eruption (8 k-years B.P.)**

This eruption (Fig. 2.4B) represents the second catastrophic Plinian eruption whose deposits are characterized by two basal levels of pumice with a thin pyroclastic surge level intercalated (Rolandi et al., 1993a). Fall-out deposits followed a E-NE oriented dispersal axis creating 0.5 m thick deposits in areas 30 km far from the vent. Instead, pyroclastic surge deposits are very close to the vent. Although no deposits related to calderic collapse are present, a partial collapse of the volcanic structure was inferred due to the huge erupted magma volume (Cioni et al., 1999).

### **The Avellino eruption (3.7 k-years B.P.)**

This catastrophic volcanic event represents one of the most massive eruptions of the Somma volcano, whose fall-out deposits were found up to 20 km far from the vent, following a dispersal axis E-NE oriented (Fig. 2.4C), with associated ash-fall and pyroclastic flow deposits. The entire volcanic event can be divided in three phases (Rolandi et al., 1993b):

1. Beginning phase, with ash-fall and pyroclastic flow deposits associated;
2. Plinian phase, with thick basal pumice and ash deposits deriving from the eruptive column;
3. Phreatomagmatic phase, characterized by pulsing Plinian eruptive column that produced several pyroclastic flows.

### **The 79 A.D. eruption or Pompeii eruption**

This historical volcanic event can be considered the most dramatic and well documented eruption of the Somma volcano (Fig. 2.4D). On August 24<sup>th</sup>, 79 A.D the

volcano erupted after about eight centuries since the last eruption, causing the destruction of Pompeii, Herculaneum and Stabiae Roman towns. Many Authors studied this eruption (Lirer et al., 1973; Sigurdsson et al., 1985; Barberi et al., 1989; Cioni et al., 1999; Gurioli et al., 2002; Rolandi et al., 2007), although the most important information derives from the two ancient letters that Plinius “The Young” sent to his friend Tacitus. These letters described the massive volcanic event during which his uncle Plinio “The Old” died. The entire eruption was characterized by the following phases:

1. Phreatomagmatic beginning phase, whose ash-fall proximal deposits are 0.15 m thick with pyroclastic surge deposits intercalated;
2. Main Plinian phase, characterized by massive fall-out associated deposits that followed a S-SE oriented dispersion axis;
3. Phreatomagmatic phase, associated to the last huge calderic collapse of Somma volcano.

### **The 472 A.D. eruption or Pollena eruption**

This volcanic event was one of the massive eruptions occurred after the 79 A.D. eruption, affecting a huge area around the vent and producing fall-out and pyroclastic flow deposits, the first ones following a E-NE oriented dispersal axis (Fig. 2.4E). During this eruption, no defined volcanic structure was present inside the Somma caldera, the latter being characterized by an amphitheater-shape, bordered in the northern area only (Rolandi et al., 2004).

### **The 1631 A.D. eruption**

This catastrophic eruption was attributed to the Vesuvius volcano activity, occurred after a quiet period of five centuries (Fig. 2.4F). The entire event lasted just two days but its beginning was massive, causing several pyroclastic flows, which affected and destroyed the southern areas close to the vent and caused about 4000 casualties. The eruption can be divided in four defined phases (Rolandi et al., 1993):

1. Plinian phase, associated to fall-out deposits formation that followed an E-NE oriented dispersal axis;

2. Vulcanian phase;
3. Pyroclastic flow and surge phase;
4. Phreatomagmatic phase, characterized by fall-out and lahar deposits.

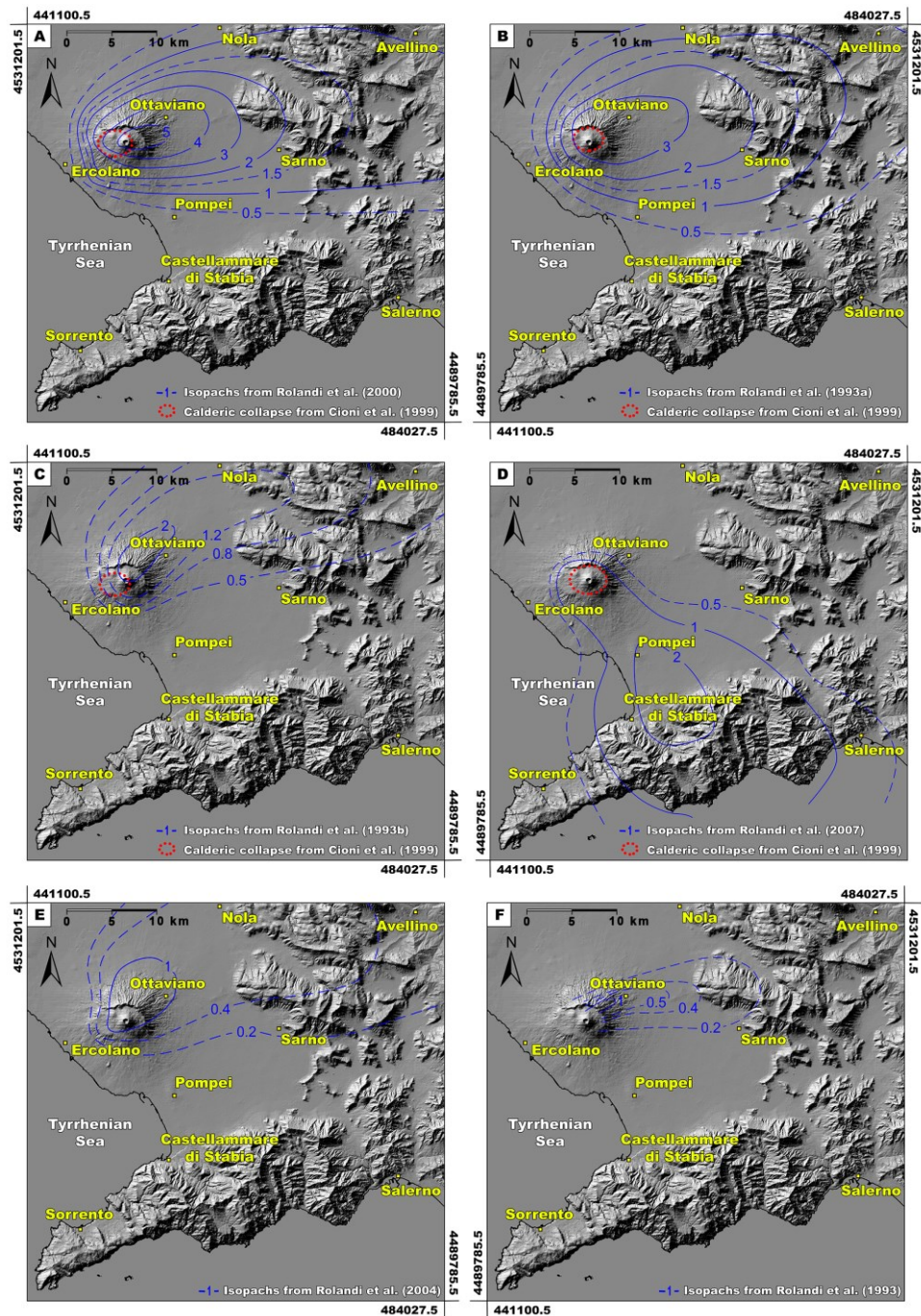


**Figure 2.4.** Isopach maps (fall deposits thicknesses in meter) of principal Plinian eruptions of the Somma-Vesuvius volcano with hypothesized calderic collapses: A) Sarno or Basal Pumice eruption (17 k-years B.P.); B) Ottaviano or Mercato Pumice eruption (8 k-years B.P.); C) Avellino eruption (3.7 k-years B.P.); D) 79 A.D. or Pompeii eruption; E) 472 A.D. or Pollena eruption; F) 1631 A.D. eruption.

### 2.1.2. Volcanological history of the Phlegraean Fields

The Phlegraean Fields are a volcanic field whose activity was related to monogenetic eruptions that strongly influenced the morphology of the area. For this reason, this volcanic district was divided in: 1) continental Phlegraean Fields; 2) insular Phlegraean fields, including Procida and Ischia islands.

The volcanic activity of the Phlegraean Fields was characterized by two massive catastrophic eruptions, which strongly affected the entire Campanian Plain. After these volcanic events, not less than 70 mainly explosive eruptions occurred in the Phlegraean Fields caldera previously formed (Orsi et al., 1996). The Ischia Island is also a volcanic field whose activity is one of the oldest occurred in the Campanian area, shown by the presence of lava flows dated about to 150 k-years B.P., whose main eruption was the Green Tuff of the Mount Epomeo (50 k-years B.P.). Using the Neapolitan Yellow Tuff (NYT - 15 k-years B.P.; Deino et al., 2004; Scarpati et al., 2013) deposits as a stratigraphic marker, which is widespreadly distributed in the Campanian Plain, the volcanic activity of the Phlegraean Fields can be divided in four cycles (Di Girolamo et al., 1984).

#### **The 1<sup>st</sup> cycle (60 ÷ 39 k-years B.P.)**

This cycle represents the beginning of the volcanic activity in the entire Phlegraean area and was characterized by a magmatic rising, which led to effusive and explosive volcanic eruptions, forming both lava domes and flows and surge/pyroclastic flow deposits (*Ancient tuffs*).

#### **The 2<sup>nd</sup> cycle (39 ÷ 15 k-years B.P.)**

During this cycle the first massive catastrophic volcanic event occurred. The *Campanian Ignimbrite eruption* (CI - 39 k-years B.P.; De Vivo et al., 2001; Fedele et al., 2008) strongly affected the morphology of the entire Campanian Plain. During this eruption, a calderic collapse of the volcanic district occurred and a massive pyroclastic flow, characterized by several successive events and a volume of Dense Rock Equivalent (DRE) more than 100 km<sup>3</sup> (Barberi et al., 1978), was erupted covering an area of 7000 km<sup>2</sup>. The CI deposits crop out along the border of the Campanian Plain

through the Apennine chain, with a variable thickness ranging between 20 and 60 m. After the CI eruption, although the geochronological data showed a gap between 30 k-years and 20 k-years B.P., probably related to the effects of the last massive volcanic event, a thick series of pyroclastic deposits separated by palaeosols and the presence of two monogenetic vents was recognized and dated back to  $17 \div 15$  k-years B.P. (Alessio et al., 1973).

### **The 3<sup>rd</sup> cycle (Neapolitan Yellow Tuff eruption)**

The Neapolitan Yellow Tuff (NYT) characterizes this cycle, which represents the second huge catastrophic volcanic event after the CI eruption. This eruption, dated back to 15 k-years B.P. (Deino et al., 2004), includes about 50 km<sup>3</sup> of DRE that buried Phlegraean Fields *sensu stricto* and the city of Naples with a thick blanket of pyroclastic-flow material, forming a major caldera collapse inside the earlier Campanian structure (Scarpati et al., 2013). In proximal areas, the thickness of this tuff is up to 150 m (Scarpati et al., 1993) but NYT is present also along the Apennine slopes bordering the Campanian Plain.

### **The 4<sup>th</sup> cycle (15 k-years B.P. ÷ 1538 A.D.)**

The recent volcanic products of the Phlegraean Fields eruptions (post-NYT deposits) filled the huge caldera created during the NYT, about 3 km deep. Loose and unconsolidated pyroclastic deposits, largely cropping out along the slopes of volcanic reliefs surrounding the city of Naples are the products of the recent Phlegraean explosive activity (Scarpati et al., 2013). The main explosive volcanic events (Fig. 2.5) were: the Gauro eruption (10 k-years B.P.; Orsi et al., 1996); the Pomici Principali eruption (10 k-years B.P.; Scherillo and Franco, 1960; Alessio et al., 1971); the Minopoli eruption (8 k-years B.P.; Armienti et al., 1983; Civetta et al., 1991); the San Martino eruption (uncertain dating); the Montagna Spaccata eruption (uncertain dating); the Baia eruptions (uncertain dating); the Pisani eruption (5 k-years B.P.; Orsi et al., 1996); the Agnano eruption (4 k-years B.P.; Orsi et al., 1996); the Paleo-Astroni eruption (4 k-years B.P.; Di Filippo et al., 1991); the Agnano-Monte Spina eruption (4 k-years B.P.; Rosi and Santacrose, 1984); the Averno and Senga eruptions (3 k-years B.P.; Alessio et al., 1973; Di Girolamo et al., 1984; Rosi and Sbrana, 1987). The

last low-intensity eruption of the Phlegraean Fields was the Monte Nuovo eruption, occurred in 1538 A.D. (Orsi et al., 1996), after a quiet period of about 3 k-years.

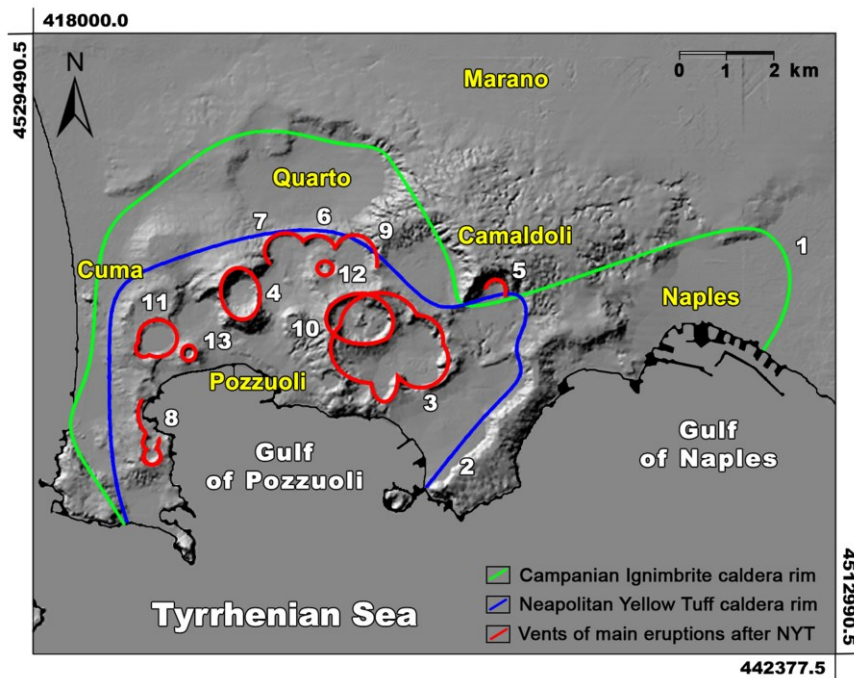


**Figure 2.5.** Vents of the main Phlegraean explosive volcanic eruptions occurred after the NYT calderic collapse: 1) Campanian Ignimbrite (CI) rim; 2) Neapolitan Yellow Tuff (NYT) rim; 3) Agnano vents; 4) Gauro vent; 5) Minopoli vent; 6) San Martino vent; 7) Montagna Spaccata vent; 8) Baia vents; 9) Pisani vent; 10) Astroni vent; 11) Averno vent; 12) Senga vent; 13) Monte Nuovo vent (modified from Orsi et al., 1996).

## 2.2. Sarno Mountains Range

### 2.2.1. Pre-Quaternary geological features

The carbonate structure of the Sarno Mountains is located to the east of the Somma-Vesuvius volcano and culminates with the highest peak of the M.t Pizzo D'Alvano (1.133 m a.s.l.). It is delimited to the West by the Nola plain, to the South by the Sarno river alluvial plain, to the East by the Solofrana valley and to the North by the Lauro valley. The carbonate ridge is NW-SE oriented, from Palma Campania to Mercato San Severino towns, and is located on the northeast border of Campanian Plain, at a mean distance of about 20 km from the Somma-Vesuvius volcano. The Sarno Mountains, as the Lattari, Avella and Salerno mountain ranges, surrounding the Campanian Plain,

are formed by a Mesozoic carbonate platform series that was deformed as tectonic units, which were piled up in the thrust and belt Apennine structure by the orogenic tectonic Miocene phases (Patacca and Scandone, 2007) (Fig. 2.6). Then, during Plio-Quaternary extensional tectonic phases, the carbonate tectonic units were faulted forming the current mountainous and steep morphological settings. Morphological settings that characterize these mountain ranges derive from faulting and erosional phases that occurred from the beginning of the orogenic processes (Brancaccio et al., 2000). In detail, the Sarno Mountains are a part of the Mesozoic carbonate tectonic unit of M.ts Picentini-Taburno. This morphological structure is characterized by a  $10^{\circ}$  -  $40^{\circ}$  NE dipping monocline structure, covered by late-Quaternary ash-fall pyroclastic deposits (D'Argenio et al., 1973). The latter, deriving from the activity of the near volcanic districts of the Somma-Vesuvius and Phlaeagraen Fields, are discontinuous and characterized by variable thickness.

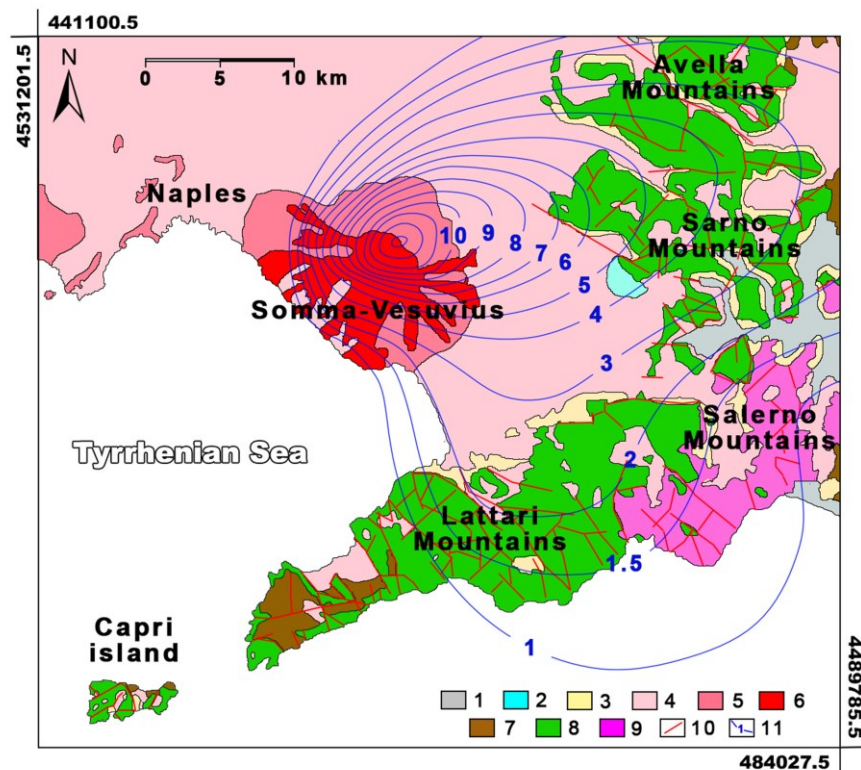


**Figure 2.6.** Geological setting of the peri-Vesuvian area (modified from De Vita et al., 2013): 1) alluvial deposits; 2) travertine deposits; 3) incoherent ash-fall deposits; 4) mainly coherent ash-fall deposits; 5) volcanic rocks; 6) debris and slope talus deposits; 7) Miocene flysch; 8) Middle Jurassic-Upper Cretaceous limestone; 9) Lower Triassic-Middle Jurassic dolomites and calcareous limestones; 10) outcropping and buried fault; 11) total isopachs line (m) of the most important Mt. Somma-Vesuvius eruptions (modified from De Vita and Nappi, 2013).

The oldest extensional tectonic phases related to the formation of the Tyrrhenian back-arc basin lasted until the Cretaceous and the beginning of Cenozoic period (Cinque et al., 1985). However, the most important tectonic phase that affected the area is related to the compressive Mio-Pliocene “Apenninic orogenetic phase” that created an important fault system characterized by sub-vertical SW–NE and NW–SE oriented direct faults (Nicotera and Civita, 1969). The lowering of the faulted Mesozoic carbonate platform along the Tyrrhenian bordered up to 3.000 m below the actual sea level, formed a regional semi-graben structure with subsidence rates of about 2.0 mm/years (Cinque et al., 1993). This structure was filled during the Quaternary by pyroclastic, alluvial and marine deposits forming the actual Campanian Plain.

Due to these tectonic phases, direct and/or reverse fault systems, transversally oriented to the principal alignment axis, characterize the mountain ridge, although faults with a strike-slip component are also supposed. Consequently, the entire carbonate ridge is characterized by several fault scarps and subsequent hydrographic network systems, creating throws of up to 250 m, which are smaller if compared to those related to master faults at the boundary. These morphological shapes are joined to flat summit palaeo-surfaces located at several hundreds of meters above the sea level. Convex-concave steepest slopes characterize the Sarno mountains ridge with decreasing slope angles from upslope to the foothill area, where colluvium deposits of alluvial fans are present.

### **2.2.2. Stratigraphic characterization of ash-fall pyroclastic deposits mantling Sarno Mountains slopes**

Ash-fall pyroclastic coverings mantling the Sarno Mts. ridge derive from fall-out deposits erupted by the nearest Somma-Vesuvius volcano, whose dispersal axes were mostly E-NE oriented. After the catastrophic landslide event occurred on May 5<sup>th</sup> and 6<sup>th</sup>, 1998 in the Sarno Mts. area, test pits carried out in different sites allowed reconstructing the stratigraphic setting of the volcanoclastic series along slopes of mountains surrounding the Campanian Plain. To describe the stratigraphic setting, considering also the pedogenetic horizons formed during the periods following each eruptions, a criterion based on the recognition of the principal pedogenetic horizons

was adopted (USDA, 2014; Terribile et al., 2000), combined with the lithostratigraphic and geotechnical classification of soils by means of the Unified Soil Classification System (USCS). Complete volcanoclastic series were found in morphological conservative areas (with slope angle, lower than 28°) of the Avella, Sarno, Lattari and Salerno mountain ranges. Due to the different orientation of dispersal axes of each eruption, different stratigraphic settings were found. The representative volcanoclastic series (Table 2.1) is characterized, from the top, by a pedogenized soil horizon (A+B), covering scarcely weathered lapilli pumiceous horizons (C-Cb), intercalated with paleosols (Bb). At the bottom, a basal paleosol (Bb<sub>basal</sub>) is always present wrapping the underlying carbonate bedrock (R).

Thickness range (m)	Lithologic description and USCS classification	Horizon
0.10	Humus (Pt)	A
0.50 ÷ 3.00	Very loose soil of pyroclastic horizons highly subjected to pedogenic processes with dense root apparatuses (SM). Generally dark brown colored.	B
0.00 ÷ 0.50	Very loose pumiceous lapilli level (gravel) with low degree of weathering (GW-GP). Dark green colored. Pollena eruption (472 A.D.)	C
0.10 ÷ 1.50	Earth of pyroclastic origin constituted by fine to coarse ash and subordinately by pumiceous lapilli. Paleosol (SM). Brown - red - dark red colored.	Bb
0.00 ÷ 0.50	Whitish pumiceous lapilli (gravel) from very angular to angular, with maximum 6 cm diameter, in place, matrix almost absent. Avellino eruption (3.670 k-years B.P.)	Cb
0.10 ÷ 1.50	Basal paleosol (SM). Yellow - red - dark colored.	Bb <sub>basal</sub>
?	Carbonate bedrock fractured by discontinuity sets. The latter presents variable opening and filling formed by pyroclastic deposits coming from overlying soil horizon.	R

**Table 2.1.** Representative stratigraphic setting of the ash-fall pyroclastic cover in conservative areas of the Sarno Mountains. The classification of volcanoclastic materials is in according to Schmidt (1981).

Complete volcanoclastic series were found on the Lattari Mts. as similarly characterized by paleosols, but with a unique C horizon ascribed to the deposits of the A.D. 79 eruption. In addition, a basal paleosol wrapping the carbonate bedrock was found also in this case. The basal paleosol was attributed to the remnants of deposits of the APC. The thinning of the pyroclastic soil mantle for slope angle greater than

28°, up to its annulment for slope angles greater than 50°, was recognized to have a strong influence on the stratigraphic settings of the volcanoclastic series along the slopes (De Vita et al., 2006) (Fig. 2.7). The reduction of the total thickness was found to determine the downstream pinch out of the pyroclastic horizons (both C and Bb), down to the direct overlying of the B horizon on the Bb<sub>basal</sub> horizon.

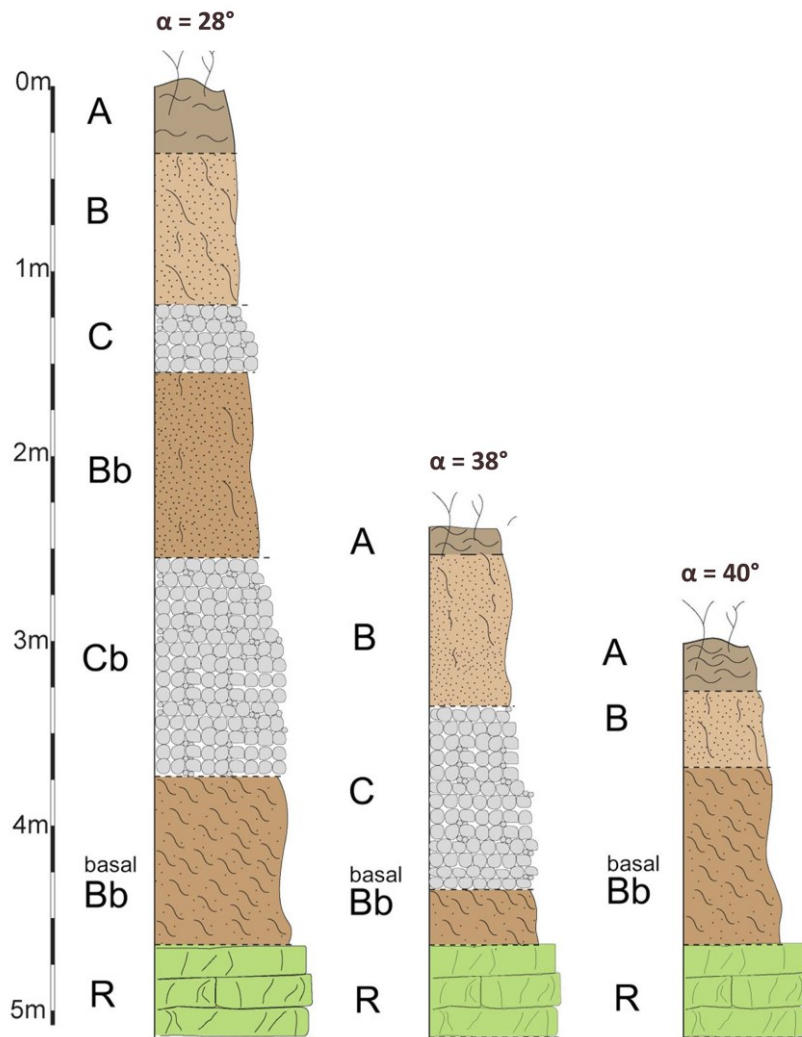


**Figure 2.7.** Stratigraphic setting variation of ash-fall pyroclastic cover for different slope angles in Sarno Mountains area (De Vita et al., 2006a): (A+B) humus and pedogenized horizons; (C-Cb) lapilli pumiceous layers; (Bb-Bb<sub>basal</sub>) paleosoils; (R) carbonate bedrock.

A distributed model of ash-fall pyroclastic cover thickness mantling the mountain slopes surrounding the Campanian Plain was obtained (De Vita et al., 2006; De Vita and Nappi, 2013). These studies were focused on empirical modelling of ash-fall pyroclastic soils along slopes to assess the strong spatial variations in thickness and

stratigraphic settings. A first step was the reconstruction of the ash-fall pyroclastic deposits distribution and the theoretical total thickness assessment at the regional scale, considering the algebraic sum of all isopach maps of principal eruptions known in the scientific literature and new data gathered in several test areas. The principal Plinian eruptions of the Phlegraean Fields and Somma-Vesuvius volcanoes, for which isopach maps of ash-fall pyroclastic products were available, were taken into account. For volcanoclastic deposits of Phlegraean Fields, belonging to the Ancient Pyroclastic Complex (APC) (Rolandi et al., 2000), only ash-fall deposits related to the eruption of the Campanian Ingnimbrite (39 k-years) (Perrotta and Scarpati, 2003) were included in calculations. Instead, for the Recent Pyroclastic Complex (Rolandi et al., 2000), the principal Plinian eruptions were considered: Codola eruption, 25 k-years B.P. (Rolandi et al., 2000); Sarno eruption, 17 k-years B.P. (Rolandi et al., 2000); Ottaviano eruption, 8.0 k-years B.P. (Rolandi et al., 1993a); Avellino eruption, 3.67 k-years B.P. (Rolandi et al., 1993b); Pompeii eruption, A.D. 79 (Lirer et al., 1973); A.D. 472 eruption (Rolandi et al., 1998); A.D. 1631 eruption (Rosi et al., 1993); A.D. 1944 eruption (Cole and Scarpati, 2010). By this reconstruction (De Vita et al., 2006), the distribution of the theoretical total ash-fall deposits was recognised as inhomogeneously distributed around the volcanic vents and characterised by two main dispersal axes, the principal was eastward oriented and the secondary southward (Fig. 2.8). Considering that isopach maps were reconstructed on the basis of observations of outcrops or boreholes mainly located within the Campanian Plain or at the base of the surrounding mountains, the total theoretical thickness and stratigraphic settings were validated by a comparison with field measurements and observations carried out along the Avella, Sarno, Lattari, Picentini and Salerno mountain ranges, which consisted of 73 field inspections (light dynamic penetrometric tests and test pits; De Vita and Nappi, 2013) (Fig. 2.6). In favorable logistical conditions and a thickness of the pyroclastic mantle lower than 4.0 m, hand-dug pits reaching always the carbonate bedrock were executed. Instead, for greater values of thickness, light dynamic penetrometric tests were executed down to the bedrock. Field investigations were carried out in slope sectors with slope angles lower than  $28^\circ$  with the purpose to make a comparison with the theoretical value of the total ash-fall pyroclastic deposits. This was established for taking into account field observations which showed the reduction of ash-fall pyroclastic soil mantle thickness for slope angle higher than  $28^\circ$  (De Vita et al., 2006; 2013), up to the approximate disappearance and lack of physical

continuity for slope angle greater than  $50^\circ$ . Data of thicknesses, considered as apparent values because measured along the vertical, were transformed in real values (stratigraphic thickness) as the projection in the plane normal to the slope. Subsequently, the actual real thickness values were compared with the theoretical real ones that were calculated by Eq. [2.1], thus considering the total theoretical thickness fallen in the area ( $z_0$ ), derived from the regional distribution model (Fig. 2.8), and the slope angle ( $\alpha$ ):

$$z = z_0 \times \cos\alpha \quad [2.1]$$

Considering the soil thickness data of ash-fall pyroclastic soils mantle collected in a wide mountain area that surrounds the Campanian Plain, the maximum values measured in each test site were observed not to exceed the theoretical value fallen in that area (Fig. 2.8), as calculated by the Eq. [2.1]. In detail, for slope angles lower than  $28^\circ$ , the ash-fall pyroclastic total thickness was observed as well comparable to that theoretically fallen in the area as it was verified by the good correlation between theoretical and actual values (Fig. 2.8).

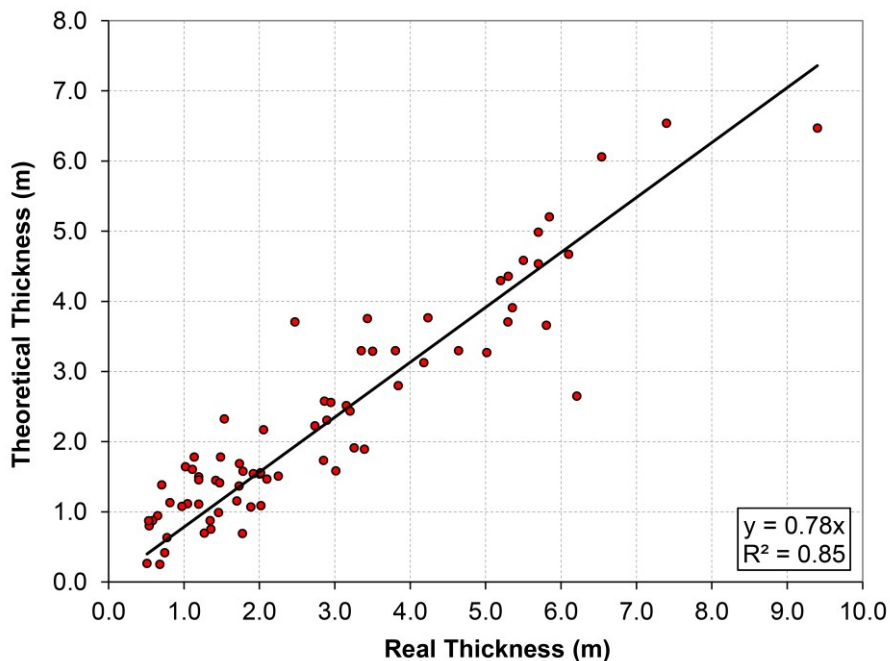


**Figure 2.8.** Correlation between the theoretical and the actual thickness of the pyroclastic mantle. Values are in real terms (modified from De Vita and Nappi, 2013).

Contrarily, for slope angles greater than  $28^\circ$ , actual stratigraphic thickness values were found lower than theoretical ones fallen in the same area. Field data confirmed the discontinuity and the negligible thickness of the pyroclastic mantle for slope angles greater than  $50^\circ$  (Fig. 2.9). Such a distribution model, basically controlled by the slope angle, was attributed to denudation or erosional processes, including landsliding, which reached a dynamic equilibrium, between resisting and driving forces, leading to slope instability, in which vegetation and rainfall triggering events play a spatially and temporally variable role.

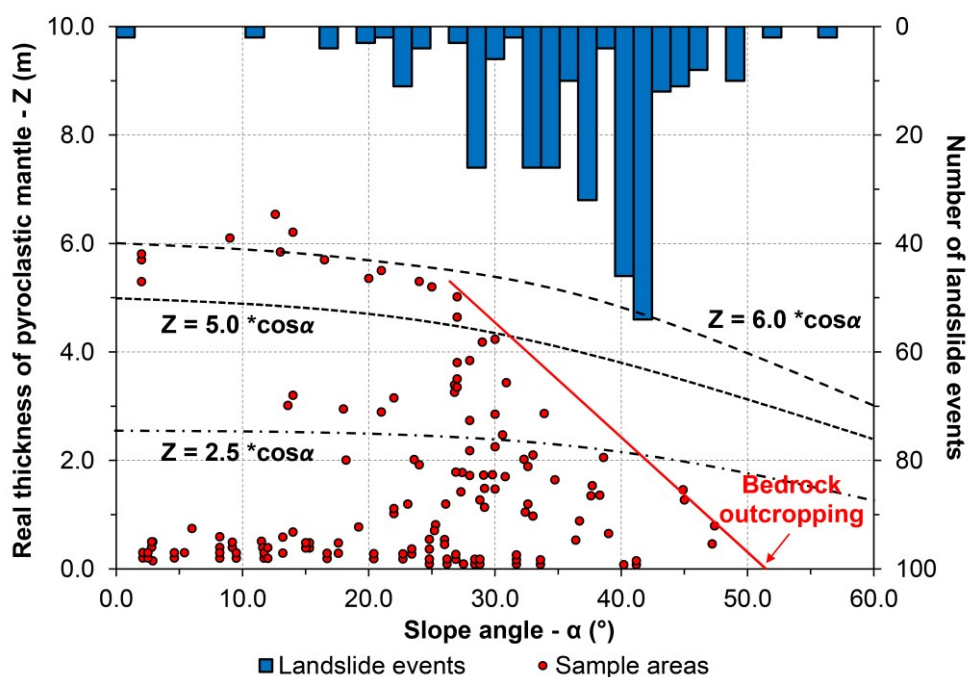


**Figure 2.9.** Comparison between real thicknesses of the pyroclastic mantle measured along slopes of sample areas (dots) and theoretical distribution of ash-fall pyroclastic soils (dashed curves). Theoretical distributions of three sample areas, characterised by different  $z_0$  values, are also showed with  $z_0$  equal to 6 and 5 m, respectively, for the southwestern and northeastern slopes of the Sarno mountain range, and 2.5 m for the north-eastern slopes of the Lattari mountain range. The continuous black line represents the upper envelope (modified from De Vita and Nappi, 2013).

Based on field data and observations, an empirical distribution model of ash-fall pyroclastic deposits along the mountain ranges surrounding the Campanian Plain was developed in a raster GIS environment (De Vita and Nappi, 2013). The model was based on the combined application of the total theoretical thickness map of ash-fall deposits, calculated by the sum of the isopach maps of principal eruptions, and the

constraints related to the observations that the thickness of the pyroclastic mantle decreases for slope angle values greater than  $28^\circ$  up to the annulment for values greater than  $50^\circ$  (Fig. 2.10).

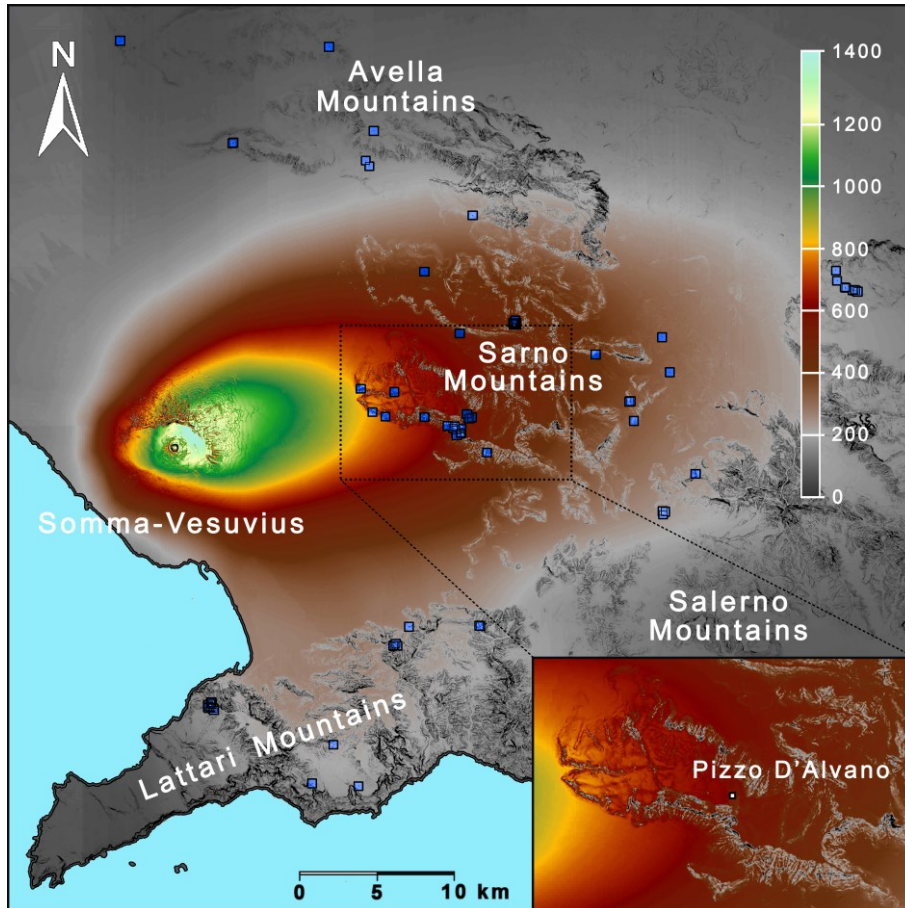


**Figure 2.10.** Distribution model of ash-fall soil pyroclastic deposits in the area surrounding the Campanian Plain. Values of real total thickness are expressed in centimeters. Sample areas for field soil thickness measurements are also shown (blue squares; De Vita et al., 2013).

## 2.3. The Camaldoli hill

### 2.3.1. Geological features of the Phlegraean area

The geology of the Phlegraean area is dominated by the eruptive history of Phlegraean Fields (Fig. 2.11), whose volcanism is related to Plio-Quaternary extensional tectonics that deformed the western margin of the Apennine chain and formed the semi-graben structure of the Campanian Plain (D'Argenio et al., 1973; Ippolito et al., 1973; Finetti and Morelli, 1974; Bartole, 1984). The beginning of

volcanism in the area is not precisely defined, though the oldest dated rocks, which are not the lowermost in the stratigraphic sequence, yield an age of about 60 k-years (Pappalardo et al., 1999) and are related to explosive volcanism, which extended beyond the present margin of the Phlegraean Fields. The complex geo-structure of this volcanic district is characterized by a large caldera resulting from the two oldest main collapses, where constructive volcanic, destructive volcano-tectonic events and sea level variations controlled the present morphological setting. The whole area is also affected by uplift or subsidence phenomena (bradyseism) that allowed erosional and depositional marine processes (Cinque et al., 1985; Orsi et al., 1996). The morphostructural setting of the Phlegraean Fields is characterized by small coastal plains and internal flat areas, located at different elevations and bordering steep volcanic rims.

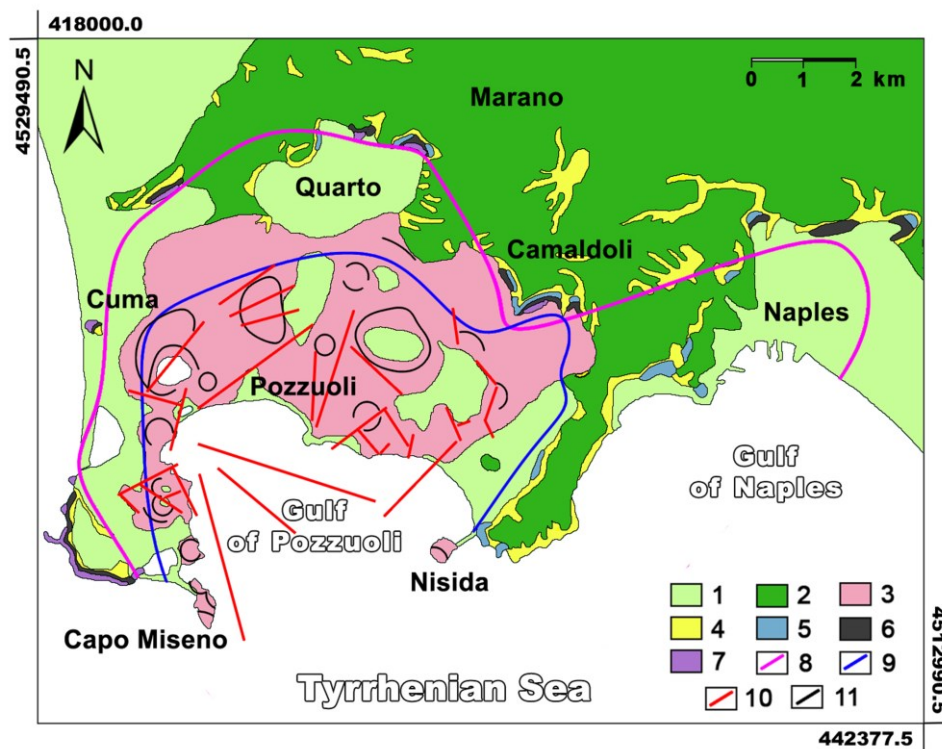


**Figure 2.11.** Geological setting of Phlegraean area (modified from Orsi et al., 1996): 1) recent and active alluvial deposits; 2) distal volcanic deposits, younger than the Neapolitan Yellow Tuff eruption (14 k-years B.P.), mostly characterized by fall-out products; 3) proximal volcanic deposits, younger than Neapolitan Yellow Tuff eruption (14 k-years B.P.), mostly composed by pyroclastic flow and/or surge; 4) Neapolitan Yellow Tuff (NYT) deposits (14 k-years B.P.); 5) volcanic deposits (39 ÷ 14 k-years B.P.); 6) Campanian Ignimbrite (CI) deposits (39 k-years B.P.); 7) volcanic pre-Campanian Ignimbrite deposits (older than 39 k-years B.P.); 8) supposed CI caldera rim; 9) supposed NYT caldera rim; 10) faults; 11) crater rim of volcanic vents younger than 14 k-years B.P.

### 2.3.2. Stratigraphic characterization of the Camaldoli hillslopes

The Camaldoli hill (458 m a.s.l.) is located in the northeastern part of Phlegraean Fields and its slopes impend over the most part of the city of Naples and adjoining municipalities. Field investigations including deep drillings, exploratory trenches and penetrometric tests allowed reconstructing the stratigraphic setting of the area (Calcaterra et al., 2007a).

The volcanoclastic series (Table 2.2) is principally characterized by alternations of scarcely weathered ash-fall pyroclastic soil horizons (SM), with accretionary lapilli, scattered pumice, pyroclasts of lavas and lithic tuff and pumiceous lapilli horizons (GP and GM). The latter are usually well sorted, with variable amounts of lithic fragments and variably in thickness from few to tens of centimeters. Paleosols (SM), usually developed on ash or reworked deposits during the quiet period of the Phlegraean Fields volcanic district, show variable degree of humification.

The entire series is formed by both NYT and, in some cases, CI proximal deposits with variable thicknesses (up to 30 m). Locally it has been reworked for terrace-cultivation and building construction.

Due to the tectonic-volcanic activity that occurred in the Phlegraean area, slopes that characterize the western and the southern parts of the Camaldoli hill represent the rim of the calderic collapse related to the NYT eruption. For this reason and also for the sub-horizontal layering of the ash-flow deposits, the entire volcanoclastic series appears truncated in proximity of the slopes and mantled by the top soil (SM), which is formed by the weathering processes that affect the primary volcanic deposits.

Due to these geological and geomorphological settings, slope instabilities with different triggering mechanisms and kinematics occur in the whole area, involving both lithoid materials (tuff and extrusive igneous rocks) and incoherent materials (top soil and loose pyroclastic deposits). The latter incoherent materials are typically subject to flow-like shallow landslides triggered by long-duration and/or intense rainfall events, particularly if preceded by significant rainy periods.

Thickness ranges (m)	Lithologic description and USCS classification	Horizon
0.50 ÷ 2.00	Very loose soil with pumiceous lapilli. Generally dark brown colored. SM	Top soil
0.50 ÷ 1.50	Very loose white pumiceous lapilli layer with low degree of weathering (GP) and greenish ash content increasing to the top (GM). Agnano Monte Spina eruption (4 k-years B.P.)	Pumice
0.50 ÷ 1.00	Soil of pyroclastic origin constituted by fine to coarse ash and subordinately by pumiceous lapilli. Paleosoil (SM). Brown - red - dark red colored.	Paleosol
0.50 ÷ 3.00	Ash layer (SM) with pumiceous lapilli and lithic fragments layer altering (GW-GP). Grey-greenish coloured. Agnano eruption (4 k-years B.P.).	Ash / Pumice
0.50 ÷ 1.00	Soil of pyroclastic origin constituted by fine to coarse ash and subordinately by pumiceous lapilli. Paleosoil (SM). Brown - yellowish colored.	Paleosols
0.50 ÷ 4.00	Alternating of fine ash (SM) and coarse sand (GP) with subordinately pumiceous lapilli. Grey-greenish colored. Pisani eruption (5 k-years B.P.)	Ash / Pumice
0.50 ÷ 1.50	Alternating of fine ash (SG) and coarse sand (SM) with subordinately pumiceous lapilli. Greenish colored. Minopoli eruption (8 k-years B.P.)	Ash
1.00 ÷ 2.00	Very loose pumiceous lapilli layer with lithic fragments (GW). Light grey coloured. Pomici Principali eruption (10 k-years B.P.)	Pumice
1.50 ÷ 3.00	Alternating of fine ash layer (SM), very loose pumiceous lapilli layer (GP) with ash content increasing to the top (GM) and lithic fragments. Grey-greenish coloured. Uncertain eruption.	Ash / Pumice
1.00 ÷ 2.50	Coarse ash layer with with-yellowish pumiceous lapilli and lithic fragments (SM). Layered texture related to the different grain sizes. Grey-greenish coloured. Loose facies of Neapolitan Yellow Tuff eruption (15 k-years B.P.).	Ash
?	Massive layer. Yellowish coloured. Lithified facies of Neapolitan Yellow Tuff eruption (15 k-years B.P.).	Tuff

**Table 2.2.** Representative stratigraphic sequence deriving from field investigations, including borehole drilling and exploratory trenches, carried out in of Camaldoli hill area (Calcaterra et al., 2007a). Thickness range, USCS classification and, in some cases, provenience of each pyroclastic horizon are shown.

# Chapter 3

---

## Hydrological processes and shallow slope instability

Shallow instabilities affecting peri-Vesuvian and Phlegraean slopes covered by ash-fall pyroclastic soils are strongly related to the hillslope hydrological processes. Geomorphological, stratigraphical and climatic factors as well as hydro-mechanical properties and hydrological conditions of involved materials represent the predisposing and triggering factors of these shallow landslides also including their kinematics. This chapter describes the hydrological processes and dynamics, which is known to affect the slope stability, and mechanisms leading to landslide triggering as well as the kinematics of flow-type landslides occurring in peri-Vesuvian and Phlegraean area.

### 3.1. Hydrological slope processes

Rainfall or snowfall events, evapotranspiration processes, surficial or sub-surficial flows as well as geomorphological, geological and stratigraphic factors strongly affect hydrological processes of a slope. Morphological conditions, land uses and management strategies are strongly related to slope stability conditions.

#### 3.1.1 Infiltration

During a rainfall event, the amount of water not intercepted by vegetation (Helvey and Patric, 1965) reaches the ground surface allowing the *infiltration* process within the soil/rock that is at the ground surface along the slope. If the infiltration rate is greater than its infiltration capacity, the exceeded water will pond on the ground surface leading the initiation of the *runoff* (Fig. 3.2).

The infiltration capacity of a soil/rock derives from its hydraulic properties and represents the maximum amount of water, which can infiltrate in a time unit. In detail,

the capability of a material to allow water infiltration is function of pore water pressure and derives from the size, number and interconnections between internal voids. For example, a soil characterized by plane-parallel macrostructures to the surface is particularly restrictive to the infiltration process.

Soil infiltration capacity is high at the beginning of the rainfall event, due to high soil suction values, and assumes a constant value, equal to the Saturated Hydraulic Conductivity ( $K_{sat}$ ), when the soil becomes saturated.

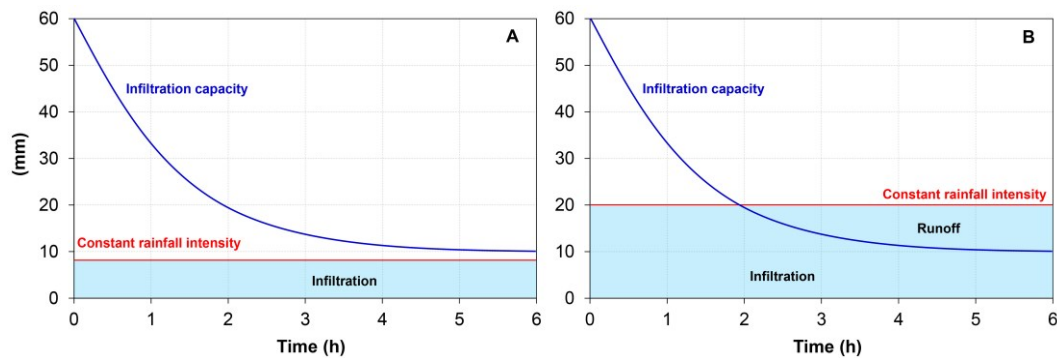


**Figure 3.2.** Representative decreasing of soil infiltration capacity ( $f$ ) with time during rainfall event. If  $f$  is higher than rainfall intensity only infiltration occurs (A). Instead, if  $f$  is lower than rainfall intensity, infiltration and runoff occur (B).

A first interpretative model of the infiltration process was described by Horton's model (1933) (Eq. 3.1):

$$f(t) = f_c + (f_0 - f_c) \times e^{-\alpha t}$$

[3.1]

where:

$f(t)$  = infiltration capacity at time  $t$ ;

$f_c$  = final constant value of infiltration capacity with a saturated soil ( $K_{sat}$ );

$f_0$  = initial maximum value of infiltration capacity;

$\alpha$  = decay constant of a soil;

$t$  = time.

Horton's model (1933) provides that:

- in concomitance of long-prolonged rainfall an initially uniform infiltration occurs along a slope;
- during stable high-intensity rainfall events a decreasing of the soil infiltration capacity occurs leading to runoff flow (Hortonian type), more or less simultaneously on the entire hydrographic basin (Amerman and McGuinness, 1967);
- when the rain intensity is less than the infiltration capacity, a reduction of the water amount available for the infiltration and no water excess for the runoff occur (Horton, 1937a).

The variability of the infiltration capacity is controlled by: a decrease of the unsaturated hydraulic gradient due to the saturation of soil from the surface; physical or mechanical soil properties changes deriving from human (removal, overloading) or natural causes (erosion, drying/imbibition cycles), which reduce the pore size or their interconnections.

After the Horton's first model, some other Authors focused their research on studying infiltration processes, proving that infiltration rate is inversely proportional to the water content existing in an unsaturated soil (Sherman, 1944) and that the infiltration process may be divided in three parts (Bodman and Coleman, 1943):

- *transmission zone*, located in the shallowest part of the soil profile and where infiltrated water percolates through this zone after the end of the absorbing process;
- *wet zone*, where the water content decreases with depth;
- *wet front*, characterized by irregular shape and high potential values.

Considering a homogeneous, one-dimensional and semi-finite soil model with uniform wetting antecedent conditions, Philip (1958) proposed a new equation (Eq. 3.2) to describe infiltration ( $i$ ) processes advancing the initial Horton's model (1933):

$$i = \frac{1}{2}st^{-\frac{1}{2}} + A$$

[3.2]

where:

$A$  = is a constant;

$s$  = a sorptivity value (a measure of the capacity of the medium to absorb or desorb water by capillarity) obtained from the rate of penetration of the wetting front;

$t$  = time.

with conditions

$$t = 0 \quad i \rightarrow \infty \quad i \rightarrow A$$

Finally, the shape of the decay curve and then the infiltration capacity is strongly affected by rainfall intensity (Smith, 1972) and pore water pressure distribution.

### 3.1.2 Runoff, sub-surficial (throughflow) and deep percolation flows

The amount of water deriving from rainfall events follows different paths along a slope (surficial flows) or leading infiltration and flowing within it (sub-surface flows). For slightly vegetated slopes characterized by a thin cover, the Horton's model (1933) assumes that the amount of infiltrated water follows different paths and can be stored within the slope or flows: part of this water feed infiltration process and the other part will flow along the slope (*runoff*) (Horton, 1937a). In this case, runoff follow the contributive partial-area model, which assumes that only the rainfall affecting a small part of a drainage basin is able to contribute to runoff (Kirkby and Chorley, 1967; TVA, 1968). Soils characterized by high hydraulic conductivity values allow infiltration deepening down to the saturated basal zone (if it exists).

Rocky slopes, such as those formed by carbonate rock-masses, if characterized by open discontinuity systems in the shallower zone, favour a high infiltration rate and, due to the decrease of hydraulic conductivity with depth, form a saturated flow parallel to the slope named *subsurface stormflow*, although the greater part of the infiltration water feeds the *groundwater* and *baseflow*. In some cases, if along the slope total or partially saturation conditions occur a *returnflow* can exist, becoming *overland flow* (Musgrave and Holtan, 1964).

Coincident with the *contributive partial-area model*, the logical extention of the *contributive variable-area model* was developed, which assumes that variability of

sources providing the formation of a quick runoff both between and within storms (Tsukamoto, 1961; 1967; Ragan, 1967, 1968; Nutter, 1969). This variation is strongly related to initial soil moisture conditions, field capacity and rainfall intensity (Betson et al., 1964; TVA, 1965; Betson et al., 1968; Betson and Marius, 1969; Dunne and Black, 1970b). In concomitance of heavy and/or prolonged rainfall events, vegetated slopes with significant humus horizon are affected by the formation of *overland flow*, occurring both in areas where a lot of water is retained on the surface or saturation condition exists (Kirkby and Chorley, 1967) (Fig. 3.3).

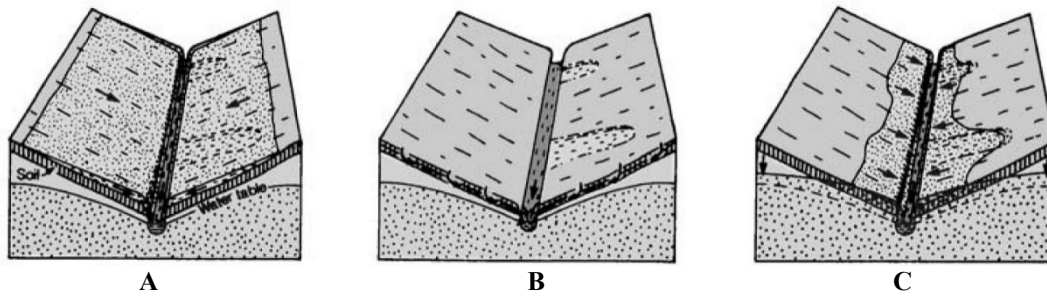


**Figura 3.3.** Models of runoff formation along a slope due to: (A) infiltration capacity less than rainfall intensity (Horton, 1933); (B) *returnflows* from *throughflows* (Kirkby and Chorley, 1967); (C) saturation conditions up to the slope ground surface.

Furthermore, slopes affected by low-intensity and short rainfall events lead to the formation of *Hortonian overland flows* (Haggett and Chorley, 1969) in different areas (Fig. 3.4): close to the hydrographic network (Kirkby and Chorley, 1967; Jamison and Peters, 1967; Carson and Kirkby, 1972), hollows (Kirkby and Chorley, 1967; Dunne and Black, 1970a) and areas characterized by thin cover.

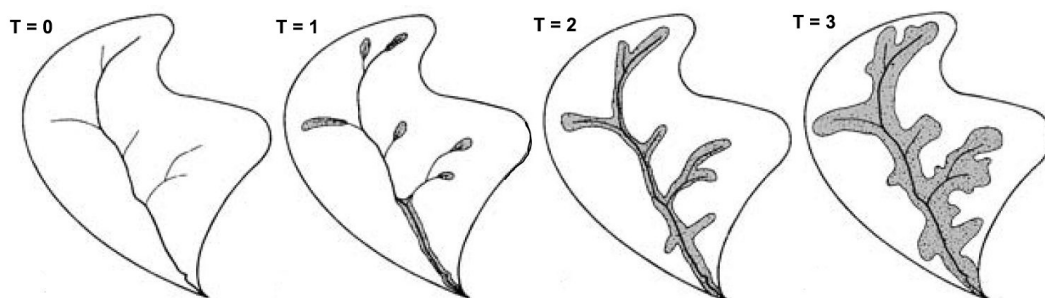


**Figura 3.4.** Representation of the saturated or near-saturated areas formation (grey areas), close to hydrographic network, and their expansion during a rainfall event (from Kirkby and Chorley, 1967).

With respect to infiltration and flow processes within a slope, several types of saturated and unsaturated sub-surficial flows may occur, whose triggering and dynamics are strongly related to geomorphological, stratigraphic, climatic, and antecedent hydrological conditions (soil water content and pressure head). Soil hydrological and geotechnical properties as well as thicknesses represent the most important parameters for initiation of sub-surficial flows.

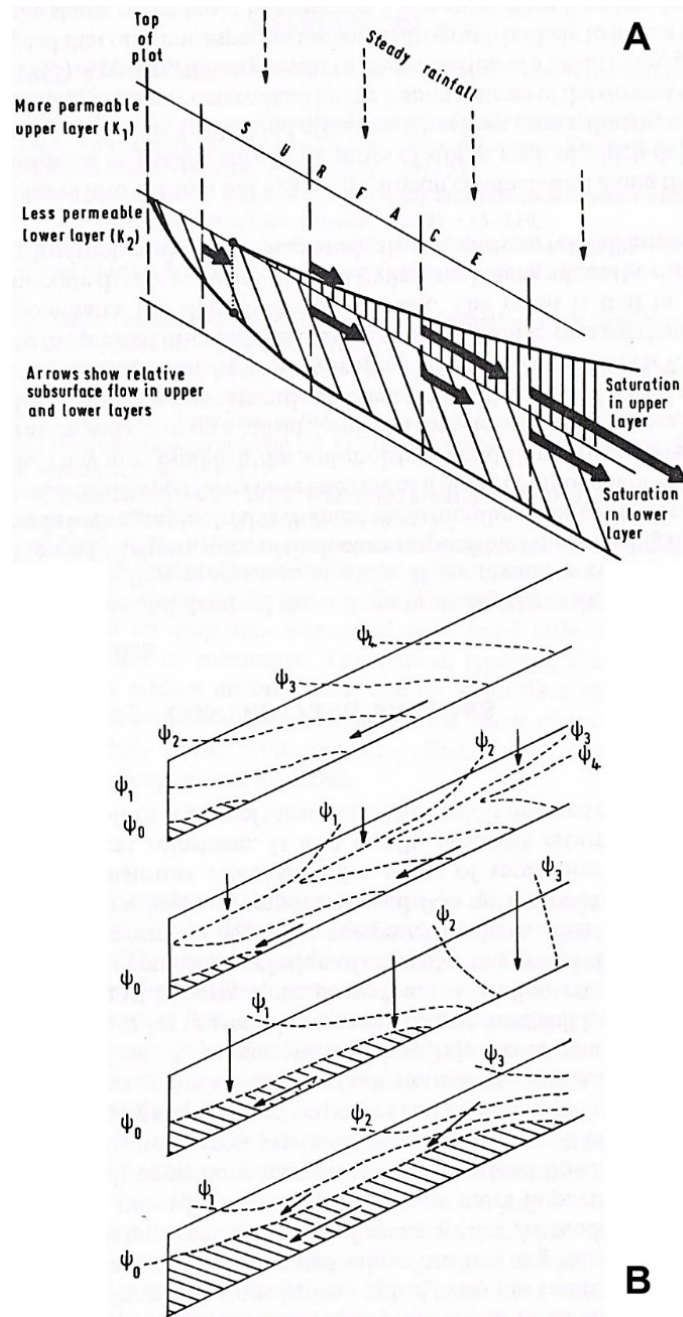


**Figure 3.5.** Formation of sub-surficial flows within a soil cover characterized by a deeper horizon with low-permeability (A). The sketches show also the pressure head ( $\psi$ ) distribution with time (B) due to the increase of water content (modified from Kirkby and Chorley, 1967).

In detail, animal burrows, radical or structural voids apparatuses as well as erosional processes (*pipe flows*) may increase hydraulic conductivity of a soil promoting sub-surficial flows (Fletcher et al., 1954; Bell, 1968; Berry, 1970) which can feed *overland flows* (Fig. 3.6). Soil pore water pressure strongly affects unsaturated flows formation, such as *capillary flows* or *bulk flows*, occurring in areas characterized by low matrix potential. Kirkby and Chorley (1967) proposed the *throughflow model* after the Horton's model (1933), related to heavily vegetated slopes with thick soil covers containing less-permeable horizons and sharply overlaying relatively impermeable unweathered bedrock. This permeability contrast promote lateral flow within the more-permeable horizon (Fig. 3.5A). If saturation conditions reach the ground surface, due to cover discontinuity or thickness decreasing, *return flow* may occurs leading to the formation of the *overland flow* (Kirkby and Chorley, 1967; Kirkby, 1969; Cakver et al., 1972) (Fig. 3.5B).

Discharge and velocity of sub-surficial flows are also affected by slope angles that control the hydraulic gradient in saturated conditions. In fact, slopes characterized by low angles and thick cover allow more infiltration than slopes with high angles and thin cover (Fig. 3.6).

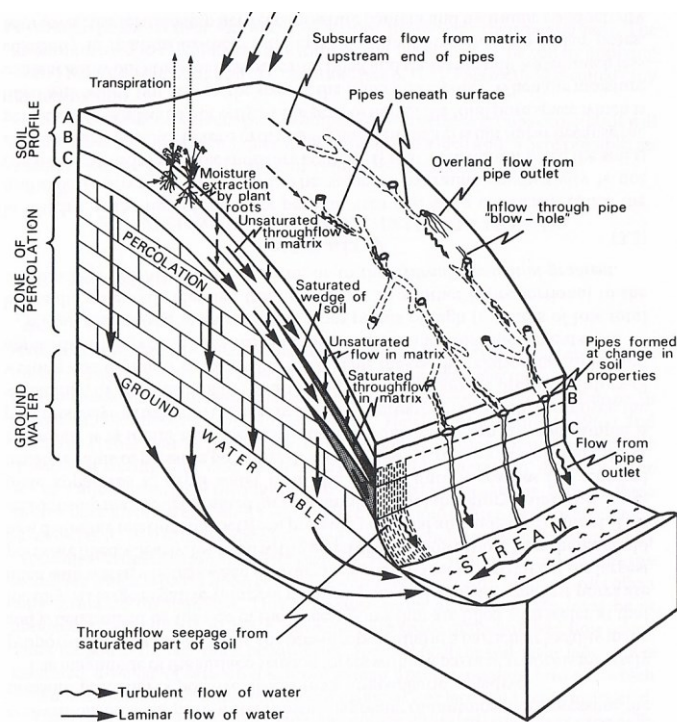


**Figura 3.6.** Different types of sub-surficial flows triggered by rainfall events and affected by slope angle and cover thickness variations existing along a slope (from Kirkby and Chorley, 1967).

Usually, *throughflows* triggered by low-intensity and short rainfall events are strongly related to the extension of the saturated or near-saturated areas close to the hydrographic network (Kirkby and Chorley, 1967; Weyman, 1970) (Fig. 3.6), whose flow may last for weeks promoting the *basal flow* (Hewlett, 1961b; Carson and Kirkby, 1972) where an impermeable bedrock exists.

If rainfall events represent the principal input for the hydrological regime of a slope, which feed surficial or sub-surficial flows, vegetation interception and mostly evapotranspiration processes represent the output, which control the variability of soil pore water pressure. The effects are related to the type, growth and activity of the vegetation, which characterize a slope, usually affecting the hydrological regime during summer (vegetative plants period and higher air temperature) more than the winter period (dormant plants period and lower air temperature).

### 3.2. Stability of soil-mantled slopes

Defined as the downslope movement, shallow to deep and rapid to slow, of a rock, debris or earth mass, controlled by the gravity force (Varnes, 1978; Carrara et al., 1985; Cruden, 1991; Cruden and Varnes, 1996), landslides represent an important factor for slope morphological evolution. Volumes of involved materials can be highly variable, from few to millions of cubic meters, as well as their nature (rocks, incoherent or cohesive materials).

Shallow flow-type landslides, which involve ash-fall pyroclastic cover mantling peri-Vesuvian and Phlegraean slopes, occur in specific slope sectors due to the combination of several unfavorable climatic, stratigraphic and geomorphological factors, whose recognition and control is useful for preventing the recurrence of these events.

Morphological shapes of *debris flows* (Hungri et al., 2001) or *soil slips* (Campbell, 1975) that affect mountains surrounding the Somma-Vesuvius volcano and Phlegraean slopes (Figure 3.7) can be described according to the classification of Cruden and Varnes (1996) (Table 3.1) and the nomenclature proposed by the “Working Party on World Landslide Inventory” (1993b).

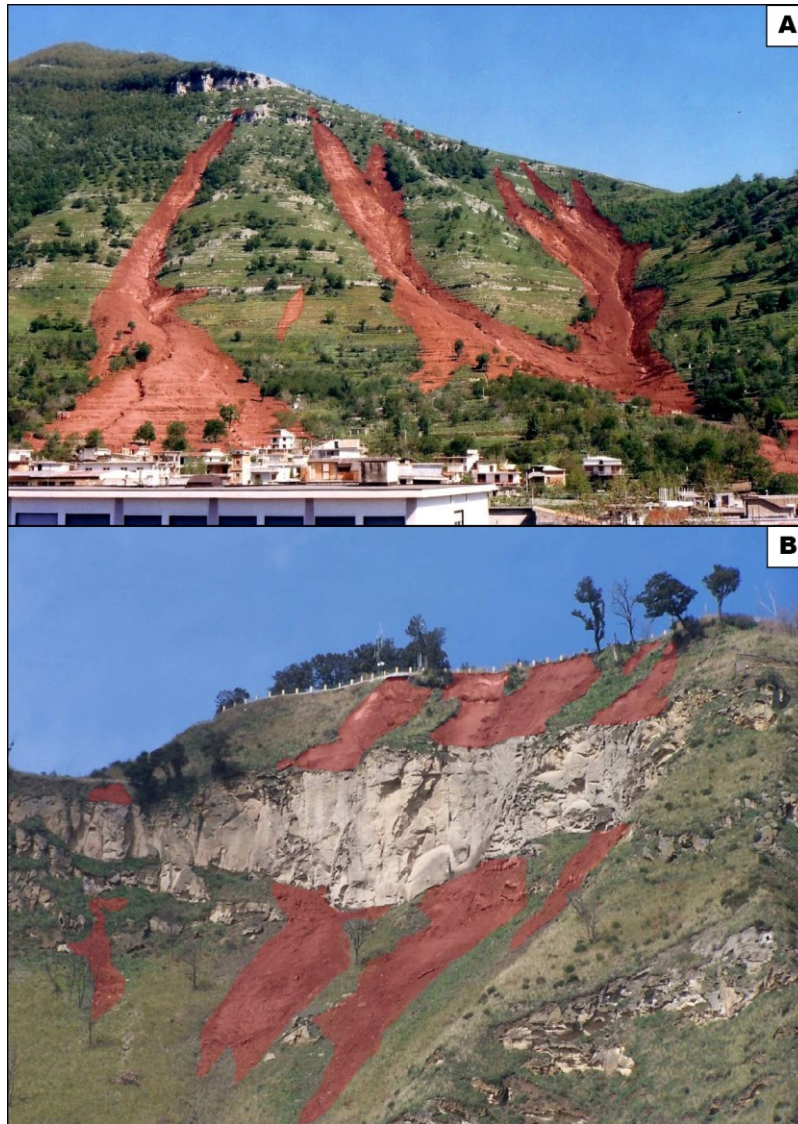


**Figure 3.7.** Detachment areas and morphological shapes of principal flow-type landslides (red coloured) involving ash-fall pyroclastic cover mantling peri-Vesuvian (A) and Phlegraean (B) slopes.

<b>Detachment area</b>	<b>Crown</b>	Uppermost sector of the landslide where undisplaced material adjoins to the main landslide scarp.
	<b>Main scarp</b>	Vertical scarp, in the downstream direction, which identifies the nearly undisturbed area around the top part of the landslide and it is caused by movement of displaced material.
	<b>Top</b>	Highest contact area between the undisturbed material and main scarp.
	<b>Flanks</b>	Undisturbed soil located laterally to the failure surface.
<b>Accumulation area</b>	<b>Main body</b>	Part of displaced material overlying the surface of rupture between main scarp and toe of surface of rupture.
	<b>Surface of rupture</b>	Forms or formed the lower boundary of displaced material.

**Table 3.1.** Nomenclature of the principal landslide structures recognizable at the ground (Working Party on World Landslide Inventory, 1993b).

As regards the shallow flow-type landslides involving ash-fall pyroclastic covers mantling peri-Vesuvian and Phlegraean slopes, it is possible to define clearly the morphological shapes. Field evidences showed that main scarps, flanks and slide surfaces of past landslide events are always recognizable, for several years after the landslide occurrence due to the limited erosional processes.

### 3.2.1. Predisposing and triggering factors to shallow landsliding

*“A landslide may have several predisposing factors but just one triggering cause”*  
(Wieczorek, 1996).

Considering this statement, landslide-triggering factors may be different and related to natural and/or anthropic causes and can change initial slope stability condition into instability one. Moreover, predisposing factors have also to be taken into account because they are boundary conditions that make a slope more or less susceptible to landsliding. In geotechnical terms, predisposing factors lead certain sectors of a slope more susceptible to slope instability due to a locally lower safety factor. Predisposing factors have to be differentiated from the triggering factors, deriving from natural (for example earthquakes, rainfall) or anthropogenic phenomena (for example excavation, overload) altering stability conditions.

Predisposing factors may be:

- *Intrinsic factors*, deriving from geological and structural factors of a slope: type (rock, incoherent or cohesive soil) and status (weak, sensitive, weathered, or fissured) of the materials; in addition, presence of main joint systems or faults, layering, adversely oriented structural discontinuity, unconformity.
- *Geomorphological factors*, related to volcano-tectonic activities, erosional processes, slope angles, hydrographic network, vegetation removal (for example wildfire).
- *Physical factors*, deriving from intense and/or prolonged rainfall, rapid snow melt, earthquakes, volcanic eruptions, freeze-and-thaw weathering, which lead to a decreasing or annulment of hydro-mechanical properties of materials forming the slope.

- *Anthropic factors*, deriving from excavation of a slope, loading of a slope or of its crest, deforestation, irrigation, mining, artificial vibrations, which can determine hydrological and /or morphological modification.

Starting from one or more of these predisposing factors, slope instability can exist if triggering factors modify the equilibrium between resisting (shear strength) and driving (shear stresses) forces. The shear strength of rocks and soils usually derives from the sum of internal friction and cohesion in different ways, according to the conditions in which they are located. Rocky slopes rarely are homogeneous and massive because they are crossed by several discontinuity sets, stratification or other surfaces of weakness along which only shear strength to the friction angle exists. In materials whose shear strength is also due to cohesion, failure occurs along more or less regular concave surfaces (spoon shaped). Materials with shear strength deriving only from internal friction do not have a true failure surface, although characterized by a surface whose inclination angle coincides with the internal friction angle.

Water represents the most important factor for slopes instabilities involving ash-fall pyroclastic covers in peri-Vesuvian and Phlegraean area. In fact, saturated soils are affected by complex failure mechanisms during deformation including drained conditions (over-pore pressure conditions) or undrained conditions. In details, the influence of water content and pore water pressure on the stability of a slope strongly depends on the nature of the material forming the slope. For example, as regards cohesion degree of rocks or soft rocks, the water content variability has a minimal destabilizing effect limited to the dissolution of the matrix binding the particles. On the contrary, incoherent materials are strongly affected by water content, whose cohesion (apparent cohesion) degree is related to their initial conditions (Bear, 1979; Fredlund and Rahardjo, 1993; Öberg and Sällfors, 1997).

In detail, when water content is lower than saturation, voids among particles are not completely saturated and thin but tenacious film exists enveloping particles (capillary meniscuses) (Fig. 3.8) with a pore pressure lower than that of the atmosphere (suction). Fine-grained materials (sand, silt or clay) are characterized by small intergranular voids and then the water film holds together particles with electrostatic forces. This phenomenon, which controls the capillarity, strongly affects hydraulic conductivity (Bouwer, 1966; Ng and Shi, 1998) and shear strength of materials,

determining an adjunctive form of cohesion (apparent cohesion) existing only under unsaturated conditions (Fredlund et al., 1978).

In fact, an increase of the water content, up to complete saturation, causes the filling of voids between particles and then the gradual decrease or annulment of the apparent cohesion. For these reasons, considering modifications of soil hydro-mechanical properties due to external factors and water content variability, triggering of shallow landslides can be related to:

- Increase of shear stresses due to natural or anthropic factors;
- Cohesion degree and internal friction angle;
- Water content and pore-water pressure of soils whose variability affects the inherent shear strength.

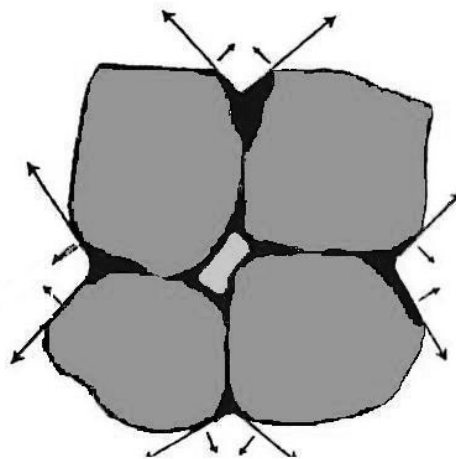


**Figure 3.8.** Schematic representation of capillary menisci, which create reciprocal attraction between grains and increase of effective stress. Arrows represent surface tension at the interface water-air.

### 3.2.2. Landslide classifications

Many landslides classifications were proposed in literature based fundamentally on type of mechanisms and involved materials.

Considering slope instabilities involving ash-fall pyroclastic covers mantling peri-Vesuvian and Phlegraean areas, the most relevant classifications, useful to describe such type of landslides, are listed below (Varnes, 1978; Pierson and Costa, 1987;

Hutchinson, 1988; Sassa, 1989; Cruden and Varnes, 1996; Hungr et al., 2001; Hungr et al., 2014).

Since not all the classifications are able to classify properly these type of landslides, also due for the progress in time to comprehend these slope instability phenomena, as well as in advancing mechanisms of flow-type landslides, following the basic features of the abovementioned classifications are described.

### **Pierson and Costa's classification (1987)**

Considering classifications based on the rheological behavior of materials involved in subaerial flow-like mass-movements that of Pierson and Costa (1987) can be applied to flow-type landslides affecting peri-Vesuvian and Phlegraean slopes. This classification was made considering velocity, ratio of mixtures between water and sediments and rheological behavior of fluids to an applied shear stress. The Authors suggest, in a two-dimensional matrix, three main thresholds forming four sediment concentration areas (Fig. 3.9) ranged between 0% (clear water) and 100% (dry sediment). The different flow-type phenomena proposed by this classification are:

- *Streamflows*:
  - *normal streamflows* (Newtonian flows with yield strength lower than 10 N/m<sup>2</sup>), defined as flowing water with transported sediments in concentration as small as to not affected the rheology of the fluid;
  - *hyperconcentrated streamflows* (non Newtonian flows with yield strength ranging between 10 and 20 N/m<sup>2</sup>), defined as flowing mixture of water and sediments with a measurable yield strength, which appear approximately flowing like a Newtonian fluid;
  - *Slurry flows* (Binghamian flows with yield strength greater than 20 N/m<sup>2</sup>), defined as as flowing mixture of sediment and water, the latter higher than liquid limit;
- *Granular flows*:
  - *viscous granular flows* (Binghamian flows), defined as flowing mixture of sediment, air and water liquefied by extreme stresses;
  - *inertial granular flow*, defined as sediments with low water content flowing for granular collisions.

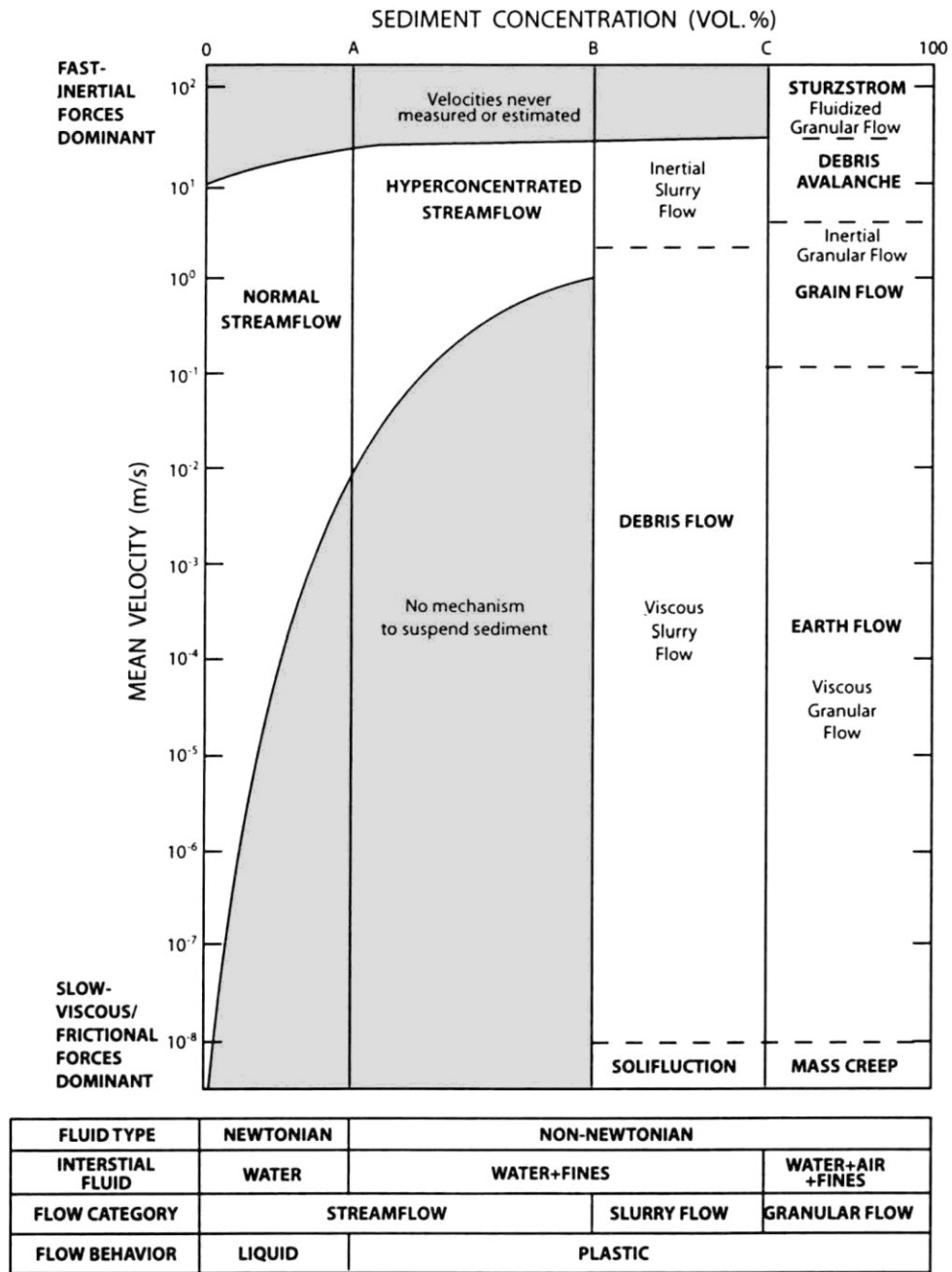


**Figure 3.9.** Scheme of rheologic classification of sediment-water flows (Pierson and Costa, 1987) (image from “<http://www.unomaha.edu>”)

Considering Pierson and Costa’s classification (1987), slope instabilities involving ash-fall pyroclastic soils in peri-Vesuvian and Phlegraean area, can be considered varying from “*viscous slurry flows*” to “*hyperconcentrated streamflows*”, according to concentration of sediments and the related yield strength.

### Hutchinson's classification (1988)

One of the main classifications of slope movements was carried out by Hutchinson (1988) based mainly on the morphology of slope movements which are strongly related to geological, morphological and hydrogeological aspects as well as geotechnical parameters of involved materials. In particular, morphological factors represent the most important parameter to recognize and classify a landslide. Among the main types of mass-movements (landslides) identified by the author, the following categories can be considered to classify the slope instabilities affecting pyroclastic soils of peri-Vesuvian and Phlegraean slopes:

A. *Landslides*, representing relatively rapid down-slope movements whose characteristically take place on one or more discrete bounding slip surfaces, which define the moving mass. Among this category a specific sub-classes can be identified:

- *Translational slide* (Fig. 3.10a), which involve shear failure on a fairly planar surface in downslope section, though often channel-shaped in cross section, usually running roughly parallel to the general slope of the ground. Their rate depth/length (D/L) (Skempton and Hutchinson, 1969) are typically 0.1 or less. Considering the involved materials (volcaniclastic deposits), in this sub-classes can be identified the *slide of debris*. The speed reached by the sliding and run-out degree tend to increase with slope angle. In particular, fall into this category:

1. *Debris slides*, characterized predominantly by translational movement, often rapid to very rapid, occurring commonly on slopes of about  $25 \div 45^\circ$ . They are characterized by low D/L ratios (often  $< 0.05$ ), high length to breadth (L/B) ratios (typically 5.0 to 10 or more), and are generally triggered by intense rainfall or by earthquakes.
2. *Debris avalanches* (Varnes, 1978) whose have a greater run-out and are regarded here a being a more rapid form of *debris slide*.

B. *Debris movements of flow-like form* (Fig. 3.10b-c-d) whose involve incoherent materials (*debris flows*). Among this category a specific sub-classes can be identified:

- *Flow slides* (Fig. 3.10b), characterized by a sudden collapse and extensive, very to extremely rapid run-out of a mass of debris following some disturbance. An essential feature is that the material involved has a metastable, loose or high porosity structure, which moves the overburden load wholly or partially onto the pore fluid, during the collapsing. The excess pressure leads to loss of strength and gives the falling material a semi-fluid character. Casagrande (1971) suggested for flow slides the terms *liquefaction slides*.
- *Debris flows* (Fig. 3.10c-d), characterized by very to extremely rapid flows of wet debris. This potentially very destructive form of slope movement is associated with mountainous areas, where a sudden access of water can mobilize debris mantling the slopes and incorporate it into a debris flow. An important mechanism in a debris flow is the generation of excess pore-fluid pressures by repeated undrained loading associated with their movements. At least two types of such loading exist, in addition to that of the liquefaction of loose debris, suggested by Sassa (1984): a) the undrained loading of a lower debris flow by fresh debris advancing over it; b) the repeated self-undrained loading of a single flow as a result of the mixing and upsetting of the fabric as it advances, so that the grains are thrown into suspension and pore-pressures approach geostatic values. In this sub-classes can be identified:
  1. *Hillslope debris flows* (Brundsen, 1979) whose form a single track down a valley side and debouch onto flatter ground at its foot where the channel may be slightly sinuous and levees are formed (Fig. 3.10c);
  2. *Channelized debris flows*, a more fully developed version of *hillslope debris flow* (Fig. 3.10d). They tend to occur on mountain slopes and generally follow the pre-existing stream courses. Speeds are reported to vary generally between about 3.0 and 12 m/sec (Campbell, 1975) though, exceptionally, speeds of 30 m/sec or more may be attained. As *debris flows* reach more gently inclined channels or debouch onto *debris fans*, they tend to decelerate, thin or spread out, but are often still capable of considerable further travel.

Based on the Hutchinson (1988) classification, landslide phenomena involving ash-fall pyroclastic deposits mantling peri-Vesuvian and Phlegraean slopes are characterized by “*slides of debris*”, “*debris slides*” or “*debris avalanches*” specifically, whose can evolve to “*debris movements of flow-like form*”, “*hillslope debris flows*” and/or “*channelized debris flows*” specifically. Field evidences in many detachment areas of initial *debris slide* allow to consider improbable the evolution of a “*slide of debris*” in a “*flowslide*” because static liquefaction of the involved material is required.

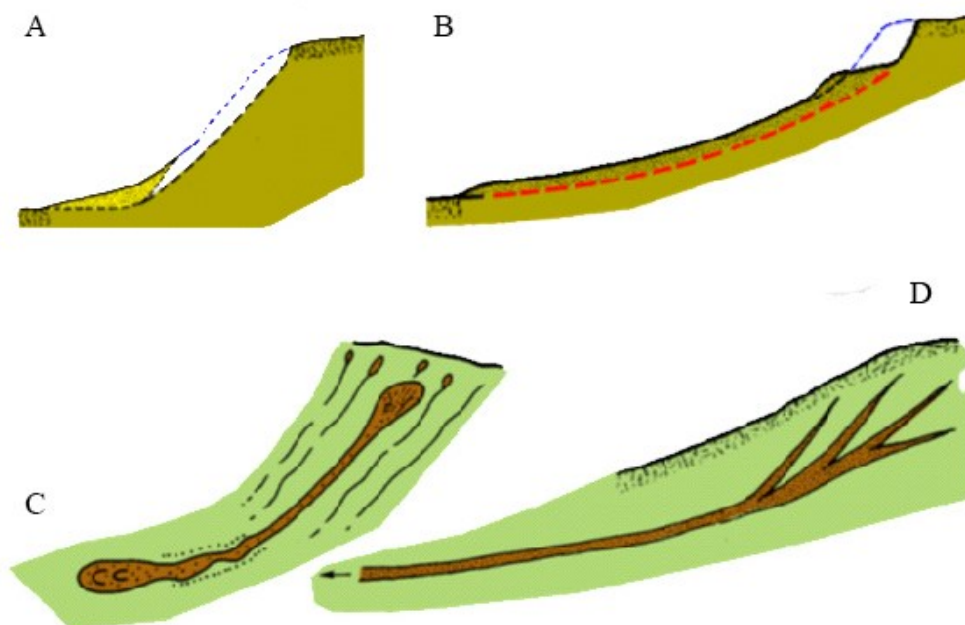


**Figure 3.10.** Types of mass-movements identified by the Hutchinson (1988) considered to classify the slope instabilities affecting pyroclastic soils of peri-Vesuvian and Phlegraean slopes: a) slide of debris; b) flowslide; c) hillslope debris flow; d) channelized debris flow.

### Sassa’s classification (1989)

Considering slope instabilities involving ash-fall pyroclastic mantle of peri-Vesuvian and Phlegraean slopes, Sassa’s classification (1989) is very useful to explain dynamics that trigger the initial landslide and then the final evolution to flow. This classification suggests three main types of landslides, considering geotechnical parameters:

- *Sliding*, when the increasing of pore water pressure may lead to a first detachment or a reactivation of a mass of materials (Fig. 3.11), following the

effective shear strength law (Terzaghi, 1943). This mechanism of instability can be related to both the reduction of the shear strength, caused by the increase of pore pressure and the inherent reduction of effective stress, and the increase of driving forces, due to downslope-oriented seepage pressure;

- *Liquefaction*, when saturated materials with low hydraulic conductivity values are affected by rapid dynamic stresses, causing the increasing of pore water pressure and then a reduction of effective strains. The final effect of this process is the reduction of the material shear strength, which will move downhill like a viscous flow;

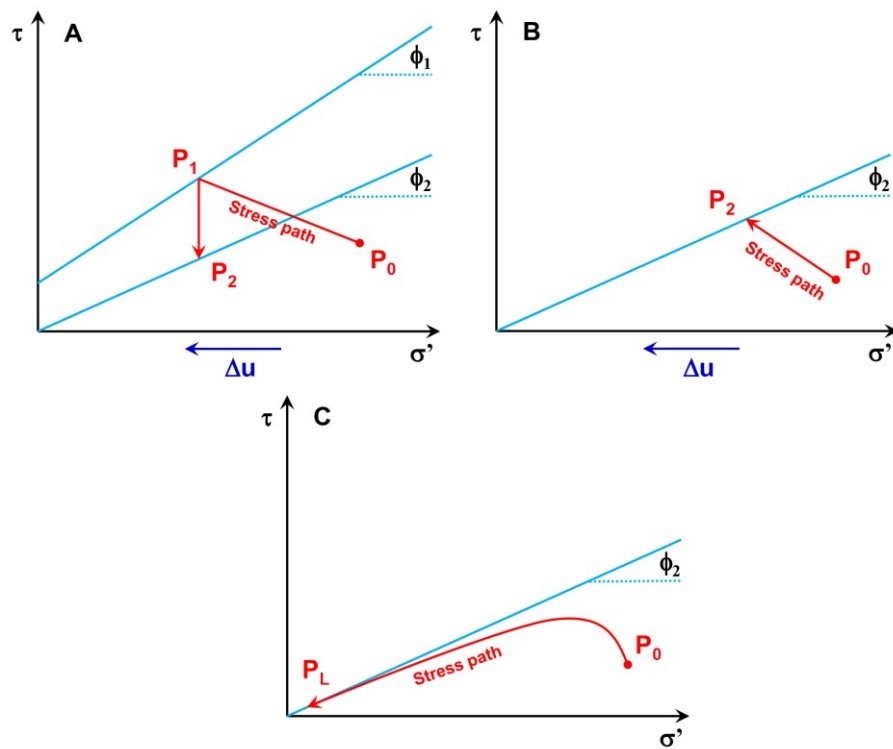


**Figure 3.11.** Graphs representing the effects of the pore water pressure variation leading to different types of instability conditions including a first detachment (A) or a reactivation (B) or liquefaction (C) of a mass of materials, following the effective strains law (Terzaghi, 1936): ( $\tau$ ) shear stress; ( $\sigma'$ ) effective strain; ( $\phi_1$ ) initial friction angle; ( $\phi_2$ ) residual friction angle; ( $\Delta u$ ) pore water pressure variation; ( $P_0$ ) initial condition; ( $P_1$ ) first detachment condition; ( $P_2$ ) reactivation condition; ( $P_L$ ) liquefaction condition.

Based on the dynamics suggested by this classification, slope instabilities that affect peri-Vesuvian and Phlegraean slopes mantled by ash-fall pyroclastic deposits are

characterized by initial *sliding* of material evolving in a *flow-type landslide* (Hutchinson, 1988) along the slope, due to a dynamic *liquefaction* mechanism.

### Cruden and Varnes's classification (1996)

The most used landslide classification is that of Cruden and Varnes (1996), deriving from an update of the previous Varnes's classification (1978), which considers both types of involved materials and movement or kinematism.

According to this classification, ash-fall pyroclastic soils affected by instability phenomena in peri-Vesuvian and Phlegraean area can be generally classified as “*debris*”, due to a gravel content greater than 20%, even if only in a very limited part involved materials cannot be excluded to belong to the “*earth*” class, due to a gravel content lower than 20%. Furthermore, involved material can be defined as “*wet*” or “*very wet*”, considering the other subdivision of the Authors based on the water content.

Considering different involved materials and type of kinematisms, Cruden and Varnes's classification (1996) suggest five main groups of landslides: *falls*, *topples*, *slides (translational and rotational)*, *spreads* and *flows*. In addition, the classification introduces seven velocity classes (based on a quantified scale) for each type of landslide, varying from *extremely slow* to *extremely rapid*.

Following nomenclature suggested by Cruden and Varnes's classification (1996) and considering the peculiar slope instabilities involving ash-fall pyroclastic soils in peri-Vesuvian and Phlegraean area, these landslides can be considered as “*complex phenomena*” characterized by a “*rapid, wet / very wet, debris slide*”, evolving to “*extremely rapid / rapid, wet / very wet, debris flow*” (Fig. 3.12).

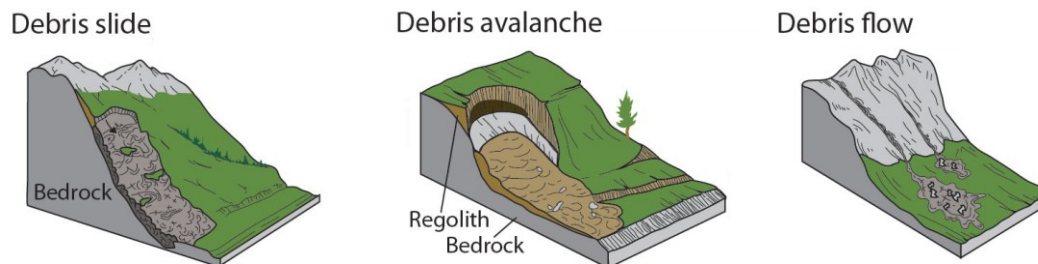


**Figure 3.12.** Types of landslides involving pyroclastic soils mantling peri-Vesuvian and Phlegraean slopes (Cruden and Varnes, 1996).

### Hungr et al. (2014) classification

Finally, it is necessary to mention a more recent and detailed classification of flow-type landslides that consider involved materials, water content, critical conditions and velocity of the landslide to get the formulation of a unique nomenclature for several landslides. Following this classification, which represent a reviewed version of Hungr et al. (2001) classification, the peculiar slope instabilities involving ash-fall pyroclastic soils in peri-Vesuvian and Phlegraean area can be identified as:

- A. *Debris slides*, characterized by slidings of a mass on a shallow, planar surface parallel with the ground over a stronger substrate. Many *debris slides* become *flow-like form* (Hutchinson, 1988) after moving a short distance and transform into extremely rapid *debris avalanches*.
- B. *Debris flowslides*, very rapid to extremely rapid flows of sorted or unsorted saturated granular material on moderate slopes, involving excess pore-pressure or liquefaction of material originating from the landslide source. The occurrence of liquefaction flowsliding is constrained to a certain, narrowly defined group of “liquefiable” materials, including ash-fall pyroclastic soils (Picarelli et al., 2008), forming a significant part of the source volume. However, as specified by the Author, earthquake and spontaneous liquefaction should be clearly separated from the processes of rapid, undrained loading, mixing, and dilution, which play a dominant role in *debris flows* and *debris avalanches*. During the undrained loading process, a sudden increase of total stress in a saturated (or nearly saturated) soil increases the pore pressure while the effective stress remains at a constant low value (e.g., Hutchinson and Bhandari, 1971; Sassa, 1985). In contrast, during liquefaction the total stress remains constant, but the effective stress is reduced by structural collapse (e.g., Lefebvre, 1995; Eden and Mitchell, 1970; Picarelli et al., 2008). Rapid undrained loading can affect all materials, even if less than 100 % saturated and is therefore controlled more by the process than by material character.
- C. *Debris flows*, very rapid to extremely rapid flows of saturated debris in a steep channel, which cause entrainment of material and water from the flow path. As described by the Author, the flow may be initiated by a slide, debris avalanche or rock fall from a steep bank, or by spontaneous instability of the steep streambed. Once material begins to move in a steep channel, the bed becomes

subject to rapid undrained loading, often so sudden that it could be characterized as impact loading (Sassa 1985). Under such conditions, even coarse material can liquefy, or at least suffer a significant increase in pore-pressure. The bulk of the material involved in a *debris flow* event usually originates from entrainment from the path, while the volume of the initiating slide is insignificant. The magnitude of *debris flows* therefore depends primarily on the characteristics of the channel and can be estimated by empirical means (Hungr et al., 2005). As a result of channelization, a *debris flow* grows and becomes fronted either by a boulder concentration (e.g., Pierson, 1986) or a turbulent “head” (Davies, 1986). Periodic damming and release may occur, contributing to flow growth.

- D. *Debris avalanches*, very rapid to extremely rapid shallow flows of partially or fully saturated debris on a steep slope, without confinement in an established channel. As described by the Author, in contrast to a *debris flow*, a *debris avalanche* is a unique event that can be found anywhere on steep slopes. In many cases, *debris avalanches* enter established channels, de-stabilize channel infills, and become *debris flows*. *Debris avalanches* initiate as *debris slides* and are associated with failures of pyroclastic covers. In some cases, it is difficult to make distinction between *debris avalanches* and *flowslides*. Cohesion loss, spontaneous liquefaction, and undrained loading can all occur simultaneously in a landslide on a steep slope. However, the Author suggested that the term *flowslide* must be reserved for failures where spontaneous or earthquake liquefaction is clearly the dominant mechanism. The rapid undrained loading process also allows *debris avalanches* to be triggered by impact from rock fall or rock slide on soil-covered slopes (e.g., Lacerda, 2007). Once initiated, rapid undrained loading continues progressively as material moves down the slope, increase the mass from few tens of cubic meters to many thousands.

In this way, slope instabilities involving pyroclastic soils mantling peri-Vesuvian and Phlegraean slopes can be identified as “*debris slides*” whose can trigger “*debris avalanches*” and/or “*debris flows*”. “*Debris flowslides*” is not the correct term to indicate these debris flows, because the rapid undrained loading processes play a dominant role in *debris flows* and *debris avalanches* occurrence (Hungr et al., 2014),

causing the liquefaction of the involved materials, more than the spontaneous liquefaction, suggested by other Authors (Picarelli et al., 2008). The presence of clear and defined failure surfaces whose characterize many detachment areas of initial slides may confirm this suggestion.

### **3.2.3. Hydrological threshold conditions leading to landslide triggering**

The assessment of hydrological threshold conditions triggering landslides has become an increasingly challenging topic of research (Campbell, 1975; De Vita and Piscopo, 2002), because rainfall thresholds are suitable for use in early warning systems (Guzzetti et al., 2007; 2008; Baum and Godt, 2010) as well as for assessing landslide temporal probability, by linking rainfall threshold values to statistical hydrological analyses (Glade and Crozier, 1996; Glade, 1998).

The identification of rainfall thresholds has been chiefly based on empirical approaches focused on identifying a rainfall event preceding the landslide, which is considered a primary climatic factor (Wieczorek and Glade, 2005) that controls the slope instability. Therefore, by the graphical or statistical analysis of rainfall events that triggered (or did not trigger) landslides, a rainfall threshold can be defined as the minimum rainfall amount that likely can trigger a landslide. In such a view, a rainfall event is supposed to modify an antecedent stability condition of a slope up to the onset of instability by exceeding a threshold value (White et al., 1996). A triggering rainfall event can be measured by means of up to 25 rainfall and climate variables (e.g. intensity, total precipitation height, etc.; Wieczorek and Glade, 2005; Guzzetti et al., 2007). The event can be identified at very different time scales (from minutes to several days), depending on permeability of materials involved in the slope instability, seasonal control and landslide dimensions (Peruccacci et al., 2012).

The more direct connection between the occurrence of rainfall events and shallow landslides, depending on the relatively limited complexity of hydrological processes as well as of physical systems involved in the slope instability, has favored the development of rainfall thresholds for shallow landslides more than for deep-seated ones (Guzzetti et al., 2007; Peruccacci et al., 2012). Depending on the extent of the analyzed areas, rainfall thresholds for triggering landslides can vary across local,

regional and global scales (Guzzetti et al., 2007 and references therein). Considering the uncertainty related to the identification of a sequence of rainfall events responsible for causing landslide triggering, an automated procedure based on objective criteria was proposed to select the triggering sequence in a rainfall time series (Melillo et al., 2014; Vessia et al., 2014). A rainfall threshold value is often related to rainfall data collected at considerable distance from the source zones; therefore, owing to spatial variability of short duration/high intensity events, the reliability of these thresholds might be questionable. In addition, empirical rainfall thresholds are affected by uncertainties due to several secondary factors such as spatial variability of hydraulic and mechanical soil properties, and different antecedent-hydrological conditions. Such types of uncertainties were found to increase for landslide-triggering rainfall events of shorter duration (Nikolopoulos et al., 2014).

Different empirical approaches have been proposed to assess rainfall thresholds for triggering landslides, according to different characterizations of critical rainfall events, which have been related mainly to the cumulative rainfall depth, duration and intensity. Besides the empirical ones, other types of hydrological thresholds have been proposed, which were based on a physical-conceptual modelling of hillslope hydrological processes (e.g. Wilson, 1989; Crosta and Frattini, 2003) and on deterministic approaches, namely taking into account complete hydro-mechanical stability modelling of a slope (e.g. Terlien, 1998; Godt et al., 2008; De Vita et al., 2013; Peres and Cancelliere, 2014; Napolitano et al., 2015, 2016; Tufano et al., 2016).

Several attempts to set hydrological thresholds also considering antecedent-hydrological conditions have been carried out, because the latter were conceived as secondary climatic factors (Wieczorek and Glade, 2005) with an indirect effect on the slope stability during triggering rainfall events. Such antecedent-hydrological conditions, accounting for the variable status of pore pressures inside the potentially unstable slope materials (Wieczorek, 1996), actually control the effects of the same rainfall event on the slope stability, thus influencing the threshold value itself. Conceptually, the antecedent-hydrological conditions predispose a slope to instability, while the rainfall event that directly precedes the landslide occurrence determines the slope instability. Nevertheless, the effects of antecedent-hydrological conditions depend on saturated/unsaturated hydraulic properties of the involved materials and on slope-boundary conditions. This control has been demonstrated by negligible effects of antecedent soil moisture observed in triggering shallow landslides in Hong Kong

(Brand et al., 1984) and in the Pyrenees (Corominas and Moya, 1999), where surficial permeability is high due to large macropores and specific water retention is low.

Various methods have been proposed to take into account antecedent-hydrological conditions, which have ranged from the recognition of a seasonal antecedent rainfall needed to trigger debris flows during intense rainstorms (Campbell, 1975; Wieczorek, 1987; Wieczorek and Sarmiento, 1988), to the identification of a rainfall amount cumulated over a long time span preceding the landslide and in assessing the seasonal effect on it (Govi et al., 1985; Cardinali et al., 2006), to the adaptation of the intensity-duration model (Caine, 1980) considering different seasonal conditions (Govi et al., 1985). Antecedent-hydrological conditions were also recognized to control the debris flow magnitude (Wieczorek and Glade 2005; Baum and Godt, 2010).

Other types of thresholds were based on the combined analysis of triggering rainfall, occurring in a period strictly preceding the landslide onset, and rainfall accumulating in a more antecedent period. Following this approach, a first attempt (Crozier and Eyles, 1980) considered a combination of the rainfall on the day of the landslide occurrence (critical) and the rainfall in the preceding day (predisposing), but more articulated combinations of time periods with different durations were tested in different areas of the world (Kim et al., 1991; Crozier, 1997; Terlien, 1998; Pasuto and Silvano, 1998; Chleborad, 2003; Aleotti, 2004; Gabet et al., 2004). In these attempts a strong influence of the antecedent precipitation, as well as of the seasonal control on rainfall amount preceding the landslide occurrence, was discovered. The antecedent rainfall was estimated over very different time spans, varying from a few days to months, in relationship to the geological, geomorphological, and climatic frameworks. For example, Chleborad (2003) identified a rainfall threshold by combining the 3-day rainfall directly preceding the landslide occurrence and the cumulative rainfall for the 15-day period before the 3-day event rainfall.

Other researchers have taken into account antecedent rainfall by developing algorithms that simulate conceptually infiltration, drainage, and soil moisture storage into the regolith cover. The Antecedent Water Status Model (AWSM), proposed by Crozier (1999) to develop a landslide-triggering threshold for Wellington, New Zealand, was conceived as an index for expressing a daily water budget of the soil mantle, which considers a drainage factor for rainfall exceeding specific water retention in the antecedent ten days. By considering landslide occurrences, this index was combined with the daily rainfall identifying a threshold value. Afterwards, an

Antecedent Water Index (AWI) was proposed (Godt et al., 2006) for the Seattle, Washington area, USA. The AWI was based on the assessment of the antecedent soil moisture conditions by a water balance and to its combination with a rainfall intensity-duration empirical threshold by a decision tree.

Regarding the debris flows involving the ash-fall pyroclastic soil-mantled slopes of Campania region, a relevant effect of the antecedent conditions was found by an empirical approach based on the combination of the critical rainfall in the day of the landslide occurrence with cumulative antecedent rainfall from the day preceding the landslide up to 5, 10, 20, 40 and 60 preceding days (De Vita, 2000; De Vita and Piscopo, 2002). By this empirical approach, the threshold values of the daily rainfall needed to trigger a landslide was found to decrease, from 110 mm to a minimum of 50 mm, depending, respectively, on the cumulative antecedent rainfall, separately varying from 0 to about 200 mm. Other authors (Fiorillo and Wilson, 2004) by applying the process-based approach of the “leaky barrel” model (Wilson, 1989) also demonstrated a dependence of the rainfall threshold value on the antecedent-moisture conditions existing in the soil column as well as by the ratio between rainfall intensity and drainage capability. Recently, Greco et al. (2013) proposed a one-dimensional hydrological model of a pyroclastic multi-layered soil mantled slope in the Cervinara area (Campania region), simplified as a single homogeneous soil layer. The authors demonstrated that the maximum variation of pore-water pressure gradient occurs during the warm season, due to the fluctuation of water table in the underlying limestone bedrock.

Finally, this research project expands results of previous experience (De Vita et al., 2013), which estimated intensity-duration (I-D) rainfall thresholds, through a deterministic approach, by focusing the effect of antecedent-hydrological conditions on critical rainfall that triggers initial landslides. Coupling hydrological monitoring and modeling (Fusco et al., 2013; Fusco and De Vita, 2015), these thresholds (Napolitano et al., 2015; 2016; Tufano et al., 2016) were obtained starting from physically-based models considered representative of test sites in Sarno Mountains area where the May 1998 landslide event occurred.

# Chapter 4

## Landslide involving ash-fall pyroclastic soil mantled slopes of the peri-Vesuvian and Phlegraean areas

The urbanized foothill areas along carbonate mountain ridges, bordering the Campanian plain, and Phlegraean Fields slopes are among the most landslide-prone areas of Italy (Figs. 4.1 and 4.2). Urban centers have been subjected to repeated occurrences of rainfall-induced shallow landslides, which represent a well-known geohazard. Since their deposition, landsliding and other denudation processes affected these deposits along mountain slopes. Nevertheless, relevant pyroclastic soil thicknesses still exist as well as a high continuous or residual hazard to debris flows triggering under heavy and/or prolonged rainfall events.

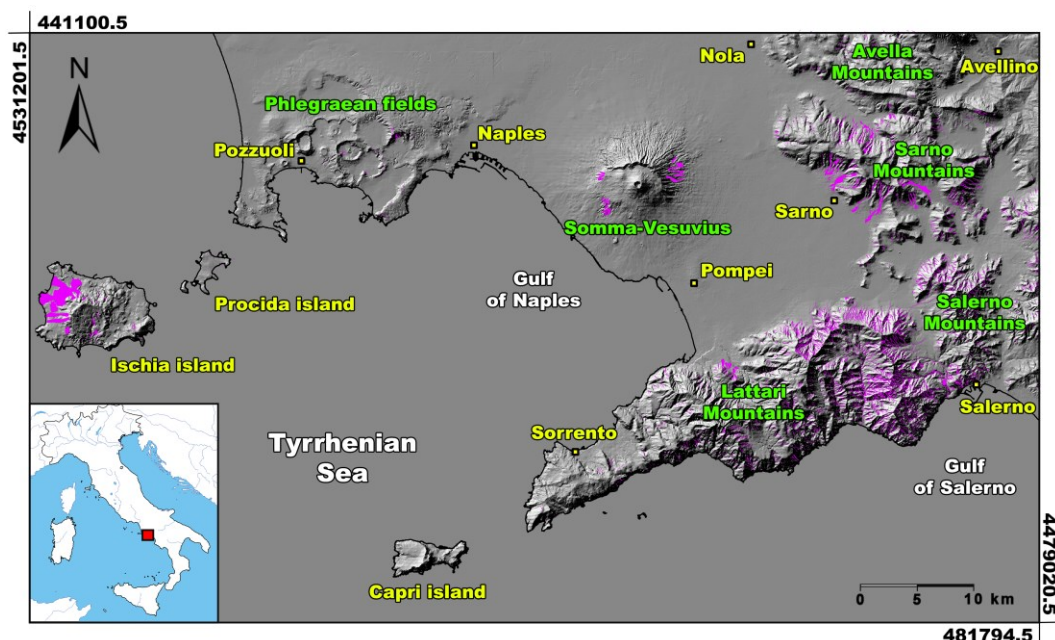


**Figure 4.1.** Recent flow-type landslide events (in violet) occurred in peri-Vesuvian and Phlegraean areas (landslides database from Campania Centrale Basin Authority, now including previous of Sarno, Nord-Occidentale and Destra Sele Basin Authorities).

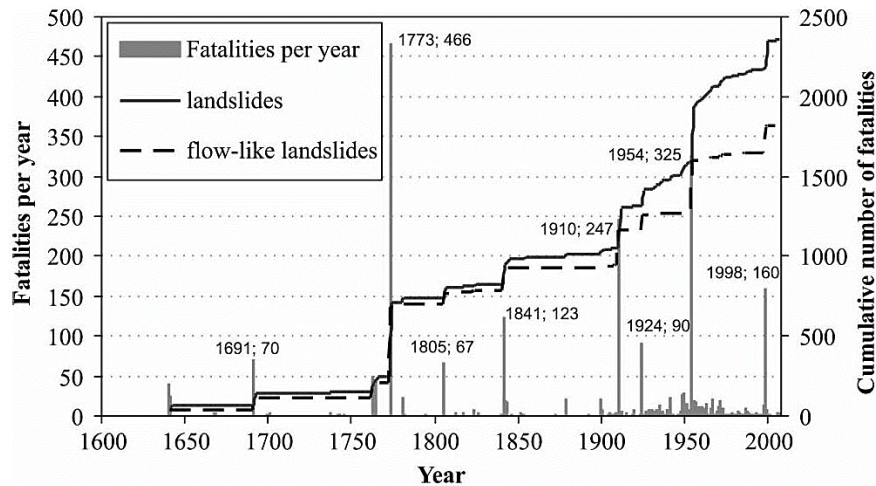


**Figure 4.2.** Histogram of fatalities per year caused by landslides and specifically by flow-type landslides in Campania region (Southern Italy) and their cumulative curves for the period 1640 ÷ 2006 (from Cascini et al. 2008).

Considering both peri-Vesuvian and Phlegraean slopes, several studies demonstrated that the spatial variability of pyroclastic soils thickness, slope angle and morphological discontinuities along the slopes, such as knick-points, abrupt increases of slope angle related to bedrock outcrops and artificial road-cuts, play an important role to rise locally the susceptibility to landslide triggering. In particular, Sarno and Lattari mountain ranges are characterized by peculiar hazardous geomorphological conditions due to the highest thicknesses of ash-fall pyroclastic deposits derived from the Somma-Vesuvius volcano (De Vita et al., 2006a), whose distance from the volcano is variable between 12 and 25 km.

## 4.1 Principal case histories

The high debris flows hazard of peri-Vesuvian and Phlegraean areas is well testified by the number of deadly debris flow events known from historical chronicles (literary works, paintings and documents) since the 17<sup>th</sup> and especially for the 20<sup>th</sup> centuries, as easily recognized in the State Archives, in the CNR archives and the AVI Project (Guzzetti et al., 1994). Historical reports described catastrophic flow-type landslide events that strongly affected respectively the towns of Maiori and Atrani (Lattari Mountains), in 1540, of Quindici (Sarno Mountains), in October 25<sup>th</sup> 1640 (Calcaterra

et al, 2003; Cascini et al., 2008), and of Gragnano on 1841 (Fig. 4.3) located in the foothill of Monte Pendolo (Salerno Mountains; Mele and Del Prete, 1999).

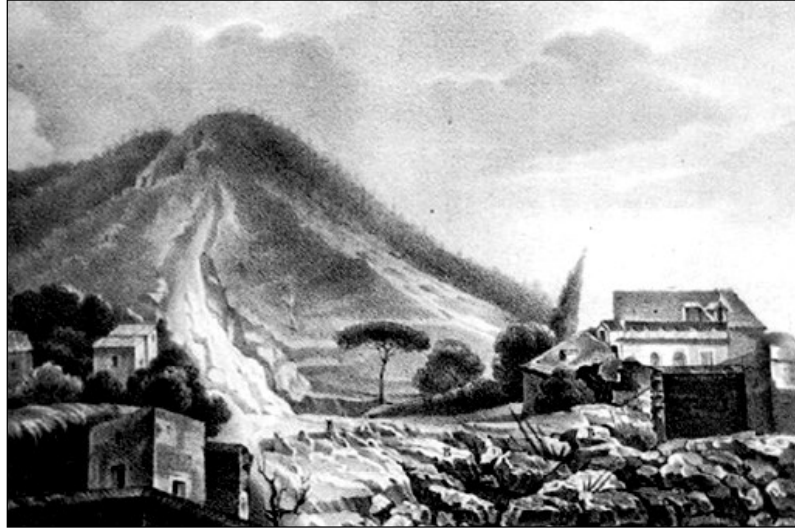


**Figure 4.3.** The historical painting representing the Monte Pendolo 1841 debris flow event, which affected the town of Gragnano (Salerno, Italy) (modified from Mele and Del Prete, 1999).

Among the most catastrophic landslide areal events involving pyroclastic soils of peri-Vesuvian slopes, those occurred on the 9<sup>th</sup> of October 1910 and on the 24<sup>th</sup> and 25<sup>th</sup> of October 1954 in the Lattari and Salerno Mountains area (Fig. 4.4) are to be considered. Heavy and long prolonged rainfall event triggered hundreds of debris flows along the Salerno Coast, which affected several towns (Vietri, Salerno, Cetara, Maiori and Amalfi) causing 150 and 318 casualties (Esposito et al., 2004) respectively. During the extreme rainfall conditions of October 1910, relevant slope instabilities also occurred on the Ischia Island, affecting the Casamicciola town (15 casualties), and the Somma-Vesuvius slopes. Besides the two previous main events, several smaller deadly debris flow events occurred in the Phlegraean Fields and, mostly, in the peri-Vesuvian area: the 1935 and 1963 events, which affected the western slope of the Monte Pendolo; the 23<sup>th</sup> of November 1966 which occurred in the Vico Equense municipality and caused three casualties; the 1971 event which affected the north-western slope of the Monte Pendolo with six casualties; the 16<sup>th</sup> of February 1973 event occurred along slopes of the Mount San Costanzo (Massa Lubrense, Lattari Mountains) causing 10 casualties; the 22<sup>th</sup> of February 1986 event occurred in Palma Campania (Sarno Mountains) with eight casualties; the 10<sup>th</sup> of

January 1997 event which hit Pozzano (Lattari Mountains) causing four casualties (Calcaterra and Santo, 2004); the January 1997 event which affected southern slopes of the Camaldoli hill (Naples) (Calcaterra and Guarino, 1999).



**Figure 4.4.** Morphological aspects and effects of main debris flow events occurred during 20th century (photos from web): Salerno coast (G, H) and Ischia Island (D, E) on October 24<sup>th</sup> and 25<sup>th</sup> 1910; Salerno Coast on October (A, B, C, F) 9<sup>th</sup> 1954; Palma Campania (I), on February 22<sup>th</sup> 1986; Pozzano (L), on January 10<sup>th</sup> 1997; Mount San Costanzo (M), on February 16<sup>th</sup> 1973.

Considered as the most documented catastrophic debris flow event, that occurred in the Sarno Mountains on the 5<sup>th</sup> and 6<sup>th</sup> of May 1998 represents a key point for the national and international scientific community, because, after this event many studies were focused on a better understanding of predisposing and triggering factors, kinematics and rheology of these flow-type landslides.

In detail, on 5<sup>th</sup> and 6<sup>th</sup> May 1998 after heavy and prolonged rainfall, several landslides (more than one hundreds) involved ash-fall pyroclastic cover mantling Sarno Mountains slopes (Fig. 4.5). The towns of Sarno, Bracigliano, Siano, Quindici and Moschiano were reached and strongly affected by massive debris flows, which caused the loss of 160 lives (Del Prete et al., 1998; Guadagno and Celico, 1998) and damaged or destroyed everything along their paths, due the their high destructive power. In addition, the town of San Felice a Canello (Caserta, southern Italy) was also hit by a minor debris flows event.

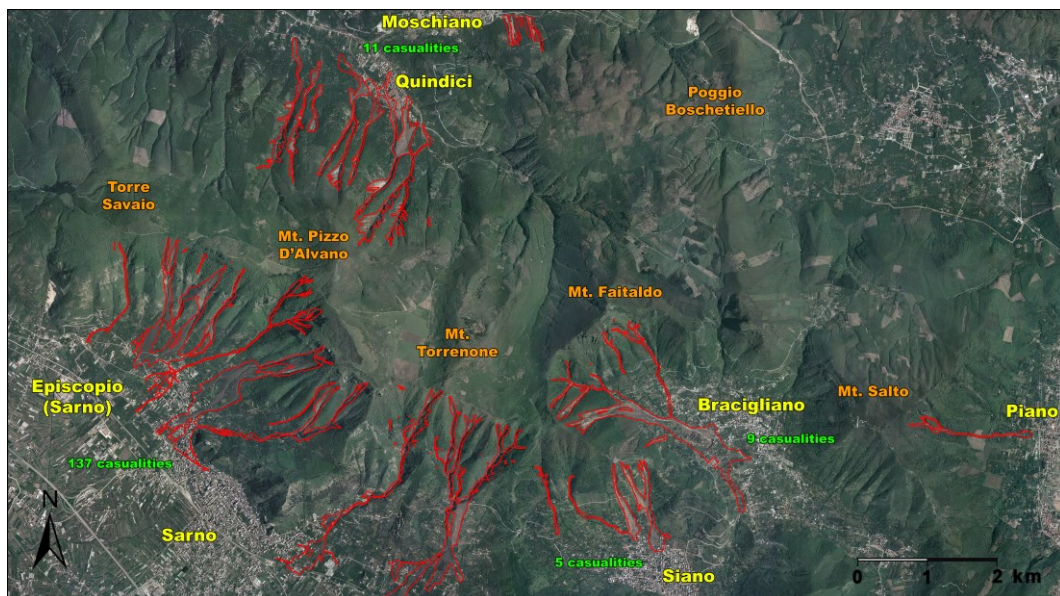


**Figure 4.5.** Debris flow event occurred on the 5<sup>th</sup> and 6<sup>th</sup> of May 1998, which affected many towns at the foothill of the Sarno Mountains.

Following this episode, further smaller events can be listed (Fig. 4.6): the San Martino Valle Caudina (Avella Mountains) event, occurred on the 15<sup>th</sup> and 16<sup>th</sup> of December 1999 with six casualties; the Nocera Inferiore (Lattari Mountains) and Camaldoli hill event, on the 4<sup>th</sup> and 5<sup>th</sup> of March 2005 that caused three and no casualties respectively; the Monte di Vezi (Ischia Island) event, occurred on the 30<sup>th</sup>

of April 2006 causing four casualties; the Casamicciola (Ischia Island) event, affecting the Monte Epomeo slope on the 10<sup>th</sup> of November 2009 causing one casualty; the Atrani (Lattari Mountains) event, occurred on the 9<sup>th</sup> and 10<sup>th</sup> of September 2010, which caused one casualty.



**Figure 4.6.** Evidence and effects of some debris flow events occurred in peri-Vesuvian and Phlegraean areas after the Sarno landslide event occurred on the 5<sup>th</sup> and 6<sup>th</sup> of May 1998: (A) Camaldoli hill event (March 4<sup>th</sup> and 5<sup>th</sup>, 2005); (B) Monte di Vezzi event (November 10<sup>th</sup>, 2009); (C) Nocera Inferiore event (March 4<sup>th</sup> and 5<sup>th</sup>, 2005).

## 4.2. Landslide kinematics and rheological behavior

Slope instabilities that involve ash-fall pyroclastic coverings mantling peri-Vesuvian and Phlegraean slopes are among the natural phenomena that represent the greatest source of risk for the population that lives in the foothill areas of these part of the Campania region. Due to their catastrophic and complex behaviour, the scientific community focused several studies on the comprehension of these landslides by using different approaches.

Debris flows involving ash-fall pyroclastic soil covers are the last evolutionary stage of complex landslides (Cruden and Varnes, 1996), which are characterized by up to three fundamental consecutive evolutionary phases (Fig. 4.7): (1) initial *debris slides* (Cruden and Varnes, 1996) or *soil slips* (Campbell, 1975), involving few tens or hundreds of cubic meters of ash-fall pyroclastic soils (debris, with more than 20% of gravel); (2) *debris avalanches* (Hungr et al., 2001), involving progressively greater volumes of pyroclastic deposits along open slopes by a dynamic liquefaction mechanism; (3) *debris flows* (Hungr et al., 2001), characterized by the channeling into the hydrographic network of rapid to very rapid flow-like debris masses. An initial small landslide always exists even if it may evolve directly into a channeled flow (*debris flow*) or stop its downslope movement and to not progress in the other stages, according to the local unfavorable morphological conditions. It follows that these flow-like landslides, in the intermediate (*debris avalanche*) and final (*debris flow*) stages, when they assume a typical rheology of a fluid, are always triggered by a small initial landslide (*debris slide - soil slip*). For this reason, they can be defined as *landslide-triggered debris flows* (Jakob and Hungr, 2005).

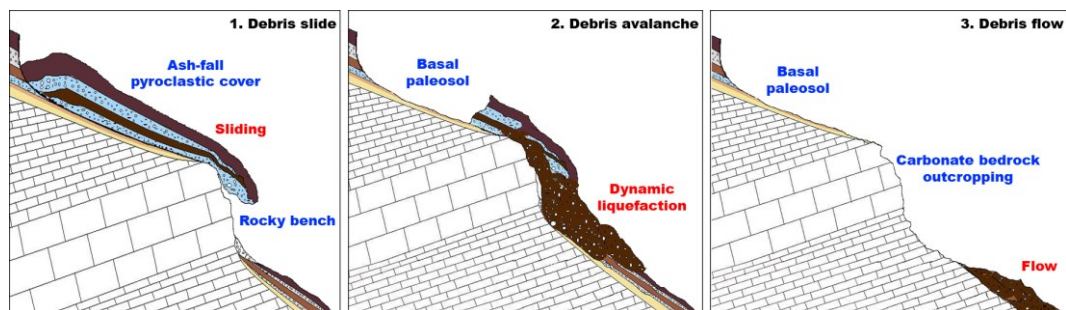


**Figure 4.7.** Three fundamental consecutive evolutionary phases which characterize debris flows involving ash-fall pyroclastic soil covers: 1) initial *debris slide*; 2) *debris avalanche*; 3) *debris flow*.

Such as for subaerial flow phenomena, also flow landslides are characterized by a viscous rheologic behaviour, which represents the frictional and cohesive resistance of the soil mass against the flow, which is inversely proportional to the water content. As regards the Newtonian flows, those fluvial for example, deformation is directly proportional to the applied shear strength. Instead, considering soil-water mixtures, such as those forming *debris flows*, the rheologic behavior is of Bingham type because the mixture can flow only if the applied shear stress exceeds a threshold value (Fig. 4.8).

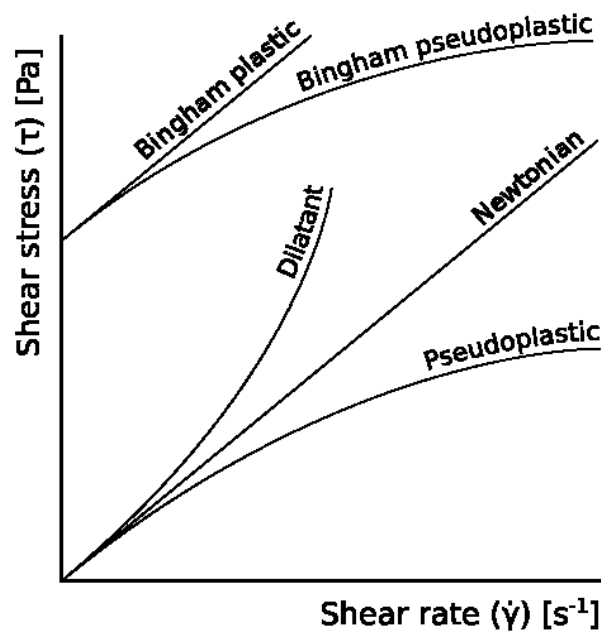
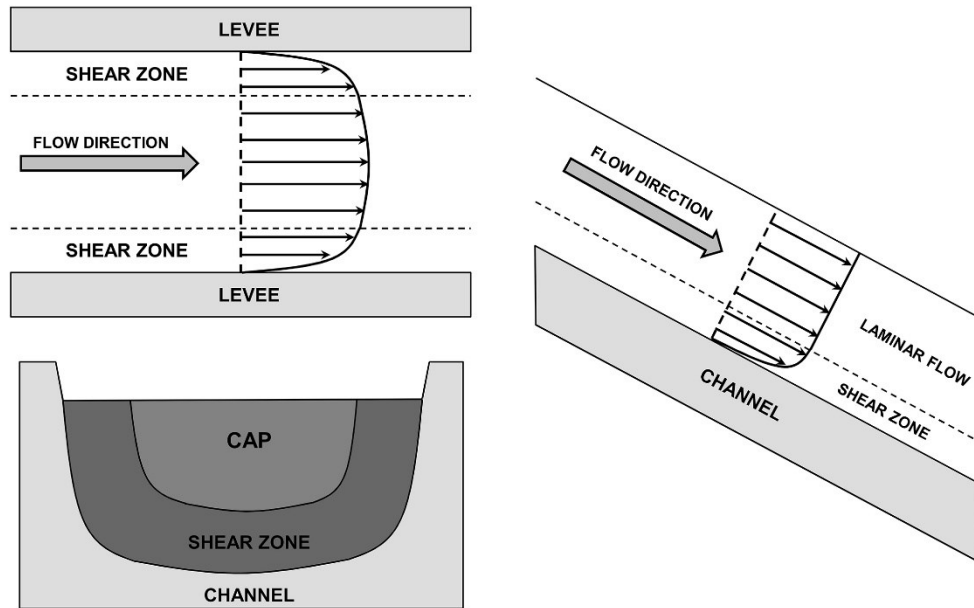


Figure 4.8. Rheological behavior of Bingham and Newtonian flows.

Therefore, the capability of a material to generate a flow phenomenon depends on *viscosity* and the applied *shear strength*, which define the threshold value for the flow movement. As regards debris flow phenomena, if the slope or channel angle is lower than the friction angle of involved material, the landslide does not evolve in a flow.

A Bingham flow in section (Fig. 4.9) shows a different velocity of the flow characterized by constant values in the middle part (*laminar flow*) and gradually lower close to the border (*shear zone*), where high shear strength values exist, allowing liquefaction of the involved material and flow core advancing (*cap*).



**Figure 4.9.** Schematic cross-sections of a Bingham flow showing differential velocity (thin black arrows) of the flow, which is characterized by constant values in the middle part (*laminar flow*) and gradually lower close to the border (*shear zone*). The latter zone is characterized by liquefaction processes of the involved material, which allow flow core (*cap*) advancing.

The velocity ( $V$ ) of a debris flow [Eq. 4.1] can be defined considering levees created close to channel bend areas by the flow (Fig. 4.10; Revellino et al., 2003 and therein):

$$V = (r_c \times g \times \cos\beta \times \tan\delta)^{0.5} \quad [4.1]$$

where:

$r_c$  = curvature radius of the channel levee;

$g$  = gravity acceleration;

$\beta$  = inclination of channel;

$\tan\delta = \Delta h/W$ ;

$\Delta h$  = difference between the height of the levees;

$W$  = width of the channel.

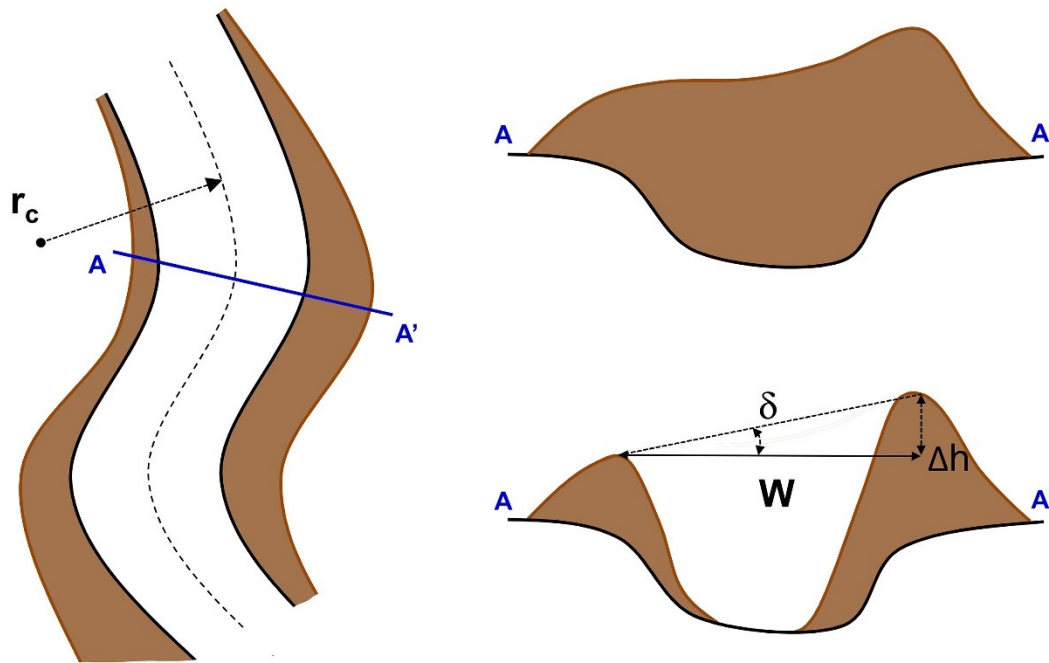


**Figure 4.10.** Schematic section of debris flow levees formed close to the channel bend areas whose morphology allows to estimate flow velocity in that area (Revellino et al., 2003 and therein): ( $r_c$ ) curvature radius of the channel levee; ( $\Delta h$ ) difference between the height of the levees; ( $W$ ) width of the channel; ( $\delta$ )  $\Delta h/W$ .

### 4.3. The role of geomorphological factors to landslide susceptibility

Flow-type landslides mostly affect steepest peri-Vesuvian and Phlegraean slopes covered by ash-fall pyroclastic covers, which have slope angles usually ranging from  $30^\circ$  to up to  $90^\circ$ .

The role of geomorphological factors is fundamental for landslides triggering and kinematics. In fact, this kind of debris flows, activated by intense and/or prolonged rainfall events, are characterized by high velocity (15-20 m/s; Calcaterra et al., 2000; 2003), high destructive power and occur without easily recognizable precursors. In addition, related to the slope morphology, they may develop on regular slopes without incisions, where unchannelled landslides take place, and along slopes close to torrential heads, where channelled landslides may develop (Di Crescenzo and Santo 2005).

Previous works, after the Sarno landslide event of the 5<sup>th</sup> and 6<sup>th</sup> of May 1998, were focused to investigate the role played by morphological and stratigraphic triggering factors of the initial slides and all the evolutionary phases (Celico and Guadagno, 1998; Calcaterra et al., 2003; Crosta and Dal Negro, 2003; Calcaterra and Santo, 2004; Di Crescenzo and Santo, 2005; Guadagno et al., 2005).

The Phlegraean district and the Campanian Apennine chain, the latter well represented by the Sorrento Peninsula and in the chain areas extending over the territories of Naples, Avellino, Salerno and Benevento provinces, are susceptible to two kinds of complex landslides, characterized by the same initial movement (*initial slide*). Typically, where high-angle and open slopes exist, the *avalanches* phase represent the second evolutionary stage while, on the contrary, if the initial mobilized mass is forced to converge in the existing steep valleys, channelled *debris-flows* may occur (Calcaterra et al., 2003).

More in detail, instability phenomena affecting Phlaegraean slopes involve shallowest soils covering volcanoclastic series, approximately 0.5 - 1.0 m thick, and detachment areas (initial *soil slip*) have slope angles ranging between 25° and 70° (Calcaterra et al., 2007a). Usually, the initial *soil slips* occurring on open slopes and within the valleys, whose characterize Phlaegraean slopes, not evolve to rapid *flows*. However, during heavy rainstorms, debris stored within the deep and narrow valleys can be mobilized as *hyperconcentrated streamflows* (Calcaterra et al., 2007a).

As regards flow-type landslide involving the ash-fall pyroclastic cover, mantling peri-Vesuvian carbonate slopes, detachment areas (initial *debris slide*) are localized close to high slope angles ranging from 35° to 45°.

In detail, natural and/or artificial breaks of the ash-fall pyroclastic cover, including road cuts or rocky benches (Celico and Guadagno, 1998; Di Crescenzo and Santo, 2005), and local stratigraphic settings, including thickness decrease due to knickpoints (De Vita et al., 2013), may cause slope instability (Fig. 4.11). Furthermore, hydrogeological conditions that, even though influencing only a minority of cases, emphasize the important role of groundwater outlet from the bedrock in the triggering mechanisms at the natural scarps, bedrock joints, or karst cavities.

As shown by field evidence of the slide surfaces in the detachment areas, initial *debris slides* start as small rotational slides (Calcaterra and Santo, 2004; Guadagno et al., 2005; Guadagno and Revellino, 2005). The initial landslide mass can stop (*aborted debris slide*) or continue along the slope if favored by the previous mentioned

local geomorphological and stratigraphic conditions. If the initial *debris slide* mass impacts on the volcanoclastic deposits downslope the cover break, the *avalanche* and/or *flow* phases may occur (Fig. 4.11) due to dynamic liquefaction. However, in some cases no morphological separation between the detachment area and the *avalanche/flow* zone exists and then it is not always easy to make a clear distinction (Di Crescenzo and Santo, 2005).

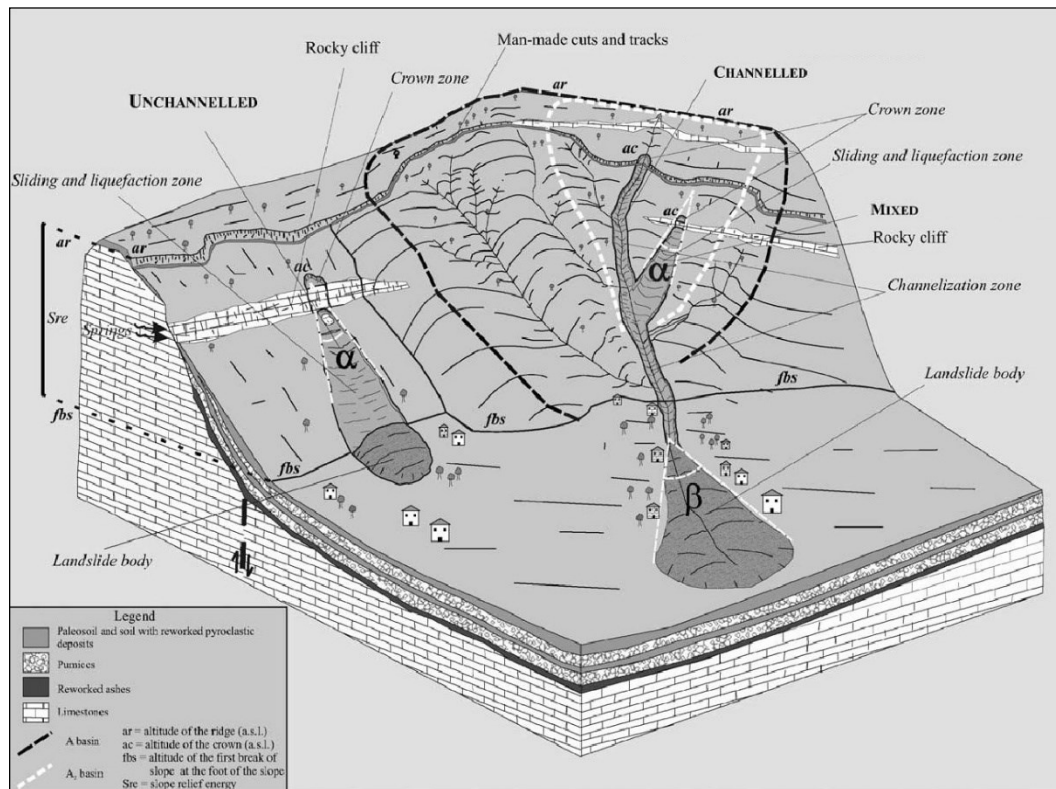


**Figure 4.11.** Scheme of the main morphological and morphometric parameters of landslides occurred in the Sarno Mountains on the 5<sup>th</sup> and 6<sup>th</sup> of May 1998 (modified from Di Crescenzo and Santo, 2005).

In fact, four types of slopes can be distinguished where channelled, unchannelled and mixed *debris slide-flow* may occur (Figure 4.12):

- planar or open slopes without drainage basin;
- slopes with a single and non-hierarchized drainage basin;
- slopes with low hierarchized basins;
- slopes with highly hierarchized basins.

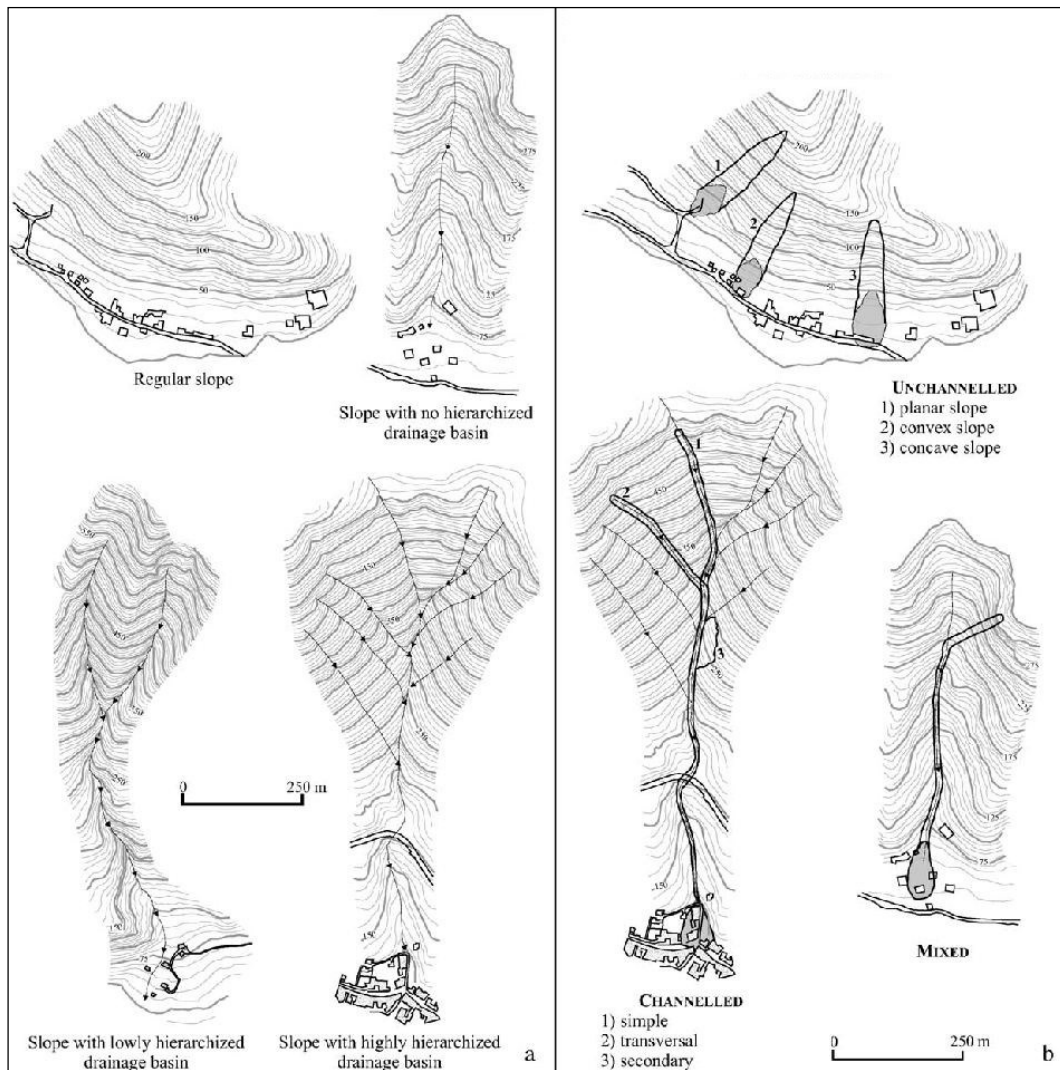


**Figure 4.12.** Different kinds of slopes and flow-type landslides occurred in peri-Vesuvian area: (a) regular slopes, discriminated in concave, convex, planar, without hierarchized drainage basins, with low and highly hierarchized drainage basins; (b) flow-type landslides channeled, not channeled and mixed (modified from Di Crescenzo and Santo, 2005).

Geomorphologic analysis to identify different types of slopes and landslides and a detailed morphometric analyses (Figure 4.13a, 4.13b, 4.13c) based on descriptive parameters were carried out by Di Crescenzo and Santo (2005), to identify semi-quantitative values of morphometric parameters useful for highlighting areas to be monitored or stabilized.

Field evidence showed that the morphology of *debris flow* involving ash-fall pyroclastic soils is characterized by small triggering areas and by *avalanche/flow* areas 10-20 times greater due to the amplification process of the landslide mass (Di Crescenzo and Santo, 2005).

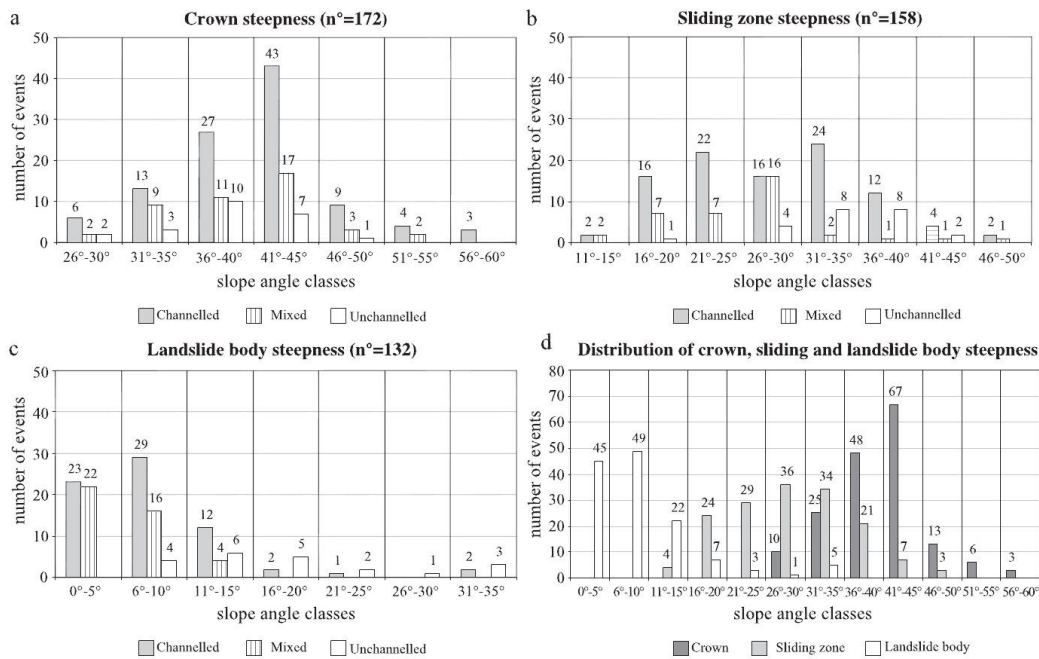


**Figure 4.13.** Morphometric data related to debris slide/flow. The classes of slope angle are differentiated between crown zone (a) slip area (b), landslide body (channeled, not channeled, mixed; (d) summary of data used for a, b and c graphs (Di Crescenzo and Santo, 2005).

The stratigraphic and geomorphological factors are responsible for the typical triangular or elongated shape of the landslides, and their apical angle appears to be the most important morphological parameter because it seems to have an important influence on the volume of material mobilized by landslides (Guadagno et al., 2005) (Fig. 4.14). The apical angles of the landslides seem to be related to the impact energy of the initial rupture and to the geometry of the pyroclastic cover. Indeed, the action of the abrupt load caused by the impact of material falling from upslope sectors leads to the undrained loading mechanism (Hutchinson and Badhari, 1971) causing the dynamic liquefaction and then the avalanche or debris flows stages.

Considering as the sliding zone also the area affected by the avalanche phase, the critical values of the apical angles ( $\alpha$ ) were calculated, ranging between  $15^\circ$  and  $29^\circ$  (Di Crescenzo and Santo, 2005) (Fig. 4.15).

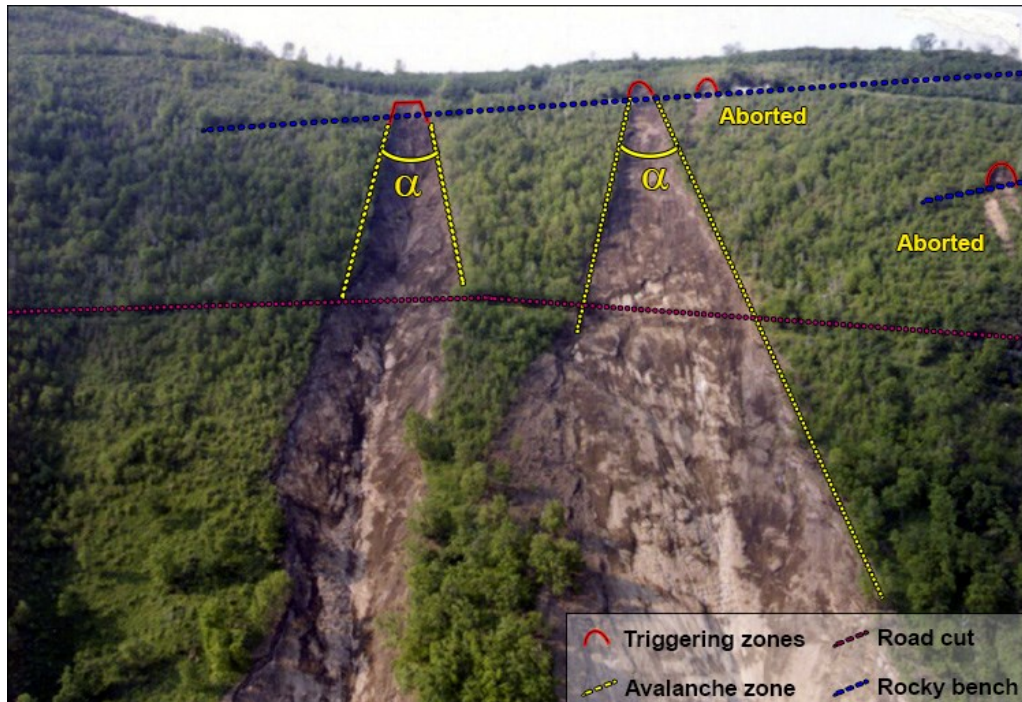


**Figure 4.14.** Example of unchannelled Sarno May 1998 debris slides characterized by very small triggering area and higher avalanche area, assuming the characteristic subtriangular morphology which apical vertex angle ( $\alpha$ ) ranged between  $15^\circ$  and  $29^\circ$  (Di Crescenzo and Santo, 2005). Slope areas characterized by ash-fall pyroclastic cover breaks, due to road cuts and rocky benches, are also showed.

Accordingly, due to local variations of morphology, the volume of material involved in the *debris avalanche* may vary significantly. However, stratigraphical differences between the two zones cannot be neglected because all detachments areas shown disappearing or thicknesses reducing of the pumiceous lapilli horizons (De Vita and Nappi, 2013). In fact, the pumiceous horizons play an important role in influencing the planar sliding and, consequently, the phase of areal enlargement of landslides. Nevertheless, where pumiceous horizons are not widespread, the landslide tends to stop near the source. Furthermore, the initial slide surface is always located in one of the interposed paleosols between several eruptions.

Other studies carried out by means of a geotechnical approach (Cascini, 2004), highlighted that the failure planes are generally located within pumice levels. Moreover, they showed that the liquefaction phases and spreading of pyroclastic soils involved in the landslide are greatly influenced by the porosity and therefore by the amount of sandy-pumice levels.

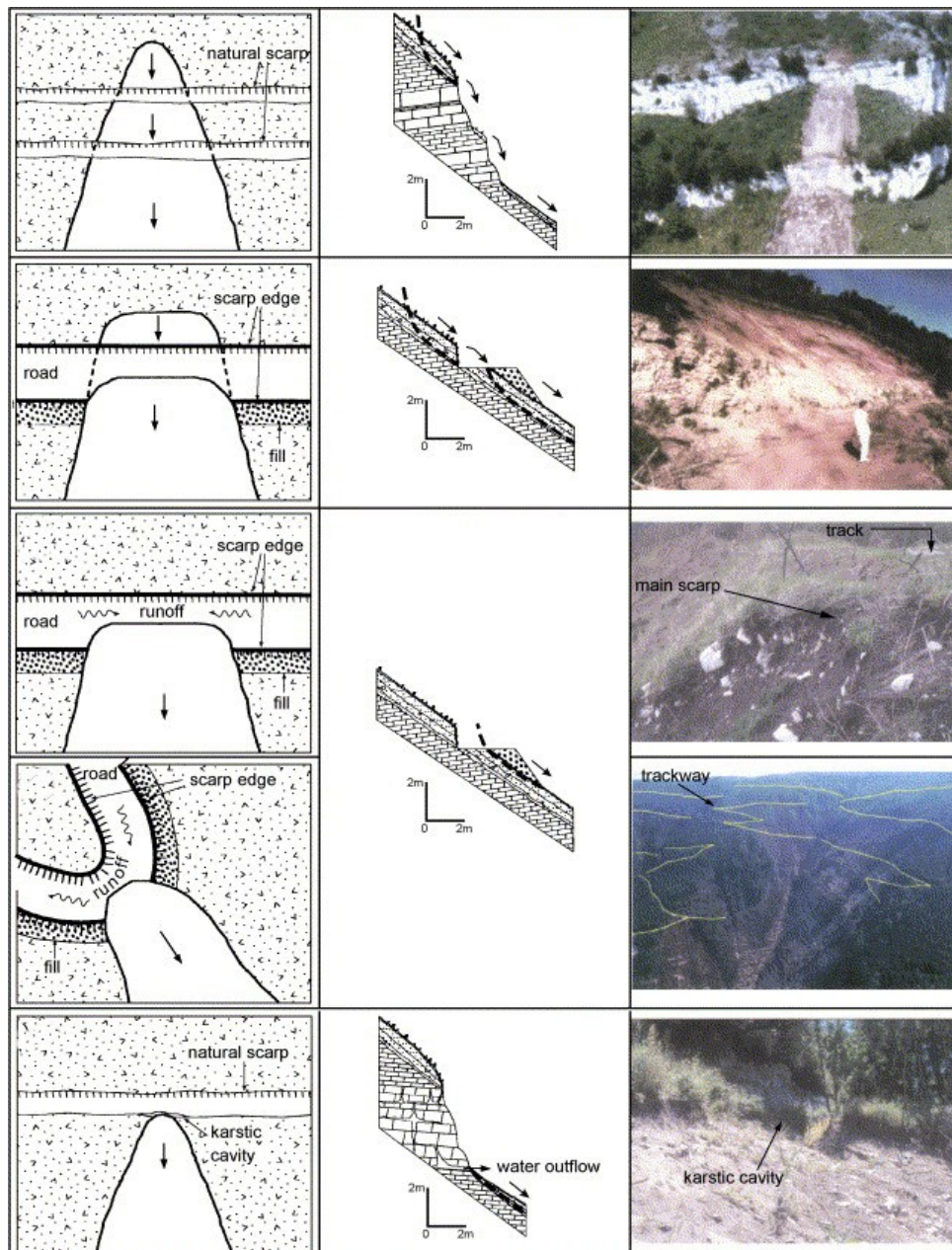


**Figure 4.15.** Geomorphological features of the main detachments areas of the 5<sup>th</sup> and 6<sup>th</sup> May 1998 flow-type landslide event occurred in the Sarno Mountains area (Guadagno et al., 2005).

Guadagno et al. (2005) performed a statistical analysis of morphometric parameters (Fig. 4.16) where it is clear that the ratio between the initial volumes and the volumes of debris avalanche ( $V_i / V_a$ ) decreases as length of the slope increases.

The role of ash-fall pyroclastic cover discontinuities was identified by a statistical study of detachment areas, finding that up to 75% of landslides occurred along and/or close to the axes of the channels or at points of convergence of shallow water flow (Crosta and Dal Negro, 2003).

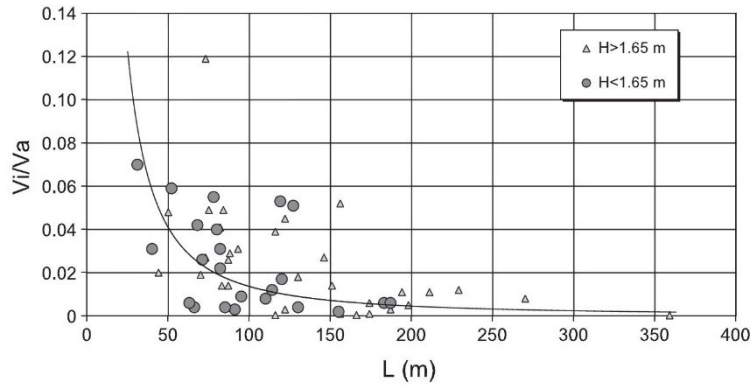


**Figure 4.16.** Relationship between volume of material involved in the initial break and volume involved in the debris avalanche against slope length (Guadagno et al., 2005).

In detail, more than a half of the Sarno May 1998 initial *debris slides* occurred upslope to morphological discontinuities and the landslides on Pizzo D'Alvano massif were associated mostly to natural discontinuities in the southern side, while mostly to artificial cuts in the northern sector (Fig. 4.17; Crosta and Dal Negro, 2003).

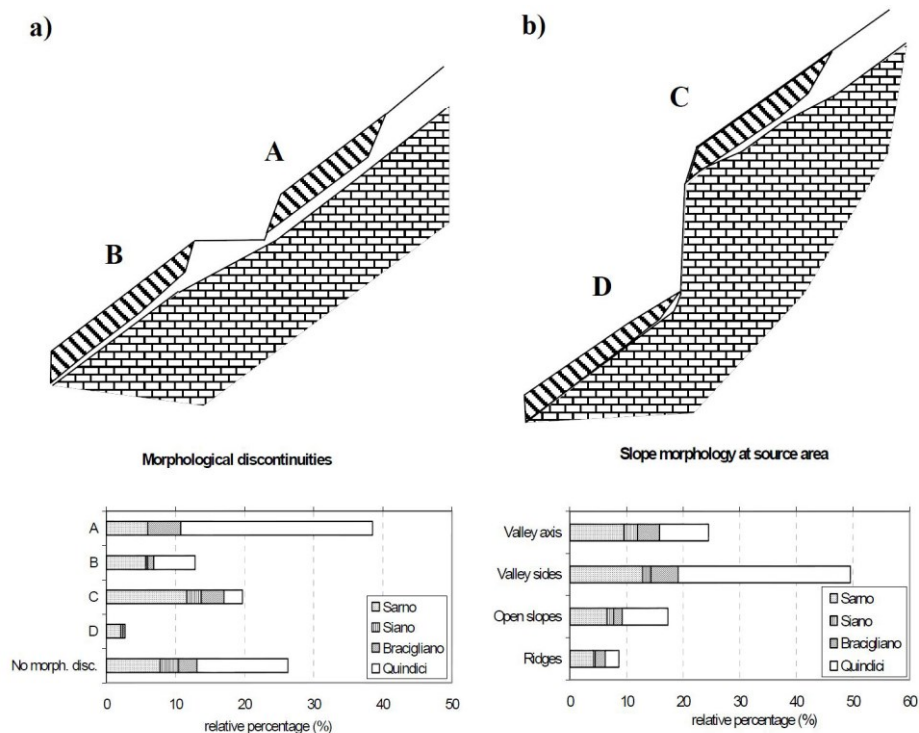


**Figure 4.17.** Morphological characteristics of source areas and relative frequency: (a) road cut with instabilities in the upslope sector and within the downslope earth fill; (b) rock cliff inducing a natural interruption of volcanoclastic cover. About 75% of the landslides took place at sites with morphologic and stratigraphic interruptions of pyroclastic covers (Crosta and Dal Negro, 2003).

Finally, a relationship between the height of the detachment area and the slope relief energy exists (Fig. 4.18). This morphometric parameter, in most of the landslides higher than 80%, is equal to the difference in elevation between the watershed line of the slope affected by a landslide and the first slope break at the foothill. This result may be used to predict the zones of potential detachment for slopes not yet affected by landslides.

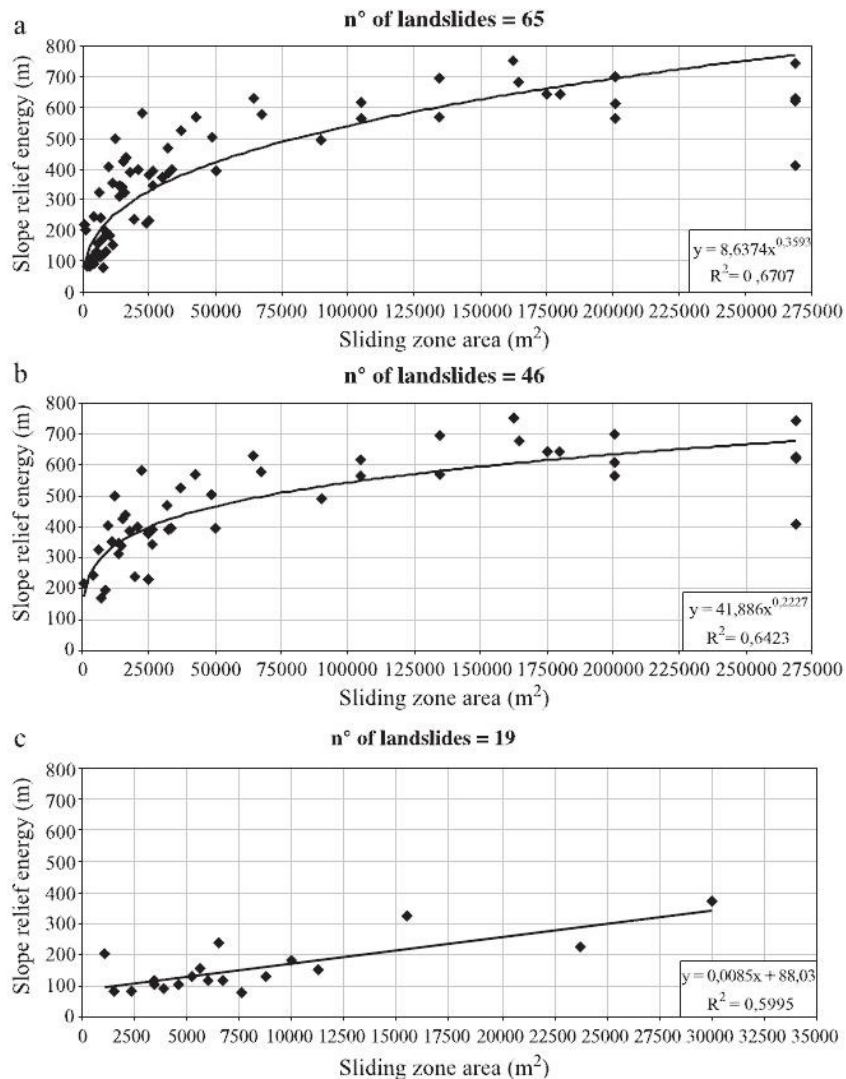


**Figure 4.18.** Relationships between the slope relief energy and the area of the sliding zone: (a) all, (b) channelled and mixed landslides, (c) unchannelled landslides (Di Crescenzo and Santo, 2005).

Cascini et al., (2008) focused their research to the comprehension of debris flow triggering mechanisms considering geomorphological, hydrological and anthropic aspects. The result was the individuation of six typical triggering areas (Fig. 4.19):

- 1- Source areas M1, located in colluvial hollows associated to zero order basins (ZOBs) (Dietrich et al., 1986; Guida, 2003) and characterized by convergent sub-superficial groundwater circulation within the pyroclastic deposits and by ephemeral springs fed by water flow deriving from the carbonate bedrock.
- 2- Source areas M2, small with a triangular shape downslope enlarged, located close uphill or downhill to the outcropping or buried bedrock scarps: at the base of bedrock scarps, where ephemeral springs associated to groundwater outlet from karst conduits can exist (Di Crescenzo and Santo, 1999; Budetta and de Riso, 2004; Guadagno et al., 2005); at the top of bedrock scarps.
- 3- Source areas M3, related to ash-fall pyroclastic cover discontinuities deriving from anthropic slope modifications, including road cuts.
- 4- Source areas M4, characterized by multiple landslides arranged like a cluster of grapes, mainly located downhill of the main channel, involving limited volume of ash-fall pyroclastic deposits with a V-shaped transversal profiles.
- 5- Source areas M5, triggered along open slopes with a convex longitudinal profile, related to the presence of deep natural or anthropogenic gullies inside the pyroclastic deposits. These source areas are characterised by rectilinear planforms with a concave transversal profile and located along the maximum slope directions.
- 6- Source areas M6, located at the base of the convex-concave hillslopes or along the flanks of the steepest hydrographic network (at the summit or along the hillslopes).

All these source areas imply that ephemeral springs at the contact between the ash-fall pyroclastic cover and the carbonate bedrock must exist, deriving from return flows fed by karstic conduits. Although in some cases field evidence confirm this assumption, the role of the hydraulic conductivity reduction of the pyroclastic cover cannot be neglected. In fact, the gradual decrease of  $K_{sat}$  values with depth allows more the formation of occasional perched water table within the pumiceous horizons than massive percolation of water through the carbonate bedrock. In addition, field evidence in the detachment areas showed the presence of the basal paleosols still covering the carbonate bedrock. For this reason, in this case, a detachment of the entire ash-fall pyroclastic cover from the bedrock can be rejected.

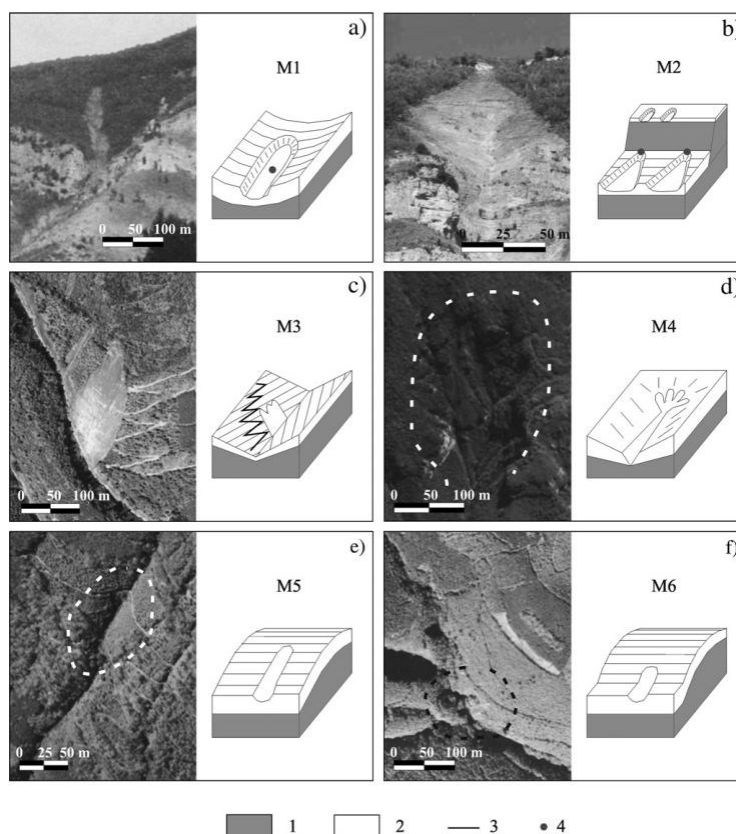


**Figure 4.19.** Proposed typical source areas of Sarno May 1998 landslide triggering debris flow event (from Cascini et al., 2008): (1) carbonate bedrock; (2) ash-fall pyroclastic cover; (3) road cuts; (4) ephemeral springs.

#### 4.4. Hydraulic and geotechnical properties of pyroclastic soils mantling peri-Vesuvian and Phlegraean Fields slopes

Ash fall-pyroclastic soils covering carbonate mountain ranges, surrounding the Campanian Plain, and Phlegraean Fields slopes, belong to the andosols category, mostly found in regions where active and recently extinct volcanoes are located (Shoji et al., 1993; Guadagno and Magaldi, 2000; Terribile et al., 2000).

Weathering processes involving tephritic rocks or similar pyroclastic materials, characterized by a significant content of volcanic glass, allow the formation of allophane, imogolite or aluminum-humus complexes minerals, which gives to these soils some peculiar andic properties. The chemical and mineralogical properties, texture, and depositional features of the parent material strongly affect the genesis of andosols (Shoji et al., 1993). In addition, some unusual hydro-mechanical properties

derive from the presence of allophane minerals, in particular high shear strength values and from high to very high water storage capacity.

#### 4.4.1 Geotechnical properties of pyroclastic soils in peri-Vesuvian and Phlegraean areas

The knowledge of physical and mechanical properties of ash-fall pyroclastic deposits, which characterize the peri-Vesuvian and Phlegraean slopes, is fundamental to understand triggering mechanism and kinematics of shallow flow-type landslides involving these materials. Several laboratory and field tests showed a strong variability and the peculiar behavior of volcanoclastic and pedogeneized horizons, which form the soil mantles. In this section, the most significant results will be discussed.

As regards ash-fall pyroclastic soils mantling Sarno Mountains slopes, including the similar contexts of the Salerno and Lattari areas, results of previous works (De Vita et al., 2013; Napolitano et al., 2015) were considered to describe physical, index and mechanical properties of pumiceous lapilli and pedogeneized horizons which characterize the pyroclastic soil cover in this area.

Grain size curves (Fig. 4.20) showed that pumice layers (C, Cb) are characterized by gravel and slightly coarse sand, while pedogeneized horizons (B, Bb, Bb<sub>basal</sub>) by coarse or fine sand, silt and clay, whose grain size rate shown the typical decreasing of particle size with depth.

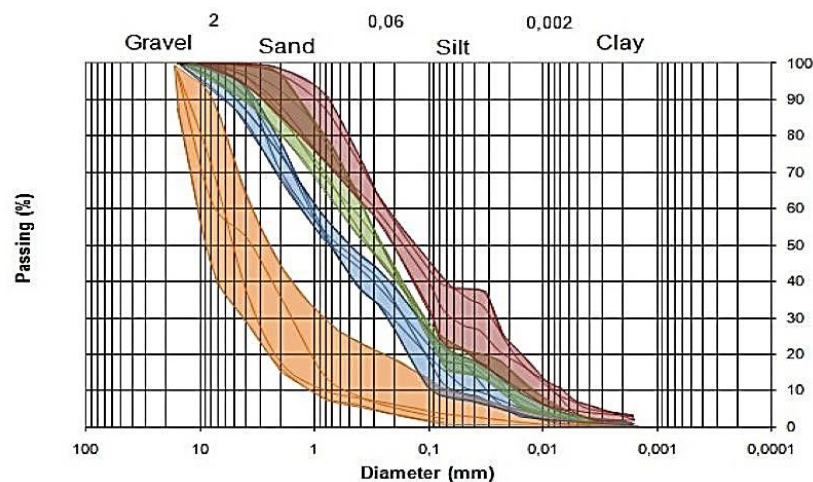


**Figure 4.20.** Grain size envelopes of soil horizons characterizing the ash-fall pyroclastic cover mantling Sarno Mountains slopes (from Napolitano et al. 2015): blue) B horizon; orange) C horizon; green) Bb horizon; red) Bb<sub>basal</sub> horizon.

This latter aspect justifies the generally recognized increase in porosity and in the void ratio of lower paleosols (Bb and Bb<sub>bas</sub>) (Fig. 4.21).

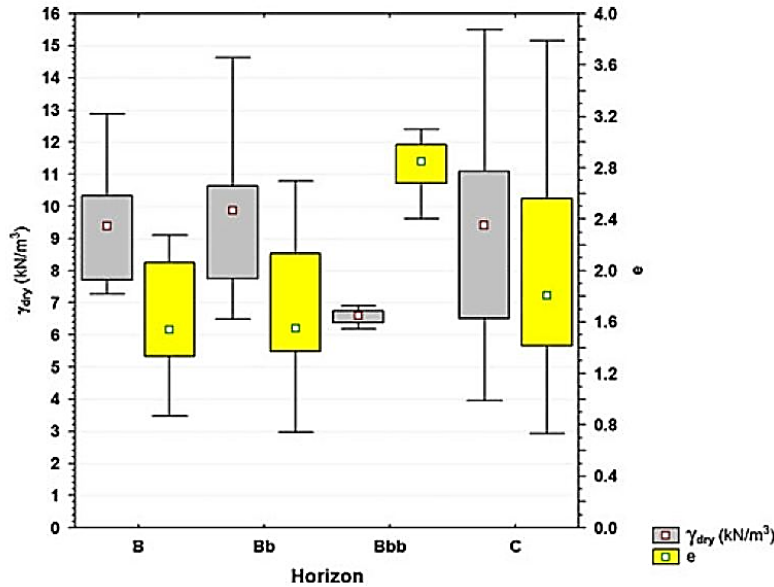


**Figure 4.21.** Box plots of dry unit weight ( $\gamma_{dry}$ ) and void ratio ( $e$ ) (from De Vita et al., 2013)

Typically, high values of these parameters are peculiar of volcanoclastic deposits characterized by vesicular structures that allow the existence of partially interconnected intraparticle voids. Other main physical and index parameters were determined (Table 4.1) including the consistency limits, which allow determining the different plasticity and liquidity indexes of the pedogeneized soils. Results showed that the decrease in grain size with depth corresponds to an increase of the plasticity index ( $I_p = w_L - w_P$ ), justifying as the transition from plastic to liquid status requires higher percentage of water.

Horizon	$\gamma_s$ $kN/m^3$	OM %	$D_{10}$ $mm$	$D_{60}$ $mm$	U	$I_p$ %
B	2.43	4	0,075	1,2	16	5.24
Bb	2.55	7	0,030	0,88	29	10.99
Bb <sub>bas</sub>	2.38	6	0,014	0,34	24	13.58

**Table 4.1.** Main physical and index parameters determined by laboratory tests carried out on disturbed and undisturbed soil specimens in the Sarno Mountains area (De Vita et al. 2013; Napolitano et al., 2015): ( $\gamma_s$ ) specific weight of solid; (OM) organic matter; ( $D_{10}$ ) diameter at 10%; ( $D_{60}$ ) diameter at 60%; (U) uniformity coefficient; ( $I_p$ ) plasticity index.

Shear tests revealed heterogeneous and variable mechanical properties of each horizon (Fig. 4.22), which characterize the ash-fall pyroclastic cover in Sarno Mountains area.

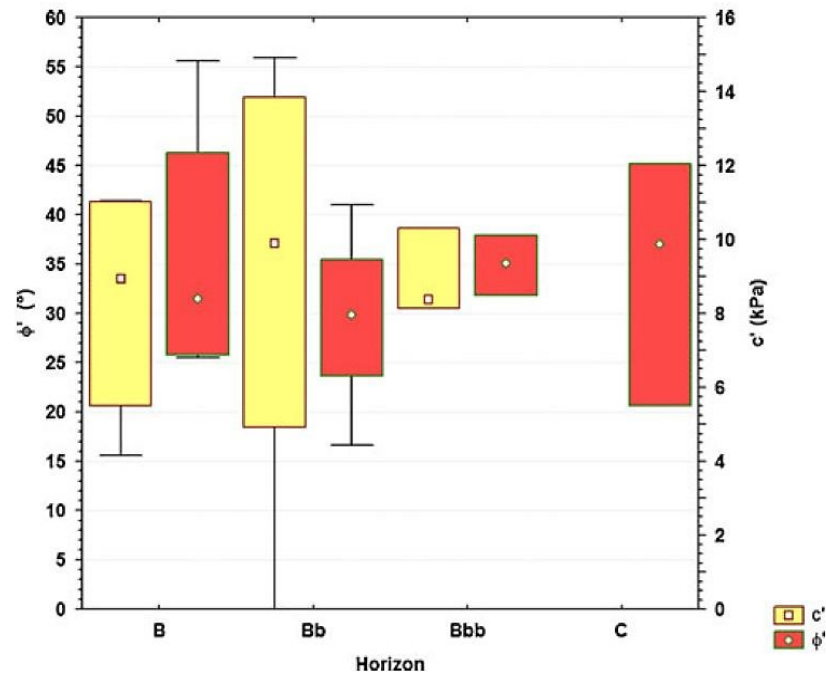


**Figure 4.22.** Box plots of  $c'$  and  $\phi'$  values obtained by means of direct shear tests (from De Vita et al., 2013)

An increase of the friction angle values ( $\phi'$ ) and then of the shear strength ( $\tau'$ ) in the pedogeneized horizons was observed, showing also the existence of a non-negligible apparent cohesion ( $c'$ ) due to the combined effect of micro-roots system and coarse pumiceous pyroclasts.

As regards volcaniclastic deposits, which characterize slopes of the Camaldoli hill sample area, disturbed, and undisturbed soil specimens of the shallowest horizons of the volcaniclastic sequences (down to 4.0 m) were tested by different geotechnical laboratory procedures to obtain index and mechanical characterizations (Fusco et al., 2016a; 2016c). Grain size curves of the volcaniclastic soils showed the uppermost stratigraphic sequence (down to 2.0 m), chiefly involved in slope instability process, as formed by the overlap of a loose sandy gravel with silt (actual B horizon) over dense silty sand horizon, formed by fine ashes, sometimes with gravel intercalations (pumiceous lapilli) (Fig. 4.23).

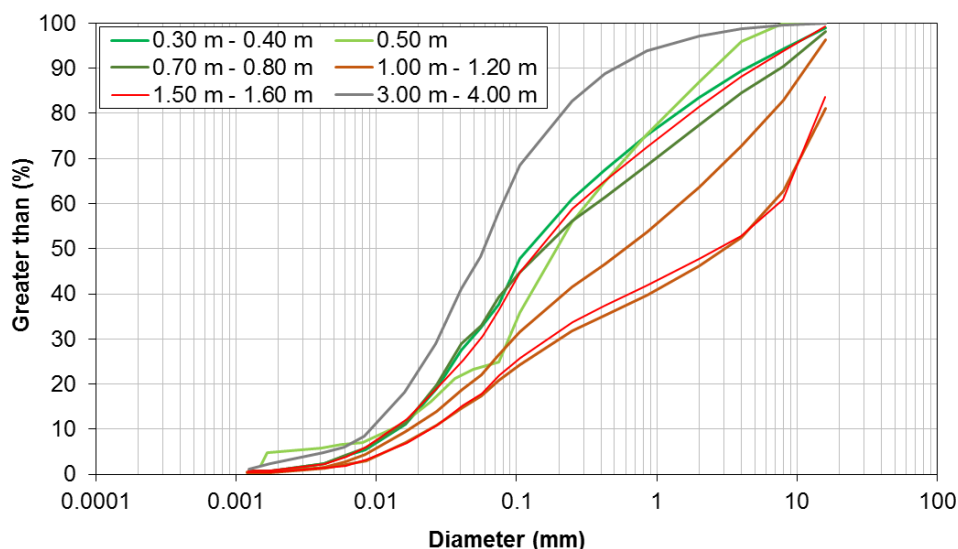


**Figure 4.23.** Grain size curves of pyroclastic soil horizons, which characterize the Camaldoli hill slopes (Fusco et al., 2016a; 2016c).

In addition, the determination of main physical and index parameters (Table 4.2) allowed the understanding of the peculiar properties of volcanoclastic soils, which are very similar to those characterizing Sarno Mountains slope area. Friction angle ( $\phi'$ ) and then shear strength ( $\tau'$ ) values of soils and fine ash horizons were determined by shear tests carried out on several undisturbed specimens (Fig. 4.24).

Horizon	$\gamma_s$ $kN/m^3$	$\gamma_{dry}$ $g/cm^3$	$n$	$e_0$	OM %	U	$I_p$ %
Top soil	2.49	0.97	59.3	1.44	3.35	26.6	8.82
Fine ash	2.51	1.09	56.3	1.29	3.34	8.47	8.91
Paleosols	2.46	0.94	61.6	1.60	3.13	20.8	8.72
Pumiceous lapilli	2.48	1.03	58.1	1.39	3.40	306.7	8.03

**Table 4.2.** Main physical and index parameters determined by laboratory tests carried out on disturbed and undisturbed soils specimens in the Camaldoli hill area (Fusco et al., 2016a; 2016c): ( $\gamma_s$ ) specific weight of solid; ( $\gamma_d$ ) dry specific weight; ( $n$ ) porosity; ( $e_0$ ) initial void ratio; (OM) organic matter; (U) uniformity coefficient; ( $I_p$ ) plasticity index.

Such as for the Sarno mountains, pyroclastic soils have a non-negligible apparent cohesion ( $c'$ ) was observed due to the combined effect of micro-roots system and coarse pumiceous and lithic pyroclasts. These latter justify the presence of this

materials along the Camaldoli hill steepest slopes despite high slope angles (more than 50°).

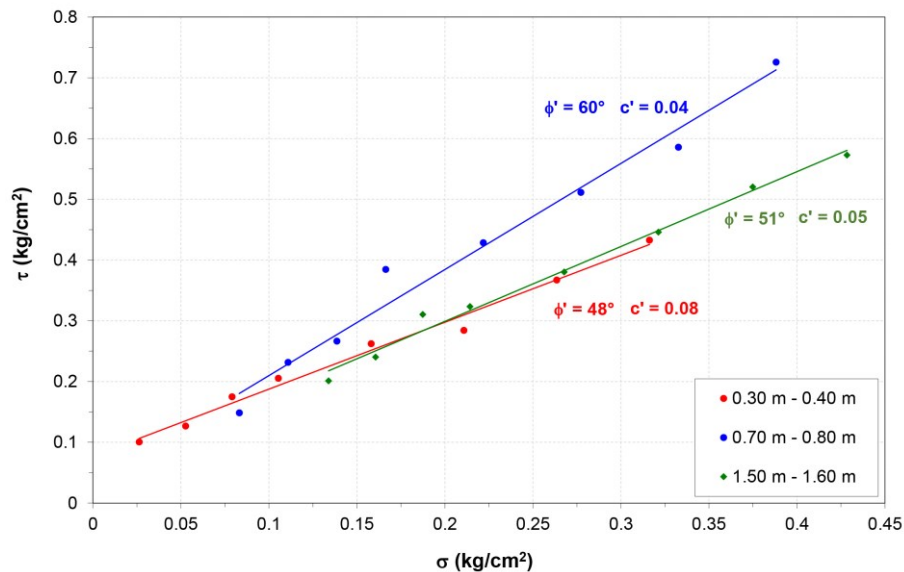


**Figure 4.24.** Shear strength ( $\tau'$ ) of collected pyroclastic soils in Camaldoli hill area obtained by means of direct shear tests: ( $c'$ ) cohesion; ( $\phi'$ ) friction angles. (Fusco et al., 2016a; 2016c).

#### 4.4.2 Saturated and unsaturated hydraulic properties of pyroclastic soils in peri-Vesuvian and Phlegraean areas

Peculiar saturated and unsaturated properties characterize the pyroclastic soils covering peri-Vesuvian carbonate ranges and Phlegraean Fields slopes. These soils are very heterogeneous and characterized by alternating horizons with different particle grain sizes (from gravel to silt) and thus by different and contrasting saturated hydraulic conductivity ( $K_{sat}$ ), sometimes up to high levels.

This section describes results of previous works focused on the hydraulic characterization of pyroclastic soils which mantle the Sarno Mountains and Phlegraean Fields sample areas, which were carried out with field and laboratory methods both regarding samples collected nearby the source areas of flow-type landslide events.

As regards slopes of the Sarno Mountains, a complex water circulation within the pyroclastic mantle-carbonate bedrock system is justified by the multilayered hydrogeological setting and the unsaturated conditions. For this reason, different field

and laboratory tests were carried out in some detachment areas of Sarno May 1998 flow-type landslide event to obtain the hydraulic characterization of different horizons constituting the pyroclastic mantle (De Vita et al. 2013; Napolitano et al., 2015). The strong influence of grain size and structural characteristics of the soil on the hydraulic conductivity induces to the high variability in space and time of this parameter, up to several magnitude orders. Results showed a decrease of  $K_{\text{sat}}$  values with depth in agreement with the decrease of the grain size (Fig. 4.25).

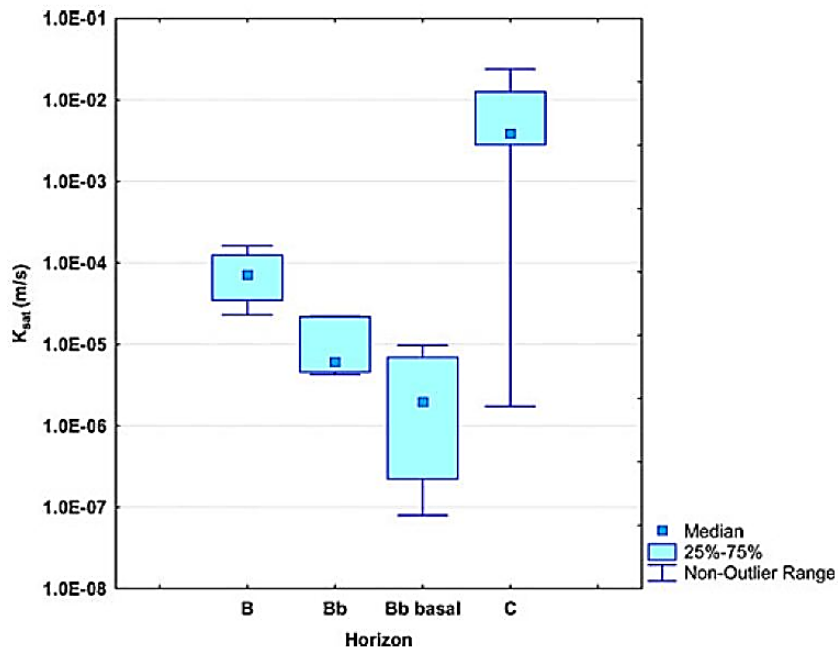


**Figure 4.25.** Box plot of hydraulic conductivity values estimated for each pyroclastic soil horizon, which characterize the ash-fall pyroclastic cover mantling slopes of the Sarno Mountains (from De Vita et al., 2013). Data derive from “single ring infiltrometer tests” (Bouwer, 1986), “CCHP permeameter tests” (Amoozegar and Warrick, 1986) and grain size empirical formulas (for C horizon only).

In detail, paleosols (Bb, Bb<sub>bas</sub>), with very similar hydraulic conductivities, are relatively less permeable than the top soil (B), while pumice horizons (C, Cb) shown the highest values.

Soil water retention curves (SWRCs) reconstructed by laboratory tests (De Vita et al., 2013) showed that pyroclastic soil horizons of the Sarno Mountains area have peculiar unsaturated hydraulic properties as well as distinguishable saturated hydraulic conductivity values, the latter strongly affected by water content. In particular, different residual water contents (the higher  $\theta_s$ , the higher  $\theta_r$ ) of each soil horizons was

observed, despite pedogenized horizons (B, Bb, Bb<sub>bas</sub>) are characterized by similar hydraulic behavior (Fig. 4.26). Furthermore, pumiceous lapilli horizons showed an unusual high water retention capacity due to high specific surface and interconnected intra-particle voids.

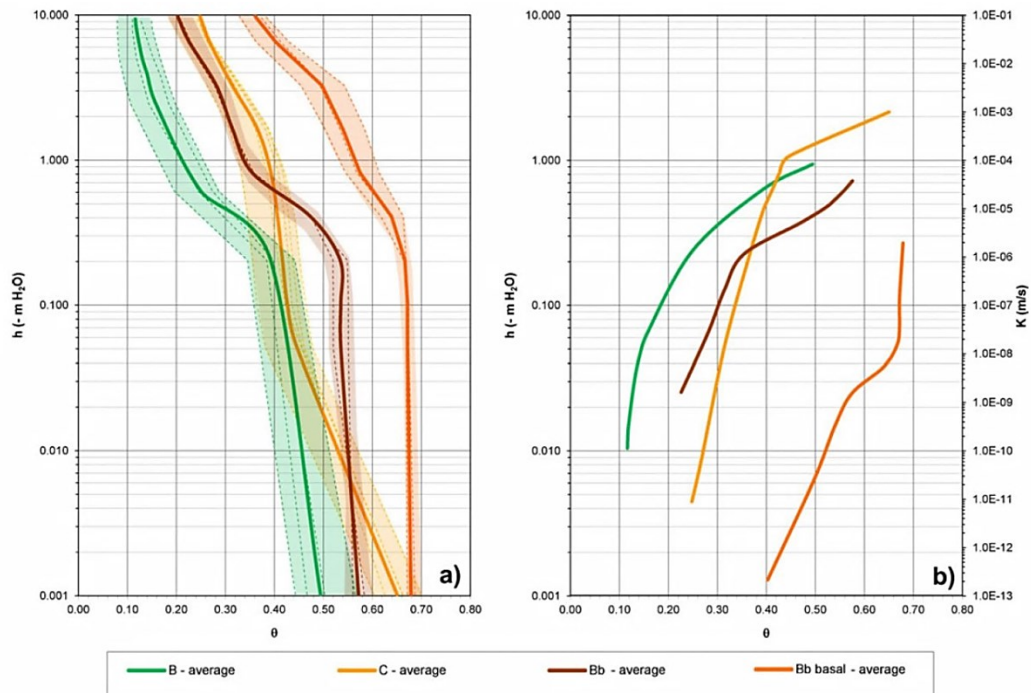


**Figure 4.26.** (a) Soil water retention curves (SWRCs) and (b) hydraulic conductivity functions (HCFs) obtained for pyroclastic soils horizons, which characterize the ash-fall pyroclastic mantle covering the Sarno Mountains area (from De Vita et al., 2013).

Finally, from field and laboratory tests a similar hydraulic behavior was recognized for pyroclastic soils characterizing Camaldoli hill slopes (Fusco et al., 2016a; 2016c). In this case, soil water retention curves obtained for the shallowest horizons of the volcanoclastic series (down to 1.70 m) showed high retention capacity (Fig. 4.27a). Furthermore, a strong variability of  $K_{\text{sat}}$  values with depth characterizes these horizons (Fig. 4.27b) due to their difference in grain size. In fact, the top soil covering the volcanic series (alternating of pumiceous and cineritic layers) has a similar hydraulic conductivity of the shallowest pumiceous horizon, due to the presence of coarse pyroclastic materials (scoriae, pumices and lithics). An important decrease of hydraulic conductivity occurs at 1.60 m of depth, where a fine ash horizon was recognized.

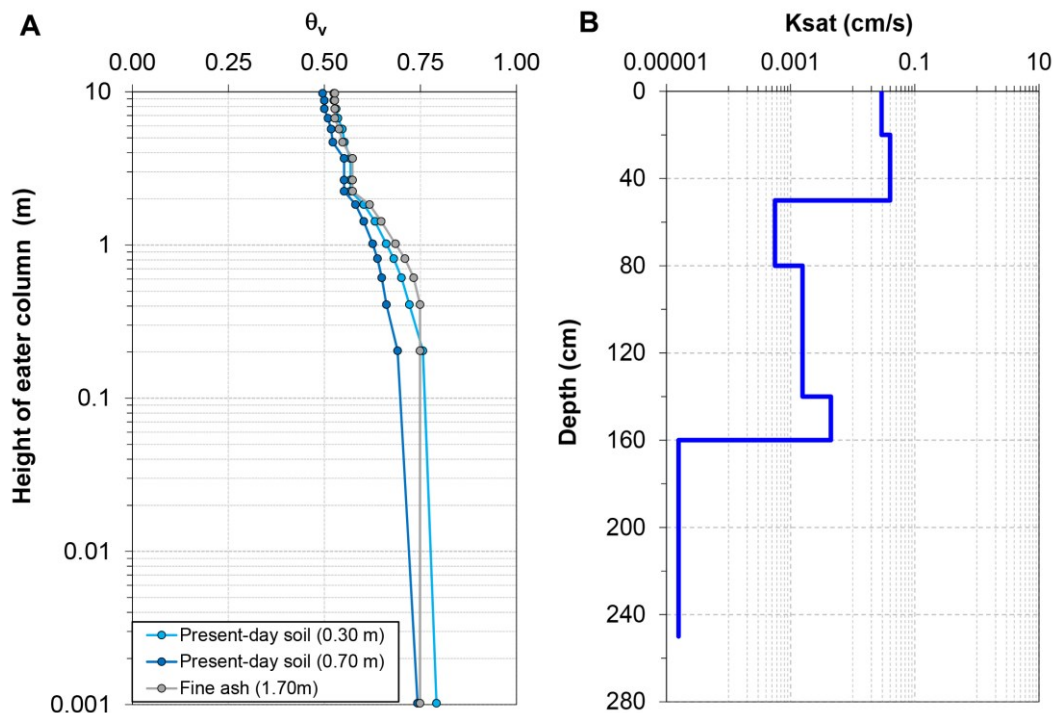


**Figure 4.27.** Soil Water Retention Curves (SWRCs) expressed as height of water column ( $h$ ) vs volumetric water content ( $\Theta_v$ ) and saturated hydraulic conductivity ( $K_{sat}$ ) variation with depth of shallowest pyroclastic soils in Camaldoli hill area (Fusco et al., 2016a; 2016c).

## 4.6 The role of hydrological conditions to landslide triggering

Flow-type landslides involving ash-fall pyroclastic soils in the peri-Vesuvian and Phlegraean areas are essentially shallow landslides triggered by peculiar hydrological conditions, such rainfall and soil moisture conditions, strongly related to the period preceding the failure. The magnitude of the event is generally proportional to the intensity and duration of rainfall triggering event. Furthermore, stratigraphic and geomorphological settings affect water infiltration and flowing processes within the pyroclastic soils.

As regards slope instabilities affecting peri-Vesuvian carbonate ridges, typically affected by landslide-triggered debris flow events, different interpretations of hydrogeological processes within the superficial system pyroclastic cover-carbonate bedrock were proposed. These different conceptual models are of extreme relevance

in the understanding of mechanisms triggering landslides as well as in proposing approaches for the landslide hazard reduction.

Volcaniclastic series covering carbonate slopes are characterized by a complex stratigraphical system of the incoherent ash-fall pyroclastic deposits (pumiceous horizons with alternating paleosols), with vertical and lateral variations of saturated hydraulic conductivity. The underlying carbonate bedrock is characterized by a hydraulic conductivity varying with the degree of fracturing and filling of open joints. In this framework, some different conceptual models were proposed for taking into account the water flow in the surficial hydrogeological system ash-fall pyroclastic coverings/carbonate bedrock (De Vita et al., 2003).

A first interpretative model promotes an occasional groundwater flow developed in the upper part of the fractured carbonate bedrock by particularly high and/or prolonged rainfall (Celico et al., 1986). The “*occasional perched water table*” feeds both basal water table, typical of carbonate mountains, and ephemeral springs, the latter following a path parallel to the slope. It is important in this context to emphasize the presence of marly interbeddings (marls with *Orbitolinae*) that behave as relative impermeable thin layers, leading to the formation of small underground reservoirs that feed the high altitude springs.

After the landslide event of the 5<sup>th</sup> and 6<sup>th</sup> of May 1998 in the Sarno Mountains, other hydrogeological models based on the observation of the existence of a low hydraulic conductivity basal paleosol that separate hydraulically the pyroclastic mantle from the bedrock were proposed (Celico and Guadagno, 1998; Del Prete et al., 1998; Celico, 2000). Also in these models the formation of a “*perched occasional water table*”, affecting also the ash-fall pyroclastic deposits, were proposed. These saturated and/or near saturated conditions lead to the increase of pore water pressure ( $u$ ), including overpressure in some cases, an effective stress ( $\sigma'$ ) decreasing and then a shear strength ( $\tau$ ) decreasing of the pyroclastic horizons. Considering also an increasing of the ash-fall pyroclastic cover density ( $\gamma_n$ ) and the buoyant unit or effective unit weight ( $\gamma'$ ), lower than the water density (approximately equal to 1), instable conditions can occur.

Field investigations and sampling for laboratory tests carried out in the triggering areas of the 1998 Sarno event allowed to propose revisited models of triggering hydrological conditions of peri-Vesuvian flow-type landslides (Fig. 4.28; Celico et al., 2002). During particularly heavy rainfall, the formation of occasional perched saturation zones within pumiceous lapilli horizons may take place. The first model

suggests an ash-fall pyroclastic mantle several meters thick and a slide surface within the mantle where two horizons exist, the shallowest with hydraulic conductivity greater than or equal to  $10^{-3}$  cm/s and the deepest less than  $10^{-4}$  cm/s. The second model is characterized by a slightly fractured carbonate bedrock covered by thinner, coarser and more permeable pyroclastic horizons. In this case, an increase of pore water pressure within the ash-fall pyroclastic mantle is possible due to the relative lower saturated hydraulic conductivity of the carbonate bedrock (less than  $10^{-4}$  cm/s). The last model, typical of most detachment areas, is characterized by thickness reduction of a very permeable ash-fall pyroclastic cover mantling a carbonate bedrock characterized by a strong variation of permeability along the vertical (due to marl intercalations).

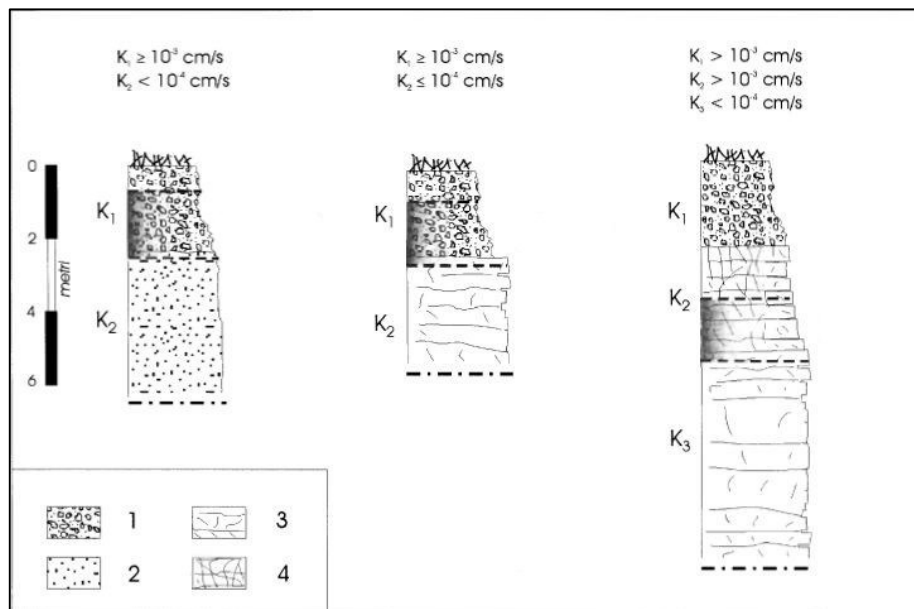


**Figure 4.28.** Possible models of carbonate bedrock - ash-fall pyroclastic cover hydrological system, assuming the existence of an ephemeral perched water table (from Celico et al., 2002): (1) predominantly pumiceous deposits; (2) ash deposits; (3) poorly fractured carbonate bedrock; (4) fractured and layered carbonate bedrock.

In these models, the formation of perched ephemeral water tables can occur during rainfall events whose intensity is not lower than the infiltration capacity at saturation of relative less permeable horizons and during the hydrological year when the demand for water retention was satisfied.

As regards flow-type landslides occurring in the peri-Vesuvian area, the hydrological triggering conditions of the previous models have a spatial variability related to stratigraphic and geomorphological settings, involved pyroclastic soils and to joint systems of shallow part of carbonate bedrock and their saturated hydraulic conductivity. For this reason these events does not occur everywhere along the slopes during rainfall events.

Recent studies based on accurate testing of unsaturated and saturated hydraulic properties of soil horizons forming the volcanoclastic series covering the carbonate bedrock, joined to a stratigraphic survey of pyroclastic covers along the peri-Vesuvian carbonate slopes (De Vita et al., 2003; De Vita et al., 2006a; 2006b; 2013; Napolitano et al. 2015), led to understand the following important aspects:

- 1) ash-fall pyroclastic mantle formed, from the top, by: A + B horizons (SM), with saturated hydraulic conductivity, ranging from  $10^{-2}$  to  $10^{-3}$  cm/s; C horizons (GP-GW), formed by pumiceous lapilli with higher  $K_{sat}$ , ranging from  $10^{-1}$  to  $10^0$  cm/s; Bb horizon, or paleosols (SM), with lower  $K_{sat}$ , ranging from  $10^{-2}$  to  $10^{-4}$  cm/s;
- 2) continuous presence of the Bb<sub>basal</sub> horizon, corresponding to a basal paleosol (SM) with lower  $K_{sat}$ , ranging from  $10^{-4}$  to  $10^{-5}$  cm/s, wrapping the carbonate bedrock;
- 3) unsaturated carbonate rock-mass underlying the ash-fall pyroclastic mantle, characterized, for the first meters, by open discontinuities, in the shallowest part filled by the overlying Bb<sub>basal</sub> paleosol.

From these observations derives a conceptual hydrogeological model of the surficial system “pyroclastic mantle/carbonate bedrock”, which is characterized by a shallower part of the pyroclastic cover with a mean value of  $K_{sat}$  higher than that of the Bb<sub>basal</sub> horizon. Moreover, the shallower part of the carbonate rock is characterized by open discontinuities filled by soil derived from the overlying Bb<sub>basal</sub> horizon and hence characterized by a  $K_{sat}$  estimable as a fraction of that of the Bb<sub>basal</sub> horizon, depending on the effective porosity of the rock-mass.

It follows that the surficial system “pyroclastic mantle/carbonate bedrock” can be described by a hydrogeological conceptual model formed by three layers in which the intermediate one, corresponding to the coupling of Bb<sub>basal</sub> horizon and of the shallower part of the carbonate rock-mass, with discontinuities filled by the overlying soil, limits

the velocity of unsaturated/saturated percolation allowing an increase of water content and soil pressure head in the first layer at the top of the Bb<sub>basal</sub> horizon. This condition, occurring especially during heavy and prolonged rainfall events, leads to the formation of a lateral throughflow in an ash-fall soil mantled slope and then to near-instability or instability conditions.

Finally, the possibility that an increase of pore pressure can occur in the ash-fall pyroclastic mantle for a groundwater outlet coming from the carbonate bedrock appears negligible due to existence of the intermediate layer, which prevents it. Field observations which show the outcrop of the Bb<sub>basal</sub> paleosol in the detachment areas of initial debris slides may confirm that finding.

# Chapter 5

## Data and methods for engineering-geological characterization, hydrological monitoring and modelling of test areas

The understanding of stratigraphic settings and hydro-mechanical properties of pyroclastic deposits involved in shallow landslides is important to carry out hillslope hydrological monitoring and modelling, from the local to regional scales, for landslide susceptibility analysis in the peri-Vesuvian and Phlegraean areas. First of all, two test sites were chosen, in the Sarno Mountains and in Camaldoli hill areas, enclosed in the municipality of Naples, (Figs. 5.1 and 5.2) to apply a coupled hydrological and mechanical modelling approach for assessing the influence of antecedent-hydrologic conditions on rainfall intensity-duration thresholds for triggering debris flows in ash-fall pyroclastic, soil-mantled slopes.

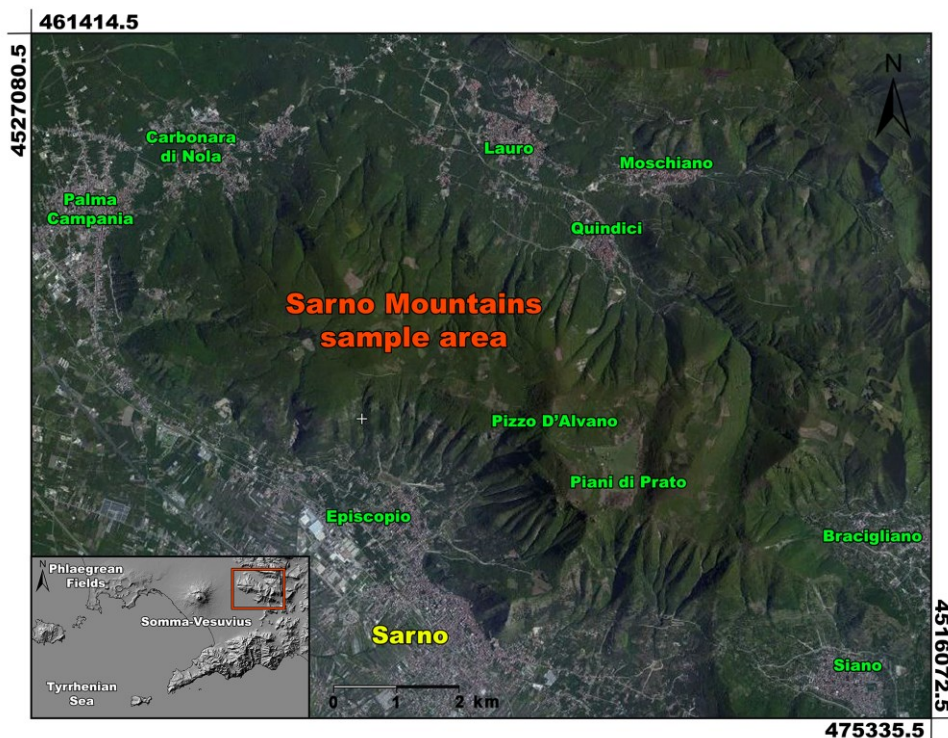


Figure 5.1. Geographical framing of the Sarno Mountains sample area.



Figure 5.2. Geographical framing of the Camaldoli hill test area in the eastern side of the Phlegraean Fields.

The next step was to extend these modelling approaches from local to regional scales in order to obtain landslide susceptibility maps considering geological, geomorphological and hydrological aspects coupled to critical rainfall conditions.

## 5.1. The Sarno Mountains test area

The test area identified in the Sarno Mountains (Fig. 5.3) is located along the slopes of the Mount Pizzo d'Alvano (1133 m a.s.l.). It was considered representative of typical source areas for debris flows occurring along mountainous slopes around the Somma-Vesuvius volcano (Calcaterra et al, 2003; Di Crescenzo and Santo, 2005; Guadagno et al., 2005).

The site, where many rainfall-induced debris flows occurred in the last main landslide event of the May 1998, includes four initial slide areas. Three of them (L1, L2 and L3 in Fig. 3) were considered to identify deterministic rainfall thresholds (De Vita et al., 2013; Napolitano et al., 2015), while one (L4 in Fig. 5.3) was chosen to carry out an extensive hydrologic monitoring network upslope from the landslide crown (Fusco et al., 2013; Fusco and De Vita, 2015; Napolitano et al., 2015), due to

favorable local logistic conditions. The landslide at this site started above a rocky cliff, triggered a debris avalanche, and evolved into a debris flow along the Tuoro Valley, in the southwestern slope of the Sarno Mountain Range. Due to the thickness and stratigraphic setting of the ash-fall pyroclastic mantle as well as to morphological settings and vegetation cover, the test area can be considered also representative for the hydrological role assessment of ash-fall pyroclastic covers on groundwater recharge of carbonate aquifer. Stratigraphic and morphological settings of the fourth sample landslide are similar to those of the other three study areas.

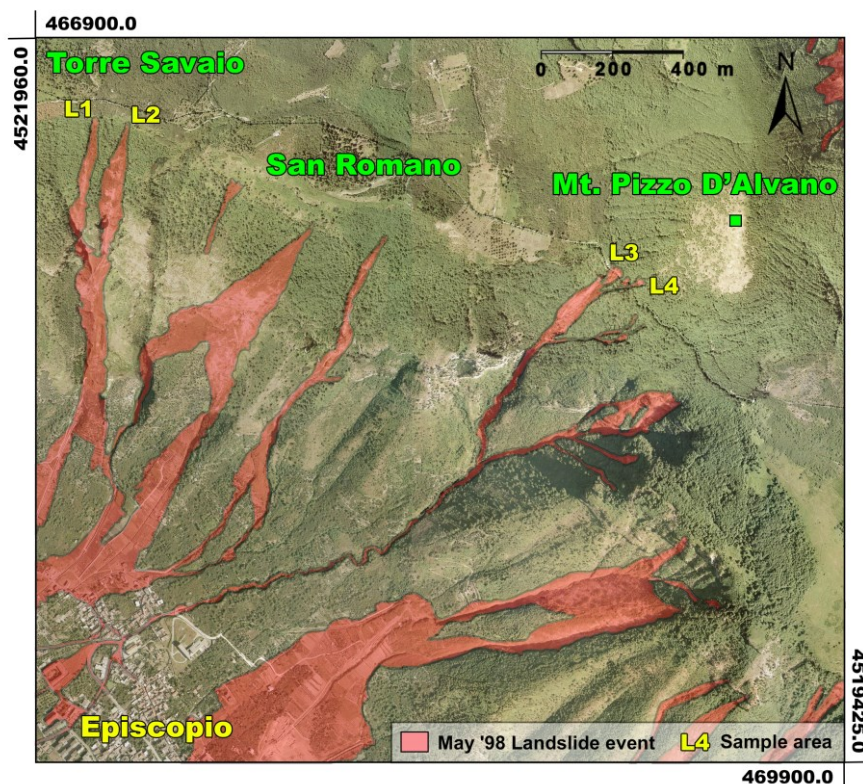


**Figure 5.3.** Location of the four studied sample areas corresponding to source areas of initial landslides, which triggered debris flows occurred in May 1998 in the Sarno Mountain Range (Campania, southern Italy). We studied stability conditions of initial landslides of areas 1 to 3 and installed a station for monitoring hydrological regime of the pyroclastic soil mantle in area 4.

### 5.1.1. Reconstruction of the engineering-geological model

Engineering geological investigations, including light dynamic penetrometer tests (DPLs) and exploratory pits, were carried out in the sample slope areas to reconstruct

a detailed stratigraphic and geometric settings. 2D engineering geological models were created by taking into account their small-scale variability and reconstructing the slope topography preceding the landslide, which determines susceptibility to initial landsliding (Fig. 5.4). The original ground profiles preceding the slope instability were reconstructed by a linear extrapolation technique from transversal topographic profiles, which were surveyed externally to the landslide flanks. Moreover, the current topographical profiles inside the landslide scars were considered as representative of the rupture surfaces. The latter assumption was based on the observation of negligible erosion of the source areas since May 1998. Finally, undisturbed samples were collected from test pits for laboratory test, including soil geotechnical identification (USCS) and characterization of unsaturated and saturated soil properties as well as mechanical properties (De Vita et al., 2103; Napolitano et al., 2015). Coupling both field and laboratory tests, a detailed stratigraphic model of the test area was reconstructed (Fusco and De Vita, 2015).

Considering the shallowness of the deposits and the effects of pedogenetic processes occurred in stages between consecutive eruptions, a criterion based on the identification of the main soil horizons was adopted (Terrible et al., 2000; USDA, 2014). An alternation of pedogenic and weathered pyroclastic soil horizons with unweathered pumiceous lapilli horizons was observed (Table 5.1), as it is commonly found in most of the peri-Vesuvian mountain slopes. Even though the ash-fall pyroclastic deposit thickness typically decreases with slope, a strong reduction of pyroclastic-mantle thickness was observed in proximity of slope-morphological discontinuities, where slope angle values become abruptly greater than  $28^\circ$ . Land use in the study area was deciduous forest of chestnut (*Castanea sativa*) with sparse evergreen underbrush, which is common along the peri-Vesuvian mountain slopes and in source areas of debris flows as well.

The engineering geological models of the areas upslope of the three landslide crowns were integrated with the characterization of saturated hydraulic conductivity and Soil Water Retention Curve (SWRC) parameter of each soil horizon, which were carried out in previous researches (De Vita et al., 2013) by means of laboratory and field tests.

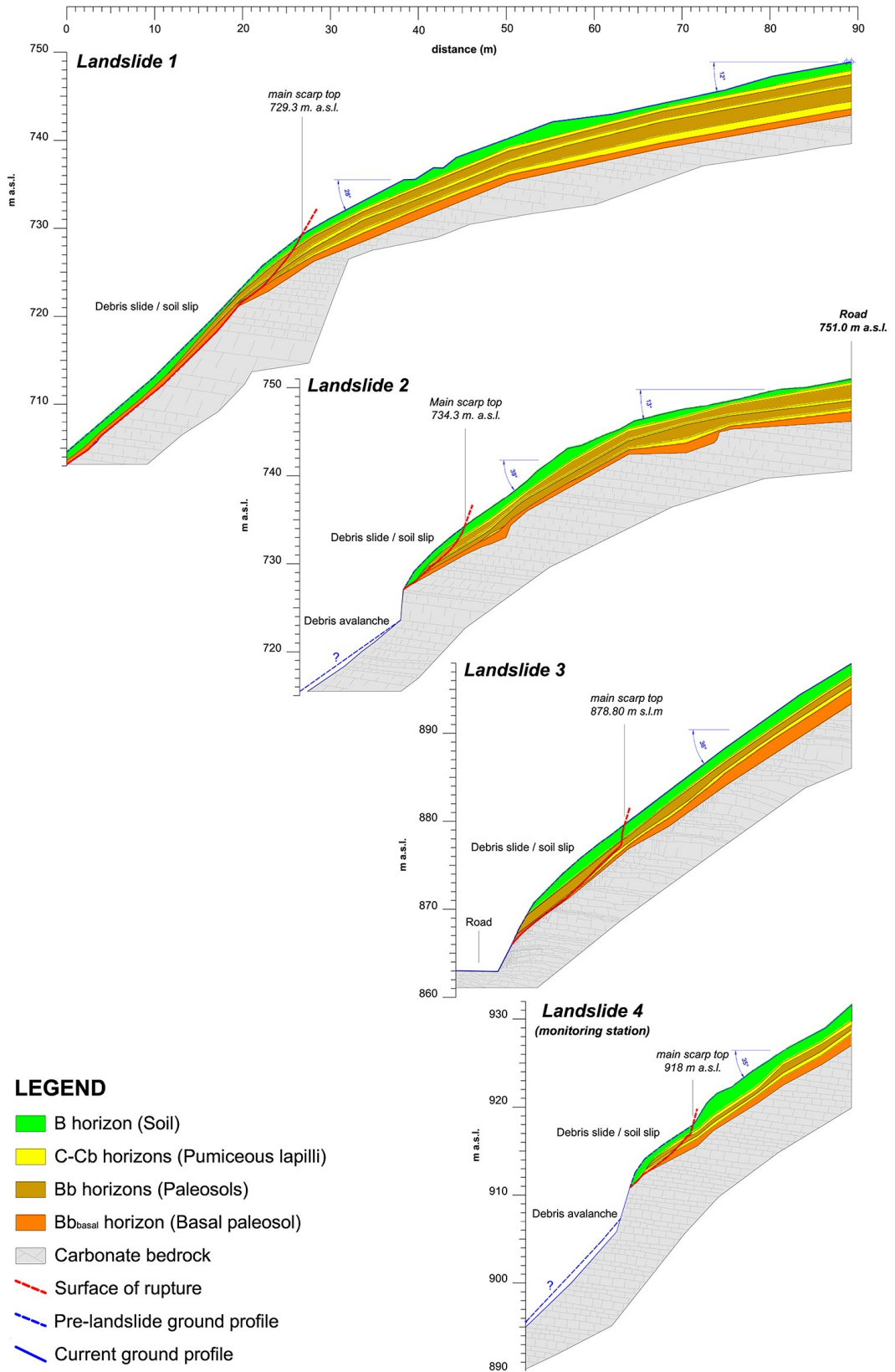


**Figure 5.4.** Geological models of the three representative initial landslides (L1, L2, and L3) and of the fourth area (L4), upslope of another initial landslide, where a monitoring station was installed (from Napolitano et al., 2015).

Bottom depth (m)	Thickness (m)	Lithological and lithostratigraphic descriptions USCS characterization	Horizon (ID)
0.10	0.10	Humus (Pt)	A
1.30	1.20	Very loose soil of pyroclastic horizons highly subjected to pedogenetic processes with dense root apparatuses (SM). Generally dark brown coloured.	B
1.60	0.30	Very loose pumiceous lapilli level (gravel) with low degree of weathering (GW-GP). Dark greenish gray coloured. Pollena eruption (A.D. 472).	C
2.50	0.90	Weathered and pedogenized soil of pyroclastic origin constituted by fine to coarse ash and subordinately by pumiceous lapilli. Paleosol (SM). Dark reddish brown coloured.	Bb
2.90	0.40	Pumiceous lapilli (gravel) from very angular to angular, with maximum 6 cm of diameter, in primary deposition, matrix almost absent. Light yellowish gray coloured. Avellino eruption (3.7 kyrs B.P.).	Cb
3.80	0.90	Weathered and pedogenized soil of pyroclastic origin constituted by fine to subordinate coarse ashes. Basal paleosol (SM). Dark yellowish brown coloured.	Bb <sub>basal</sub>
?	?	Carbonate bedrock, fractured and altered, by discontinuities from open to closed, filled by material coming from the overlying horizon. Light gray coloured.	R

**Table 5.1.** Stratigraphic setting of the hydrological monitoring test area.

### 5.1.2. Setting up of the hydrological monitoring station

In order to assess hydrological processes occurring within the pyroclastic mantle and variability of soil hydrological parameters from hourly to seasonal scales, an automated field soil hydrological monitoring station was set up in the southwestern sector of Mount Pizzo D'Alvano (Fig. 5.6).

The area of the soil hydrological monitoring station, located upslope of the landslide main scarp, is characterized by a fairly regular profile, with an average slope angle of about 35°. Instead, downslope of the main scarp a slope morphological discontinuity, characterized by an abrupt increase of the slope angle and the outcrop of the carbonate bedrock, forms a rocky scarp whose height is up to 5.0 m (Fig. 5.5). At the top of the limestone bedrock, a variation of the ash-fall pyroclastic soil

stratigraphic setting, corresponding to the absence of one or both pumiceous lapilli levels (C and Cb horizons), was recognized. Instead the shallower B horizon was always recognized.



**Figure 5.5.** Geomorphological features that characterize the initial debris slide area of L4 test site: (A) main scarp and slide surface, (B) and (C) rocky bench border.

Given the aim of the study, the setting of the monitoring station was designed based on the geological model previously reconstructed and specifically focused on monitoring hydrological parameters in each soil horizon of the ash-fall pyroclastic cover, thus it was designed in the perspective of collecting data selectively in each soil horizon.

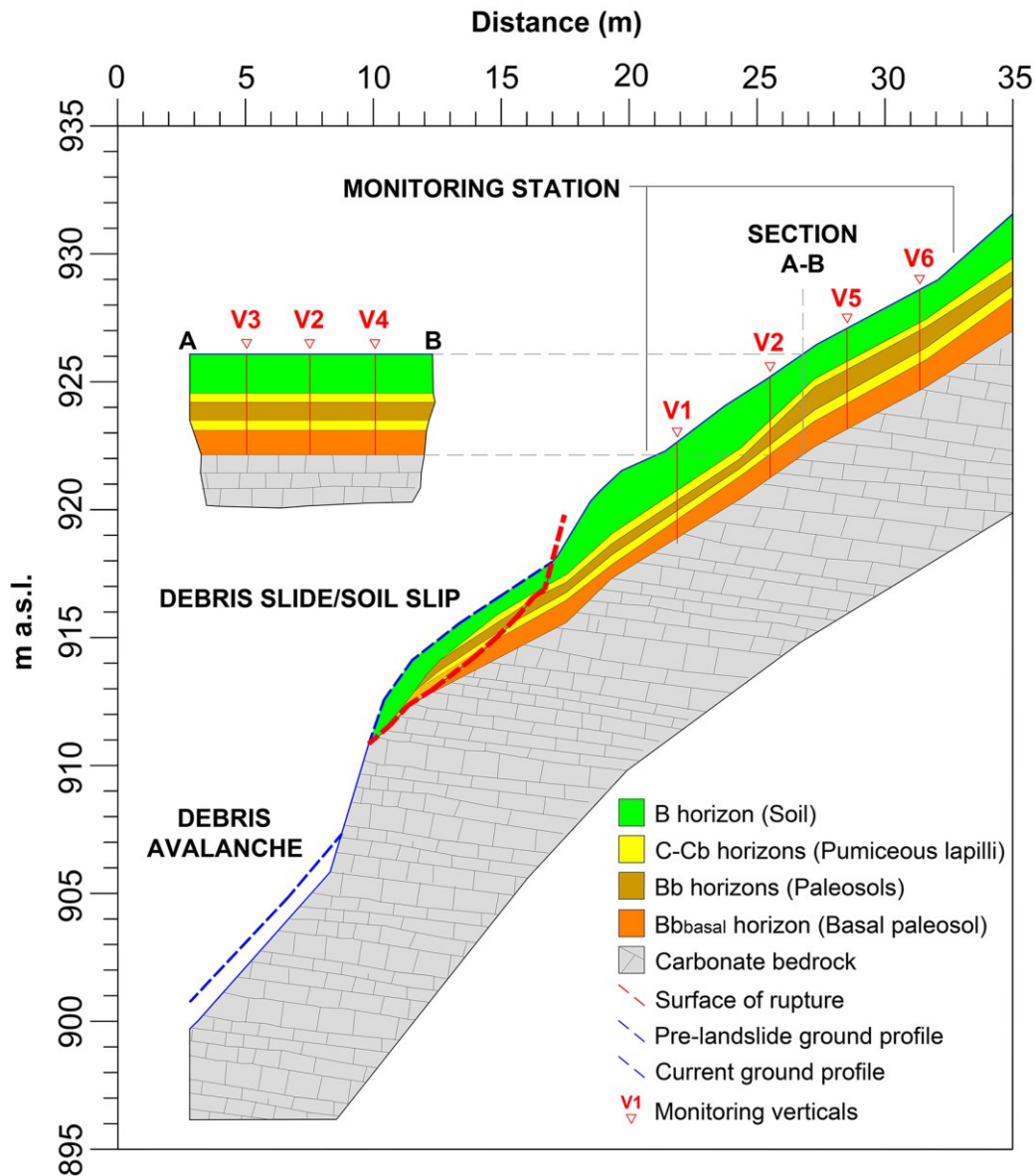


**Figure 5.6.** Engineering geological model of the L4 test area obtained by in situ investigations with schematic indication of the monitoring verticals.

Jet Fill tensiometers (Soilmoisture Inc.) and tensiometers provided at the top by rubber septum stoppers (Soil Measurement System Inc.), whose pressure range is well known to be comprised between 0.0 and -9.0 m at sea level, were used for pressure head monitoring to measure accurately higher pressure head during the rainy winter season (Fig. 5.7). For the latter, measurements were made by Tensicorder (Soil Measurement System Inc.), consisting of an electronic pressure dial to be connected to the internal part of the tensiometer tube by a nylon tubing and a syringe needle, puncturing the self-sealing rubber septum stopper. Instead, to measure lower pressure

head values Watermark sensors (Irrometer, Riverside, CA) were also installed, whose measurement is based on the electrical resistivity of a gypsum lamina and it is extended over a wider range of pressure head, down to -20.4 m (Fig. 5.7). Considering pressure head values recorded at the beginning of the monitoring period lower than the capability of Watermark sensors similar devices, MPS-2 sensors (Decagon technologies) (Fig. 5.7), were installed in the area. This devices allow to record very low pressure head values, due to their wider range of measurements (0 to -500 kPa). Moreover, soil temperature and volumetric water content were monitored by means of soil temperature sensors and ECH<sub>2</sub>O sensors (Irrometer, Riverside, CA).



**Figure 5.7.** Devices and wiring setting up of hydrological monitoring station in Sarno Mountains test area: A) Watermark sensors (Irrometer, Riverside, CA); B) automated tensiometers (Soil Measurement System Inc.); C) ECH<sub>2</sub>O sensor; D) MPS-2 sensor (Decagon technologies); E) Watchdog datalogger (Irrometer, Riverside, CA); F) EM50 datalogger (Decagon technologies); G) Field downloading phase of recorded data.

Assuming that the highest pressure head variations occur in the shallower horizons being more strongly influenced by rainfall events and evapotranspiration process, we decided to install the most part of sensors in the A and B soil horizons. Other sensors were distributed in the deeper Bb and Bb<sub>basal</sub> horizons (Table 5.2). No sensors were installed in the C horizon due to its coarse grain size, which prevents a good hydraulic coupling between soil and sensors and inhibits a reliable functioning.

Horizon	Tensiometer	Watermark	MPS-2	N° of sensors	Range depth (m)
B	16	8	3	27	0.0 ÷ 1.5
Bb	5	2	1	8	1.8 ÷ 2.5
Bbb	2	2	1	5	3.5 ÷ 4.0

**Table 5.2.** Number of sensors installed in the ash-fall pyroclastic mantle for suction monitoring at different depth (except for the C horizon).

For protecting measuring equipment against environmental damaging, plastic boxes were buried in the upper part of the B horizon (Fig. 5.8). Sensors were nested in six verticals arrangements and their upper terminations, including manometers, septum stoppers and dataloggers (Watchdog, Spectrum Technologies, Inc.; EM50, Decagon Technologies), were enclosed in as many sealed plastic boxes.



**Figure 5.8.** Installation phases of devices used for hydrological monitoring in L4 test area: 1) protective plastic boxes for devices; 2) automated tensiometers; 3) Watermark sensors; 4) MPS-2 sensors; 5) connecting cables; 6) protective plastic boxes for dataloggers.

Verticals were installed in alignment with two straight lines, respectively parallel and perpendicular to the slope direction line. The one in the slope direction line,

consisting of four verticals, was set starting from the crown zone and extended upslope for a length of 10.0 m. That normal to the slope direction line intersects the latter in the second vertical from the bottom and it is formed by two additional verticals extending for about 5.0 m (Fig. 5.9).

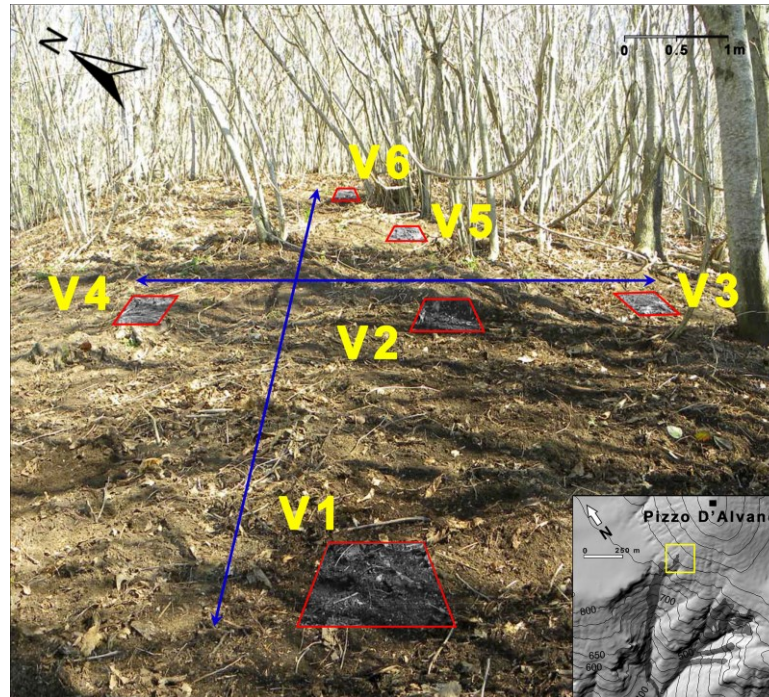
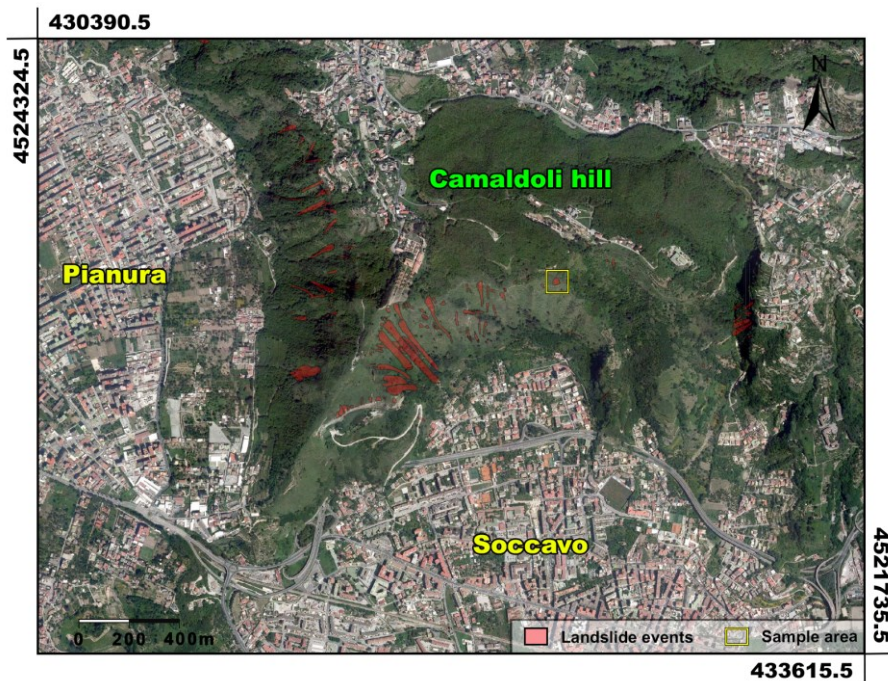


Figure 5.9. Location of boreholes that characterize the hydrological monitoring station.

In addition, a rain gauge was installed close to the monitoring station to comprehend the effect of rainfall processes on the hydrological regime of ash-fall pyroclastic soils and in the perspective of studying a possible formation of a throughflow, both in saturated and unsaturated conditions. Moreover, air temperature and air humidity sensors were installed to estimate evapotranspiration process. For the short periods of not working due to accidental damages, the rainfall time series was integrated with records derived by another rain gauge station installed by the Civil Protection Department in the nearby locality of Torriello (ID rain-gauge 15285). The monitoring period is comprised between December 2010 and December 2014 (about four years). The measurement frequency was set differently from tensiometers not provided of automated recording and other devices connected to dataloggers. In the first case the reading frequency was weekly. Instead, for the others the frequency was set with a periodicity of 10-15 minutes.

## 5.2. Camaldoli hill test area

The Camaldoli hill (458 m a.s.l.) is located in the northeastern part of Phlegraean Fields and its slopes impend above a large part of the city of Naples and its adjoining municipalities (Fig. 5.10). Field activities were carried out in a sample area along the southern slope of the Camaldoli hill, which is situated directly above the Soccavo borough (Naples town district), close to one of the triggering areas of the landslide event occurred on March 2005, whose geometries are still preserved and recognizable.



**Figure 5.10.** Location of the sample area corresponding to a source area (initial landslides) of debris flows occurred in the Camaldoli hill area before the March 2005 landslide event (Campania, southern Italy). A station for monitoring hydrological regime of the pyroclastic soil mantle was installed here.

Morphologically, the sample area is characterized by slope angles varying between  $5^\circ$  and  $35^\circ$ , upslope of the landslide scarp, where bamboo, ginestre bushes and sparse trees are present (Fig. 5.11). Starting from the main scarp, the volcanoclastic series is truncated and characterized by slope angles from  $50^\circ$  up to  $80^\circ$ , the latter where the NYT outcrops. This stratigraphic setting, not parallel to the slope, is related both to volcano-tectonic processes that characterized all the evolutionary phases of the Phlegraean Fields and to landslide processes. Further, although this area is actually vegetated by reeds, genista bushes and shrubs, the reconstruction of landslide

geometry and pre-landslide profile were carried out to estimate the volume of involved material to be approximately 900 m<sup>3</sup> (Fig. 5.11).

### 5.2.1. Reconstruction of the engineering-geological model

Different in-situ investigations consisting of borehole excavations, exploratory trenches, dynamic penetrometric tests and topographic surveys, were carried out to reconstruct an engineering-geological model of the area (Fig. 5.11; Fusco et al., 2016a; 2016c). The representative stratigraphic setting of the sample area exhibits a multilayered unconsolidated volcanoclastic series overlaying a bedrock formed by the NYT (15 k-years B.P.).

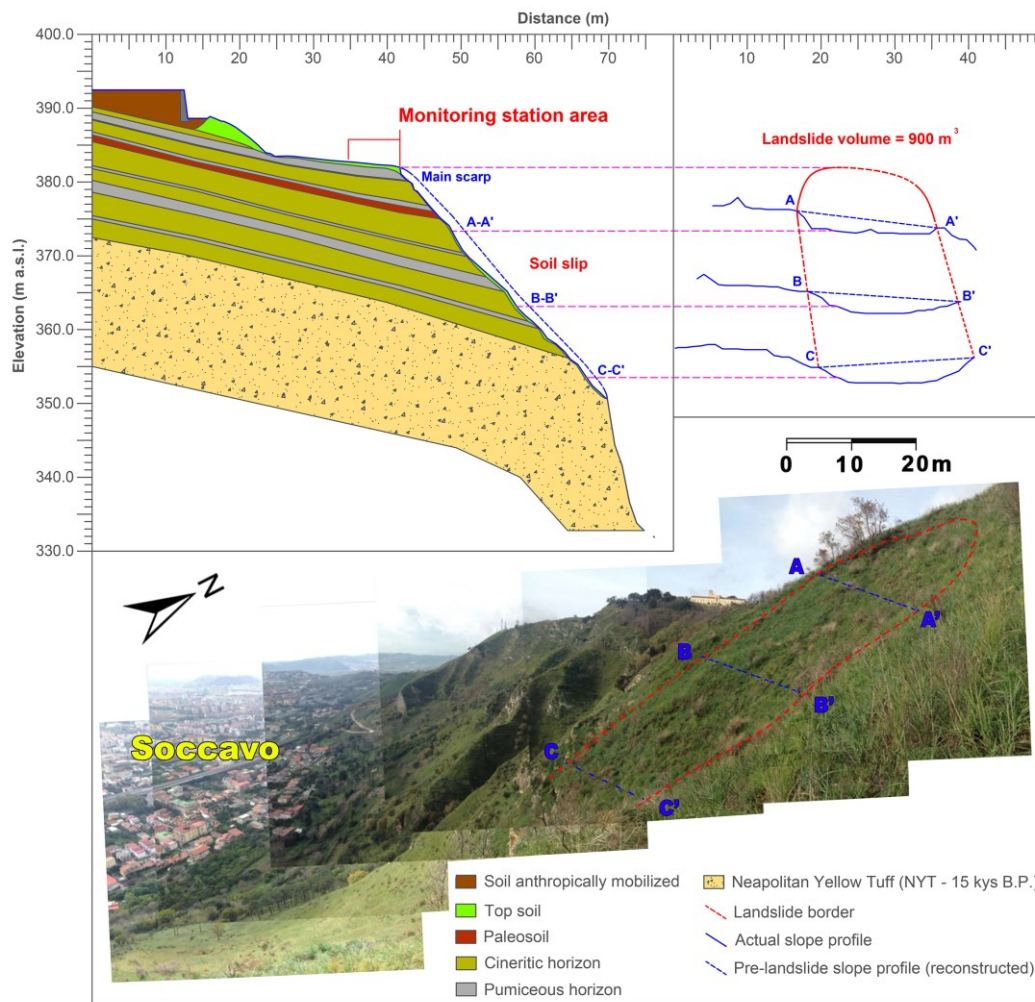


**Figure 5.11.** Engineering-geological model of the sample area reconstructed by field investigation with the monitoring station area are indicated. Geometry and actual photo of the landslide are also shown.

The volcanoclastic series (Table 5.3) is characterized by alternating pedogenized, cineritic and pumiceous horizons, derived by cycles of eruptive and dormant phases of the Phlegraean Fields volcanic district.

Range depth (m)	Lithological description	Horizon
0.00 ÷ 1.00	Very loose soil of pyroclastic horizons highly subjected to pedogenetic processes with dense root apparatuses and pumiceous lapilli. Generally dark brown colored (SM)	Topsoil
1.00 ÷ 2.50	Very loose white pumiceous lapilli layer with low degree of weathering (GP) and greenish ash content increasing to the top (GM). Agnano Monte Spina eruption (4 k-years B.P.)	Pumice
2.50 ÷ 2.60	Soil of pyroclastic origin constituted by fine to coarse ash and subordinately by pumiceous lapilli and burned remnants. Paleosoil (SM). Brown - red - dark red colored.	Paleosol
2.60 ÷ 4.60	Ash layer (SM) with pumiceous lapilli layer alternating (GW). Grey-greenish coloured Agnano eruption (4 k-years B.P.).	Ash / Pumice
4.60 ÷ 5.10	Pumiceous lapilli layer with low degree of weathering and lithic fragments (GP). White coloured. Agnano eruption (4 k-years B.P.)	Pumice
5.10 ÷ 6.10	Soil of pyroclastic origin constituted by fine to coarse ash and subordinately by pumiceous lapilli and carbon residues. Paleosoil (SM). Brown - yellowish colored.	Paleosols
6.10 ÷ 9.60	Alternation of fine ash (SM) and coarse sand (GP) with subordinately pumiceous lapilli and carbon residues. Grey-greenish coloured. Pisani eruption (5 k-years B.P.)	Ash
9.60 ÷ 10.0	Very loose light grey pumiceous lapilli layer with low degree of weathering (GP) and greenish ash increasing to the top (SM). Pisani eruption (5 k-years B.P.)	Pumice
10.00 ÷ 11.50	Alternating of fine (SM) and coarse (GM) ashes with subordinately pumiceous lapilli and carbon residues. Greenish colored. Minopoli eruption (8 k-years B.P.)	Ash
11.50 ÷ 13.50	Very loose pumiceous lapilli layer with low degree of weathering and lithic fragments (GW). Light grey coloured. Pomici Principali eruption (10 k-years B.P.)	Pumice
13.50 ÷ 17.00	Fine ash layer (SM) with pumiceous lapilli, lithic fragments and carbon residues. Grey-greenish coloured. Uncertain eruption.	Ash
17.00 ÷ 17.50	Very loose pumiceous lapilli layer with low degree of weathering (GP) and ash content increasing to the top (GM). Grey-greenish coloured.	Pumice
17.50 ÷ 20.00	Coarse ash layer with with-yellowish pumiceous lapilli and lithic fragments (SM). Layered texture related to the different grain sizes. Grey-greenish coloured. Loose facies of Neapolitan Yellow Tuff eruption (15 k-years B.P.).	Ash
> 20.00	Massive layer. Yellowish coloured. Lithified facies of Neapolitan Yellow Tuff eruption (15 k-years B.P.).	Tuff

**Table 5.3.** Reference stratigraphic setting of the sample area, derived by a borehole drilling. USCS classification of each horizon is also shown.

Disturbed and undisturbed soil specimens of the shallowest horizons of the volcanoclastic series (top-soil and uppermost cineritic horizon), were collected at different depths (down to 4.0 m) by manual digging and specific steel sampler boxes. Samples were tested by different geotechnical laboratory procedures to obtain saturated and unsaturated hydraulic properties as well as index and mechanical geotechnical characterizations (Fig. 5.12a-d). Further in situ investigations, consisting in infiltrometric tests by open single ring (Bouwer, 1986) and Amoozemeter (Amoozegar and Warrick, 1986) devices, were carried out to define the hydraulic conductivity of the first 2.50 m of the volcanoclastic series (Fig. 5.12c).

The characterization of index properties of the volcanoclastic soils showed the uppermost stratigraphic setting (down to 2.0 m), chiefly involved in slope instability process, as formed by the overlap of a loose sandy gravel with silt (SM), corresponding to the actual pedogenized horizon, over dense silty sand (SM) horizon, formed by fine ashes, sometimes with gravel (GP) intercalations (pumiceous lapilli). The fine ash (cineritic) horizon is characterized by higher shear strength and low saturated hydraulic conductivity values, in contrast to the uppermost pedogenized horizon, characterized by relatively lower shear strength and higher hydraulic conductivity.

Finally, water retention curves obtained using a pressure cell, showed high retention capacity for all the horizons, which is typical for pyroclastic soils (Table 5.3 and Fig. 5.12b).

Horizon	$K_{sat}$ (m/s)	$\theta_s$	$\theta_r$	$\alpha$	$n$
Top soil	$2.92 \times 10^{-4}$	0.619	0.180	3.080	1.670
Pumiceous layer	$2.82 \times 10^{-4}$	0.582	0.001	4.200	1.430
Paleosol	$4.45 \times 10^{-5}$	0.616	0.160	0.930	2.320
Ash layer	$1.57 \times 10^{-7}$	0.564	0.160	0.930	2.320

**Table 5.3.** Saturated ( $K_{sat}$ ) and unsaturated model parameters for SWRC, determined for each pyroclastic horizon by laboratory tests and ratio between vertical and horizontal hydraulic conductivity of the representative physical model. Key to symbols:  $\theta_s$  = saturated volumetric water content;  $\theta_r$  = residual volumetric water content;  $\alpha$  and  $n$  = van Genuchten (1980) model fitting parameters.

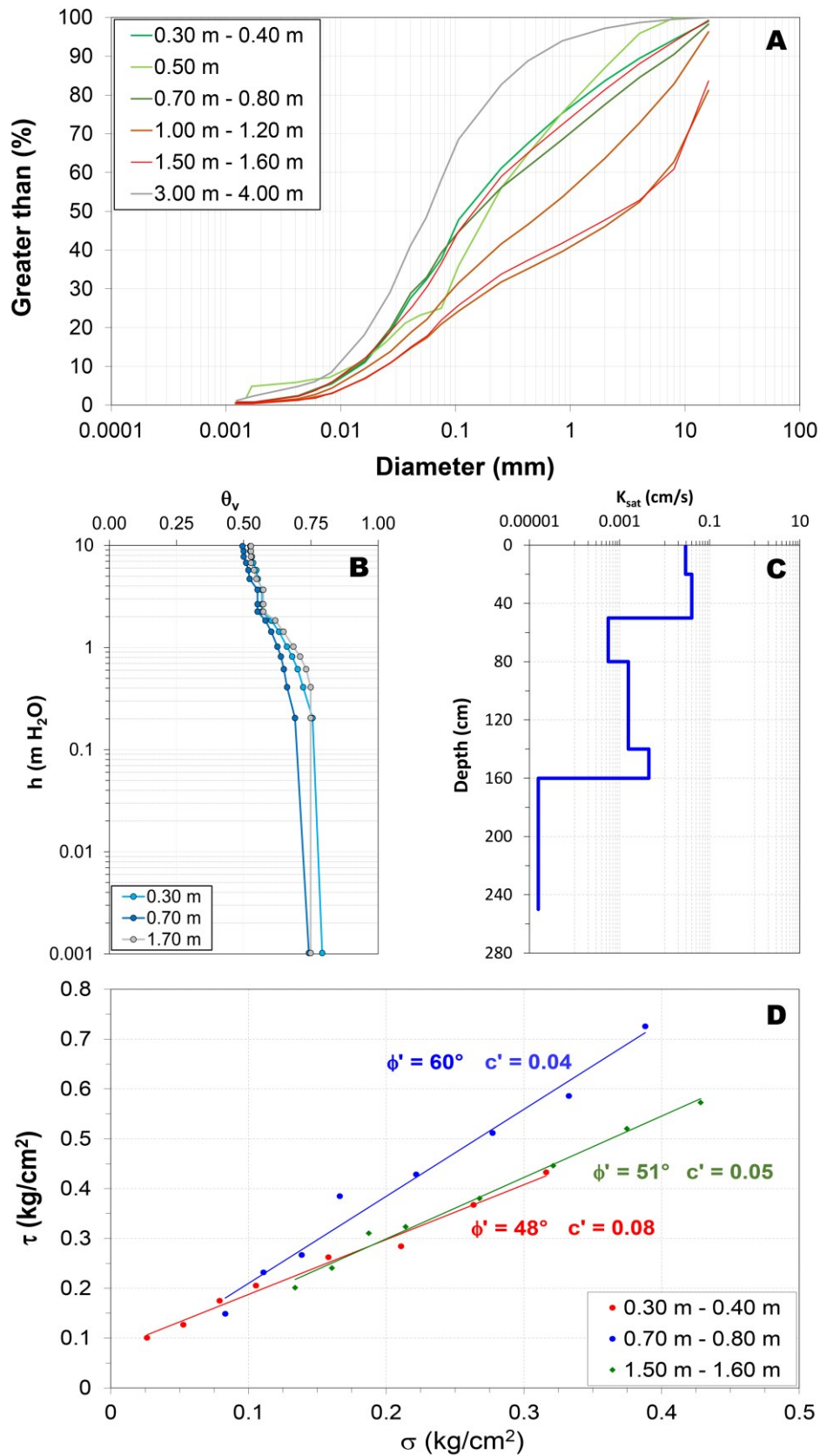


**Figure 5.12.** Mechanical and hydraulic properties deriving from laboratory and in situ tests: A) Grain size; B) Soil Water Retention Curves (SWRCs); C) Vertical log of saturated hydraulic conductivity ( $K_{sat}$ ); D) Shear strength ( $\tau$ ) and friction angle ( $\phi'$ ) values variation with depth (Fusco et al, 2016).

### 5.2.2. Setting up of the hydrological monitoring station

As for the Sarno monitoring station, also for the sample area of the Camaldoli hill, soil pressure head values were monitored upslope of the landslide source area using the same type of sensors, characterized by different measuring ranges (Table 5.4).

Horizon	Tensiometer	Watermark	MPS-2	N° of sensors	Range depth (m)
Top soil	2	2	3	7	0.0 ÷ 1.5
Ash	2	1	1	4	1.5 ÷ 2.5
Fine ash	0	1	1	2	4.0 ÷ 5.0

**Table 5.4.** Number of sensors installed in the shallowest part of the volcanoclastic series for suction monitoring at different depth.

Due to the aim of this research, all the devices were distributed following the morphology of the triggering area, most of them located in the shallowest part of the volcanoclastic sequence, and buried at different depths using enclosure boxes to preserve their integrity from wild fire (very frequent in this area) and damage from humans and/or grazing animals (Fig. 5.13). No sensors were installed into the pumiceous horizons due to their coarse grain size that does not allow hydraulic continuity with the devices.

The recordings of tensiometers and all other instruments were controlled by automatic dataloggers (Watchdog, Spectrum Technologies, Inc.; EM50, Decagon Technologies) with a 10 ÷ 15 minutes periodicity. Unfortunately, pressure head monitoring was affected by some data gaps due to accidental damage by animals and humans, maintenance works, and reaching the upper limit of the sensors' range.

Finally, rainfall and other basic hydrological and environmental parameters needed for the assessment of evapotranspiration rates at the daily time scale were obtained from a rain gauge station managed by the Civil Protection Department located upslope of the monitoring area (ID rain-gauge: 18891).

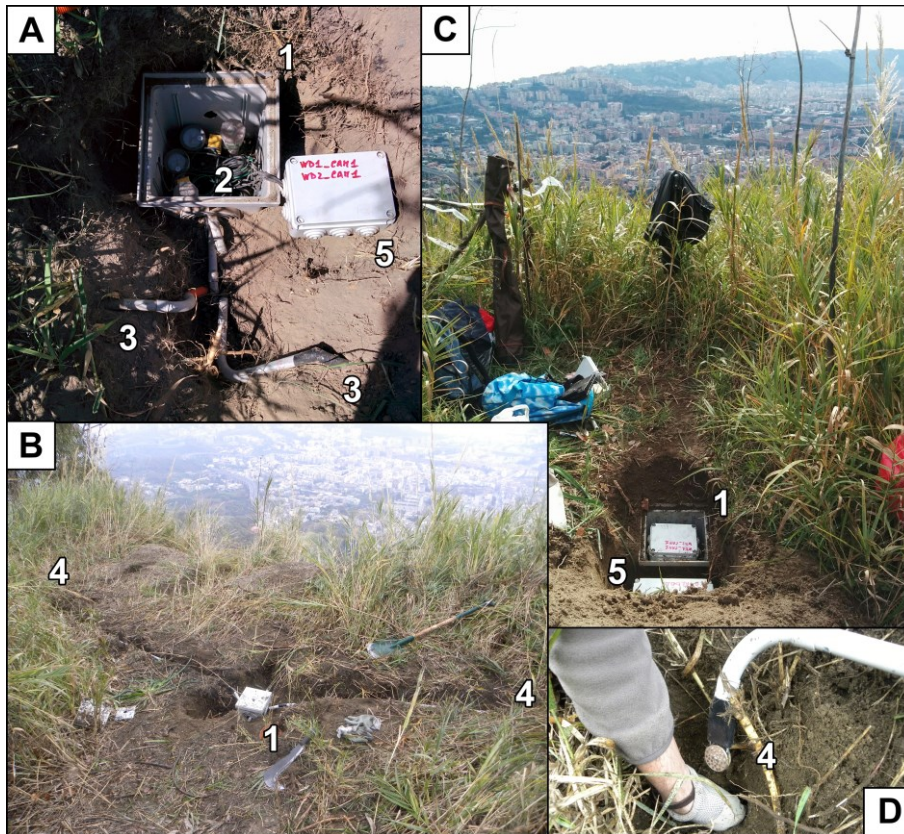


**Figure 5.14.** Installation phases of devices used for hydrological monitoring in L4 test area: 1) protective plastic boxes for devices; 2) automated tensiometers; 3) Watermark sensors; 4) MPS-2 sensors; 5) enclosure boxes for dataloggers.

### 5.3 Local scale hydrological and slope stability modelling for deterministic rainfall thresholds estimation

The hydrological and stability modelling at local scale was carried out using a physically-based 2D hillslope hydrologic model. Pore-pressure response to different rainfall intensities was simulated allowing the estimation of Intensity/Duration rainfall thresholds (Caine, 1980) by a deterministic approach. The used approach will be described in the following sub-paragraphs.

#### 5.3.1 Overview of VS2DTI code

The VS2DTI code is a graphical software package for simulating fluid flow and solute or energy transport in variably saturated porous media, suitable for the unsaturated/saturated domains. This code simulates two-dimensional movement of

water, or any other solute flow and transport through variably saturated systems, considering planar or cylindrical geometries. The package integrates a graphical interface (Hsieh et al., 2000), where the user can draw the simulated domain and enter or modify model parameters with existing models of flow and a standalone post-processor, for displaying results saved from previous simulation runs.

The finite difference method is used by VS2DTI to approximate the flow equation, which is developed by combining the law of conservation of fluid mass with a nonlinear form of Darcy's equation (Richards' equation). The resulting mathematical model or flow equation is written in terms of total hydraulic potential, considered as the dependent variable, thus allowing dealing with both saturated and unsaturated conditions.

As previously mentioned, the equation of water movement [Eq. 5.1], under isothermal and equal or constant salinity conditions, is developed by combining the conservation of mass for water, and the equation for fluid flux and storage (Lappala et al., 1987):

$$\int_f \frac{\partial(\rho s \Phi)}{\partial t} dv + \int_{\bar{s}} \rho \vec{u}_n d \bar{s} - \int_f \rho q dv = 0$$

[5.1]

where:

$\rho$  = liquid density [ML<sup>-3</sup>];

$s$  = liquid saturation [adimensional];

$\phi$  = porosity [adimensional];

$t$  = time [T];

$\vec{u}_n$  = liquid flux per unit area in the direction  $n$ , that is normal to  $\bar{s}$  that is the surface [LT<sup>-1</sup>];

$q$  = volumetric source-sink term accounting for liquid added (+ $q$ ) or taken away from (- $q$ ) the volume  $v$ , per unit volume and unit time.

This equation states that the rate of mass change in a volume  $v$  must be balanced by the sum of liquid flux across the surface boundary of  $v$  and of liquid added (by

source) or removed (at sink) [Eq. 5.4]. Besides, it is assumed that volume  $v$  is small enough that  $\rho$ ,  $s$ , and  $\phi$  can be considered constant:

$$\int_f \frac{\partial(\rho s \Phi)}{\partial t} dv = v \frac{\partial(\rho s \Phi)}{\partial t} \quad [5.2]$$

and:

$$\int_f \rho q dv = p q v \quad [5.3]$$

Finally, the equation can be simplified as:

$$v \frac{\partial(\rho s \Phi)}{\partial t} + \int_{\bar{s}} \rho \vec{u}_n d\bar{s} - \rho q v \quad [5.4]$$

As regards the flux normal to the surface  $\bar{s}$  that bounds  $v$ , it is described by Darcy's law extended to variably saturated conditions [Eq. 5.5]:

$$\vec{u}_n = \frac{K K_r(h) \rho g}{\mu} \times \frac{DH}{\partial n} \quad [5.5]$$

where:

$K$  = intrinsic permeability of the medium [ $L^2$ ];

$K_r(H)$  = relative hydraulic conductivity to liquid as function of pressure head [ $L^0$ ];

$H$  = pressure head [ $L$ ];

$g$  = gravitational acceleration [ $LT^{-2}$ ], [ $ML^{-1}T^{-1}$ ];

$\mu$  = dynamic viscosity of the liquid, expressed as height of the liquid column [ $L$ ].

Pressure head below water table is measured while total hydraulic potential  $H$  was chosen as the principal independent variable, thus allowing a simple treatment both in saturated and unsaturated conditions. For this reason, the solution of the non-linear flow equation requires that the initial values of  $H$  is specified everywhere in the solution domain. However, the non-linear equation used by VS2DTI does not have a general analytic solution and then numerical approximations of spatial and temporal derivatives are required. Spatial derivatives are approximated by a *block-centered* regular finite difference scheme, whose grid can be rectangular or cylindrical and nodes are located in the center of each block or cell (Fig. 5.15).

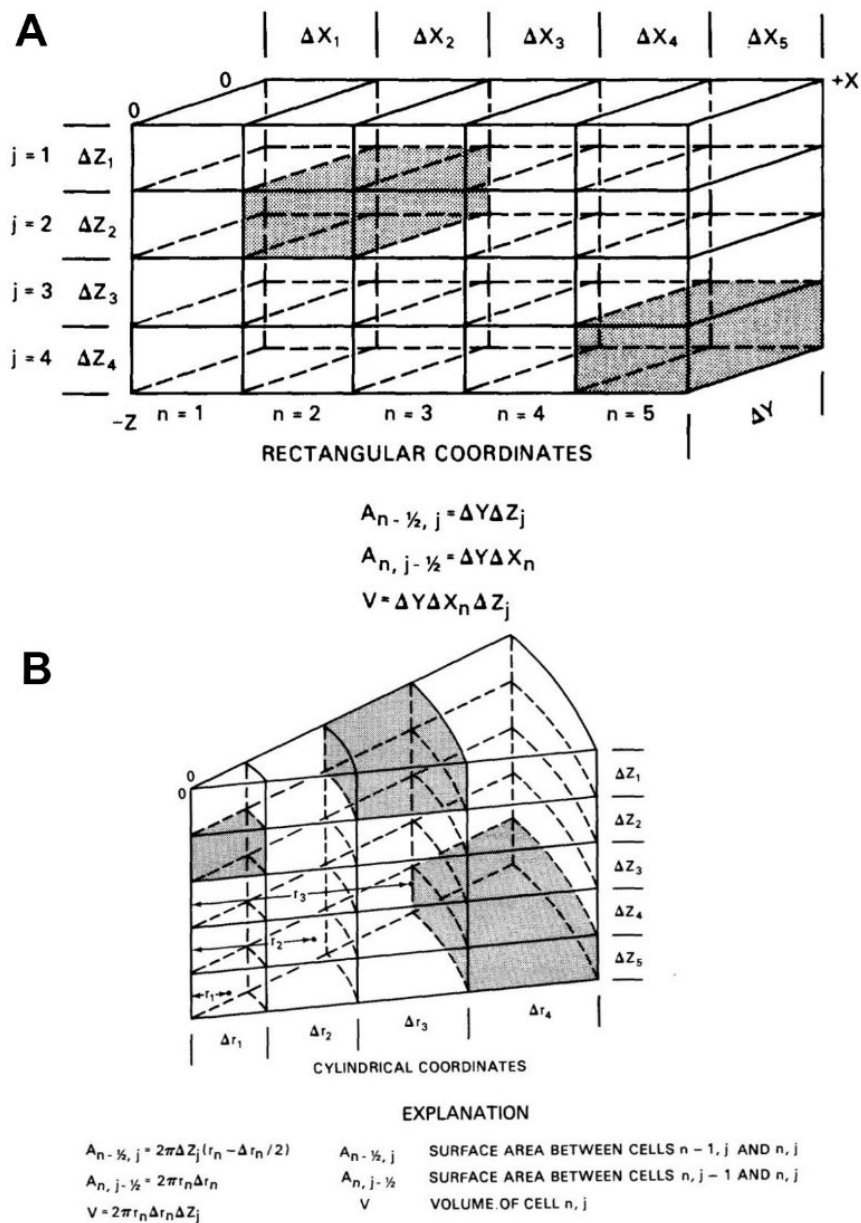


Figure 5.15. Representative block-centered scheme (Lappala et al., 1987)

Using this finite difference scheme, saturated hydraulic conductivities (conductance) must be evaluated at cell boundaries considering a harmonic mean (Appel, 1976), for multilayered saturated systems, and a geometric mean (Haverkarap and Vauclin, 1979), for unsaturated systems.

As regard the temporal derivatives approximation, VS2DTI requires to specify the duration of the temporal step and the maximum variation of next temporal step. Furthermore, the user must specify the maximum duration of the temporal step and the maximum computed pressure head value of each cell.

Finally, initial conditions required for the solution of the flow equation can be specified by reading initial volumetric moisture content ( $\theta$ ) or the initial pressure head (H).

The program computes the pressure head, or the volumetric moisture content, using the appropriate moisture content/pressure head function, or its inverse (Brooks and Corey, 1964; Gardner, 1958; Haverkamp et al., 1977; van Genuchten, 1980). Several boundary conditions that are specific to flow under unsaturated conditions can be defined:

- *specific flux and potential*, respectively described by the Neumann boundary condition (specified  $\nabla H$ ) and Dirichlet boundary conditions (specified H). The Neumann boundary conditions can be properly specified, but the Dirichlet conditions cannot; with a *face-centered* grid, the Dirichlet condition specification is straight-forward, because the nodes are located on the boundaries; flux boundary conditions require special formulation of the equations for each face across which the flux takes place. The specified flux boundary condition is implemented in the code by an equation in which each term represents the flux across a cell face;
- *evapotranspiration*, where the loss of water from the system, by plants transpiration or direct ground evaporation, can be simulated. In this case evaporation and transpiration values and different plants parameters are required;
- *seepage faces*, along which the water can leave from the system (usually at the domain/atmosphere interface);
- *gravity drainage*, where the water affected by gravity force can leave from the block, or cell, following a vertical path.

### 5.3.2. Short-term and long-term hydrological modelling for Sarno tests area

Taking into account the engineering-geological models of Sarno Mountains sample initial areas, finite-difference hydrological modeling by means of the VS2DTI numerical code was performed. The physical model of L4 sample area was used for the model calibration phase considering a period corresponding to the monitoring activity between January 2011 and December 2011. In this stage, simulated and measured pressure head time series were compared. Then, a second phase with a long-term simulation was carried out over about 11 hydrological years running from January 2000 to December 2011 to analyze the hydrological behavior of ash-fall pyroclastic cover.

#### 5.3.2.1. Estimation of daily evapotranspiration rate

An early step to set up the representative models was to verify the ability to estimate actual evapotranspiration. Given the availability of climatic data of daily rainfall and air temperature for the period 2000 ÷ 2011, gathered by a meteorological station (ID Station - 18285 - Torriello) which was installed after the events of May 1998, the potential evapotranspiration was estimated by the Thornthwaite (1948) formula [Eq. 5.6], at a monthly time scale:

$$(ET_p)_i = K \left[ 1.6 \times \left( \frac{10 \times T_i}{I} \right)^a \right] \quad [5.6]$$

with:

$I$  = heat index, which depends on the 12 monthly mean air temperatures ( $T_i$ ) and is a constant for a given location:

$$I = \sum_{i=1}^{12} \left( \frac{T_i}{5} \right)^{1.514} \quad [5.7]$$

where:

$(ET_p)_i$  = mean potential evapotranspiration for the  $i$  month (cm);

$K$  = latitude correction coefficient referred to the  $i$  month, equal to the ratio between the actual daylight hours and half the hours per day (12);

$T_i$  = mean air temperature of the  $i$  month (C°);

$$a = (6.75 \times 10^{-7} \times I^3) - (7.71 \times 10^{-5} \times I^2) - (1.79 \times 10^{-2} \times I) + 0.49$$

Potential evapotranspiration obtained by the Thornthwaite formula was compared with soil moisture losses of the entire ash-fall pyroclastic column measured by pressure-head monitoring (January 2011 ÷ December 2011). Such a comparison was based on the experimental observation that the greatest part of soil moisture loss occurs between late spring and late summer due to the intense evapotranspiration related to activity of the deciduous forest (*Castanea sativa*), while moisture loss is very low in the rest of the year owing to the activity of a scarce brushwood vegetation only. Another assumption was the negligibility of water losses through the carbonate bedrock, between late spring and late summer, which is motivated by scarce rainfall events, pressure-head values below the Field Capacity (FC), and the great soil moisture consumption of the deciduous forest. In detail, pressure-head data recorded in 2011 were used to determine water-content variations along the whole pyroclastic soil column through soil-water retention curves previously estimated (De Vita et al., 2013). Indeed, having monitored the pressure-head regime of the whole soil column down to the bedrock, this approach was considered reliable for taking into account the soil-moisture loss of the entire ash-fall pyroclastic mantle (Fig. 5.16).

The validation of the applicability of the Thornthwaite equation and the assessment of the pressure-head regime through weekly measurements were completed as follows:

- the first was to verify the applicability of the Thornthwaite method to estimate monthly actual evapotranspiration in the antecedent period, beginning in 2000, when soil hydrological monitoring data were not available.
- the second was to model the regime of evapotranspiration, related to the activity of the deciduous forest, in order to downscale estimates of monthly actual evapotranspiration to the daily time scale.

Given these assumptions and considering the pressure-head range, recorded between the beginning of June 2011 and the end of September 2011, SWRCs of each pyroclastic-soil horizon (De Vita et al., 2013) and their thicknesses, the model estimated a total soil moisture loss of about 633mm. This result was found as comparable to the estimation of potential evapotranspiration by the Thornthwaite (1948) formula, thus permitting to apply it for other years without monitoring and consider actual evapotranspiration as corresponding to the potential one.

Therefore, we considered the Thornthwaite equation applicable to estimate actual evapotranspiration.

Moreover, the pressure-head regime recorded during the monitoring period (2011) showed a strong seasonal variability, strictly controlled by the transpiration process of the deciduous forest. This understanding allowed to downscale at the monthly scale actual evapotranspiration according to the variability of the Leaf Area Index (LAI) for deciduous forests (Maass et al., 1995; Rautiainen et al., 2012).

More precisely, a Gaussian-shape time-distribution model of daily rates of actual evapotranspiration was adopted (Fig. 5.16) according to the common seasonal pattern of LAI for deciduous forests. A peak value of about  $7 \text{ mm day}^{-1}$  was set during the period of maximum root activity (June to September), and a constant minimum value of about  $0.05 \text{ mm day}^{-1}$  was set throughout the dormant period of the deciduous forest characterized by no leaf retention (October to March).

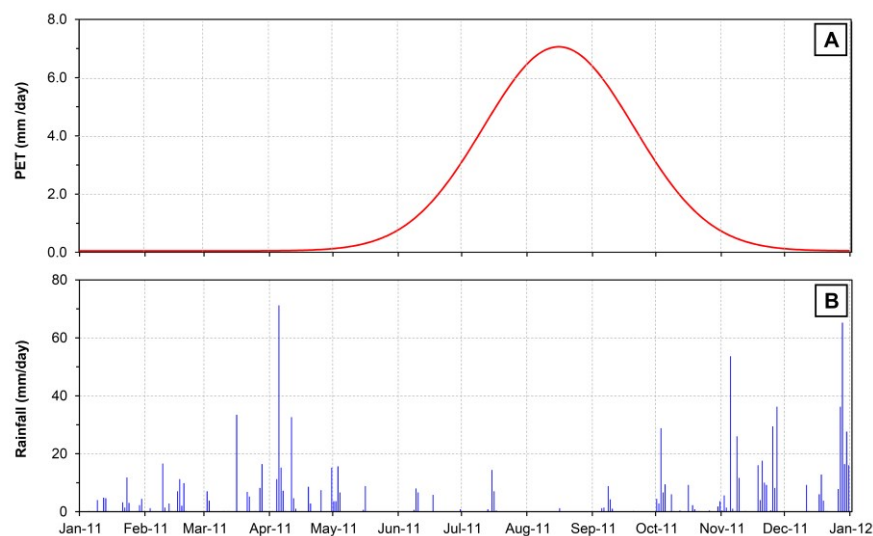


**Figure 5.16.** A) Gaussian-shape time-distribution model of daily rates of actual evapotranspiration estimated with Thornthwaite (1948) equation; B) rainfall data series obtained by the Civil Protection Department database (ID Station - 18285 - Torriello - Sarno Mountains).

### 5.3.2.2. Model calibration (short-period) and long-period hydrological modelling

The first phase of the VS2DTI hydrological modelling at the site-specific scale was addressed to calibrate the representative slope model of the Sarno Mountains sample area. At this scope was considered only the L4 test site, where a monitoring station was installed.

Starting from the 2D engineering-geological model, corresponding to a longitudinal cross-section of the slope passing through the initial debris slide, the physical model was set up (Fig. 5.17). The unsaturated and saturated hydraulic properties of pyroclastic horizons (Tables 5.5 and 5.6) were derived from previous research (De Vita et al., 2013).

Soil Horizon (USDA)	$K_{sat}$ (m/s)			No.
	25 <sup>th</sup> percentile	Median	75 <sup>th</sup> percentile	
B	$4.82 \times 10^{-5}$	$8.34 \times 10^{-5}$	$1.26 \times 10^{-4}$	24
C	$2.82 \times 10^{-3}$	$3.82 \times 10^{-3}$	$1.26 \times 10^{-2}$	29
Bb	$6.00 \times 10^{-6}$	$2.22 \times 10^{-5}$	$2.64 \times 10^{-5}$	7
Bb <sub>basal</sub>	$2.48 \times 10^{-7}$	$1.94 \times 10^{-6}$	$6.84 \times 10^{-6}$	15

**Table 5.5** Statistics of saturated hydraulic conductivity ( $K_{sat}$ ) determined for each ash-fall pyroclastic soil horizon (De Vita et al., 2013) in Sarno Mountains area. The number of measurements related to statistic values was reported in the last column.

Soil horizon	$K_{sat}$ (m/s)	$\theta_s$	$\theta_r$	$\alpha$	n	$K_z/K_h$
B	$8.34 \times 10^{-5}$	0.505	0.083	0.884	1.307	1
C	$3.82 \times 10^{-3}$	0.500	0.001	20.39	1.081	1
Bb	$2.22 \times 10^{-5}$	0.663	0.001	0.884	1.307	1
Cb	$3.82 \times 10^{-3}$	0.500	0.001	20.39	1.081	1
Bb <sub>basal</sub>	$1.94 \times 10^{-6}$	0.500	0.001	20.39	1.081	1
R	$3.82 \times 10^{-3}$	0.030	0.020	4.310	3.100	10

**Table 5.6** Saturated hydraulic conductivities ( $K_{sat}$ ), SWRC parameters and ratios between vertical and horizontal hydraulic conductivity determined for each pyroclastic horizon of the three initial landslide models (De Vita et al., 2013) for the Sarno Mountains area. Key to symbols:  $K_z$  = vertical hydraulic conductivity;  $K_h$  = horizontal hydraulic conductivity;  $\theta_s$  = saturated volumetric water content;  $\theta_r$  = residual volumetric water content;  $\alpha$  and n = fitting parameters.

The ground surface was set as a vertical flux boundary, to which a variable daily rainfall intensity and an evapotranspiration rate were assigned, according to measurements and estimates. The boundary conditions both at the upstream and downstream ends were set as seepage faces. The bedrock was assumed to be a rock-mass whose fractures are filled by pyroclastic soils of the basal paleosol ( $Bb_{\text{basal}}$  in Table 5.6). Therefore, the saturated hydraulic conductivity of the bedrock was set to 5% of that of the lowest pyroclastic soil horizon, according to a correspondent value of the rock-mass porosity of discontinuity systems, and the unsaturated hydraulic properties were set equal to the basal paleosol. The bedrock thickness was assumed equal to 5 m, with a free seepage lower boundary to simulate open fractures, not filled by pyroclastic soil, and free percolation to basal groundwater of the carbonate aquifer.

Time-varying parameters controlling water extraction by evapotranspiration, such as Rooting Depth (RD), Activity at Root Base (ARB), Activity at Root Top (ART), and the Pressure Head in Root (PHR) were set according to field observations and adjustments related to the model calibration (Table 5.7). Two RD values were considered to simulate respectively the activation of the deepest root system of the deciduous chestnut forest (4.0 m), during spring and late autumn, and the soil moisture removal due to the evapotranspiration of the evergreen shrubby brushwood which continues also during winter (0.5 m). The ARB and ART, both considered as the ratio between the total length of root apparatuses and the soil volume, were determined by field observations and measurements. Such root parameters were successively adjusted by the calibration of the numerical model after several trials and the assessment of their effects of transpiration rates during vegetative and dormant periods of forest growth. The PHR were set approximately equal to that of the PWP (-150.0 m). Furthermore, to assess pressure head distribution within the pyroclastic mantle, three observation verticals were identified for different slope sectors of the model. The verticals were aligned along the longitudinal profile of the slope and consisted of four to five observation points, located in the middle of each pyroclastic horizon. Therefore, simulated pressure head values were considered representative of the correspondent stratigraphic horizon. The locations of the observation verticals were set in proximity of the field monitoring verticals, in order to facilitate direct comparison of measured and observed hydrologic data. Initial pressure-head conditions were set up equal to those measured in January 2011, which varied in the range between -1.0 m and -2.0 m (Fusco et al., 2013; Fusco and De Vita, 2015). These values were comparable with

those previously measured during winter for shallower pyroclastic soil horizons (Bilotta et al., 2005; Sorbino, 2005).

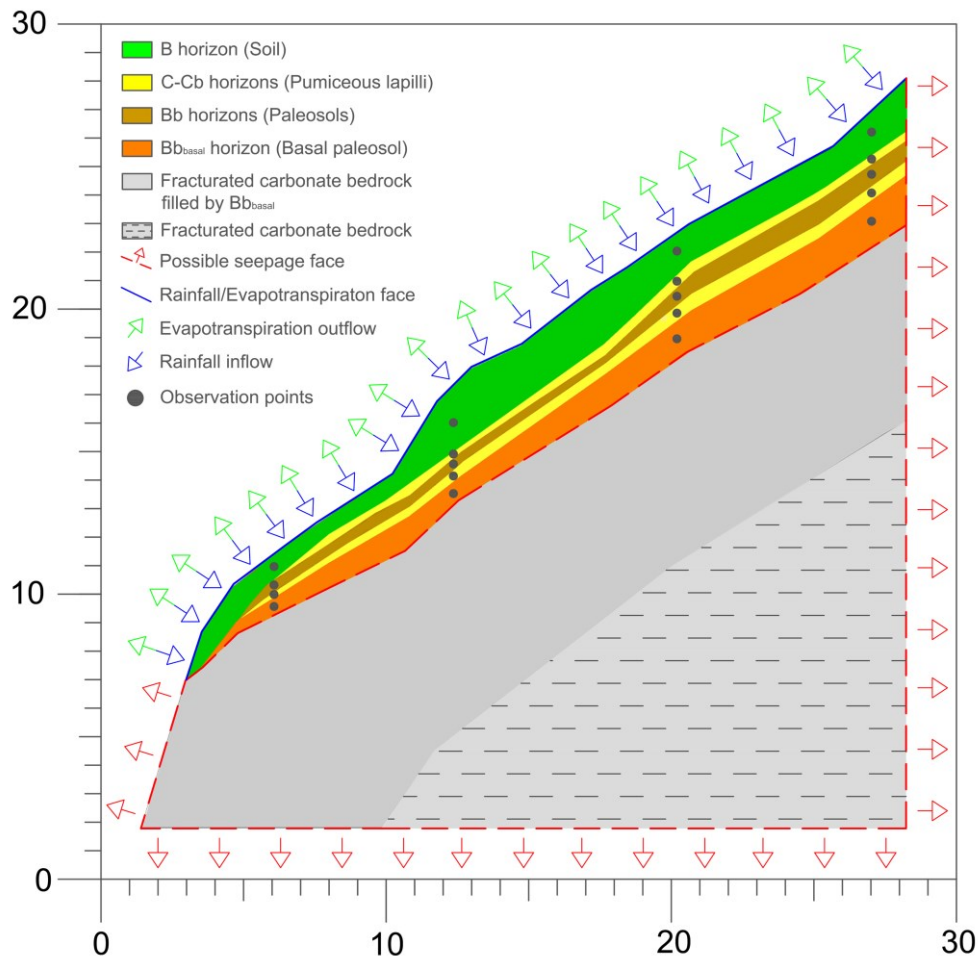


Figure 5.17. Setting of the slope hydrological model used in VS2DTI for Sarno Mountains area.

Period (month-month)	RD (m)	ARB (m <sup>2</sup> )	ART (m <sup>2</sup> )	PHR (m)
Jan - Feb	0.5	0.1	0.1	-150.0
Mar - Dec	4.0	1.5	1.5	-150.0

Table 5.7. Root parameters adopted in VS2DTI model for Sarno Mountains area to simulate soil moisture extraction by plant transpiration within the pyroclastic mantle. RD = Rooting Depth; ARB = Activity at Root Base; ART = Activity at Root Top; PHR = Pressure Head in Root.

The numerical model was calibrated for the monitoring period (2011) by adjusting iteratively saturated hydraulic conductivity (Table 5.6) and root parameters (Table 5.7), until the lowest value of the sum-of-squared residuals between measured and

simulated values (objective function) was reached.

Once achieved the best calibration for the L4 physical model, a second phase of long-term hydrological modelling was carried out to analyze the hydrological behavior of ash-fall pyroclastic cover. During this phase, 11 hydrological years, from January 2000 to December 2011, were modeled considering the same set up of L4 physical model previously used in the calibration phase. Also in this case, climate data, including rainfall and air temperature and humidity, derived from the Italian Civil Protection database while the evapotranspiration distribution, already estimated for 2011 year, was used for each year, from 2000 to 2011. The initial pressure head conditions were estimated by two consecutive runs in order to achieve typical hydrological conditions of January:

- 1) warm-up run, based on measured pressure head values during monitoring of December 2011 and extended over the period 2000-2011;
- 2) second run, in which median values obtained for each January of the whole modelled period (2000-2011) were considered.

The aim of this modelling phase was to obtain representative soil-moisture conditions of the ash-fall pyroclastic cover, by using a statistical approach, to be used for simulating critical rainfall conditions for slope stability and then to define deterministic rainfall thresholds.

### **5.3.3. Short-term and long-term hydrological modeling for the Camaldoli test area**

Similarly to the sample area of the Sarno Mountains, a representative physical model of the Camaldoli hill test site was developed by the reconstruction of an engineering-geological model and the unsaturated/saturated hydraulic characterization of the volcanoclastic series (Table 5.8). Following the same approach previously used, the first step was the calibration of the model by adjusting plant root parameters and temporal distribution of evapotranspiration to match as better as possible simulated and measured pressure head time series for the 2015 hydrological year. The second step was to extend backward in time the calibrated model over a long-term time span (2006-2015), for which rainfall and air temperature data were collected by the regional meteorological network of the Civil Protection Department

(ID Station - 18891 - Napoli Camaldoli) (Fig. 5.18). Despite the high thickness of the volcanoclastic series, considering the typical shallowness of slope instabilities, which usually involve the top soil only, the domain of the numerical model was limited at the first 10 m of the series. The ground surface of the physical model was set as a vertical flux boundary, to which a variable daily rainfall or evapotranspiration rates were applied. The boundary conditions in the upstream and downstream ends and at the bottom of the domain were set as seepage faces. Unsaturated and saturated hydraulic properties of the horizons derived from field and laboratory tests were used to complete this physical model, thus setting values of van Genuchten's (1980) model parameters of Soil Water Retention Curves (SWRCs) and of saturated hydraulic conductivity ( $K_{sat}$ ) for each horizon considered.

Horizon	$K_{sat}$ (m/s)	$\theta_s$	$\theta_r$	$\alpha$	$n$	$K_z/K_h$
Top soil	$2.92 \times 10^{-4}$	0.619	0.180	3.080	1.670	1
Pumiceous layer	$2.82 \times 10^{-4}$	0.582	0.001	4.200	1.430	1
Paleosol	$4.45 \times 10^{-5}$	0.616	0.160	0.930	2.320	1
Ash layer	$1.57 \times 10^{-7}$	0.564	0.160	0.930	2.320	1

**Table 5.8.** Saturated ( $K_{sat}$ ) and unsaturated model parameters for SWRC, determined for each pyroclastic horizon of Camaldoli hill area by laboratory tests and ratio between vertical and horizontal hydraulic conductivity of the representative physical model. Key to symbols:  $K_z$  = vertical hydraulic conductivity;  $K_h$  = horizontal hydraulic conductivity;  $\theta_s$  = saturated volumetric water content;  $\theta_r$  = residual volumetric water content;  $\alpha$  and  $n$  = fitting parameters.

As regards the time-varying parameters controlling water losses by evapotranspiration, such as Rooting Depth (RD), Root Activity at Base (RAB), Root Activity at Top (RAT), and the Root Pressure Head (RPH) were set according to field observations and adjustments related to the model calibration (Table 5.9). Two RDs values were considered to simulate the activation of the reeds and genista bushes root systems during spring and late autumn (1.5 m deep) and during winter (0.3 m), respectively. According to January 2015 field measurements, the initial pressure head values were set to match typical winter values, ranging from -1.5 m to -40.0 m (Evangelista et al., 2003; Evangelista and Scotto Di Santolo, 2004; 2007; Fusco et al., 2016a; 2016c). Furthermore, to assess pressure head distribution within the considered

volcaniclastic series, four measurement verticals were selected for different slope sectors, aligned along the longitudinal transect and consisting of ten observation points located every 0.20 cm of depth. One of the observation profiles was set coincident to the field monitoring vertical, to allow direct comparison of simulated output with measured data. Following a trial and error approach, previously used for the Sarno Mountains area, the model was calibrated by means of the adjustment of the evapotranspiration rate, which was regulated. The greatest proportion of water loss via evapotranspiration was assumed to occur during the late spring through late summer, when rainfall is limited and plants are actively transpiring. Using Thornthwaite's equation (Thornthwaite, 1948) the annual evapotranspiration rate was estimated and distributed throughout the year following a Gaussian-shape time-distribution model of daily rates with a peak in summer and minimum in winter (Fig. 5.18). Considering monitored pressure head data, the hydrological numerical model (Fig. 5.19) was calibrated by optimizing the matching between measured and simulated pressure head values.

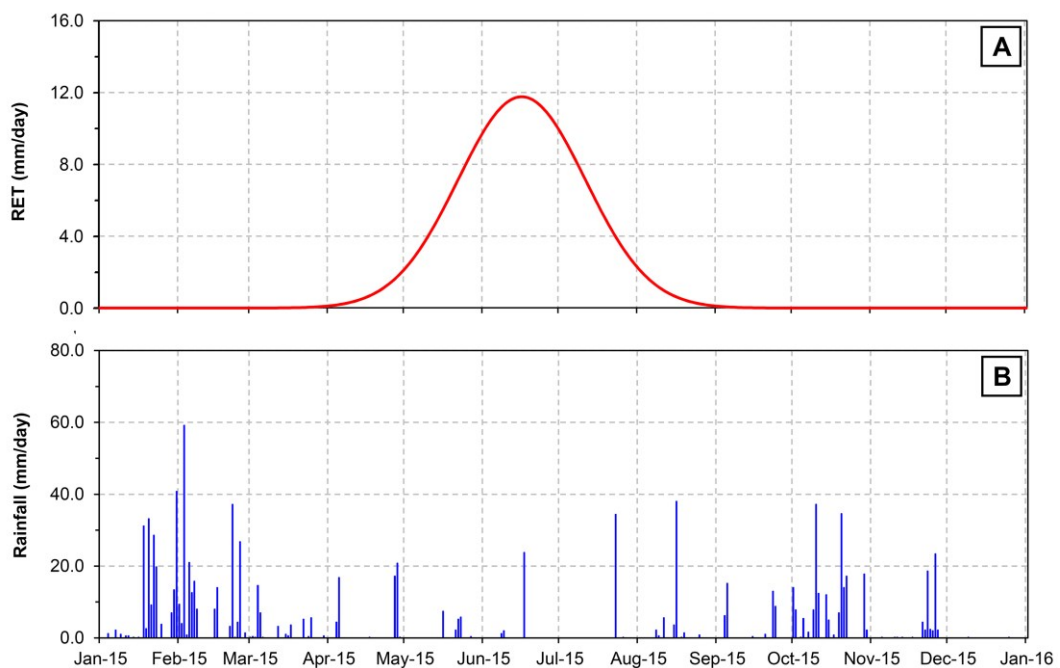


**Figure 5.18.** A) Gaussian-shape time-distribution model of daily rates of actual evapotranspiration estimated with Thornthwaite equation (1948); B) rainfall daily series obtained by the Italian Civil Protection Department database (ID Station - 18891 - Napoli Camaldoli - Camaldoli hill).

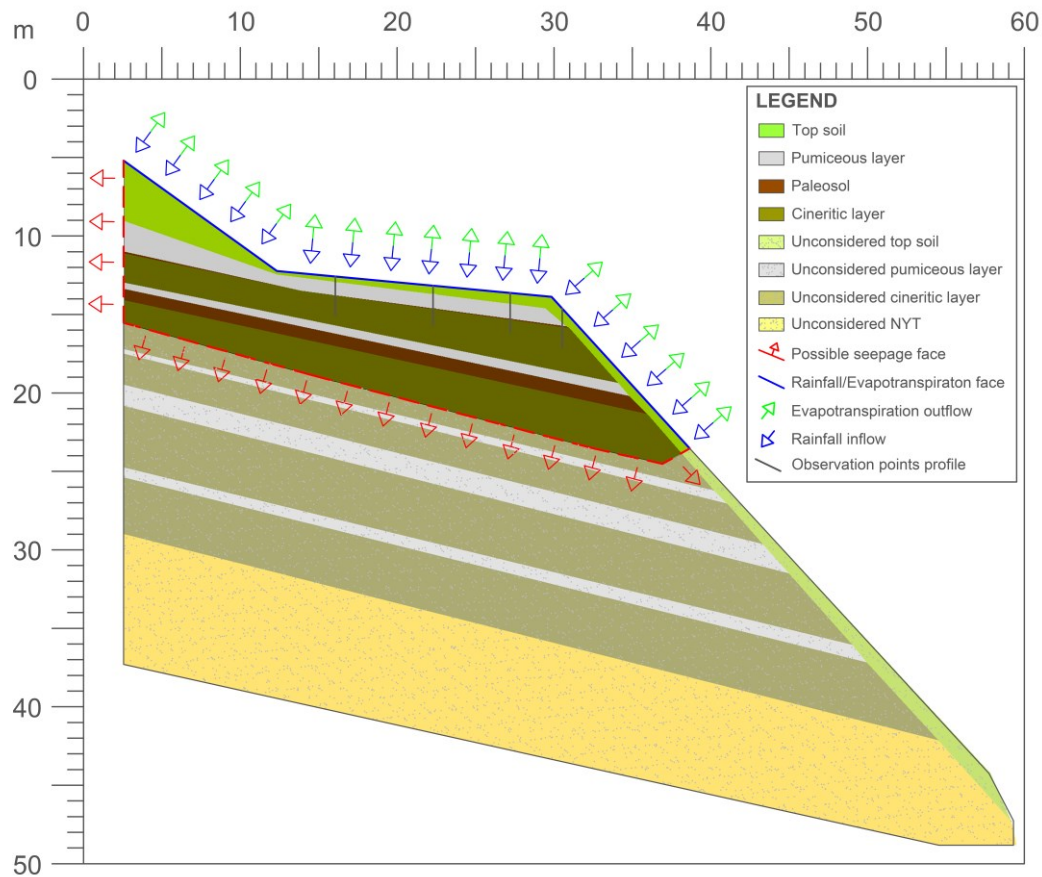


**Figure 5.19.** Setting of the slope hydrological model for Camaldoli hill area used in VS2DTI.

Period (month-month)	RD (m)	ARB (m <sup>2</sup> )	ART (m <sup>2</sup> )	PHR (m)
Jan ÷ Feb	0.3	0.1	0.1	-100.0
Mar ÷ Sep	1.5	0.5	3.0	-600.0
Oct ÷ Dec	0.3	0.1	0.1	-100.0

**Table 5.9.** Root parameters used in VS2DTI model to simulate plant transpiration and soil moisture extraction from the volcanoclastic soil covering of Camaldoli hill study area.

### 5.3.4 Estimation of I-D rainfall thresholds for the Sarno Mountains sample areas using a deterministic approach

The hydrological effects of rainfall events, potentially triggering landslides, were simulated by hydrological and slope stability analysis for Sarno Mountains area, considering L1, L2 and L3 test sites. This phase allowed defining rainfall thresholds using a deterministic approach. Triggering rainfall events were simulated with constant intensities (2.5, 5.0, 10.0, 20.0 and 40 mm h<sup>-1</sup>) and variable durations.

Accordingly, the stability of the three sample slopes under simulated hydrological conditions was analyzed by a limit equilibrium approach, which was applied to the engineering-geological cross sections passing through the median axes of the initial debris slides (Fig. 5.20a).

Finite slope stability analysis, which characterizes the methods of limit-equilibrium, subdivides the landslide (actual or potential) into a number of slices. Because the equations of equilibrium are statically indeterminate, the distribution of inter-slice forces must be assumed by introducing stress-strain relationships to make the problem statically determinate. In general, according to the limit equilibrium principle, that assumes a brittle-plastic rheologic behavior, a slope is considered stable if the resistance forces available are greater than the driving forces.

The method of the slices is generally used for 2D slope stability analysis, in which the sliding mass above the failure surface is divided into a number of slices. The forces acting on each slice are obtained by considering the mechanical equilibrium of the slices and then a Factor of Safety (FoS) is calculated [Eq. 5.7]:

$$FoS = \frac{F_R}{F_D} \quad [5.7]$$

where:

$F_R$  = forces resisting to the movement;

$F_D$  = forces driving to the movement.

Thus, unstable conditions are expected when  $FoS < 1$  and stable conditions expected when  $FoS > 1$ .

Different methods known in the scientific literature allow to carry out slope stability analysis: the Fellenius' method (1927), Bishop's simplified method (1955) and the Janbu's method (1973). The slope-stability analyses to obtain deterministic rainfall thresholds were calculated by the simplified Bishop method (Bishop, 1955) for each time step of the numerical hydrologic simulation. This method is an extension of the ordinary method of slices and assumes that the forces on the sides of each slice are horizontal and the resulting forces in the vertical direction are null (Fig. 5.20b).

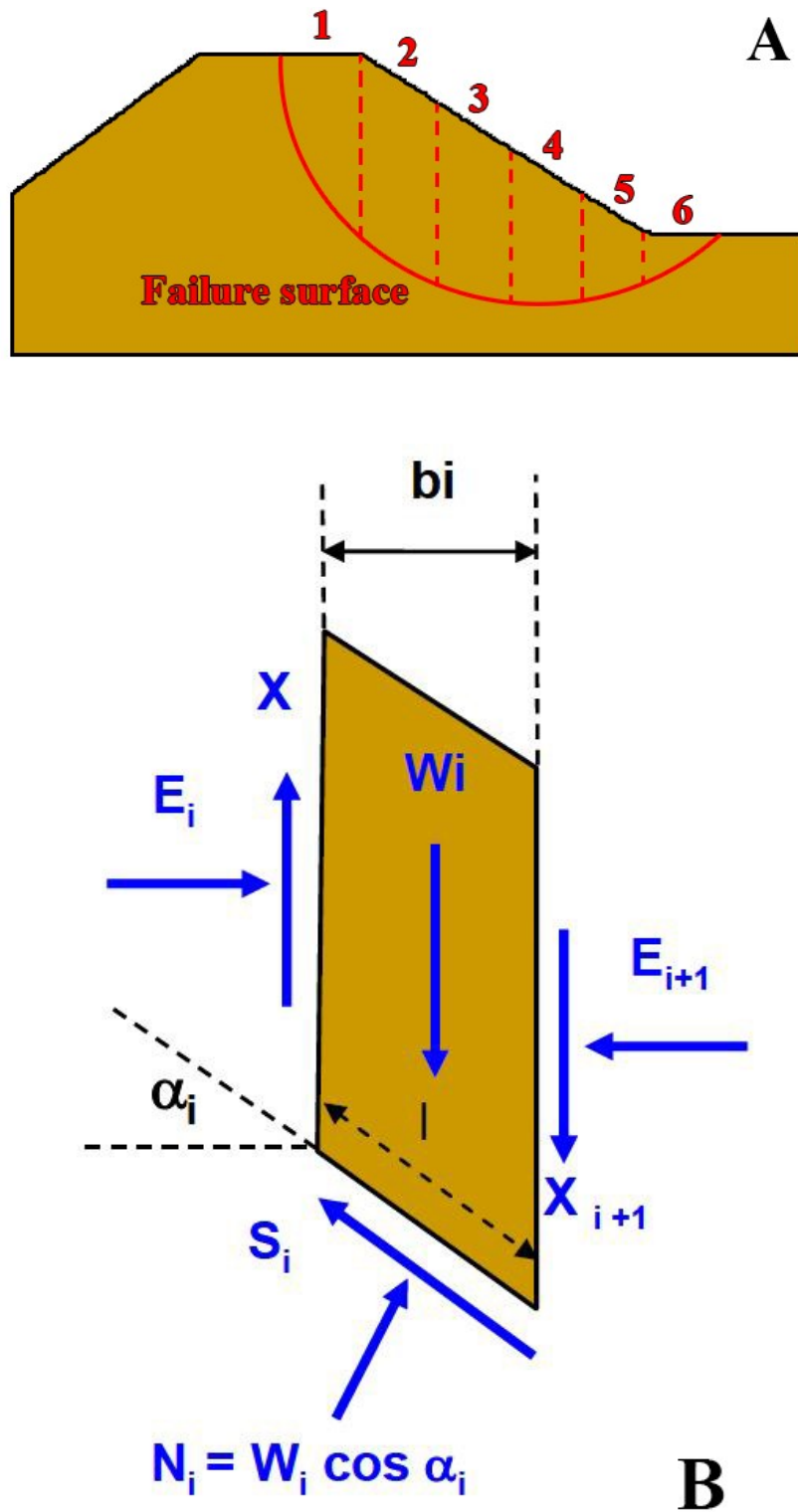


**Figure 5.20.** Schematic representation of (A) slices subdivision and (B) relative forces acting on a single slice following the Bishop's simplified method (1955).  $\alpha_i$  = slope angle;  $l_i$  = slices length;  $b_i$  = slices width;  $W_i$  = Weight of slice;  $E_i$  = horizontal force, acting perpendicular to the sides of the slice;  $X_i$  = vertical forces, acting parallel to the sides of the slice;  $N_i$  = Forces acting perpendicular to the base of the slice;  $S_i$  = Shear stress acting at the base of slices.

Considering these assumptions, the total factor of safety of the slope is the sum of those calculated for each slice using the follow equation [Eq. 5.8] for drained conditions:

$$FoS = \sum FoS_i = \frac{[c'_i b_i + (W_i - u_i b_i) \tan \phi'] \frac{1}{m_a}}{W_i \sin \alpha_i} \quad [5.8]$$

where:

$W_i$  = weight of slice;

$u_i$  = pore water pressure;

$\phi'_i$  = internal friction angle;

$c'_i$  = cohesion;

$\alpha_i$  = slope angle;

$b_i$  = slices width;

$m_a$  = coefficient =  $\cos \alpha \left( 1 + \frac{\tan \alpha \times \tan \phi}{F} \right)$ , where F is the unknown factor or variable represented by FoS values iteratively added each time until the achievement of max convergence (100%) with F;

In detail, slices subdivision was carried out for the reconstructed landslide bodies and failure surfaces of L1, L2 and L3 sample areas. For VS2DTI modelling, observation points were set along the reconstructed failure surface, at the base of each slice, to obtain pressure head, volumetric water content and saturation degree values for each time step (Fig. 5.21).

Furthermore, same hydraulic properties previously used during the calibration phase with L4 representative VS2DTI model and drained shear strength parameters (Table 5.10) were adopted, specifically determined for each soil horizon (De Vita et al., 2013; Napolitano et al., 2015).

Specifically, effective cohesion ( $c'$ ) and friction angle ( $\phi'$ ) were respectively set to the 5<sup>th</sup> and 50<sup>th</sup> (median value) percentiles of the dataset. This statistical approach was adopted to account for the significant variability of results of laboratory tests, which is basically due to the low level of normal stress adopted and the existence of coarser pyroclasts (pumiceous lapilli) dispersed in a sandy-silty matrix (coarse and fine ashes).

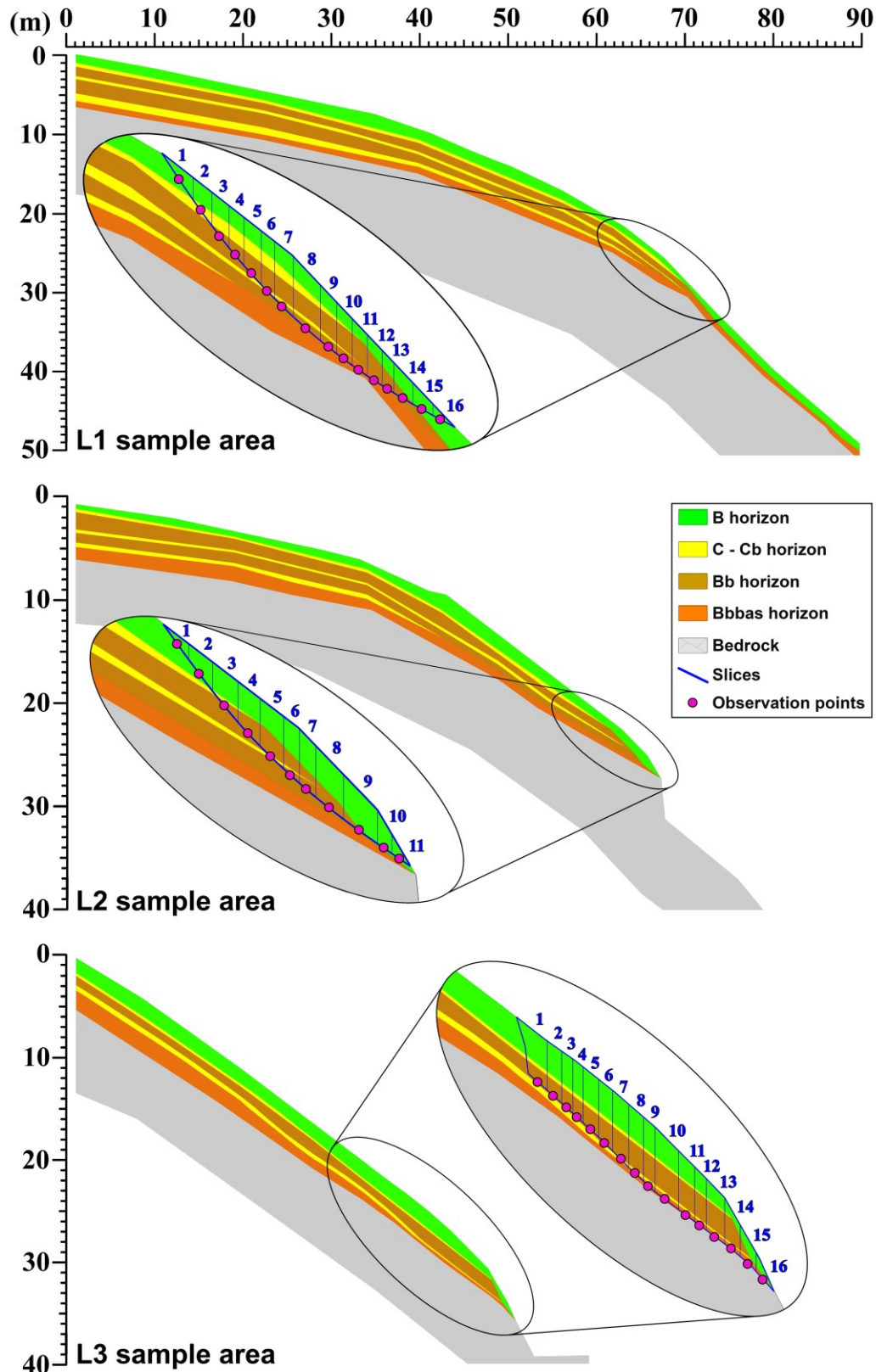


**Figure 5.21.** VS2DTI models of L1, L2 and L3 test sites in Sarno Mountains area used for rainfall critical condition modeling. Slices subdivision, for slope stability analysis, and setting up of observation points, to obtain pressure head, volumetric water content and saturation degree values, were carried out considering the reconstructed landslide body and failure surface.

In detail, a lower percentile for effective cohesion ( $c'$ ) was chosen in order to eliminate effects due to crushing of coarser pyroclasts (cohesion intercept).

Horizon	B	Bb	Bb <sub>bas</sub>	C-Cb
$c'$ (kPa)	4.5	1.8	8.1	0
$\phi'$ (°)	32	34	35	37

**Table 5.10.** Mechanical parameters of pyroclastic soils used to set up the representative slope models of Sarno mountains area for VS2DTI modeling. Cohesion ( $c'$ ) and friction angle ( $\phi'$ ) values were respectively set to the 5<sup>th</sup> and 50<sup>th</sup> (median value) percentiles of the dataset (De Vita et al., 2013; Napolitano et al., 2015).

The effect of unsaturated conditions on the stress state was considered by using the suction stress concept (Lu and Likos, 2004) and the unified effective stress criterion for both saturated and unsaturated conditions (Lu et al., 2010). Accordingly, suction stress,  $\sigma^s$ , is equivalent to pore-water pressure,  $u_w$ , for saturated conditions:

$$\sigma^s = -(u_a - u_w) \quad \text{for} \quad u_a - u_w \leq 0$$

Assuming the effective saturation degree ( $\theta_e$ ) equal to [Eq. 5.9]:

$$\theta_e = \frac{\theta - \theta_r}{\theta_s - \theta_r} \quad [5.9]$$

suction stress corresponds to the product of effective saturation degree ( $\theta_e$ ) and matric suction ( $u_a - u_w$ ) for partially saturated conditions (Vanapalli et al., 1996)

$$\sigma^s = -\theta_e(u_a - u_w) \quad \text{for} \quad u_a - u_w > 0$$

where:

$u_a$  = pore-air pressure;

$u_w$  = pore-water pressure;

$\theta$  = volumetric-water content;

$\theta_r$  = residual volumetric water content;

$\theta_s$  = saturated water content.

The Mohr-Coulomb failure criterion can then be written as [Eq. 5.10]:

$$\tau_f = c' + [(\sigma - u_a) - \sigma^s] \tan \phi \quad [5.10]$$

where:

$\tau_f$  = shear strength at a given matric suction;

$c'$  = drained cohesion;

$\sigma$  = total stress;

$\phi'$  = drained friction angle.

Daily pressure head values deriving from the long-term modeling were considered for taking into account typical seasonal hydrological conditions and their effect on Intensity-Duration rainfall thresholds. At this scope, a statistical analysis allowed identifying representative pressure head values for winter (wet condition) and summer (dry condition). Finally, considering values of rainfall intensity and durations to failure and different hydraulic and mechanical parameters derived from the sensitivity analysis, deterministic rainfall thresholds, representative of the Sarno Mountains test area, were obtained for winter and summer conditions.

#### **5.4. Distributed scale hydrological and slope stability modelling for hazard maps definition**

Considering results of in situ hydrological monitoring and deterministic rainfall thresholds carried out for the Sarno Mountains test areas (Fusco and De Vita, 2015; Napolitano et al., 2015; 2016), the objective of this part of the research was to integrate the hydrologic thresholds obtained at individual points into regional susceptibility maps that define the spatial and temporal probability of landslide occurrence via the initial debris slide stage. This specifically considers different rainfall return periods

and actual geomorphological and geological factors. To obtain distributed hydrological and slope stability modelling, the Transient Rainfall Infiltration and Grid-Based Regional Slope-Stability (TRIGRS) model (Baum et al., 2010) was applied. Due to the preliminary results of hydrological monitoring and modeling carried out for the Camaldoli hill test area, the distributed hydrological-stability modeling was performed only for the sample area of the Sarno Mountains.

#### 5.4.1. Overview of the TRIGRS model

The TRIGRS model represents a state-of-the-art numerical model to simulate infiltration, unsaturated/saturated soil water flow within a slope and slope stability by the infinite limit equilibrium approach, allowing predicting the temporal and the spatial variation of landslide susceptibility. By the assumption of a single-layered, homogeneous model and wet initial conditions, the governing equations of TRIGRS are based on a linearized solution of the Richards (1931) equation proposed by Iverson (2000) and implemented by Baum et al. (2002), again implemented within a Heaviside step series (Baum et al., 2010). The vertical distribution of pressure head through time [Eq. 5.11] for infinite depth is thus computed by:

$$\Psi(Z, t) = (Z - d)\beta + 2 \frac{I_{nZ}}{K_{sat}} \sqrt{D_1} \text{ierfc} \left[ \frac{Z}{2\sqrt{D_1 t}} \right] \quad [5.11]$$

where  $\Psi$  is the pressure head,  $t$  is time,  $Z = z/\cos \delta$  is the vertical depth,  $z$  is the slope-normal coordinate direction,  $\delta$  is the slope angle,  $d$  is the steady-state depth of the water table,  $\beta = \cos 2\delta - (I_{ZLT}/K_{sat})$  is the steady initial surface flux,  $I_{ZLT}$  is the steady (initial) surface flux,  $K_{sat}$  is the saturated hydraulic conductivity,  $I_{nZ}$  is the surface flux at the  $n^{\text{th}}$  interval, and  $D_1 = D_0/\cos 2\delta$ . The function  $\text{ierfc}$  is of the form  $\text{ierfc}(\eta) = 1/\sqrt{\pi} \exp(-\eta^2) - \eta \text{erfc}(\eta)$ , where  $\text{erfc}(\eta)$  is the complementary error function.

The TRIGRS code considers a two-layer soil as analytical solution for unsaturated groundwater flow considers, consisting of an unsaturated zone above a saturated zone characterized by a capillary fringe on a water table. Infiltration process is characterized by absorbing of part of the infiltrated water by unsaturated zone and percolation of the

remaining water at the base, leading to rise the water table. Under this condition, TRIGRS uses four parameters including residual water content ( $\theta_r$ ), saturated water content ( $\theta_s$ ), inverse of capillary fringe ( $\alpha$ ), and hydraulic conductivity ( $K_{sat}$ ) to approximate the soil water retention curve (SWRC; Gardner, 1958) and thus the one-dimensional infiltration flux (Srivastava and Yeh, 1991), with no lateral flow/throughflow. In this case, the vertical pressure head changes in the unsaturated zone are thus computed [Eq. 5.12]:

$$\Psi(Z, t) = \frac{\cos\delta}{\alpha_1} \ln \left[ \frac{K(Z, t)}{K_S} \right] + \Psi_0 \quad [5.12]$$

where  $\alpha_1 = \alpha \cos 2\delta$ ,  $\Psi_0$  is the pressure head at the water table ( $\Psi_0 = 0$ ) or at the top of the capillary fringe ( $\Psi_0 = -1/\alpha$ ),  $K(Z, t)$  is the hydraulic conductivity function of time and depth in the unsaturated zone (Srivastava and Yeh, 1991; Baum et al., 2008; Baum and Godt, 2013).

In the saturation zone, TRIGRS computes the pressure head increasing for finite depth basal boundary using a formula [Eq. 5.13] based on a Fourier series solution:

$$\Psi(Z_w, t) = \Psi_{hn} \left\{ 1 - \frac{4}{\pi} \sum_{m=1}^{\infty} (-1)^{m-1} \frac{1}{2m-1} \exp \left[ -\frac{(2m-1)^2 \pi^2 D_1 t}{4d_{LZ_w}^2} \right] \cos \left[ \frac{\pi}{2} (2m-1) \left( \frac{Z_w}{d_{LZ_w}} - 1 \right) \right] \right\} \quad [5.13]$$

where  $Z_w = Z - d$  is the vertical depth below the initial water table,  $\Psi_{hn} = \beta_{hn}$  is the pressure head applied after the accumulation of water above the initial water table, and  $d_{LZ_w}$  is the vertical height of the saturated layer. Finally, a one-dimensional infinite-slope-stability analysis (Taylor, 1948) is used by TRIGRS to determine the Factor of Safety (FoS), following the equation [Eq. 5.14]:

$$FoS(Z, t) = \frac{\tan\phi'}{\tan\delta} + \frac{c' - \Psi(Z, t)\gamma_w \tan\phi'}{\gamma_s Z \sin\delta \cos\delta} \quad [5.14]$$

where  $\phi'$  and  $c'$  are respectively the soil friction angle and cohesion for effective stress,  $\gamma_w$  is unit weight of water and  $\gamma_s$  is unit weight of soil.  $\Psi(Z, t)$  is the transient pressure head at depth  $Z$  and time  $t$  obtained from either Eqs. 11, 12 or 13 depending on the particular conditions modeled. Regarding the unsaturated zone, TRIGRS computes the Factor of Safety above the water table multiplying the matric suction  $\Psi(Z, t)\gamma_w$  by  $\chi = (\theta - \theta_r)/(\theta_s - \theta_r)$  (Vanapalli and Fredlund, 2000).

#### 5.4.2. Setting up of the distributed modelling for the Sarno Mountains

Within the framework of the Sarno Mountains, two different sample areas were chosen for distributed hydrological and slope stability modeling (Fig. 5.22): a “slope scale area”, located on the south-western slope of Mount Pizzo D’Alvano (1133 m a.s.l.) and being coincident with L4 test site where a hydrological monitoring station was installed (Fusco and De Vita, 2015); and a “regional scale area”, divided in three sectors and coincident with the entire Sarno Mountains slopes involved by Sarno May 1998 landslide event.

The Sarno Mountain slopes, as for similar frameworks of the peri-Vesuvian area, including the Salerno and Lattari Mountains (southern Italy), are characterized by peculiar geomorphological factors predisposing to shallow landsliding. Flow-like landslides involve ash-fall pyroclastic cover, whose thickness and continuity are strongly affected by slope angle variability and by the presence of rocky benches and/or narrow road cuts along the slopes.

Also considering the small extension of initial triggering areas ( $<100 \text{ m}^2$ ), a 5 m resolution DEM of the area was used for TRIGRS modelling, obtained by the resampling of the 1 m resolution DEM of the Campania region (Fig. 5.22), which was acquired through LIDAR surveys.

This new high resolution DEM (Fig. 5.23) allowed to reconstruct a new distribution map of ash-fall pyroclastic soil thickness, considering the variation of theoretical cover thickness related to the slope angle values (De Vita and Nappi, 2013). Furthermore, other input GIS data required for TRIGRS simulation, including flow direction and slope angles raster (Fig. 5.24) were obtained considering the high-resolution DEM previously reconstructed.

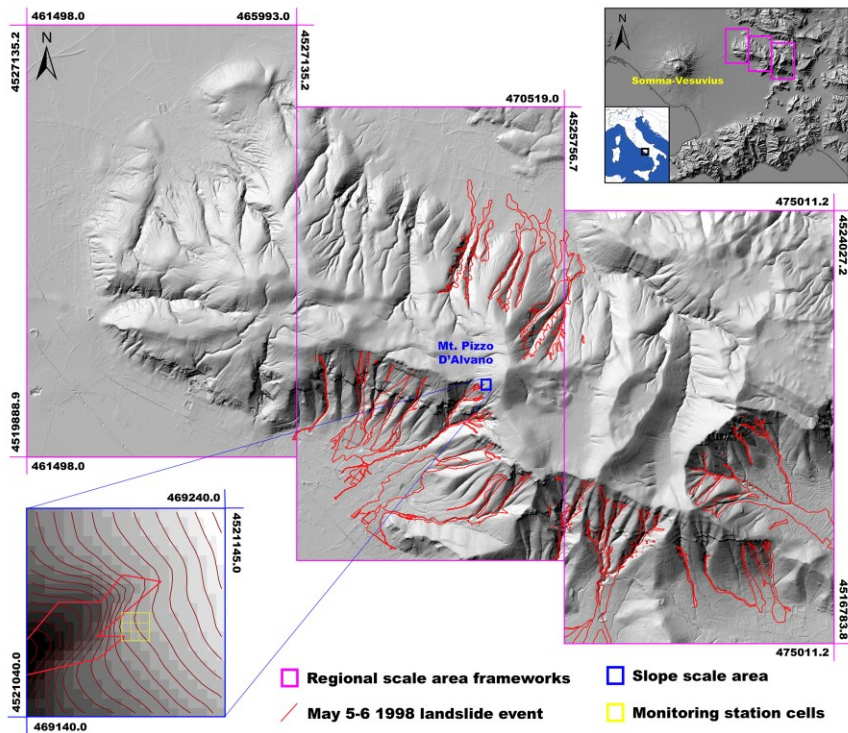


**Figure 5.22.** Map showing the sample areas from the site-specific to the distributed scales. Key to symbols: blue box) site specific sample area with analyzed cells (small yellow squares), located on the southwestern slope of the Mt. Pizzo D'Alvano and coinciding with the area of the monitoring station; magenta boxes) regional scale area coinciding with a sector of the Sarno Mts. carbonate ridge and including the most part of debris flows (red irregular shapes) occurred in May 1998.

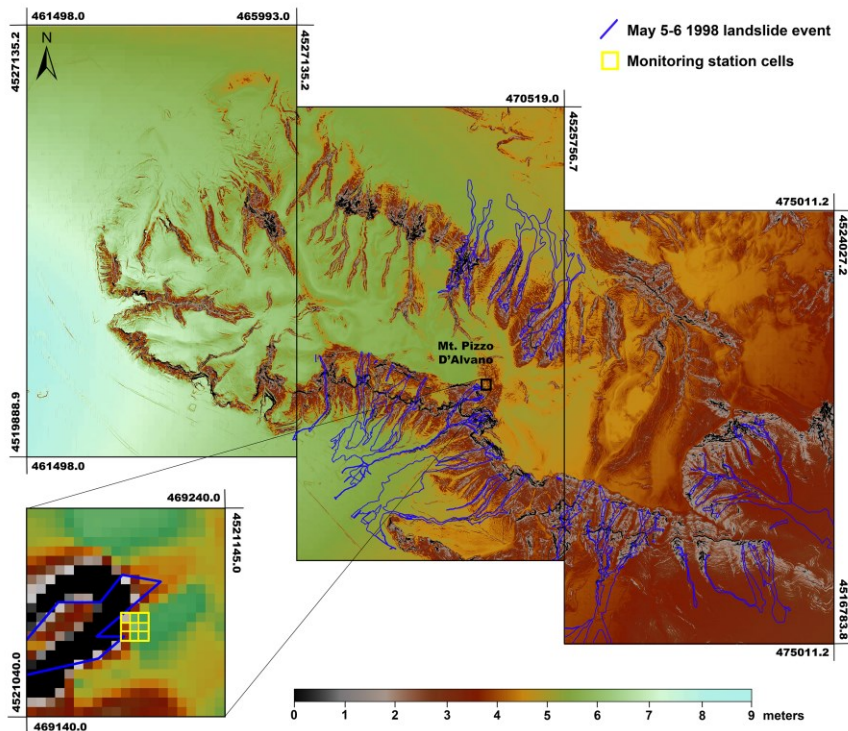


**Figure 5.23.** Thicknesses map of the ash-fall pyroclastic soil cover mantling the Sarno Mountains area. The 5 x 5 m DEM and the De Vita and Nappi (2013) model were considered.

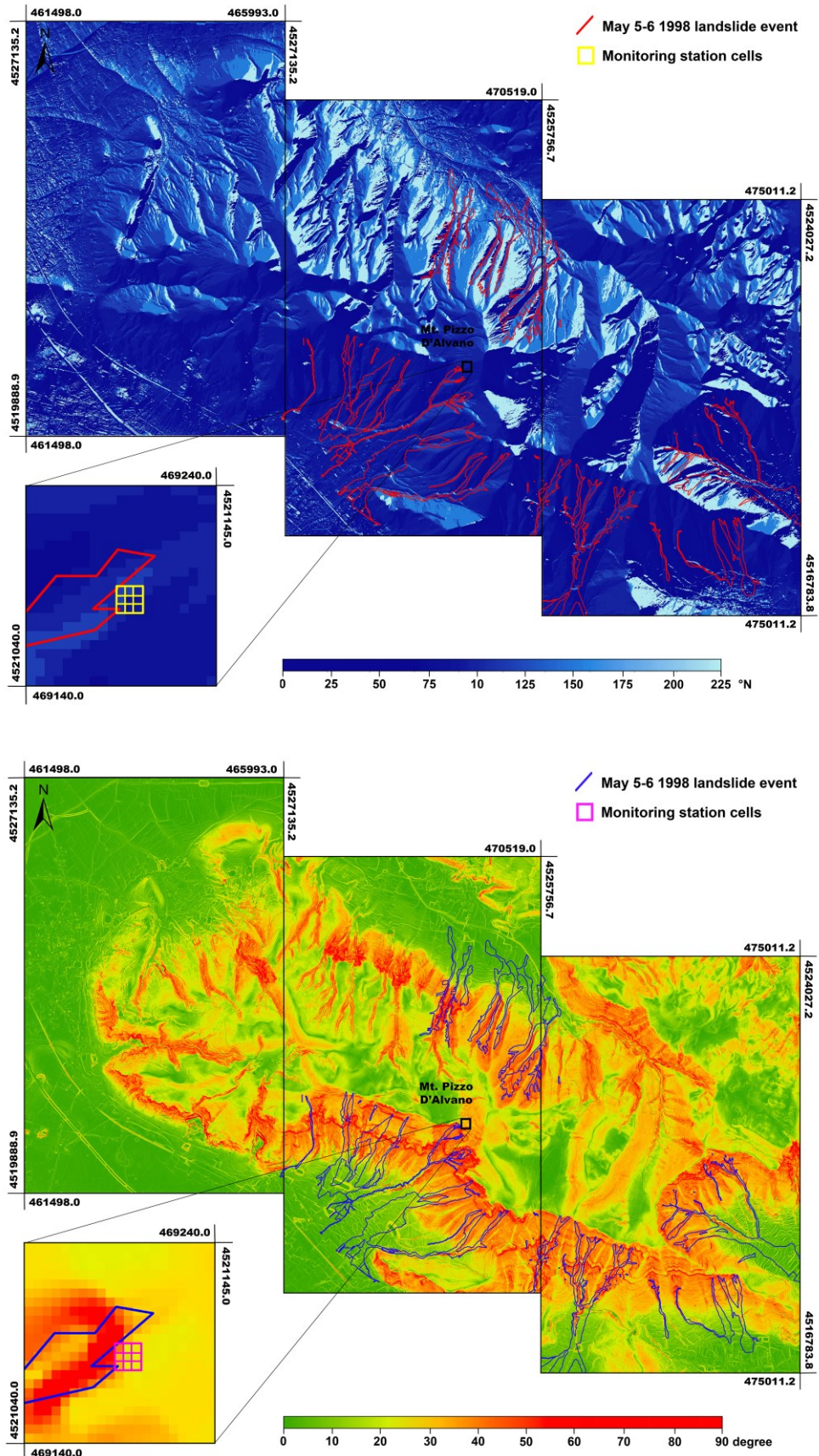


**Figure 5.24.** Flow direction and slope angle raster obtained for the Sarno Mountains sample areas considering the 5 x 5 m DEM.

A key aspect to apply TRIGRS model for the Sarno Mountains area was to set a representative model of the ash-fall pyroclastic cover simplifying the multilayered stratigraphic setting, characterized by non-uniform heterogeneous horizons, into a single-layered, variable-thickness cover with representative unsaturated/saturated hydraulic and mechanical soil properties. A step-by-step approach was used starting from the simplification of the reconstructed slope engineering-geological model, already used to calibrate numerical hydrological modelling by VS2DTI code (Hsieh et al., 2000) and to estimate deterministic rainfall thresholds (Napolitano et al., 2015). The simplified model was identified in a single-layered and variable-thickness ash-fall pyroclastic cover (Fig. 5.25).

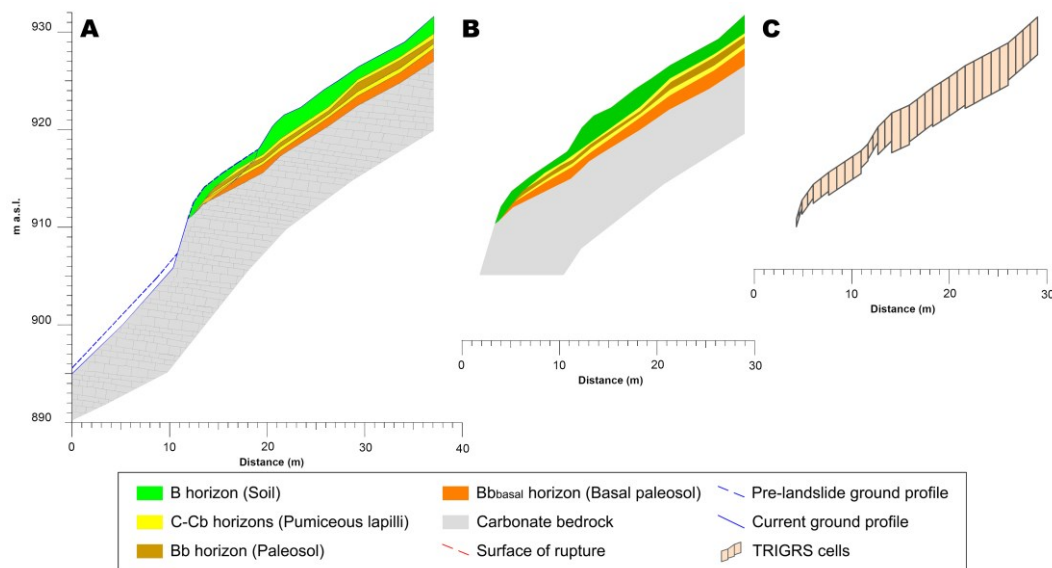


**Figure 5.25.** Simplification of a multilayered slope model from field characterization (A) and VS2DTI modeling (B) into a single-layered model with non-uniform thickness for each TRIGRS cell (C).

Representative soil properties for the TRIGRS simulations were estimated using a weighted average of measured property values for individual soil horizons based on their relative thicknesses. The measured hydraulic and mechanical properties of the individual soil horizons at our three monitoring locations, L1, L2, and L3 are reported by De Vita et al. (2013) and Napolitano et al. (2015). At each of these three monitoring locations three vertical profiles at the upslope, midslope, and downslope location were selected to account for observed variability in horizon thicknesses.

Using these representative thicknesses and measured properties of the individual horizons a weighted average of the hydro-mechanical properties for the entire profile at all nine locations were calculated by the harmonic mean (Table 5.11), which is a standard approach in hydrogeology (e.g., Freeze and Cherry, 1979). We then used the median value of these nine representative profiles to assign effective hydro-mechanical properties for the ash-fall pyroclastic soil cover throughout the TRIGRS domain.

<b>Properties</b>	<b>B</b>	<b>Bb</b>	<b>Bb<sub>basal</sub></b>	<b>C</b>
<b>K<sub>sat</sub> (m/s)</b>	$4.82 \times 10^{-5}$	$6.00 \times 10^{-6}$	$2.48 \times 10^{-7}$	$2.82 \times 10^{-3}$
<b><math>\theta_s</math></b>	0.505	0.663	0.505	0.50
<b><math>\theta_r</math></b>	0.083	0.001	0.083	0.001
<b><math>\alpha</math></b>	0.884	0.884	0.884	20.39
<b><math>\phi</math></b>	32.0	37.0	35.0	34.0
<b>c</b>	4.5	0.0	8.1	1.8

**Table 5.11.** Effective mechanical and hydraulic soil properties (De Vita et al., 2013; Napolitano et al., 2015) used to define those representative for TRIGRS modelling by statistical analysis: friction angle ( $\phi$ ) at 50<sup>th</sup> percentile; cohesion (c) at 5<sup>th</sup> percentile; saturated hydraulic conductivity ( $K_{sat}$ ) at 25<sup>th</sup> percentile; saturated volumetric water content ( $\theta_s$ ) at 25<sup>th</sup> percentile; residual volumetric water content ( $\theta_r$ ) at 25<sup>th</sup> percentile; fitting parameter of water retention curve ( $\alpha$ ) at 25<sup>th</sup> percentile.

To calibrate these mechanical and hydraulic properties, a trial-and-error approach was considered. Hydrological modelling at the slope scale area was carried out using the same rainfall intensities (I) adopted for the above mentioned deterministic rainfall thresholds (2.5, 5.0, 10.0, 20.0 and 40.0 mm/h). Time (D) with Factor of Safety (FoS) values equal to 1 of sample cells corresponding to the monitoring station area previously mentioned were also considered. Taking into account intensity/duration values found for rainfall thresholds (Napolitano et al., 2015), the TRIGRS code was applied for the three sample areas of the Sarno Mountain Ridge. Results of this modelling were compared with the map of debris flows occurred in May 1998. During this phase, typical winter pressure head values of the ash-fall pyroclastic soil cover, equivalent to those recorded by monitoring activities (Fusco and De Vita, 2015), were set as initial conditions. Based on TRIGRS' setting, an initial vertical distribution of pressure head within the ash-fall pyroclastic soil cover was defined by an iterative approach varying water table depth from the bottom of the modeled cover.

Using representative soil properties (harmonic mean) and initial winter conditions, hydrological and slope stability distributed modelling for the regional scale area were carried out. Susceptibility maps based on spatial and temporal probabilities of landslide triggering were calculated by considering morphological and geological factors, variable thickness of ash-fall pyroclastic soil cover and using the same rainfall intensities already applied in the site-scale modelling efforts described in previous sections. These maps show the distribution of unstable areas, or pixels with  $FoS \leq 1$  values, and likely unstable areas, or pixels with  $FoS$  values ranging between 1.01 and 1.05, according to different rainfall intensities and durations. The choice of  $FoS$  range to assume as indicative of slope instability follows by the consideration that these values can be approximate to the limit equilibrium condition ( $FoS = 1$ ) by truncation. Also in this case, mapping results were compared with the map of debris flows that occurred in May 1998.

# Chapter 6

---

## Results

### 6.1 Hydrological monitoring and modeling for the Sarno Mountains test area

#### 6.1.1 Hydrological regime of ash-fall pyroclastic soil mantle

The continuous hydrological monitoring of the ash-fall pyroclastic soil coverings for the L4 sample area (Sarno Mountains) allowed measuring pressure head for six years by having a greater number of sensors with a diverse functioning limit. By the pressure head time series, the hydrological regime of the ash-fall pyroclastic cover was analyzed.

In a first analysis, the six monitoring years showed a significant seasonal control (Fig. 6.1) characterized by a marked variability of the soil pressure head values, consistently limited to unsaturated conditions and strongly influenced by precipitation regime and water losses due to evapotranspiration processes. Data show that during the monitoring period, saturated conditions were not observed in the cover, even if conditions of near saturation with pressure head values greater than  $-0.1$  m were occasionally recorded in the shallowest part of the cover after heavier rainfall events. Regrettably, there were several data gaps in the pressure head time series from a few days to a few weeks, during which time the actual pressure head values were outside the functioning limit of tensiometers and Watermark sensors. Moreover, the functioning of few sensors was interrupted for a limited period of time due to damages to the equipment caused by wild boars. However, the different functioning limit and the great number of the installed devices allowed a very continuous monitoring of the soil pressure head values. In detail, the pressure head time series was analyzed by a statistical approach to obtain minimum, median and maximum values reached by each horizon (Table 6.1). In addition, considering the rainfall time series, a subdivision of the hydrological years in rainy periods, typically occurring from November to April,

and dry periods, characteristically happening from May to October, were carried out.

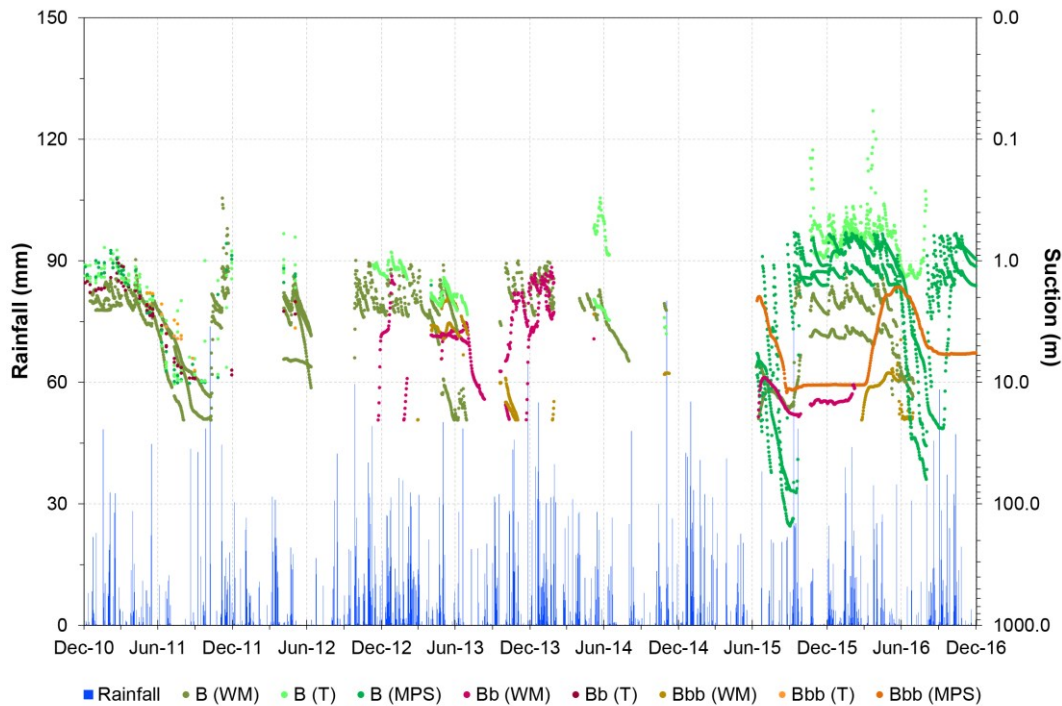


**Figure 6.1.** Pressure head (PH) time series of B, Bb and Bb<sub>basal</sub> horizons and daily rainfall data. Data obtained at different depth by using tensiometers (T), Watermark (WM) and MPS-2 sensors (MPS) were grouped for each horizon.

As regards the rainy periods, higher soil pressure head values were recorded due to the combined effects of higher rainfall and lower evapotranspiration rates. In these periods, pressure head values in the whole ash-fall pyroclastic cover were observed to change in a range limited between -0.1 m and lower than the functioning limit of the Watermark sensors (-20.4 m). In addition, the trend was characterized by a series of peaks of pressure head, which generally correspond to rainfall events or follow them shortly. The B horizon showed the major temporal fluctuations of the values as well as the correspondence between peaks of pressure head and rainfall events was observed being more direct for shallowest horizon (B) and damped and delayed for deeper ones (Bb and Bb<sub>basal</sub>). During periods with snow cover, principally occurring in February, pressure head values showed that infiltration processes were strongly limited to just the shallower part of the ash-fall pyroclastic soil cover.

At the end of March, a gradually decrease of pressure head values was recorded in all the six hydrological years. Leaf growth of deciduous chestnut forest occurring

during this period was also recognized as playing a predominant role in water loss from the pyroclastic cover. The decreasing trend became exponential at the beginning of the dry periods due to the combined effect of the loss of water by evapotranspiration processes and the decreasing of number of rainfall events. These periods were characterized by lower pressure head values ranged between -0.7 and -152.2 m. In addition, as during the rainy periods, a correspondence between peaks of pressure head values and rainfall events was observed mostly in the first 0.20 ÷ 0.30 m of depth, while no appreciable effects were observed at greater depth. However, as showed by the pressure head time series, the loss of water due to the evapotranspiration is so fast and marked that during small rainfall events peaks are significantly smoothed.

During the dry periods pressure head values, hypothetically reached by the pyroclastic cover, were lower than the functioning limit of tensiometers and Watermark sensors. In particular, for the B horizon, it was possible to measure soil pressure head only after the installation of the MPS-2 sensors.

Starting from the late September, corresponding approximately to the end of the dry period, the trend of the pressure head time series was affected by an abrupt increase of values attributable to the rainfall occurrence, mostly rainstorms, and secondly to the stop of leaf activity. This condition occurred early and markedly in the upper part of the ash-fall pyroclastic mantle, while it was recognized slightly delayed and damped for the deep horizons (Bb and Bb<sub>basal</sub>).

	2011	2012	2013	2014	2015	2016	
<b>B</b>	-2.2	-1.6	-2.2	-2.4	-4.0	-1.0	<b>Median</b>
<b>Bb</b>	-2.5	-2.7	-4.5	-2.5	-14.7	-14.2	
<b>Bb<sub>bas</sub></b>	-3.2	-3.6	-4.2	-8.4	-10.5	-5.9	
<b>Cover</b>	-2.3	-2.1	-3.4	-2.5	-7.6	-5.8	
<b>B</b>	-0.3	-0.6	-0.8	-0.3	-0.1	-0.1	<b>Max</b>
<b>Bb</b>	-1.0	-2.2	-1.3	-1.1	-9.2	-10.4	
<b>Bb<sub>bas</sub></b>	-1.8	-3.6	-2.0	-2.8	-2.0	-1.6	
<b>Cover</b>	-0.3	-0.6	-0.8	-0.3	-0.1	-0.1	
<b>B</b>	< -20.4	-11.1	< -20.4	-6.7	-152.2	-62.8	<b>Min</b>
<b>Bb</b>	-9.3	-20.4	< -20.4	-4.4	-19.2	-15.1	
<b>Bb<sub>bas</sub></b>	-8.0	-3.6	< -20.4	< -20.4	-12.2	< -20.4	
<b>Cover</b>	< -20.4	-20.4	< -20.4	< -20.4	-152.2	-62.8	

**Table 6.1.** Median, maximum and minimum pressure head values of the whole ash-fall pyroclastic cover recorded at different depth during the monitoring period 2011÷2016.

Seasonal fluctuations of pressure head time series is more appreciable considering the trend of monthly median, maximum and minimum values (Fig. 6.2). In fact, the shapes assumed by the SWRCs of each horizon shown how the variability of pressure head values due to the combined effects of rainfall events and evapotranspiration processes appear more fast and marked in the shallowest B horizon than the deepest ones (B and Bb<sub>basal</sub>).

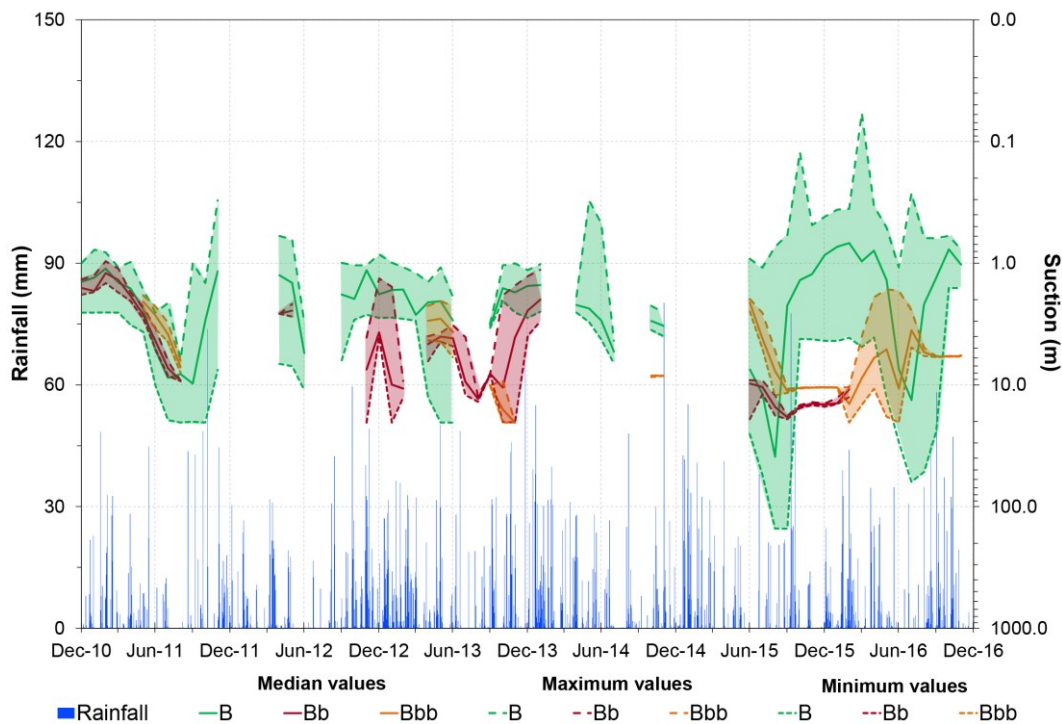


**Figure 6.2.** Median, minimum and maximum pressure head (PH) values of pedogeneized horizons (B, Bb and Bbb or Bb<sub>basal</sub>), which characterize the ash-fall pyroclastic cover of the Sarno Mountains, and daily rainfall data.

Finally, comparing pressure head values recorded at different depths of sample days of September ÷ December periods, including 2011 to 2016 years (2014 was excluded due to lack of significant data), a progressive deepening of the infiltration front was observed. In detail, in these periods three hydrological stages were identified and analyzed (Fig. 6.3).

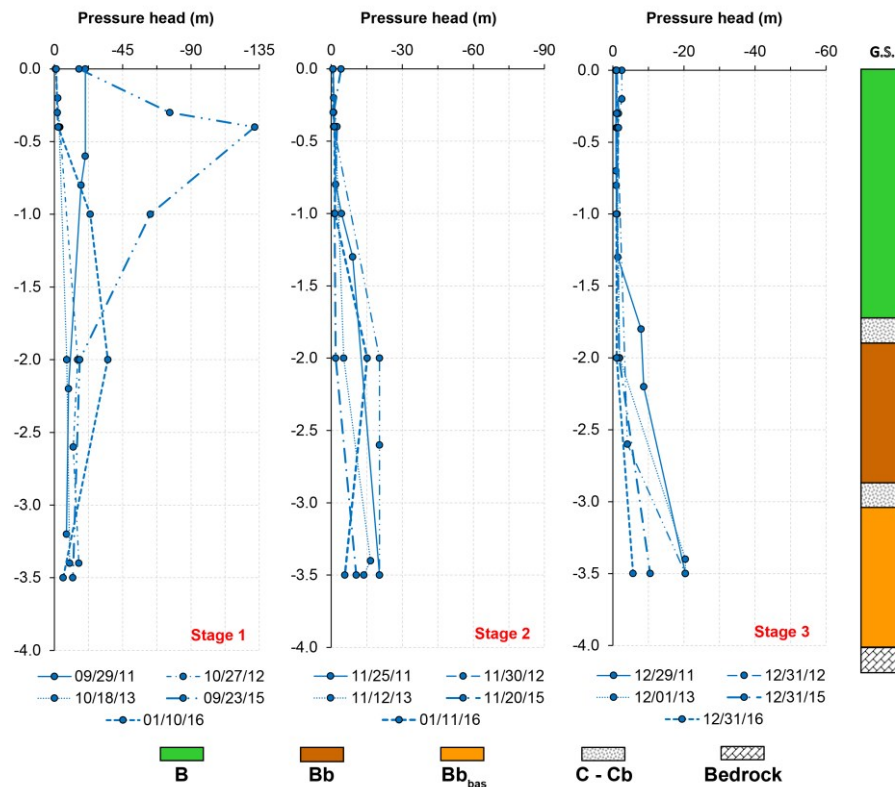


**Figure 6.3.** Observations of infiltration front deepening at the beginning of the rainy period by analysis of vertical profiles of pressure head measured at hydrological stages 1, 2 and 3, from 2011 to 2016 years (2014 was excluded due to lack of significant data).

The stage 1 is representative of the beginning of the rainy season, typically September ÷ October, and characterized by a vertical distribution of pressure head. Values varying from the near saturation (-0.8 m) to very dry conditions (-132.0 m) in the uppermost part of the cover (down to 0.5 m of depth), depending on the inconstant timing of rainfall events. Instead, for depths greater than 1.0 m, pressure head values were recorded varying in a narrower range between -8.0 m and -63.3 m. The stage 2 characteristically represents the stabilization of the rainy period occurring in November. During this period the infiltration front is uniformly formed in the B horizon, giving near saturation conditions (-0.8 m) down to depths lower than 1.0 m, despite lower pressure head values (-4.2 m) were observed in some cases due to long period of rainfall absence. Contrastingly, the deeper horizons showed higher pressure head values. The Bb horizon from -1.4 m to below the lower functioning limit of Watermark sensors (-20.4 m), while the Bb<sub>bas</sub> between -5.8 m down to < -20.4. The last stage (3), corresponding to the advanced rainy season occurring in December, data shown that the infiltration front reaches the Bb horizon down to 2.6 m of depth with

pressure head values varying from the near saturation (-0.8 m) down to -4.1 m. As regarding the lowest Bbbasal horizon, in this stage pressure head values remains with pressure head values ranged between -5.7 and < -20.4 m.

### 6.1.2. Intensity-Duration deterministic rainfall threshold

As previously mentioned, hydrological modeling to define deterministic rainfall thresholds was characterized by two phases: a preliminary model calibration phase and the effective hydrological modeling phase.

The numerical model of L4 sample area was calibrated for the monitoring period January 2011-December 2011, therefore obtaining simulated pressure-head values (Fig. 6.4). The comparison between the outcomes of the calibrated model and field monitoring data were recognized being consistent and well matching with the pressure-head regime recorded at all observation verticals. The fluctuations of pressure head values due to rainfall events were simulated showing how the effects are fast and strong in the shallowest part of the cover, while they are delayed and damped in depth.

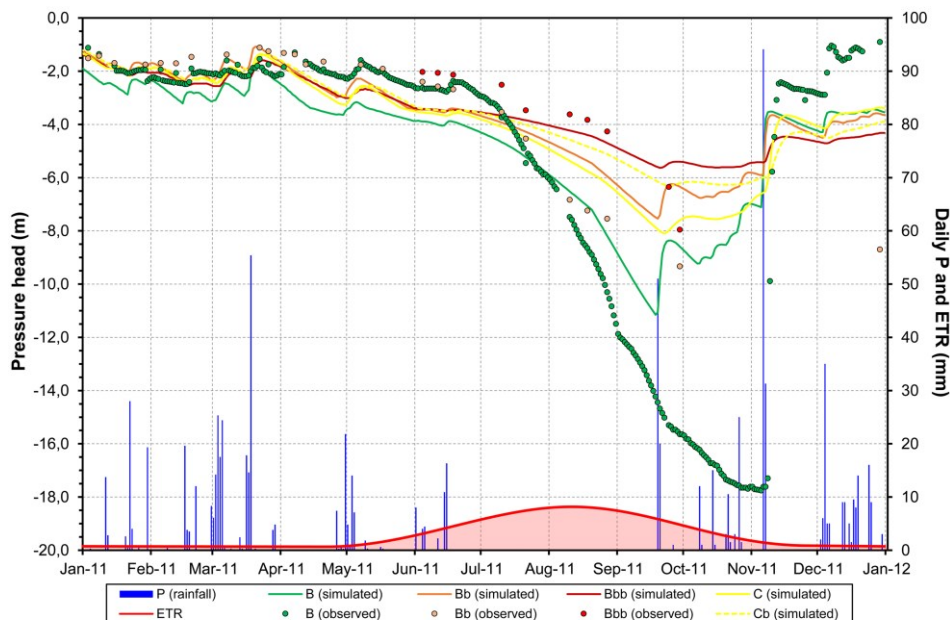


**Figure 6.4.** Model calibration for the period January 2011 ÷ December 2011. Daily rainfall, actual evapotranspiration rates, measured (circles) and simulated (continuous lines) pressure-head values are shown (from Napolitano et al. 2015).

In detail, during the period between January 2011 and April 2011 (rainy period) the results of modeled pressure head time series, calibrated on the basis of field monitoring data, showed pressure-head values above -3.0 m at all depths of pyroclastic deposits (Fig. 6.4). During this period, the highest values were measured after the rainfall events occurred between February and March 2011, when pressure head increased locally up to -0.4 m. In fact, during heavier rainstorm events the ephemeral existence of a restricted near-saturated zone, within about 2.0 m upslope of the landslide scar, which is in correspondence to an abrupt reduction of the pyroclastic mantle thickness. Such observation confirmed the buildup of pressure head in correspondence to slope segments where the pyroclastic soil thickness undergoes a significant reduction due to an abrupt increase in slope angle. As confirmed by field data, saturated conditions were not simulated, even after stronger rainfall events. Starting from April 2011 through September 2011, the drying period was modeled, in particular the exponential decreasing of pressure head values, due to a combined effect of lower rainfall and higher evapotranspiration rates, well matched with the measured data (Fig. 6.4). Moreover, in this period the inversion of the hydraulic gradient into the ash-fall pyroclastic soil cover, which is related to an upward water flux toward root apparatuses, was successfully simulated.

During the period between the late September 2011 and October 2011 more enhanced differences between monitored and simulated pressure head values exists. The return of rainfall characterized the new recharge period, which interrupted the general decreasing of the modeled pressure head trend and culminated in an increasing of water content from the shallower to deeper soil horizons (Fig. 6.4), with a downward hydraulic gradient. In this case, despite the new rainy period was modeled, there is an initial discrepancy between modeled and monitored pressure head values, especially for the shallowest part of the ash-fall pyroclastic cover (B horizon). In fact, intense rainfall and thunderstorms affected results of the simulated pressure head values making them not precisely overlapping with in situ monitoring data. This behavior can be related to hysteresis of unsaturated hydraulic properties and to the possible presence of entrapped air within the soil pores. In addition, the influence of raindrop interception by leaves, the drainage through the carbonate bedrock, and the 3D components of unsaturated/saturated flows, not taken into account into the 2D model, can be excluded due to the general low moisture content of the pyroclastic soil

cover at the end of the summer and the limited velocity of the infiltration front (Fig. 6.4).

Finally, the calibration of the representative model of L4 sample area permitted the long-term hydrological modelling of ash-fall pyroclastic mantle over about 12 years from January 2000 to December 2011 (Fig. 6.5).

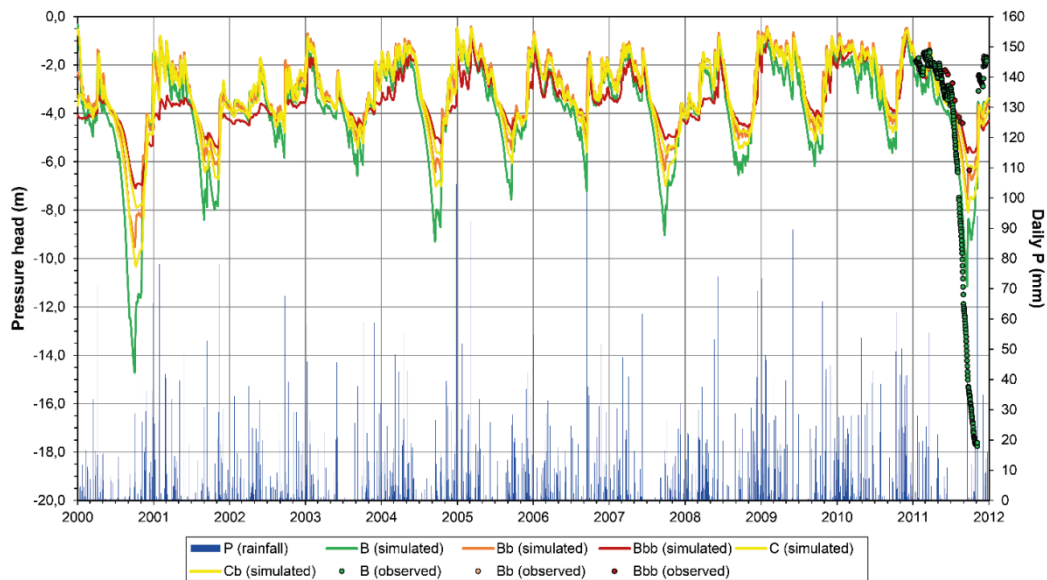


**Figure 6.5.** Long-term (January 2000 to December 2011) pressure-head simulation, differentiated for each principal soil horizon (lines), and short-term (January 2011 to December 2011) monitoring data (circles). Daily rainfall was also shown (from Napolitano et al., 2015).

Seasonal variations of pressure head values within the ash-fall pyroclastic soil mantle were observed, with damped dynamics among the soil horizons depending on depth. Following the approach previously described in Chapter 5, a first modeling (*warm up run*) was carried out by using the initial pressure-head values measured at the end of December 2011. Then, median values of January months simulated for the period 2000-2011 were used as initial conditions for a *second run* to obtain the seasonal fluctuation of the modeled pressure head time series. The availability of a relatively long time series of simulated pressure head permitted an assessment of the range of seasonal variations (Fig. 6.6). Among the most relevant observations, a greater variability for the B horizon and a relevant difference of lower annual extremes of pressure head were recognized. Considering the B horizon, simulated pressure head reached extreme lower values in 2000 and 2011, reaching -14.7 m and -11.2 m,

respectively (Fig. 6.6). Moreover, the lowest annual values were found varying around an average value of  $-8.2 \text{ m} \pm 2.6 \sigma$  (Table 6.2).

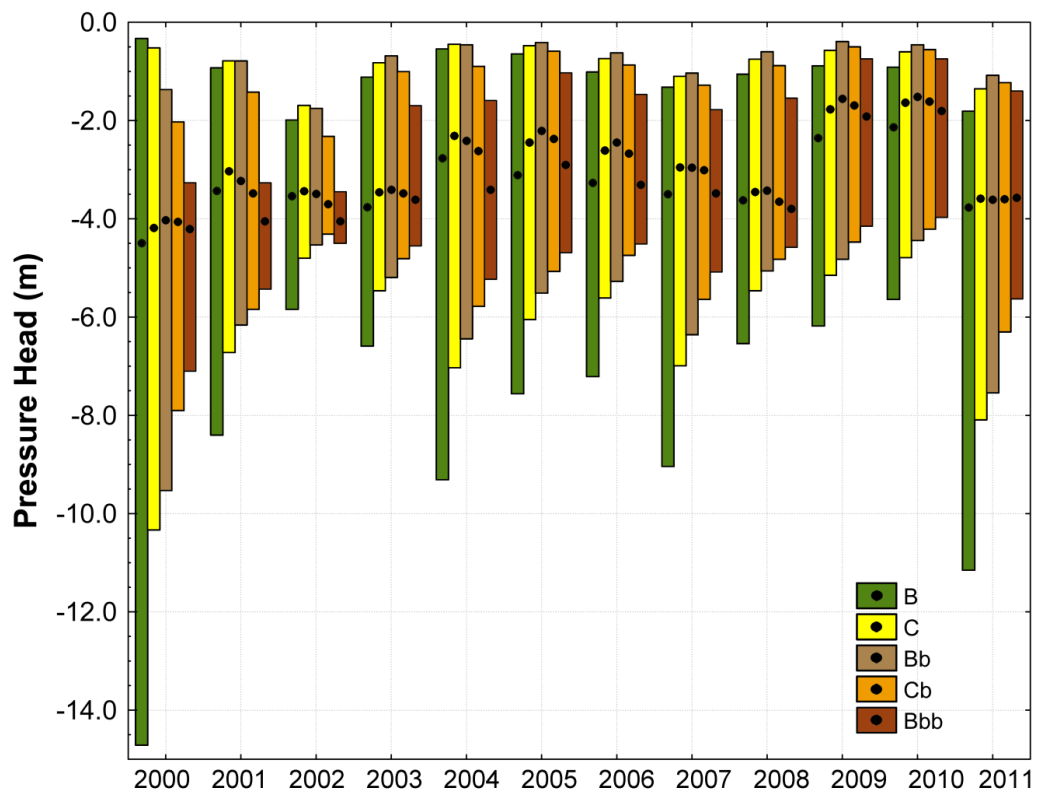


**Figure 6.6.** Range plot of annual maximum, minimum and median pressure-head values simulated for each ash-fall pyroclastic soil horizon during the period January 2000-December 2011 (from Napolitano et al., 2015).

Also considering the more variable B horizon, the maximum annual pressure-head values were observed with a lower variability because ranging around a mean value of  $-1.0 \text{ m} \pm 0.48 \sigma$ . In particular, the long-term simulated pressure-head time series was applied to choose representative initial hydrological conditions, which were used to simulate pressure head and slope stability conditions under rainfall with different intensities and durations. Specifically, to assess the effects on rainfall thresholds, representative antecedent-hydrological conditions were identified for each soil horizon and for both winter and summer seasons by considering respectively maximum and minimum average values of the whole simulated pressure-head time series (Table 6.2).

Soil horizon	Min					Max				
	B	C	Bb	Cb	Bbbas	B	C	Bb	Cb	Bbbas
Mean PH (m)	-8.2	-6.4	-5.9	-5.3	-5.0	-5.0	-1.0	-0.8	-0.8	-1.1
Dev. St. ( $\sigma$ )	2.63	1.61	1.46	1.05	0.84	0.84	0.48	0.38	0.43	0.57

**Table 6.2.** Minimum and maximum pressure head (PH) values simulated for principal soil horizons of the pyroclastic mantle in the period January 2000 ÷ December 2011 (Napolitano et al. 2015).

Statistical analyses of minimum and maximum pressure-head values allowed identifying the year 2005 as representative for average conditions of the entire simulated time series. In detail, effects of antecedent-hydrological conditions, representative of 2005 wet and dry seasons, characterized by pressure-head values ranging among pyroclastic soil horizons respectively from -1.0 m to -0.4 m and from -7.6 to -4.7 m, were estimated. Therefore, the extreme values from 2005 were adopted to set initial pressure head conditions for L1, L2 and L3 VS2DTI models. Different constant rainfall intensities, corresponding to 2.5, 5.0, 10.0, 20.0, and 40.0 mm/h, were considered and their effects on pressure-head distribution and slope stability for each landslide were calculated.

Hydrological dynamics occurring within the ash fall pyroclastic cover were observed, considering Pressure Head (PH), saturation degree (Sr) and volumetric water content (VWC) values by the observation points for each time step. In detail, the resulting numerical models shown that infiltration processes lead to vertical and lateral flows formation within the ash-fall pyroclastic cover. Unsaturated throughflow parallel to the slope was observed, which caused saturated or near saturated conditions close to morphological discontinuities controlling a reduction of the pyroclastic mantle thickness. These morphological discontinuities were identified (De Vita et al., 2013) in the case of: knickpoint (L1), rocky cliff (L2) and road cut (L3). For each modeled rainfall intensity and initial pressure head distribution, this phenomenon occurred within the slope despite showing different behavior of the ash-fall pyroclastic soil cover.

Finally, a step-by-step slope stability analysis were carried out considering the PH, Sr and VWC time series of each model. Results allowed defining the hydrological conditions of the ash-fall pyroclastic cover at the slope failure time step and then to verify the real triggering areas, which characterize the three test sites (Figs. 6.7 and 6.8).

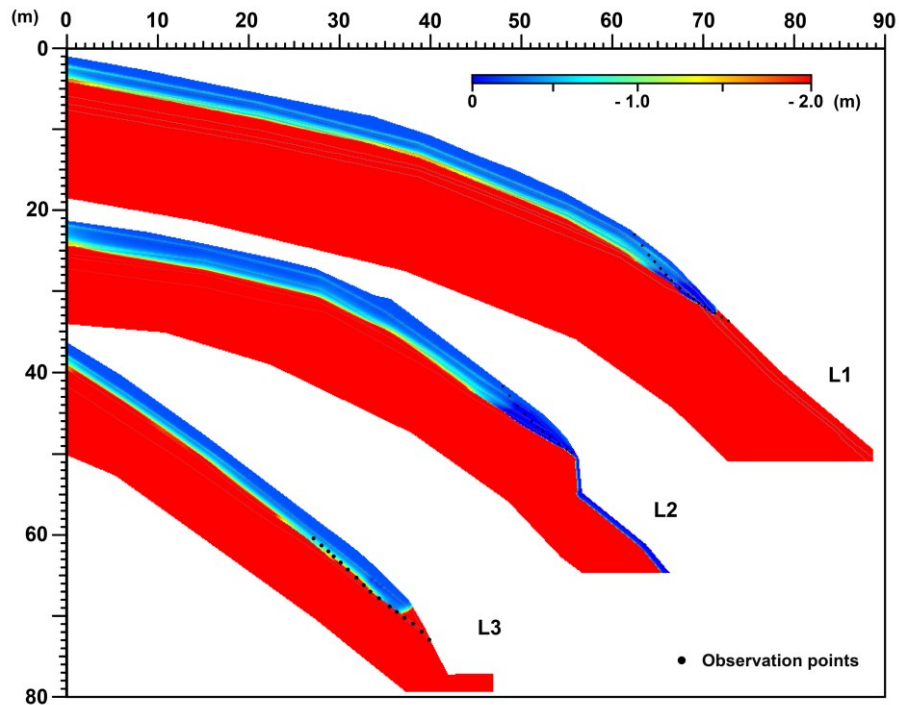


**Figure 6.7.** Pressure head distribution of the ash-fall pyroclastic cover at the slope failure time step obtained modeling 5 mm/h of rainfall intensity and winter antecedent conditions. Numerical models show the formation of saturated or near-saturated zones close to cover discontinuities or thicknesses reducing.

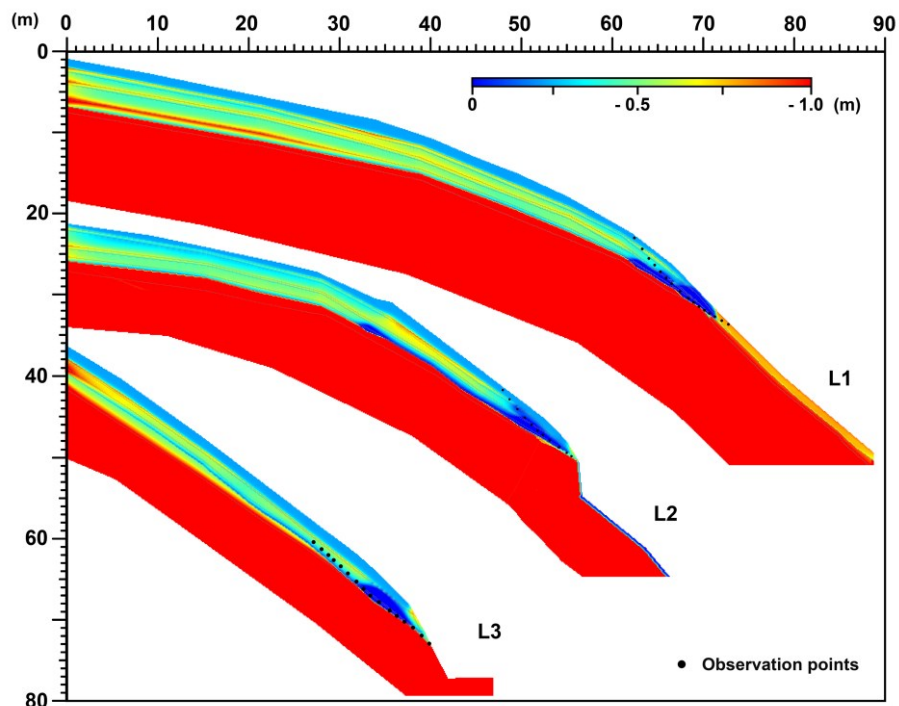


**Figure 6.8.** Pressure head distribution of the ash-fall pyroclastic cover at the slope failure time step obtained modeling 5 mm/h of rainfall intensity and summer antecedent conditions. Numerical models show the formation of saturated or near-saturated zones close to cover discontinuities or thicknesses reducing.

Considering rainfall intensity ( $I$ ) and durations ( $D$ ) values leading to slope failure, deterministic rainfall thresholds for winter (Fig. 6.9a) and summer (Fig. 6.9b) conditions were reconstructed for each modeled slope.

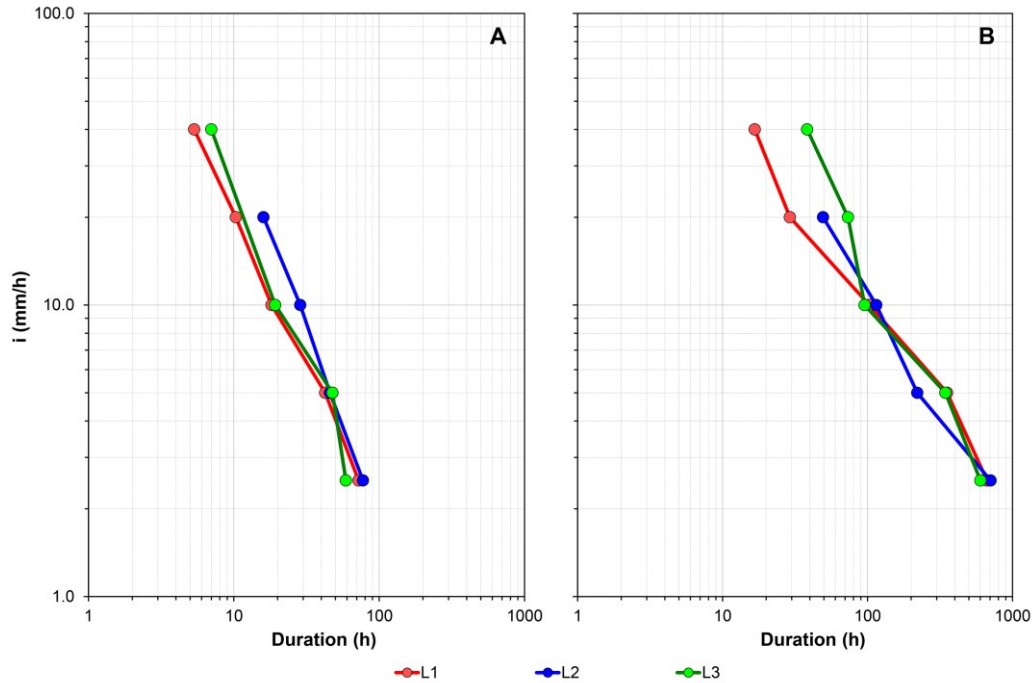


**Figure 6.9.** Intensity-Duration (I-D) thresholds calculated considering, for each test site (L1, L2, L3) of the Sarno Mountains sample areas, different rainfall intensities and antecedent winter (A) and summer (B) conditions.

In a first analysis, a well matching of I-D threshold values obtained for each test site was observed, considering both summer and winter conditions. However, results shown that antecedent low soil pressure head values (summer conditions) of the ash-fall pyroclastic cover caused a strong increasing of the rainfall duration and/or intensity necessary to generate slope instability, relatively to winter antecedent conditions.

Finally, a power-law best-fit regression of intensity/duration rainfall conditions, leading to slope instability of each representative landslide, was carried out to estimate both winter and summer deterministic rainfall thresholds (Fig. 6.10 and Table 6.3), representative of the Sarno Mountains area.

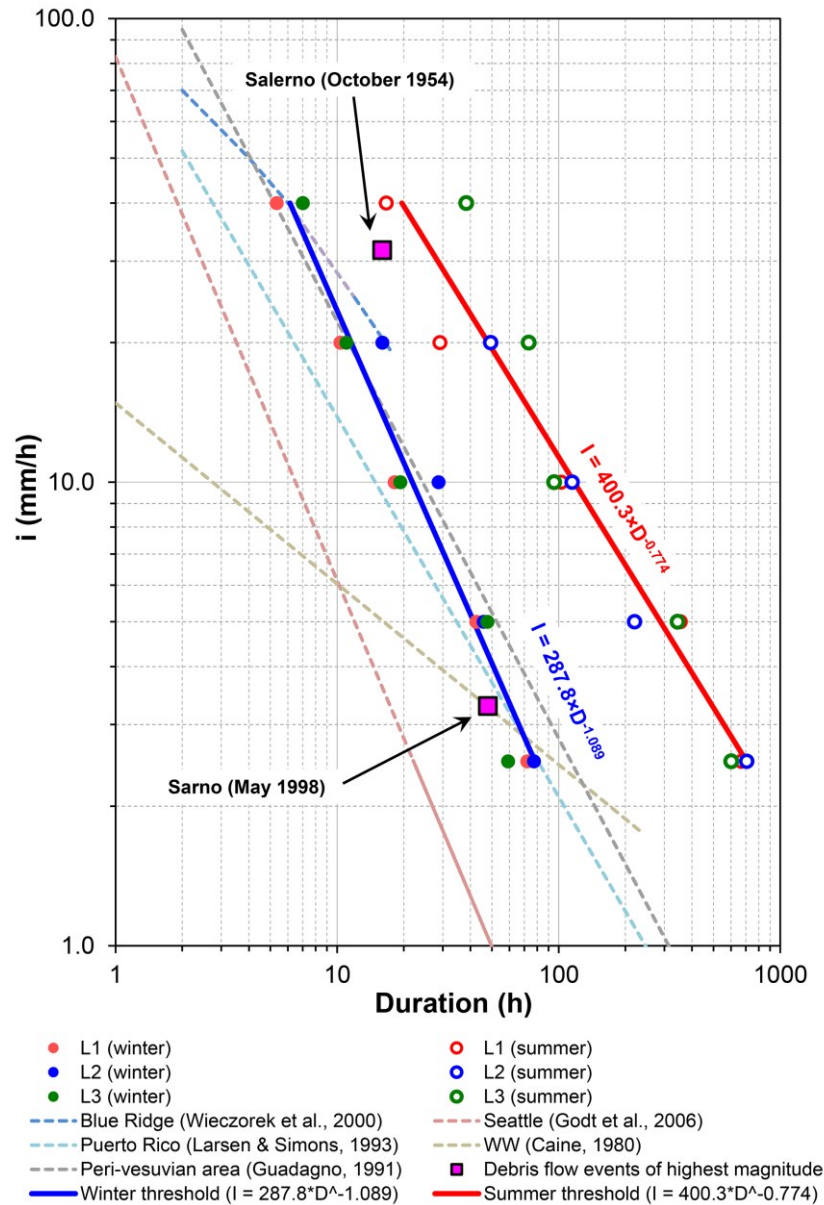


**Figure 6.10.** I-D hydrological thresholds calculated by a hydro-mechanical deterministic approach for three representative landslides (L1, L2 and L3) and taking into account antecedent conditions existing at the end of the dry season and at the late winter. The rainfall amounts that caused high magnitude debris flow events of Salerno (October 1954) and Sarno (May 1998) are also shown (from Napolitano et al., 2015).

Antecedent hydrological condition	I/D rainfall threshold (equation)	$\rho$	Prob. Fisher
Winter	$I = 287.8 \times D^{-1.089}$	0.9807	3.7%
Summer	$I = 400.3 \times D^{-0.774}$	0.9719	4.4%

**Table 6.3.** Deterministic rainfall threshold equations calculated for winter and summer antecedent hydrological conditions. Values of correlation coefficient ( $\rho$ ) and significance level of the null hypothesis (Probability of Fisher) are also shown (Napolitano et al., 2015)

### 6.1.3. Distributed hazard map

As previously described, the approach used to extend the hydrological modelling from the slope scale to distributed one by using the TRIGRS code was defined taking into account results deriving from VS2DTI modeling. In addition, to set up the representative hydro-mechanical properties of the cover modeled, a trial and error approach based on a statistical analysis of the measured properties known by scientific literature (De Vita et al., 2013; Napolitano et al., 2015) was used.

In detail, the first step was to understand how to simulate the hydrological dynamics within a slope mantled by ash-fall pyroclastic covers during a rainfall event. As confirmed by the VS2DTI modeling results, vertical infiltration and lateral throughflow may lead to near-saturated or saturated zone formation upslope of discontinuities in the ash-fall pyroclastic cover. This process, which is strongly affected by stratigraphic setting and unsaturated/saturated hydrological properties, conditions pressure head regime in ash-fall pyroclastic soils, leading to slope instability. Considering how the TRIGRS code works, only vertical flows (infiltration) can be modeled because there is no connection between each cell (or pixel) which discretizes the model. Then, lateral flows (throughflow) were modeled following a very particular and simple assumption. Rather than to simulate flows parallel to the slope, which move downslope through each cell and lead to near-saturated or saturated conditions, the vertical rise or decrease of an hypothetical water table was modeled, starting from a defined depth below the bottom of the cover (Fig. 6.11).

In detail, this approach is based on two fundamental assumption, deriving from in situ evidence and VS2DTI modeling results: slope areas close to cover discontinuity (rocky cliffs and road cuts) or thicknesses reduction (knickpoints) represent the initial slide triggering areas; saturation or near saturation conditions occur in these areas during heavy and/or long prolonged rainfall.

To verify this approach, the first step was to calibrate the hydro-mechanical properties of the representative cover, considering the slope scale test area and rainfall intensities used to reconstruct the I-D rainfall thresholds. Hydro-mechanical properties were assigned iteratively to the simplified one-dimensional ash-fall pyroclastic cover model and the resulting pressure head (PH) and Factor of Safety (FoS) values variability with time of three cells of the slope scale area were analyzed (Fig. 6.12 and Table 6.4)

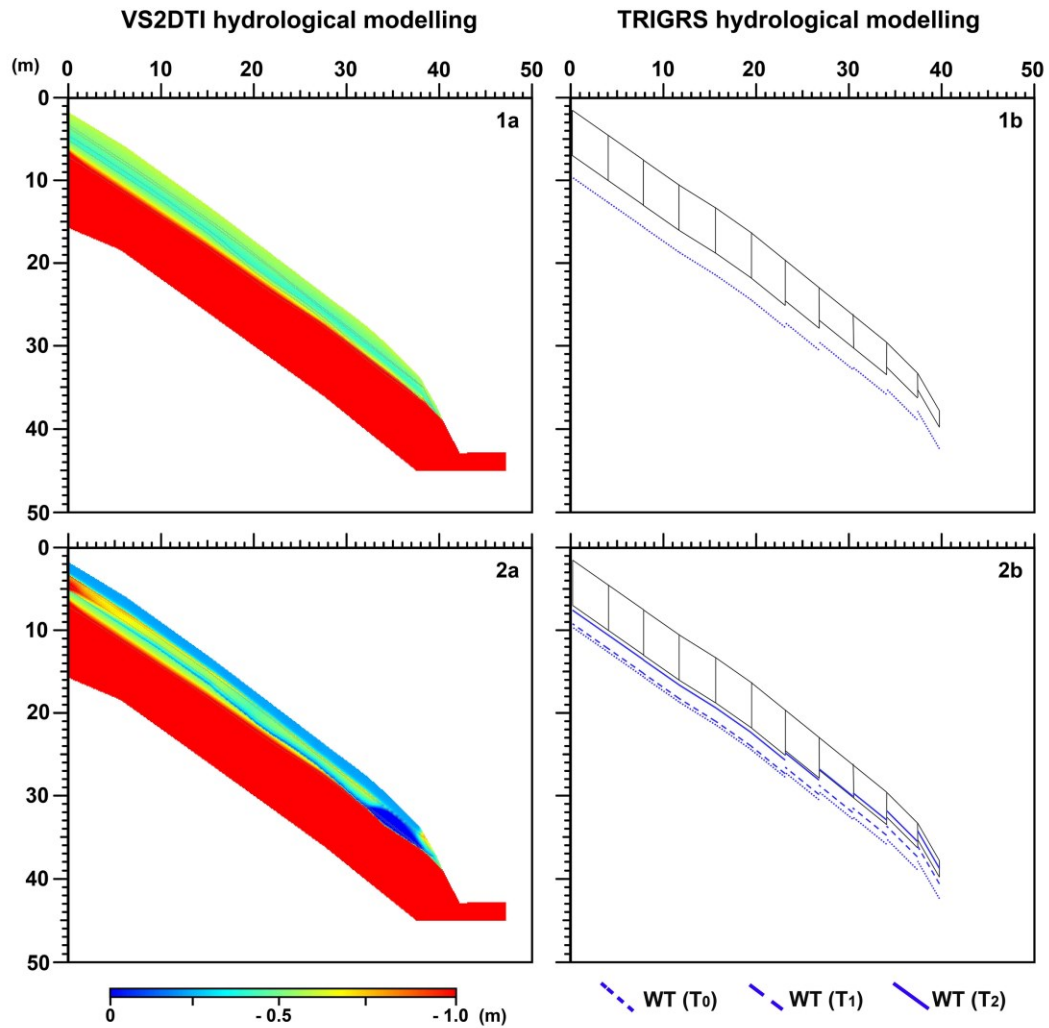


**Figure 6.11.** Modeling of throughflow and near saturated/saturated zone formation closely upslope of morphological discontinuities controlling reduction of ash-fall pyroclastic soil cover thickness, which characterize a representative slope, by using VS2DTI (1a, 2a) and TRIGRS (1b, 2b - WT for water table at time 0, 1 and 2) code.

These cells of the 5 m resolution DEM correspond to a section, which includes the initial slide area (cell 1) and part of the monitoring station area (cell 2 and 3) which characterize L4 test site.

According to the structure of the TRIGRS numerical code, pressure head values in unsaturated conditions (soil suction) are expressed as a correspondent depth of the groundwater table, which can be considered just as virtual in the studied case. In such a sense, the pressure head time series obtained at different depth for each assigned rainfall intensity (2.5, 5.0, 10, 20 and 40 mm/h) show how the infiltration process controls the rising of the virtual water table. It is important to remain here that in the

studied case the groundwater table and the saturation zone exist constantly during the hydrological year only in the carbonate bedrock at a depth of hundreds of meters.

During the rainfall event, a gradually increasing of PH and a decreasing of FoS values was observed occurring more in the cell 1 than in the cells 2 and 3 (Figs. 6.14, 6.15, 6.16 and 6.17).

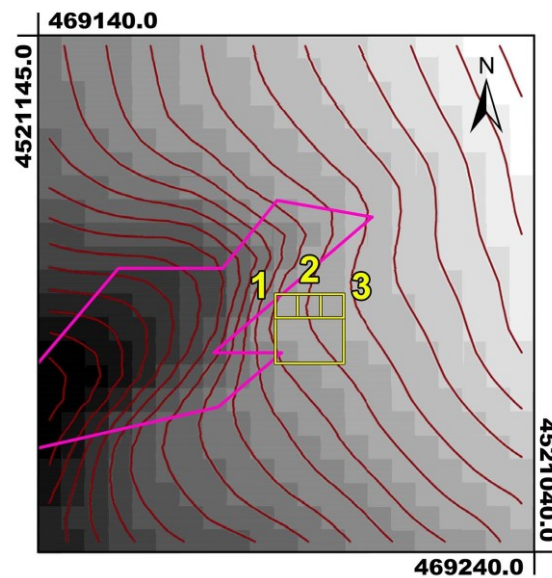


**Figure 6.13.** Considered cells used to calibrate the cover model and to verify the modeling approach. The cells correspond to the initial slide area (cell 1) of one May 1998 landslide event (pink contour) and part of the monitoring station area (cell 2 and 3) which characterize L4 test site.

Cell	Slope (°)	Thickness (m)
1	44	1.31
2	24	5.55
3	26	5.45

**Table 6.4.** Slope angles and cover thicknesses of the sample cells considered for the model calibration phase. Values derive from the 5 m resolution DEM and the ash-fall pyroclastic distribution model.

For 2.5, 5.0 and 10.0 mm/h of rainfall intensities, the rising of the water table lead to saturated and/or near saturated conditions in the cells with different times, except for 20 and 40 mm/h. These conditions strongly affected the cell 1 where instability conditions were observed due to the higher slope angle. In addition, FoS higher than 1 characterized the cells 2 and 3, despite the increasing of the PH up to 0 or slightly positive values in depth, presumably due to higher cover thicknesses.

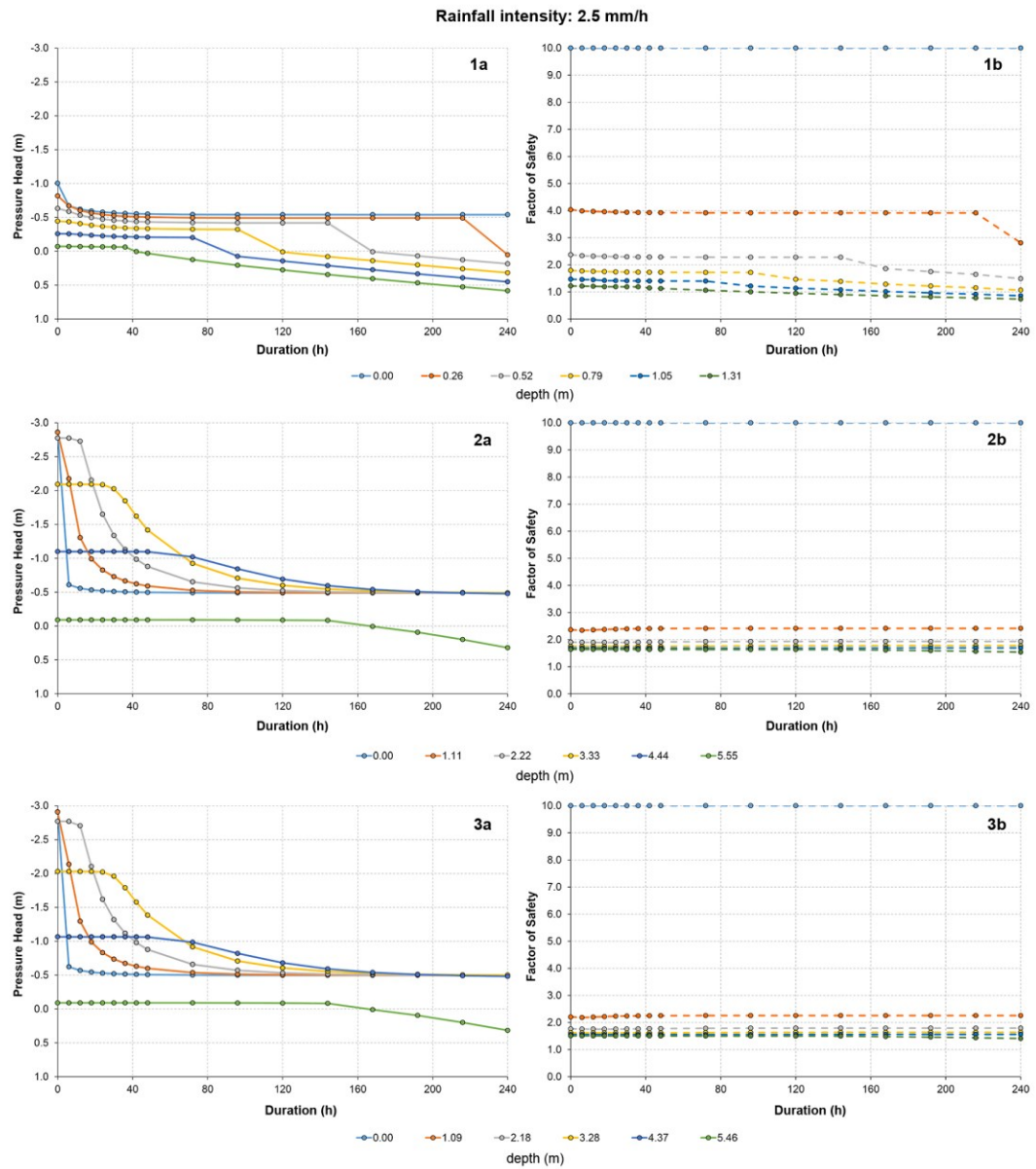


**Figure 6.14.** Time series of modeled pressure head (1a, 2a, 3a) and Factor of Safety (1b, 2b, 3b) variability at different depths for each sample cell (1, 2, 3) obtained for 2.5 mm/h of rainfall intensity.

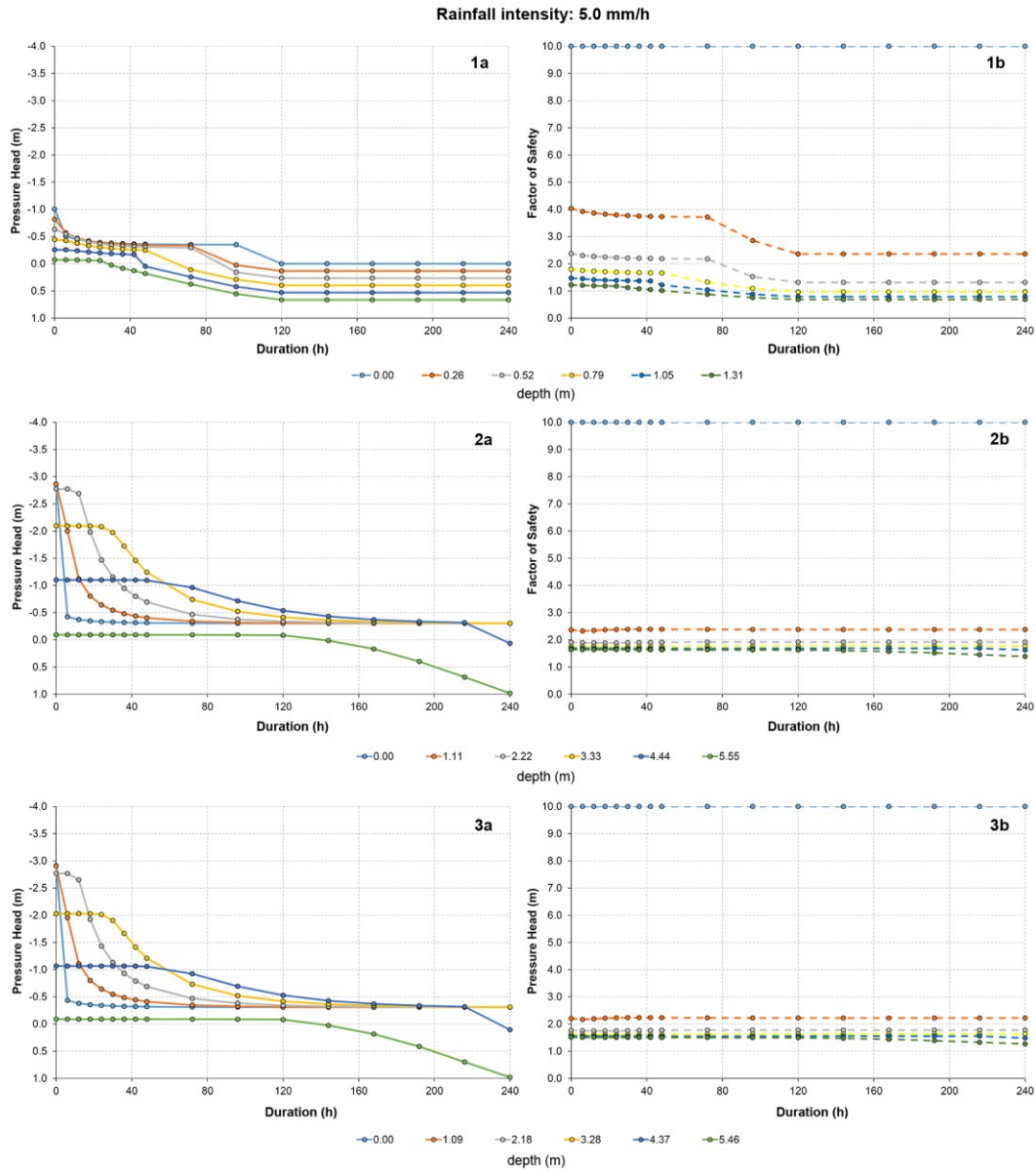


**Figure 6.15.** Time series of modeled pressure head (1a, 2a, 3a) and Factor of Safety (1b, 2b, 3b) variability at different depths for each sample cell (1, 2, 3) obtained for 5.0 mm/h of rainfall intensity.

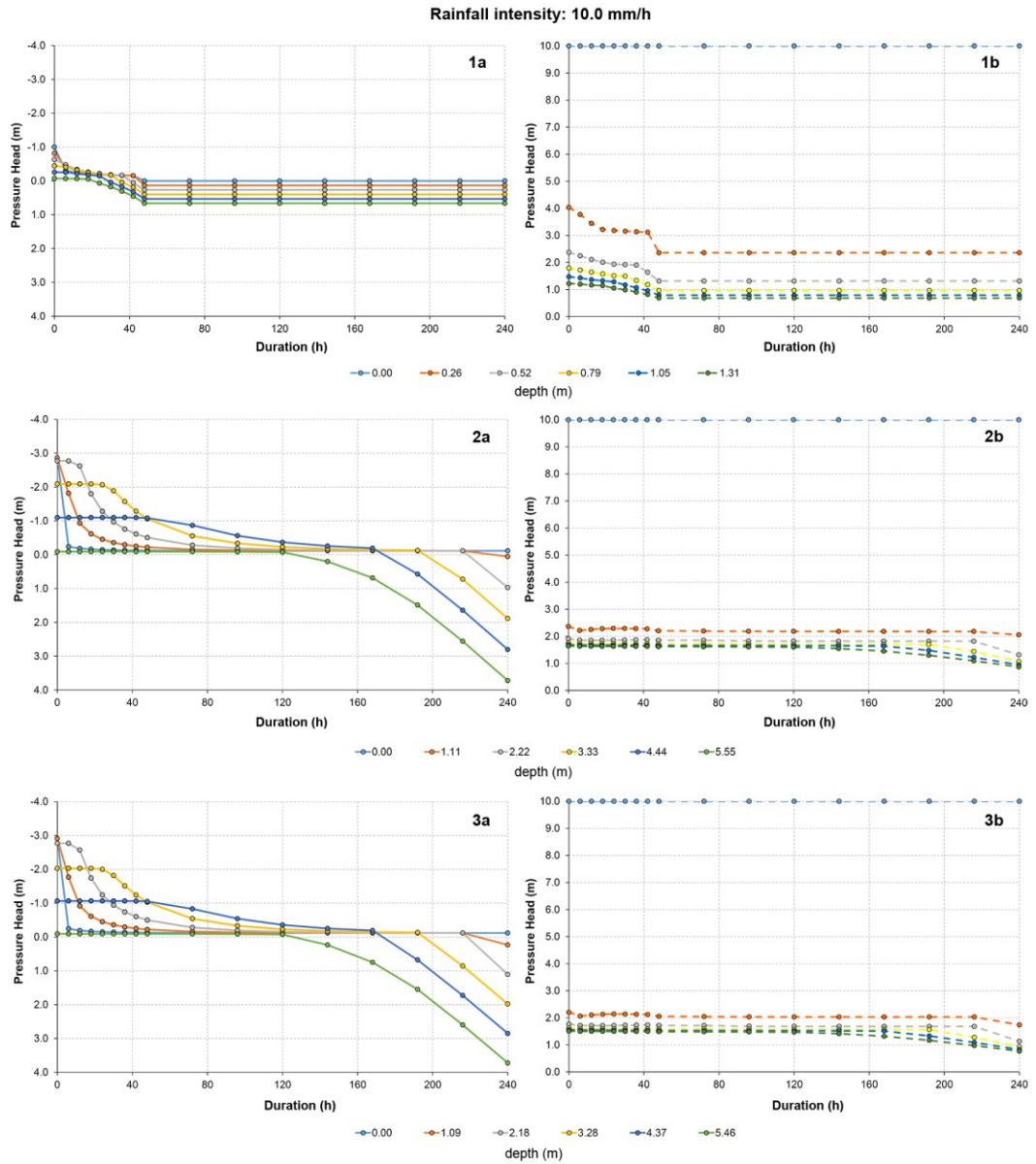


**Figure 6.16.** Time series of modeled pressure head (1a, 2a, 3a) and Factor of Safety (1b, 2b, 3b) variability at different depths for each sample cell (1, 2, 3) obtained for 10 mm/h of rainfall intensity.

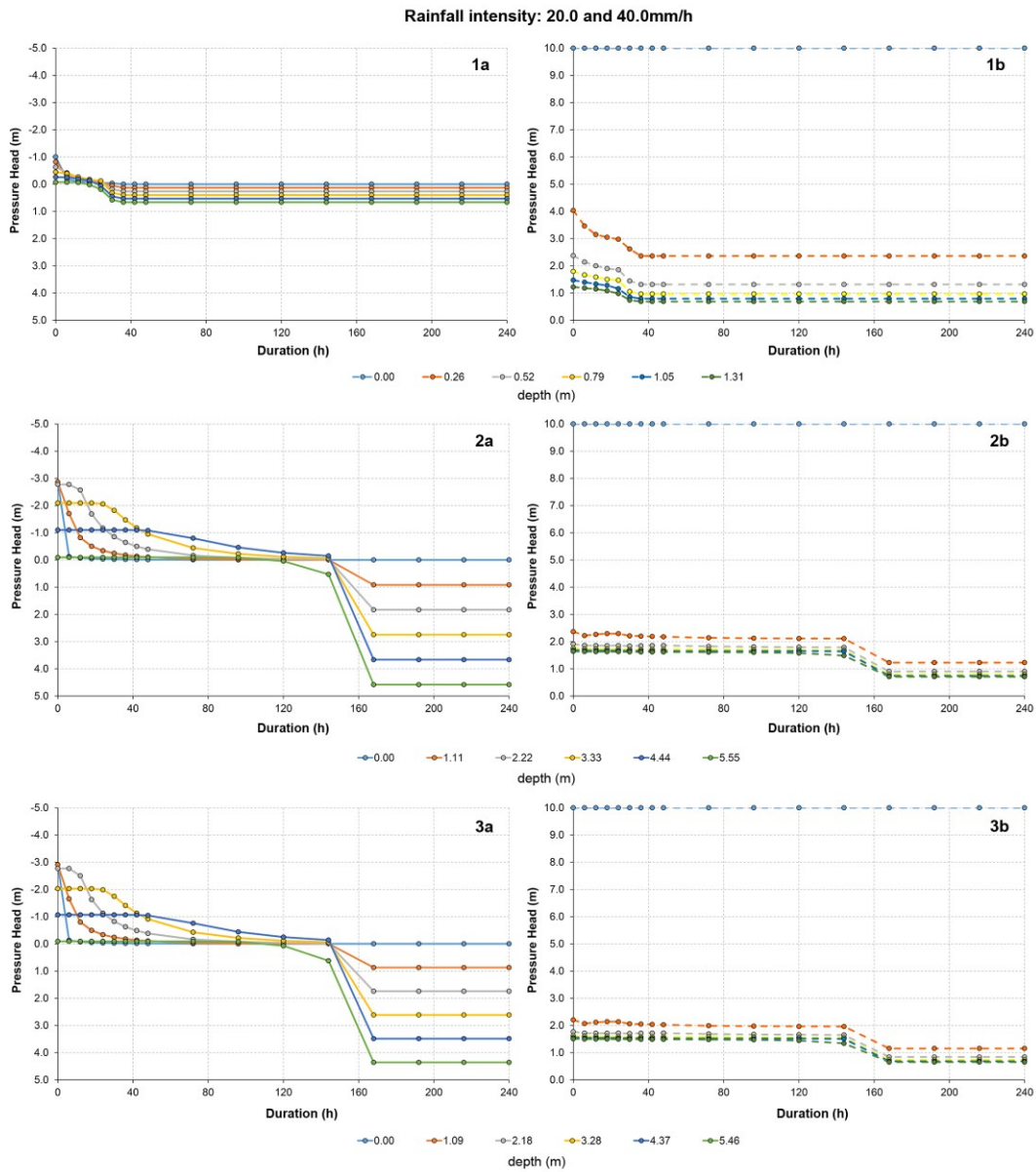


**Figure 6.17.** Time series of modeled pressure head (1a, 2a, 3a) and Factor of Safety (1b, 2b, 3b) variability at different depths for each sample cell (1, 2, 3) obtained for 20 and 40 mm/h of rainfall intensities.

The second step to calibrate the TRIGRS model was to consider rainfall intensity (I) and duration (D) values leading to slope instability conditions in the cell 1, which allowed defining a deterministic rainfall threshold for L4 test site. This latter threshold was compared with those obtained for the other three test sites (L1, L2 and L3) by using the VS2DTI code. Results showed a good correlation between rainfall I-D values calculated by means of the TRIGRS code and those belonging to the other three thresholds, especially for lower rainfall intensities (Fig. 6.18). In addition, obtained maps at local scale (Fig. 19A, 20A, 21A and 22A), for each considered rainfall intensity (2.5, 5.0, 10.0, 20.0, 40.0 mm/h) confirmed the slope instability condition of the triggering area of the May '98 initial debris slide (Fusco and De Vita, 2015), which characterize L4 test site. In fact, the observed instability conditions were confirmed by the presence of the initial slide area exactly in correspondence of the cell 1.

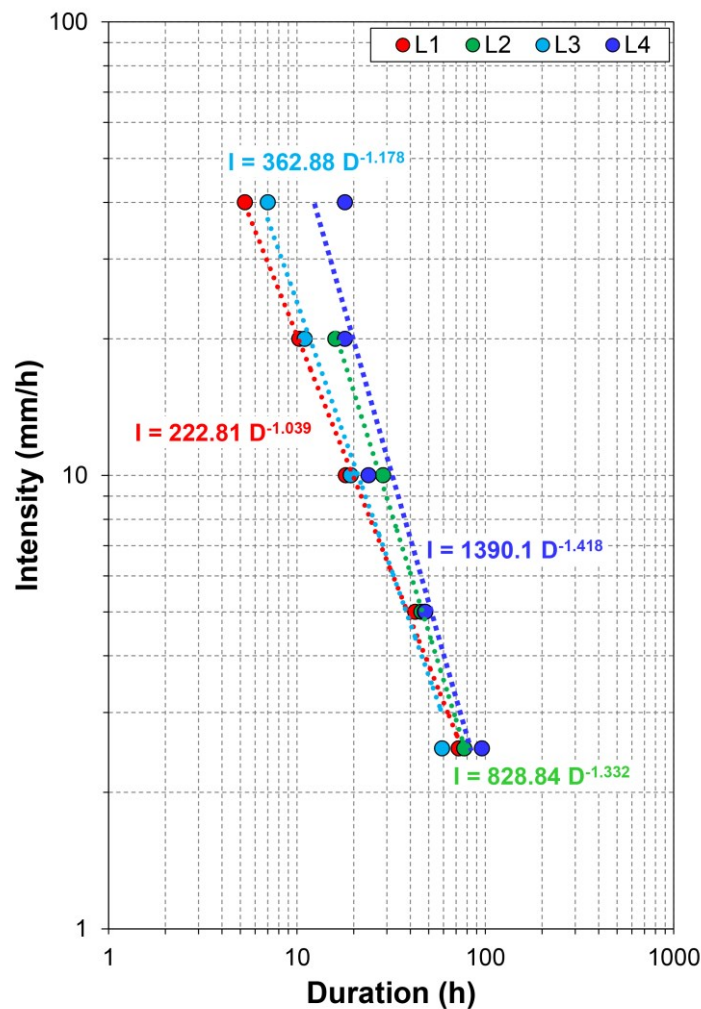


**Figure 6.18.** Comparison between deterministic rainfall threshold obtained by using TRIGRS code (L4) and those from Napolitano et al. (2015) obtained by using VS2DTI code (L1, L2 and L3).

Results derived by the calibration phase allowed validating both the methodological approach and simplified ash-fall pyroclastic cover model. Moreover, the calibration of hydro-mechanical properties (Table 6.5) allowed extending hydrological and slope stability modeling from the site-specific slope scale to the distributed one. Starting from these results, susceptibility maps were developed using the same constant rainfall intensities and duration previously considered (2.5, 5.0, 10.0, 20.0, 40.0 mm/h) to define the deterministic rainfall thresholds. Resulting maps show the distribution of stable and unstable pixels computed at the same time step of the slope failure previously obtained for the slope scale area (Figs. 19B, 20B, 21B and 22B). As mentioned in the Chapter 5, considering the numerical approximation of values close to the unit, pixels with computed FoS values  $< 1.0$ , and ranging between  $1.0$  and  $< 1.05$ , were considered respectively unstable or likely unstable. Finally, susceptibility maps were compared with the May 1998 Sarno and pre-May 1998 landslide events. In particular, the four source areas of the May 1998 initial debris slides (L1, L2, L3 and L4) were considered (Figs. 19C, 20C, 21C and 22C).

In a first analysis, observing these maps, it can be understood how unstable/likely unstable cells (or areas) affect the entire sample area. In particular, they are located both close to the main drainage network and along open slope areas where slope angles increase, cover thicknesses decrease, or discontinuities exist. The areal extension of initial slope instabilities (debris slides) were recognized inversely related to rainfall intensity (Figs 19, 20, 21 and 22). In fact, an expansion of unstable areas was observed with the reduction of the rainfall intensity.

$K_{sat}$ (m/s)	$\theta_s$ (ad.)	$\theta_r$ (ad.)	$\alpha$ (ad.)	$\phi'$ (°)	$c'$ (kPa)
$4.28 \times 10^{-6}$	0.574	0.105	4.099	33.7	4.4

**Table 6.5.** Calibrated hydro-mechanical soil properties deriving from statistical analysis of bibliographic data (De Vita et al., 2013; Napolitano et al., 2015) and assigned to the representative one-dimensional cover model used for TRIGRS modelling: effective friction angle ( $\phi'$ ); effective cohesion ( $c'$ ); saturated hydraulic conductivity ( $K_{sat}$ ); saturated volumetric water content ( $\theta_s$ ); residual volumetric water content ( $\theta_r$ ); van Genuchten's fitting parameter of water retention curve ( $\alpha$ ).

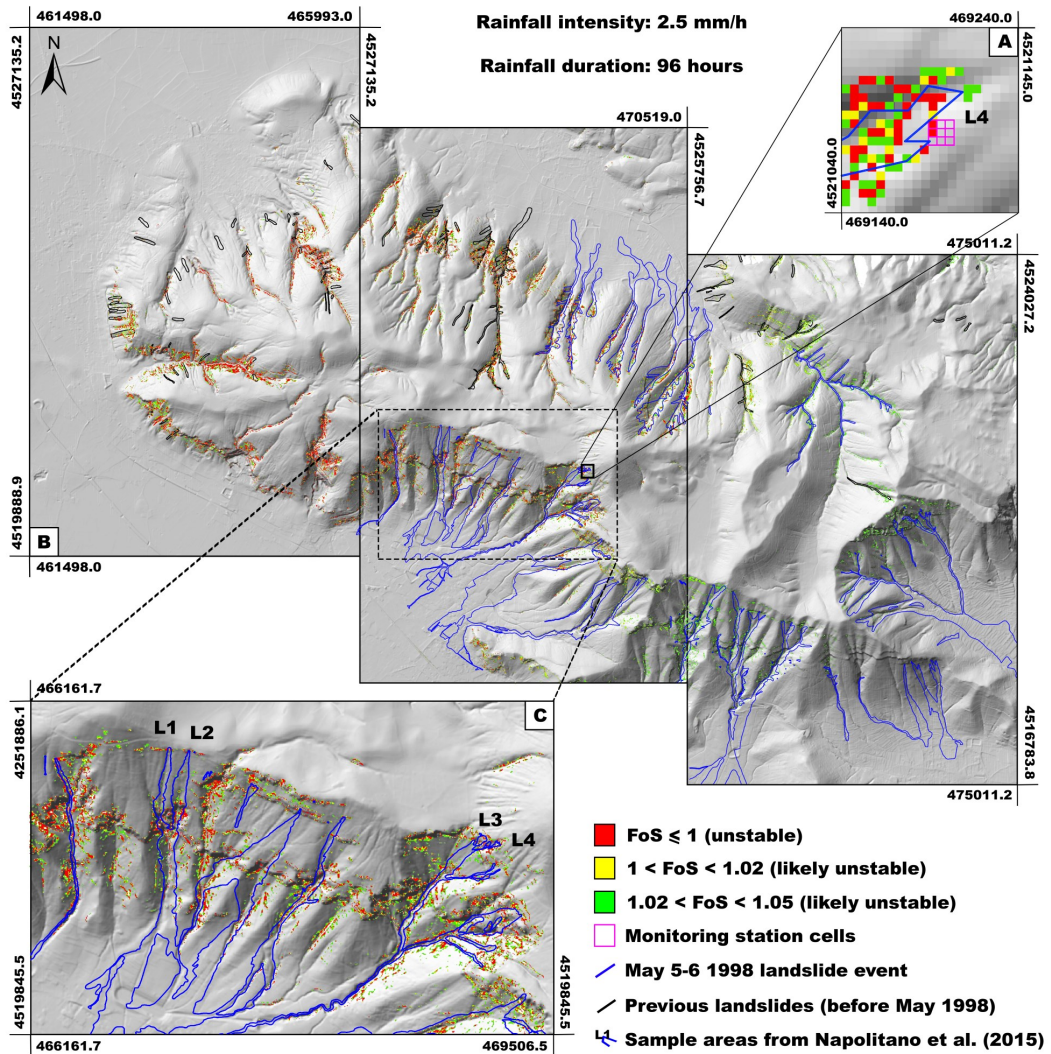


**Figure 6.19.** Susceptibility maps at a distributed scale, for the whole area (A) and at local scale (B), resulting from a modeled constant rainfall intensity of 2.5 mm/h for 96 hours. Unstable and likely unstable cells were compared within sample areas (C) L1, L2, L3 (Napolitano et al., 2015), L4 and the entire Sarno Mountains landslide database containing the May 1998 Sarno landslide event. Monitoring station cells used for local scale modeling and L4 threshold definition are also shown (C).

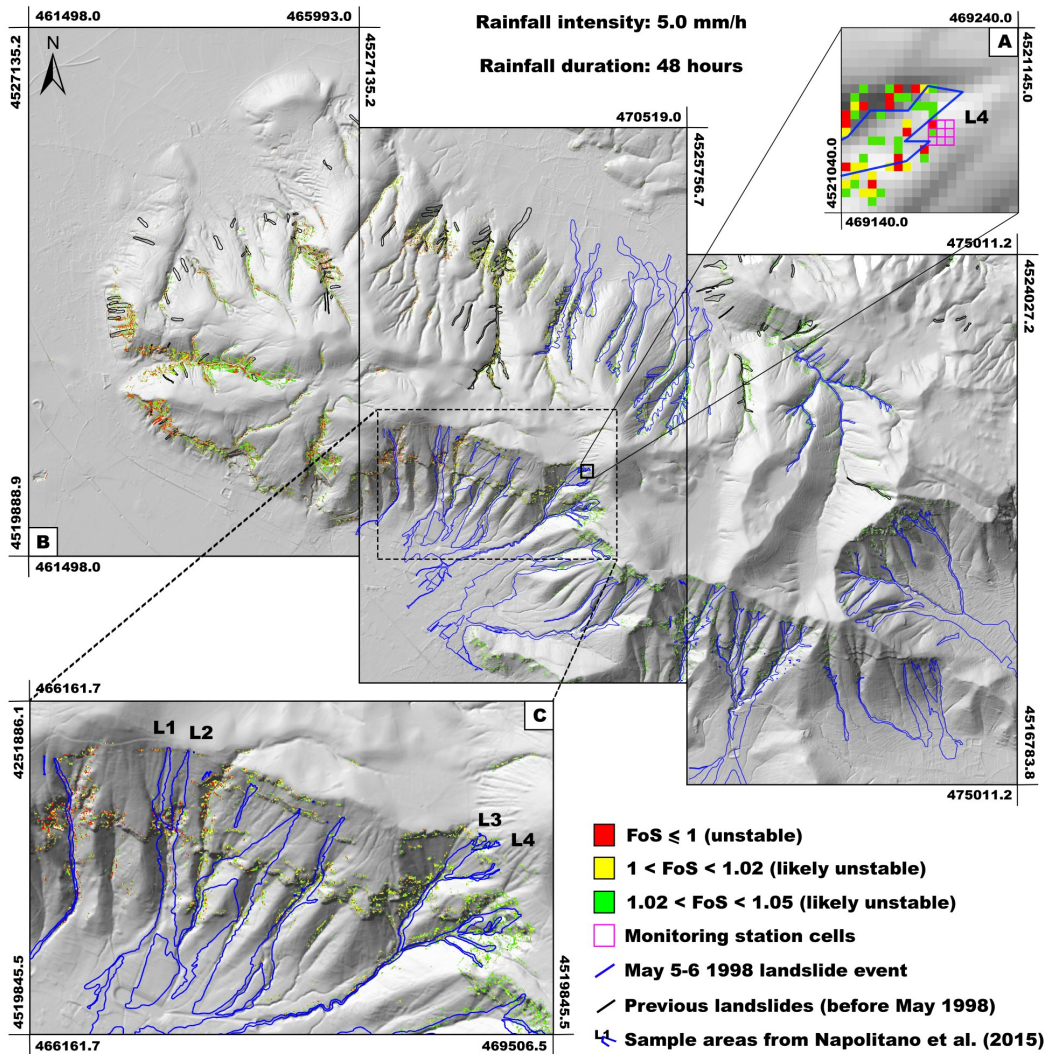


**Figure 6.20.** Susceptibility maps at a distributed scale, for the whole area (A) and at local scale (B), resulting from a modeled constant rainfall intensity of 5.0 mm/h for 48 hours. Unstable and likely unstable cells were compared within sample areas (C) L1, L2, L3 (Napolitano et al., 2015), L4 and the entire Sarno Mountains landslide database containing the May 1998 Sarno landslide event. Monitoring station cells used for local scale modeling and L4 threshold definition are also shown (C).

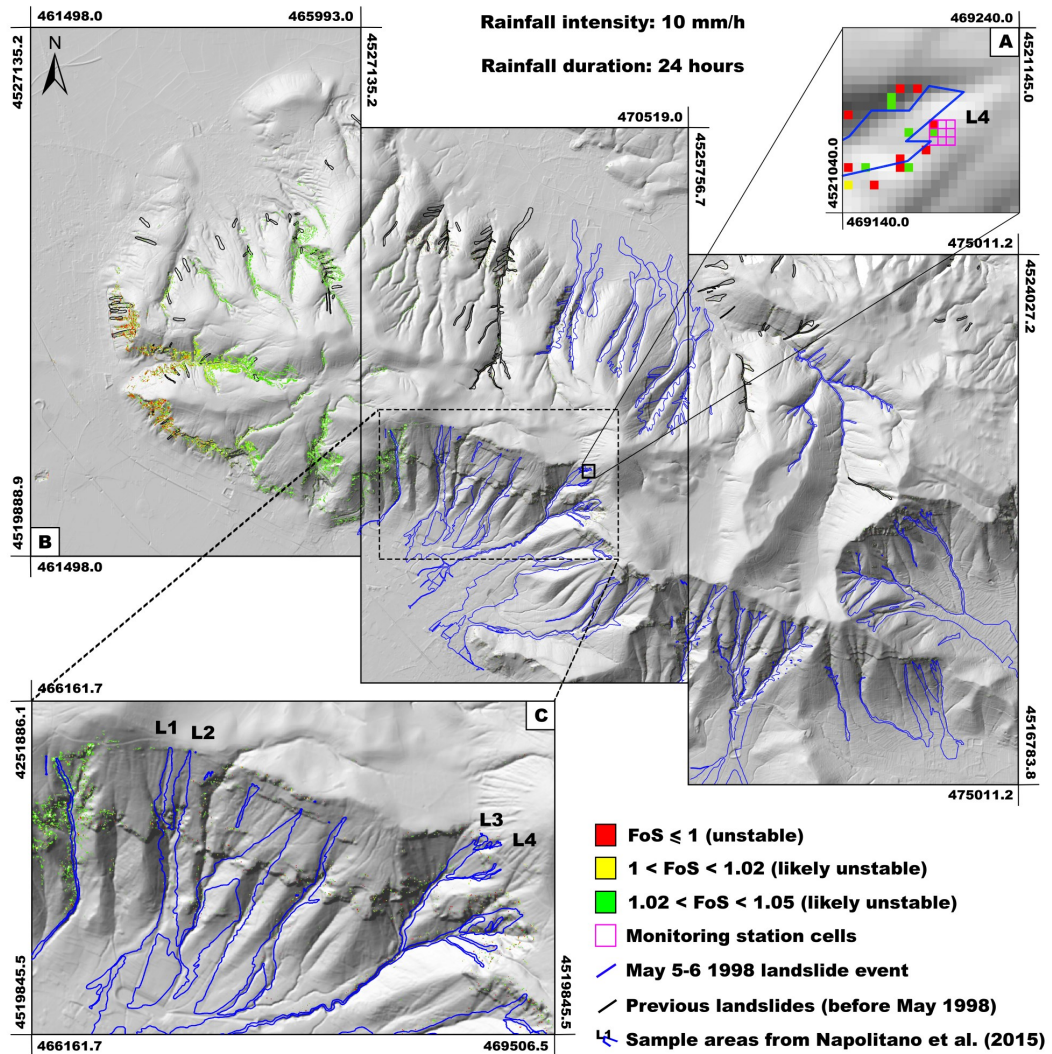


**Figure 6.21.** Susceptibility maps at a distributed scale, for the whole area (A) and at local scale (B), resulting from a modeled constant rainfall intensity of 10.0 mm/h for 24 hours. Unstable and likely unstable cells were compared within sample areas (C) L1, L2, L3 (Napolitano et al., 2015), L4 and the entire Sarno Mountains landslide database containing the May 1998 Sarno landslide event. Monitoring station cells used for local scale modeling and L4 threshold definition are also shown (C).

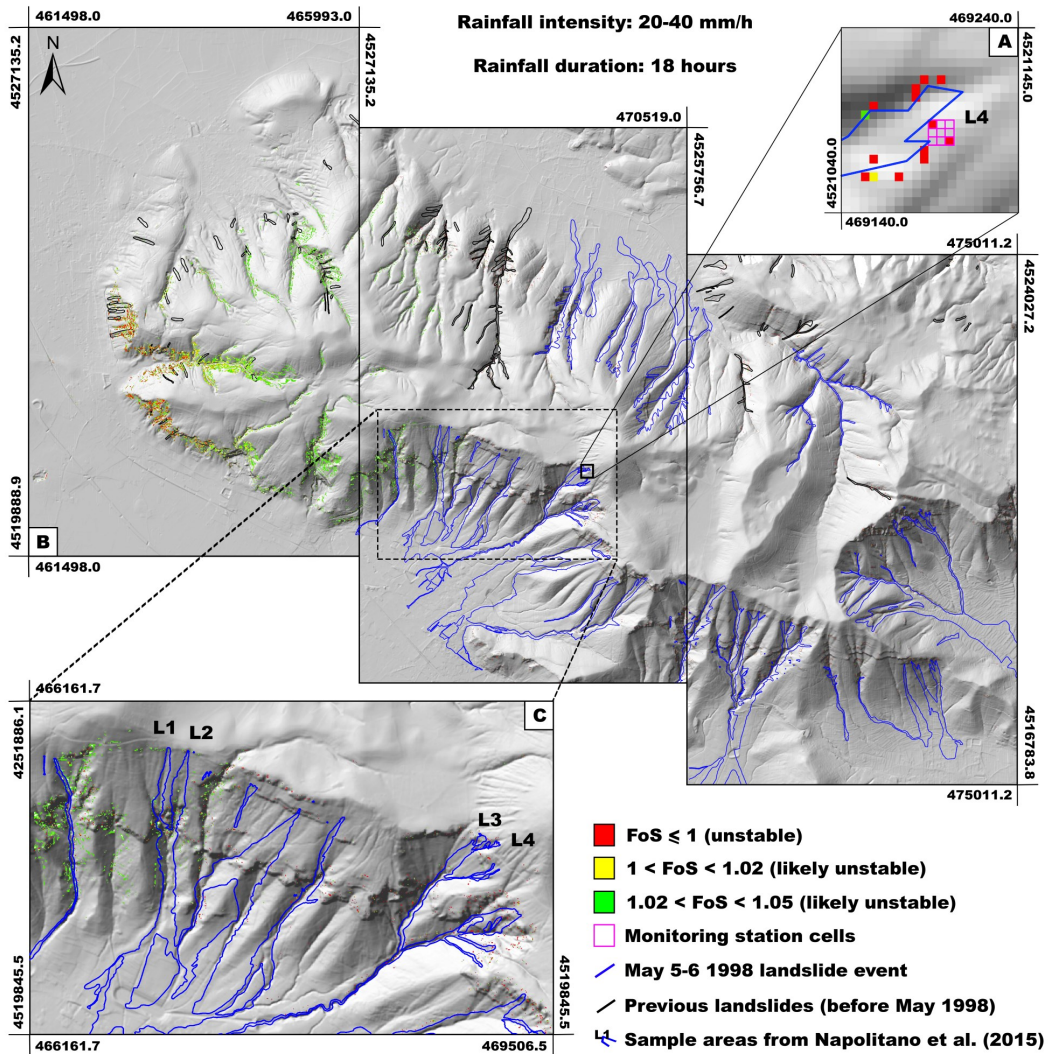


**Figure 6.22.** Susceptibility maps at a distributed scale, for the whole area (A) and at local scale (B), resulting from a modeled constant rainfall intensity of 20 and 40 mm/h for 18 hours. Unstable and likely unstable cells were compared within sample areas (C) L1, L2, L3 (Napolitano et al., 2015), L4 and the entire Sarno Mountains landslide database containing the May 1998 Sarno landslide event. Monitoring station cells used for local scale modeling and L4 threshold definition are also shown (C).

In detail, unsaturated throughflow can converge in small zones, where thickness and drainage section of the ash-fall pyroclastic soil cover reduce due to morphological factors, leading to the localized formation of near saturated/saturated conditions. In these areas FoS values became lower than 1.05 and then slope instabilities were observed, due to the combined effect of slope angles value higher than 35° and the reduction of the cover thickness from 5 to 1 m or less.

Moreover, the map showed that stable zones are located where low slope angles and high cover thicknesses exists. Observing the zoomed area of the susceptibility maps (Fig. 6.19C, 20C, 21C and 22C), the spatial variability of the unstable/likely unstable cells, obtained for each modeled rainfall intensity and duration, was more evident.

Comparison of the landslides events that occurred on the 5<sup>th</sup> and 6<sup>th</sup> May 1998, in particular with those affecting the four test sites, showed that the model simulated many of the cells for the triggering areas (*initial debris slide*), but performed more accurately for lower than for higher rainfall intensities. In addition, in some cases the distribution of the unstable cells along slopes fall within, or are coincident with, the border of the *debris avalanche* and *flow* zones.

Moreover, observing the maps, other potential susceptibility areas not affected by slope instability phenomena were correctly identified by the TRIGRS simulations. The same results were observed for susceptibility maps obtained for 20 and 40 mm/h, presumably due to lower infiltration rate ( $K_{sat}/I$  - Hydraulic Conductivity/Rainfall intensity) when high rainfall intensities are modeled.

## **6.2 Hydrological monitoring and modeling results for Camaldoli hill test area**

### **6.2.1. Pressure head regime of pyroclastic soils covering Camaldoli hill slopes**

Hydrological monitoring data recorded from January 2015 to December 2016 (Fig. 6.23 and Table 6.6) reveals the effects of the rainfall events and of the evapotranspiration processes on the top soil and the shallowest part of the

volcaniclastic series (down to 2.2 m), which characterize the Camaldoli hill test site area. Maximum fluctuations of pressure head values were observed in the shallowest horizon (top soil), even though significant, but damped variation, were recognized in the deeper soil horizons (ash horizon). As with the monitoring data from the Sarno Mountains site, pressure head time series revealed some gaps of data from a few days to several weeks, due to the limited functional range of tensiometers and Watermark sensors as well as damage by wild boars.

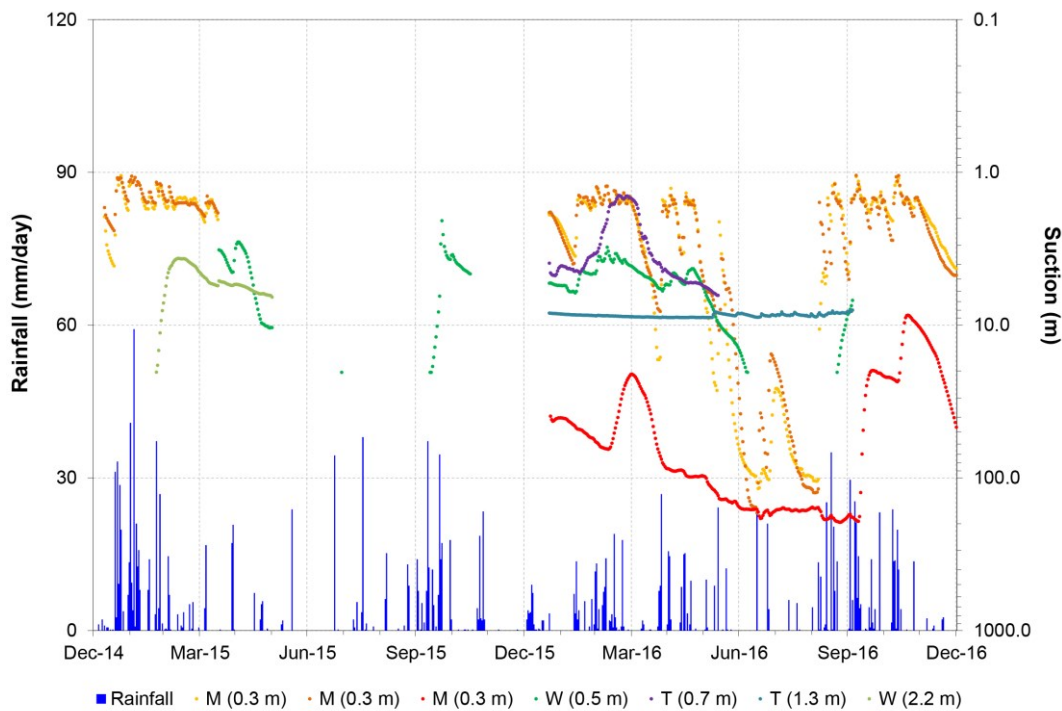


**Fig. 6.23.** Pressure head (PH) time series of the shallowest part of the volcaniclastic series of the Camaldoli hill test site. Monitoring activities were carried out from 2015 and 2016 hydrological years by using MPS-2 (M), Watermark (W) sensors and tensiometers (T). Daily rainfall is also showed.

In detail, the winter and early-spring periods of 2015 and 2016 (wet periods) showed strong fluctuations of the pressure head regime in the shallowest part of the top soil (down to 0.3 m), ranging between - 1.0 m and - 98.6 m. Moreover, different pressure head value trends were recorded at this depth: M1 and M2 sensors, ranging between -1.0 and -19.5 m, and M4 sensor, between -8.0 and -98.6 m. These conditions were due to an approximate balance between infiltration and gravity drainage taking place in this rainy period of the hydrological year. Furthermore, these wet conditions

are consistent with the combined effects of frequent heavy rainfall events, lower evapotranspiration rate during vegetation dormancy, and unsaturated water flow percolating downslope and into the deeper horizons. From the depth range between 0.5 m and 0.7 m, pressure head values varied between -1.4 and -8.0m, despite values lower than -20.4 were recorded in the early-September. Data obtained at 2.2 m of depth (fine ash horizon) showed pressure head values above the measuring capability of Watermark Sensors (-20.4 m) until early March 2015. As with the test area of the Sarno Mountains, these effects were damped and delayed with depth. In fact, observed data recorded at 1.3 m of depth, pressure head values were constantly about - 9.0 m.

Starting from spring through the early summer periods, a progressive and rapid decreasing of pressure head in the upper 0.7 m of the top soil was recorded (down to -195.6 m), due to the combined effects of less frequent rainfall events, increasing of the air temperature and higher evapotranspiration rate. On the contrary, as shown by the time series, these effects were not observed at 1.3 m, where pressure head values were consistently higher (- 9.0 m), and at 2.2 m where an abrupt increase (up to -4.0 m) was recorded. Unfortunately, after these recordings, no more data were obtained at 2.2 m depth due to equipment malfunction. Summer periods were characterized by consistently lower pressure head values, as recorded by the M4 sensor, despite strong fluctuation observed in the M1 and M2 sensors due to the combined effect of heavy rainfall events and high evapotranspiration rate. These differences may be attributed to different location of these devices in the monitoring area.

Depth (m)	2015			2016			
	min (m)	median (m)	max (m)	min (m)	median (m)	max (m)	
0.3	-4.1	-1.6	-1.0	-98.6	-2.9	-1.2	<b>Wet period</b>
0.5	-10.4	-4.2	-2.9	< -20.4	-4.6	-2.1	
0.7	-	-	-	-5.6	-4.1	-1.4	
1.3	-	-	-	-8.9	-8.8	-8.3	
2.2	< -20.4	-5.4	-3.7	-	-	-	
0.3	-	-	-	-195.6	-88.4	-1.2	<b>Dry period</b>
0.5	< -20.4	< -20.4	< -20.4	< -20.4	-11.4	-6.1	
0.7	-	-	-	-6.4	-6.0	-5.6	
1.3	-	-	-	-8.9	-8.6	-8.1	
2.2	-	-	-	-	-	-	

**Table 6.6.** Statistical analysis of field pressure head measurements recorded during 2015-2016 monitoring activities. Wet periods are related to Oct-May 2015 and 2016, while Dry period to Jun-Sep 2015 and 2016.

Starting in the late October, thus from the beginning of the rainy period, an abrupt rise of pressure head values was recorded involving initially the shallowest part of the volcanoclastic horizons and then followed by a delayed response in the deeper horizons. During these periods pressure head values increase up to - 1.0 m.

### **6.1.2. Short and long-term hydrological modelling results**

Considering monitored pressure head data during 2015, the hydrological numerical model was calibrated (*calibration phase*), minimizing visually the difference between the simulated and measured pressure head values (Fig. 6.24).

During the rainy period (January-May and October-December 2015), the simulated pressure head values in the shallowest part of the volcanoclastic series were very similar to those observed, showing also the same temporal dynamics (fluctuations) related to the infiltration of rainfall events. At 2.2 m of depth, numerical modeling succeeded in simulating the advance of the infiltration front observed in the late February 2015, with values of pressure head varying from -20.4 to -4.0 m, but afterwards draining more slowly than that observed during the transition back to the dry season.

The simulations reproduced with a somewhat overestimation the progressive decline in observed pressure head at 0.5 m depth, starting in the late April 2015. Despite the differences between simulated and measured data, the similar trend and timing of this seasonal transition indicates that the combined effects of rainfall and mostly of evapotranspiration were adequately captured by the VS2DTI model. A similar result was obtained at the same depth also during the summer-rainy transition period (during October 2015), when the abrupt increase in pressure head values was well simulated. Although the model captured the timing of transitions between winter and summer period, the magnitude of simulated pressure heads varied considerably from the observed values during the summer period (June-September 2015). The difference in magnitude can be attributed to the effects of the capillary barrier on the infiltration processes following only occasional, but intense thunderstorms occurring in this period. During such events, the effects of hysteresis of unsaturated properties, during drying and wetting conditions, could have a considerable impact on hydrologic

response, but this was not considered in the model since no information on the wetting SWRC was available.

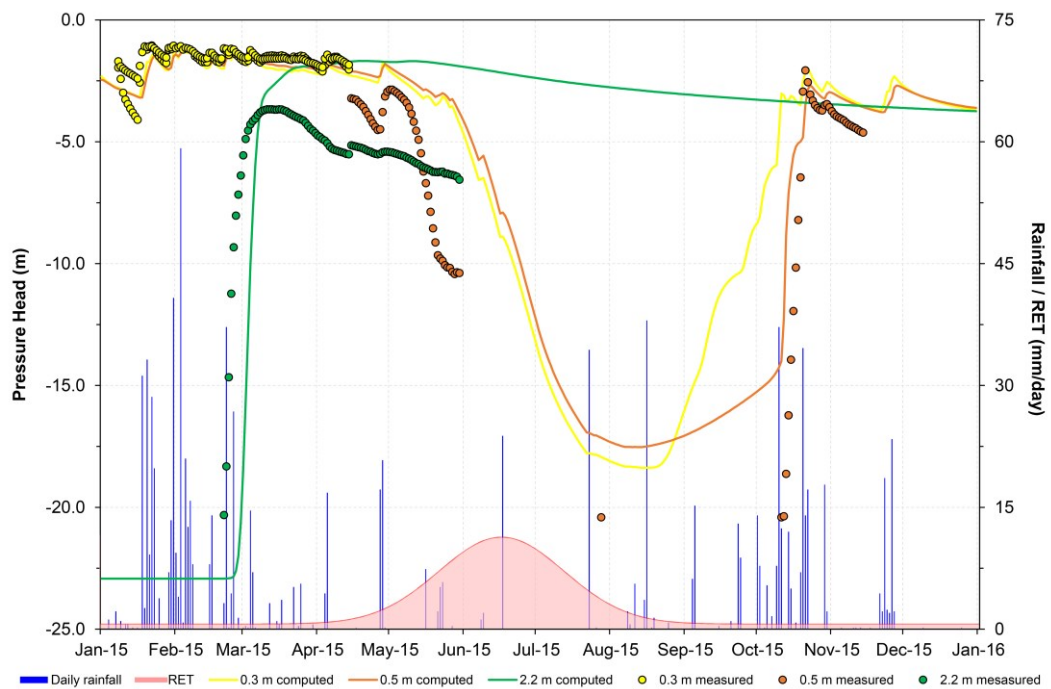


**Figure 6.24.** Pressure head distribution deriving from measured and simulated data of 2015 hydrological year. Daily rainfall and evapotranspiration rates (RET) are also shown.

The calibrated model was applied for the long-term hydrological simulations (*second phase*) from January 2006 to December 2015, which used an initial pressure head distribution based on the January 2015 monitoring data. Results showed a seasonal fluctuation of the pressure head time series characterized by summer lows and winter highs, strongly influenced by rainfall distribution and evapotranspiration processes effects (Fig. 6.25).

Analyzing the simulated hydrological behavior of the volcaniclastic series, similar pressure head values at different depths and different lower values in the summer periods were observed, the latter showing a periodicity characterized by three substantially lower values (2007, 2011 and 2015) and one considerably higher value (2009). Regardless, all the transitions from winter to summer and the reverse transitions were characterized by the same trend related to pressure head values decreasing and increasing, respectively. Median values (Table 6.7) showed that rainy

periods were characterized by pressure head values ranging from -1.7 m to -2.7 m, down to 0.5 m of depth, and from -1.0 m to -4.0 at 2.2 m of depth.

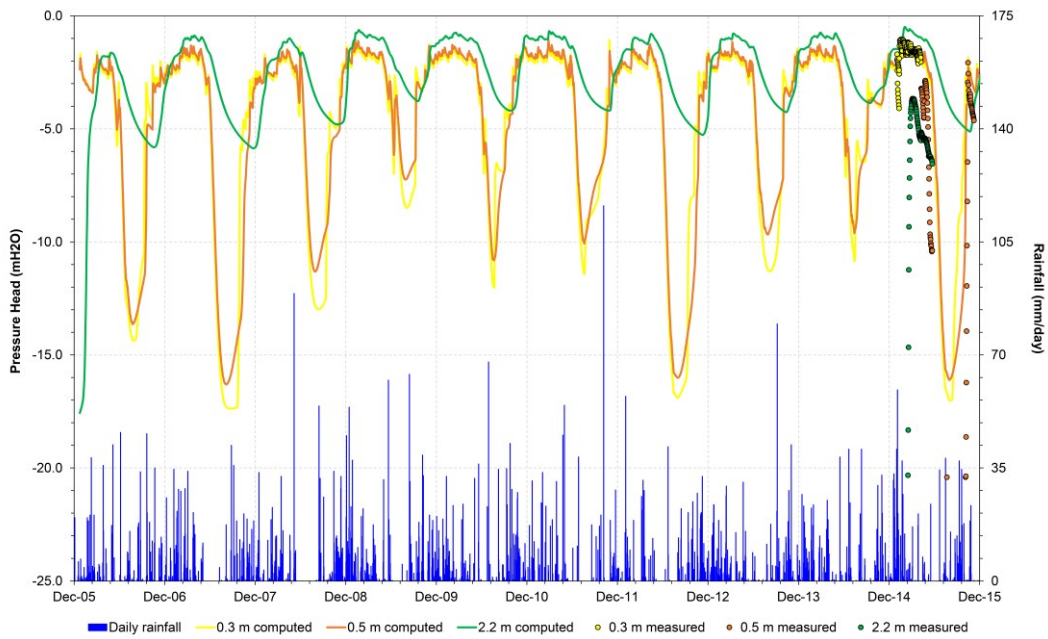


**Figure 6.25.** Pressure head distribution deriving from measured 2015 hydrological year and simulated data, derived from long-term modeling 2006-2015.

	Depth	2006	2007	2008	2009	2010	2011	2012	2013	2014	2015	
<i>M</i>	0.3m	-1.6	-1.3	-1.3	-1.0	-1.3	-1.1	-1.2	-1.2	-1.3	-1.0	Winter period
<i>Me</i>		-2.7	-2.5	-2.5	-1.9	-1.9	-2.0	-2.3	-2.1	-2.0	-2.4	
<i>m</i>		-5.8	-16.3	-6.0	-4.3	-4.2	-7.1	-8.1	-7.5	-4.1	-7.0	
<i>M</i>	0.5m	-1.7	-1.3	-1.5	-1.0	-1.2	-1.0	-1.2	-1.1	-1.3	-0.9	
<i>Me</i>		-2.7	-2.3	-2.4	-1.7	-1.8	-1.9	-2.1	-2.0	-1.9	-2.5	
<i>m</i>		-5.0	-14.1	-8.3	-3.7	-4.5	-6.8	-12.9	-7.4	-3.9	-16.3	
<i>M</i>	2.2m	-1.6	-0.9	-1.0	-0.6	-0.7	-0.7	-0.8	-0.8	-0.7	-0.5	
<i>Me</i>		-4.0	-1.7	-2.0	-1.1	-1.0	-1.1	-1.5	-1.4	-1.2	-1.7	
<i>m</i>		-17.6	-5.9	-4.8	-3.7	-4.2	-4.2	-5.3	-4.3	-3.8	-5.9	
<i>M</i>	0.3m	-2.9	-2.6	-1.4	-2.3	-3.0	-1.7	-3.6	-2.0	-2.8	-4.1	Summer period
<i>Me</i>		-11.7	-16.8	-11.6	-6.9	-6.8	-8.5	-15.7	-9.9	-6.3	-12.1	
<i>m</i>		-14.4	-17.4	-13.0	-8.5	-12.0	-11.4	-16.9	-11.3	-10.8	-17.0	
<i>M</i>	0.5m	-3.7	-2.7	-1.7	-2.9	-3.2	-1.8	-3.2	-2.0	-3.0	-3.6	
<i>Me</i>		-12.0	-14.8	-9.7	-6.2	-7.1	-7.6	-14.4	-8.2	-6.3	-14.3	
<i>m</i>		-13.6	-16.3	-11.3	-7.2	-10.8	-10.1	-16.0	-9.7	-9.6	-16.1	
<i>M</i>	2.2m	-2.2	-1.5	-1.6	-1.6	-1.5	-1.3	-1.5	-1.4	-1.4	-1.6	
<i>Me</i>		-4.3	-3.9	-3.4	-3.0	-3.4	-3.2	-3.8	-3.2	-3.3	-3.8	
<i>m</i>		-5.6	-5.2	-4.5	-3.8	-4.2	-4.0	-4.9	-4.1	-3.9	-4.9	

**Table 6.7.** Maximum (M), minimum (m) and Median (Me) values of simulated pressure head regime obtained with long-term modeling (2006-2015). Winter period are related to Oct-May, while to Jun-Sep for summer period.

The median values during the summer periods were similar, ranging from -6.2 m to -14.3 m, down to 0.5 m of depth, and from -3.0 m to -4.3 m at 2.2 m. The hydrological regime at depths of 0.3 and 0.5 m exhibited higher fluctuations in the pressure head values than those simulated at 2.2 m, which is likely due to dampening of infiltration fronts by not only increased depth, but also by the greater distance below the root systems from reeds and brooms.

# Chapter 7

---

## Discussion

### 7.1. Interpretation and comparison of results in the framework of scientific literature

#### 7.1.1. The Sarno Mountains test area

Results from monitoring activities, carried out from 2011 and 2016 years in a sample triggering area (L4 test site) in the Sarno Mountains, which failed during the 5<sup>th</sup> and 6<sup>th</sup> May 1998 landslide event, facilitated the analysis of hydrologic response in the ash fall pyroclastic cover. In detail, during the rainy periods, all recordings of B and Bb horizons showed typical higher pressure head values well matching with those previously measured, which were similarly recognized ranging in unsaturated conditions (Sorbino, 2005; Damiano et al., 2012; Fusco et al., 2013; Greco et al., 2013). On the contrary, the new recordings obtained for the Bb<sub>basal</sub> horizon (Fusco et al., 2015) during the most part of the rainy period, showed relatively dryer conditions, which previous studies had failed to observe in the deepest parts of the ash fall pyroclastic cover (Sorbino, 2005; Damiano et al., 2012; Greco et al., 2013). These conditions were related to the combined effect of frequent and abundant rainfall events and lower evapotranspiration rates, due to the dormant stage of the deciduous forest, which justifies the wetter condition occurring early in the shallower horizons (B and Bb horizons) and very tardily in the deepest one (Bb<sub>basal</sub> horizon). Specifically, the latter showed a temporally shifted hydrological regime in comparison to that of the shallower soil horizons. Since the late spring until the early autumn, the decrease of rainfall events and the increase of evapotranspiration rate causes a strong lowering of pressure head values, which strongly exceed those known by preceding measurements (Sorbino, 2005; Damiano et al., 2012). In this case, recordings obtained by using of Watermark and MPS-2 sensors allowed improving monitoring of the much dryer condition reached in the summer period by the ash-fall pyroclastic soil cover. In

addition, the dampening with depth of both rainfall events and effects of evapotranspiration processes was clearly observed. Pressure head distribution within the ash-fall pyroclastic soil cover is influenced mostly by temporal distribution of rainfall that causes a different velocity in deepening of the infiltration front.

As shown by pressure head measurements recorded at different depth, the gradual deepening of the infiltration front was strongly controlled by capillary barrier effects existing at the top of coarser pumiceous lapilli horizons and by the general progressive decrease of saturated hydraulic conductivity with depth (De Vita et al., 2013; Fusco et al., 2015; Napolitano et al., 2015). Rainfall events occurring at the end of the summer determine infiltration in the uppermost part of the ash-fall pyroclastic cover, which is initially characterized by lower pressure head values going in many cases below the functioning limit of the Watermark sensors (-20.4 m). At this stage the occurrence of occasional and slight runoff was inferred by traces at the ground surface of sheet-wash, rill and gully erosion observed after rainfall events with heavy intensities. The runoff formation appears unlikely if comparing saturated hydraulic conductivity values of the upper B horizon (Napolitano et al., 2015), ranging in the interval between the 25<sup>th</sup> and 75<sup>th</sup> percentiles from 173.5 to 453.0 mm/h, with usual rainfall intensities, which have not been recorded to exceed 150 mm/h (Tranfaglia and Braca, 2004). Instead, the occasional runoff was addressed to the ephemeral existence of a strong contrast between saturated hydraulic conductivity reached in the uppermost zone of the B horizon and the lower unsaturated hydraulic conductivity below the infiltration front (Loague et al., 2010).

The analysis of pressure head time series showed that the hydrological behavior of the ash-fall pyroclastic soil mantle is typically similar in all recording periods, except for extreme pressure head values, which depends on patterns and amount of rainfall. Furthermore, the composite hydrological dynamics of the ash-fall pyroclastic soil horizons, mostly at the beginning of the rainy season, when pressure head values increase in the shallower soil horizons, while they continue to reduce in the deeper ones, can be motivated by a re-equilibrium process of pore pressure within the deeper horizons due to the effects of the deeper root systems of chestnut trees (Fusco and De Vita, 2015).

Finally, the hydrological monitoring activity carried out by tensiometers, Watermark and MPS-2 sensors allowed the discover of a complex hydrological regime of the ash-fall pyroclastic soil mantle, and improved understanding of the relevant role

played by antecedent hydrological conditions on slope stability for a given rainfall event. This finding is very relevant to estimating rainfall thresholds for the triggering of shallow flow-type landslides and a related early warning system. In fact, the reconstruction of the latter needs to take into account the antecedent hydrological status of the pyroclastic cover in order to limit uncertainties due to analyze the last rainfall event only.

Starting from results of previous works (De Vita et al., 2013; Fusco et al., 2013) both short and long-term hydrological modeling were carried out for four test sites in the Sarno Mountains area, to reconstruct rainfall thresholds using a deterministic approach (Napolitano et al., 2015; 2016).

In detail, physically-based models were calibrated by using pressure head measurements of 2011 monitoring year, also considering the daily evapotranspiration rate estimated by the Thornthwaite (1948) equation (Napolitano et al., 2015). Results showed a good match between measured and simulated pressure head values. Thus, the long-term hydrological modelling over the whole reference period (2000÷2011) were carried out, whose results allowed definition of average hydrologic conditions of the ash-fall pyroclastic cover typical of the winter and summer period.

Different results were obtained by previous modeled seasonal hydrological slope conditions (Comegna et al., 2013; Papa et al., 2013; Cascini et al., 2014), which however did not simulate pressure-head values lower than -8.0 m in the dry season, depending on the characteristics of the installed equipment (tensiometers). The great variation of water content and pressure head involving the whole pyroclastic-mantle thickness observed, allowed new insights regarding the effect of antecedent-hydrological conditions (secondary climatic factors) on the slope stability, under rainfall of variable intensity and duration (primary climatic factors *sensu* Wieczorek and Glade, 2005).

Hydrological and slope stability modelling of critical rainfall conditions allowed the reconstruction rainfall thresholds for wet (winter) and dry (summer) seasons, for each of the three representative landslides (L1, L2 and L3 test sites).

The winter hydrological threshold matches well with other empirical hydrological thresholds, such as that found for the peri-Vesuvian area (Guadagno, 1991) or for the Blue Ridge area in central Virginia, USA (Wieczorek et al., 2000). In addition, they show higher intensity and duration values than other hydrological thresholds reconstructed for other areas of the world, such as those found for Puerto Rico (Larsen

and Simons, 1993) and Seattle, Wash., USA (Godt et al., 2006), as well as for the worldwide estimates (Caine, 1980). These greater I-D values can be related to peculiar characteristics of pyroclastic deposits mantling peri-Vesuvian slopes such as low unit weight, high hydraulic conductivity and high shear strength, relative to other types of soil. A further validation of the deterministic I-D thresholds for the wet season is inferred by the closeness with rainfall that caused the major high-magnitude debris flows events of Salerno (October 24<sup>th</sup> and 25<sup>th</sup> 1954) and Sarno Mountains (May 5<sup>th</sup> and 6<sup>th</sup> 1998), which falls within the envelope of experimental results.

As regards the hydrological threshold obtained for dry seasons, a marked positive shift in duration with a less narrow envelope was observed. Such results demonstrate a strong influence of antecedent hydrological conditions on rainfall I-D thresholds. These results explain the very limited possibility to have a rainfall-triggered flow-type landslide during or at the end of the summer owing to the extreme rainfall conditions needed. No other intensity-duration conditions were ever observed as is shown by the lower position of rainfall that caused the major high-magnitude debris flows events for the peri-Vesuvian area. The highlighted behavior confirms the noteworthy role of antecedent hydrological conditions in ash-fall pyroclastic soils as a factor controlling the threshold values of rainfall (De Vita and Piscopo, 2002; Fiorillo and Wilson, 2004) that trigger landslides.

Results deriving from hydrological monitoring and modeling activities carried out in the Sarno Mountain sample area (Fusco and De Vita, 2015; Napolitano et al., 2015; 2016; Tufano et al., 2016), allowed the reconstruction of a preliminary distributed hydrological and slope stability model, thus extending the approach used in this research from the site-specific slope scale to the regional one. The common approaches used to define susceptibility maps of rainfall-induced flow-type landslides, considers geomorphological and stratigraphic setting aspects, including slope angles, cover thicknesses and presence of natural or artificial discontinuities (Perriello Zampelli et al., 2011). The approach used in this research project represents a further step. In fact, climate and soil hydrological dynamics, which are the triggering factors of flow-type landslides involving ash-fall pyroclastic mantling peri-Vesuvian slopes, were considered. In detail, distributed hydrological and slope stability modelling were carried out using the TRIGRS code and assuming that landslide triggering is due to saturated or near saturated conditions occurring in areas close to cover discontinuities or reducing zones of ash-fall pyroclastic soil thicknesses, as also confirmed by

previous hydrological modeling results (De Vita et al., 2013).

A representative model of ash-fall pyroclastic cover, including hydro-mechanical properties, was calibrated taking into account rainfall I-D values resulting from the Napolitano et al. (2015) winter thresholds. The agreement between rainfall threshold obtained by the calibrated TRIGRS model with those previously reconstructed using VS2DTI for the three landslide sample areas (Napolitano et al., 2015) support the implementation of distributed hydrologic and slope stability modeling for the entire Sarno Mountains range.

The obtained landslide hazard maps showed good agreement with the entire landslide inventory database for the Sarno Mountains. Thus the results from the new approach can be considered an advance of those obtained with previous approaches.

The first hydrological and slope stability modeling to define susceptibility maps were carried out after the 5<sup>th</sup> and 6<sup>th</sup> May 1998 Sarno landslide event by Frattini et al. (2004). Analyzing their approach, the Authors supported the hypothesis that the triggering factors of this main rainfall-induced landslide event were related to infiltration process and throughflow occurring within the ash-fall pyroclastic cover. For this reason, both vertical (infiltration) and lateral (throughflow) flows were modeled, by using a diffusion model (Iverson, 2000) and a quasi-dynamic model (Barling et al., 1994). Their resulting maps of FoS distribution showed that slope instabilities mostly coincide with the areas located upslope of morphological discontinuities, despite both an overestimation and a not clear sub-division of instable/almost-instable areas resulted.

Maps obtained during this research project by using TRIGRS showed potentially unstable areas whose spatial resolution is finer than that identified in Frattini et al. (2004). Furthermore, for each critical rainfall intensity modeled, a different distribution of FoS values leading to slope instability was observed. Areas close to cover discontinuity (rocky cliffs, knickpoints or road cuts) or characterized by high slope angles (more than 35°), resulted potentially more unstable. Cover thickness as well as both rainfall intensity and duration, strongly affect the infiltration processes within the cover and then the occurrence of saturated or near-saturated conditions in those “critical” areas. These conditions were clearly observed by comparison of susceptibility maps obtained for each rainfall intensity value. In fact, clustered and more localized unstable areas for higher rainfall intensity were observed.

Results of distributed slope stability modelling in the Sarno Mountains sample area

emphasized the importance of the spatial variability of a rainfall event (cells), which distribution is strongly affected by morphological conditions. Considering the May 1998 Sarno landslide event, the maps showed many potentially unstable areas located in the western part of the mountains ridge not affected by these instabilities, which were confirmed by previous landslide events (for example Palma Campania 1986 event), instead. This means that the rainfall event, which triggered those landslides, hypothetically affected areas close to Mt. Pizzo D'Alvano.

### **7.1.2. The Camaldoli hill test area**

Results deriving from a soil pressure head monitoring station located along the southern slope of the Camaldoli hill (Naples, southern Italy) allowed recognizing for 2015 and 2016 years the hydrological behavior of the shallowest part of the volcanoclastic series, which characterizes the sample area. In particular, pressure head time series of the top soil, involved by the 4<sup>th</sup> and 5<sup>th</sup> March 2005 landslide event, were analyzed.

During the wet periods, typically occurring from October to May, measured pressure head values in the shallowest part of the top soil (down to 2.2 m) were mostly in disagreement with those reported in previous studies (Evangelista and Scotto Di Santolo, 2003; Evangelista et al., 2004; 2007). These differences are due to the functioning limits of devices (tensiometers) used during their monitoring activities. In fact, a behavior of the top soil not observed previously through pressure head values recorded by MPS-2 and Watermark sensors. During the dry periods, typically from June to September, after a strong decrease of pressure head values occurred (down to -195.6 m), lower than the limit previously observed (Evangelista and Scotto Di Santolo, 2003; Evangelista et al., 2004, 2007). By the analysis of the pressure head regime, characterized by high seasonal fluctuations, saturation conditions were not observed although probably occurred in the first few centimeters (< 0.10 m) of the top soil during heavy rainfall events, especially when lower pressure head and unsaturated hydraulic conductivity conditions allowed the capillary barrier effect. The higher values of pressure head measured during winter period, up to -0.5 m, are controlled by the combined effect of rainfall and unsaturated flow processes as well as by the very low evapotranspiration demand. Contrarily, between April and June periods, an

important lowering of pressure head values was recorded, strongly controlled by the rainfall decreasing, increasing of air temperatures and of evapotranspiration demand, the latter depending on the fast growth of the reeds and genista bushes that characterize the sample area.

Pressure head in the uppermost part of the volcanoclastic soil covering varies more rapidly than at depth, where hydrological response is delayed and damped during the hydrological year. At the beginning of the wet periods (rainy period), usually an abrupt increase of the pressure head values was recorded due to the deepening of the infiltration front. Specific conditions, such as composite layering of the surficial volcanoclastic series (alternating pumiceous lapilli and fine ash horizons), spatial variability of soil horizon thickness and slope angle (up to  $80^\circ$ ) control the distribution of pore pressure within hillslopes during rainfall events. Furthermore, the progressive decrease of saturated hydraulic conductivity with depth, in the shallowest part of the volcanoclastic series, and the constant low permeability of the fine ash horizon favor the existence of ephemeral throughflow processes, especially during the wet season and under heavy rainfall events.

These experimental observations had a strong influence on the setup and calibration of the numerical model used to simulate the hydrological regime of the uppermost volcanoclastic series, which is prone to landsliding. Values obtained by short-term modeling reproduced overall patterns of the field data, especially during the rainy and rainy/dry transition periods. Results represent both an advancement and improvement of results deriving from previous preliminary hydrological modeling carried out by using representative slope model (Evangelista et al., 2004; 2007).

The pore pressure dynamics during the rainy period and the timing of the seasonal transitions represent critical hydrological conditions for understanding slope instability.

A seasonal pressure head regime was reconstructed by a long-term modeling, characterized by similar pressure head values during the rainy period and variable lower peaks during the summer dry period, due to the later dependent on rainfall distribution during the different hydrological years. Furthermore, abrupt decreases and increases during the transition periods showed similar timing and trends each year.

The results obtained by monitoring and numerical modelling demonstrate the strong influence of antecedent hydrological conditions on slope stability, which explains the highest probability of landslide occurrence during rainy or transition

winter/summer periods (and conversely). The top soil horizon, which is primarily involved in slope failures at Camaldoli Hill, is characterized by friction angle values lower than the slope angle and, overall, by unconsolidated material with cohesion derived just from roots and apparent cohesion contributions. During heavy and/or prolonged rainfall, infiltration process causes increased pressure head values within the top soil that consequently determines a reduction (or annulment) of the apparent cohesion and a strong reduction of the shear strength, thus determining the triggering of the slope instability.

# Chapter 8

---

## Conclusions

The research described in this thesis is an effort to understand more deeply the relationship existing between the seasonal hydrological regime of pyroclastic soils mantling mountain slopes, which surround the Campanian Plain, and rainfall conditions, which trigger shallow flow-type landslides. Such geohazards represent one of the principal geological risks of the Campania region (southern Italy), particularly in the peri-Vesuvian and Phlegraean area. In the last century, flow-type landslides in this region have led to hundreds of casualties.

After the catastrophic landslide event of the 5<sup>th</sup> and 6<sup>th</sup> May 1998 occurred in the Sarno Mountains, several studies were focused on the comprehension of the landslide triggering mechanisms. As a result, there have been relevant advances in understanding the geomorphological aspects (Del Prete et al., 1998; Calcaterra et al., 1999; 2003; Guadagno et al., 2005; Calcaterra and Santo, 2004; Di Crescenzo and Santo, 2005; Calcaterra et al., 2006; Cascini et al., 2008; Palma et al., 2009; De Vita et al., 2013) and hydrological triggering factors (Cascini, 2003; Cascini et al., 2008; Cascini et al., 2010; De Vita et al., 2013, Napolitano et al., 2015; 2016). Direct connections between rainfall patterns and shallow-landslide occurrences are widely recognized in the scientific literature (e.g. Campbell, 1975; Caine, 1980; Guzzetti et al., 2008; Baum and Godt, 2010; Peruccacci et al., 2012). Indeed, hillslope hydrological processes such as infiltration and unsaturated throughflow determine an increase of pore pressures and their redistribution along the slope, which cause a reduction of the Factor of Safety of a slope due to a series of mechanisms, such as the reduction of apparent cohesion, buoyancy, etc. (Wieckzorek, 1996). Such general conditions cause slope instability in the pyroclastic soil-mantled slopes, which characterize the peri-Vesuvian and Phlegraean areas.

The study carried out in this PhD thesis was based on hydrological field monitoring and modelling, the latter at slope and regional scale, carried out in two test sites located in the Sarno Mountains (Fusco and De Vita, 2015; Napolitano et al., 2015; 2016; Fusco et al., 2016b; Tufano et al. 2016) and the Camaldoli hill area (Fusco et al., 2016a;

2016c). This approach was used to understand unsaturated/saturated hydrological critical conditions leading to initial instability. The same hydrological monitoring and physically-based modelling approach could be used in similar contexts throughout the world.

In detail, among the principal results of the monitoring activities, a particular hydrological behavior of the ash-fall pyroclastic coverings was found, which was unexpected if considering results of previous research. A peculiar seasonal hydrological regime, strongly affected by seasonal variability of rainfall and evapotranspiration effects, was recognized characterizing the ash-fall pyroclastic mantle. This hydrological behavior can be related both to the distinctive water retention properties of pyroclastic deposits, capable of storing a large amount of moisture by capillary retention, and to the sparse vegetation, in which evapotranspiration is concentrated in spring and summer seasons.

Based on the pressure head regime, it can be assumed that the major probability of triggering an initial debris slide occurs during the rainy period, from the late autumn to late spring. In such a hydrological period, due to the higher antecedent pressure head values, heavy and/or prolonged rainfall events can more readily result in unsaturated throughflow and near-saturated conditions within the ash-fall pyroclastic cover. Conversely, during the dry period, more stable conditions prevail due to both lower antecedent pressure head values and the minor probability of heavy and/or prolonged rainfall events occurrence.

The monitoring approach used in this research was fundamental to set up physically-based models to estimate the deterministic rainfall thresholds for the Sarno Mountains area (Napolitano et al., 2015; 2016; Tufano et al., 2016). The aim was to reduce uncertainty in the existing empirical rainfall thresholds for landslide initiation (Nikolopoulos et al., 2014), which are still used in the peri-Vesuvian and Phlegraean areas for Civil Protection purposes (Decreto del Presidente della Giunta Regionale della Campania, No 299 of June 30, 2005).

The results obtained by the analysis of the influence of antecedent conditions on the I-D hydrological thresholds show how the antecedent-hydrological conditions have a primary role in enhancing or diminishing the effect of single rainfall events on the slope instability. This is particularly relevant in soils of pyroclastic origin, due to their enhanced water retention characteristics. Specifically for the Sarno Mountains area, by the strong shift of the I-D deterministic thresholds toward longer durations

and/or higher intensities, the study shows that the hydrological status existing at the end of the summer strongly inhibits the slope instability under most rainfall conditions, because of the greater amount of water-retention capacity available in the pyroclastic mantle. Another factor in defining hydrological thresholds is the thickness of the pyroclastic cover, because water-retention capacity is proportional to the thickness. Such insight suggests the possibility that areas far away from the eruptive center and characterized by a lower pyroclastic soil thickness require lower rainfall amounts for triggering landslides at the end of the dry season than other areas with thicker pyroclastic covers. This conclusion is supported by field monitoring and modelling results, which demonstrated that to create hydrological conditions leading to near-saturation and unsaturated throughflow into the pyroclastic cover, a global increase of pressure head is necessary, even in the soil horizons deeper than the surface of rupture and not involved in landsliding.

Considering results of the hydrological monitoring and modeling at slope scale, susceptibility maps for the Sarno Mountains sample area were obtained (Fusco et al., 2016b). The approach was based on considering hydrological antecedent conditions of the ash-fall pyroclastic cover in addition to the geological and geomorphological aspects. Results may represent an advance of those already present in literature (Frattini et al., 2004; Perriello Zampelli et al., 2011).

Among the most important observations about the results obtained through TRIGRS modeling, several complexities were showed for the definition of representative model of involved pyroclastic cover and in particular of the hydrological dynamics modeling, triggering flow-type landslides. However, encouraging results from distributed hydrological and slope stability modelling were obtained. Susceptibility maps showed that during critical rainfall intensity, FoS values leading to instability was observed in areas close to cover discontinuity or characterized by high slope angles. Stratigraphic setting as well as both rainfall intensity and duration strongly affect the infiltration process within the cover and then the distribution along the slope of saturated or near saturated areas.

Results emphasized how the topography and the type of precipitation phenomena strongly control the spatial variability of a high-intensity rainfall event, determining its precise and narrow spatial position. The 5<sup>th</sup> and 6<sup>th</sup> May 1998 landslide event, which were determined to be potentially unstable by the TRIGRS simulation, were in fact subject to landliding events prior to 1998.

In conclusion, the definition of the spatial distribution of the landslide occurrence probability, related to a specific value of rainfall threshold, is essential to obtain landslide hazard maps at a large-scale. In this way, results of this research could facilitate the development of a consistent early-warning system, taking into account the seasonally variable landslide hazards. This could be defined by using deterministic thresholds and the triggering maps of large areas, coupled with a real-time monitoring and rainfall forecasts to assess landslides hazards across broad regions.

The next step, with the collaboration of local institutions, would be to place additional monitoring stations with near-real-time broadcasting capabilities in potentially unstable areas identified on the basis of the findings of the produced cartography.

## References

---

- Aleotti P. (2004) - A warning system for rainfall-induced shallow failures. *Engineering Geology*, 73, pp. 247-265.
- Alessio M., F. Bella, S. Improta, G. Belluomini, C. Cortesi and B. Turi (1971) - Carbon-14 Dates IX. *University of Rome, Radiocarbon*, 13(2), pp. 395-411.
- Alessio M., F. Bella, S. Improta, G. Belluomini, C. Cortesi and B. Turi (1973) - Carbon-14 Dates X. *University of Rome, Radiocarbon*, 15(1), pp. 165-178.
- Amerman C.R. and J.L. McGuinness (1967) - Plot and small watershed runoff: its relation to larger areas. *Trans. Am. Soc. Agric. Engrs.*, 10(4), pp. 464-466.
- Appel C.A. (1976) - A note on computing finite difference interblock transmissivities. *Water Resources Research*, Vol 12, 3, pp. 561-563.
- Barberi F., F. Innocenti, L. Lirer, R. Munno, T. Pescatore and R. Santacroce (1978) - The Campanian Ignimbrite: a major prehistoric eruption in the Neapolitan area (Italy). *Bull. Volcanol.*, 41(1), pp. 1-22.
- Barberi F., M. Carapezza, F. Innocenti, G. Luongo and R. Santacroce (1989) - The problem of volcanic unrest: the Phlegraean Fields case history. *Atti Conv. Lincei*, 80, pp. 387-405.
- Barling R.D., I.D. Moore and R.B. Grayson (1994) - A quasi-dynamic wetness index for characterizing the spatial distribution of zones of surface saturation and soil water content. *Water Resources Research*, 30, pp. 1029-1044.
- Baum R.L., W.Z. Savage and J.W. Godt (2002) - TRIGRS - A Fortran program for Transient Rainfall Infiltration and Grid-Based Regional Slope-Stability Analysis. *U.S. Geological Survey Open-File Report 02-0424*.
- Baum R.L., W.Z. Savage and J.W. Godt (2008) - TRIGRS - A Fortran program for transient rainfall infiltration and grid-based regional slope-stability analysis, version 2.0. *U.S. Geological Survey Open-File Report 2008-1159*.
- Baum R.L. and J.W. Godt (2010) - Early warning of rainfall-induced shallow landslides and debris flows in the USA. *Landslides*, 7, pp. 259-272.
- Baum R.L. and J.W. Godt (2013) - Correction to "Estimating the timing and location of shallow rainfall-induced landslides using a model for transient, unsaturated infiltration". *J. Geophys. Res. Earth Surf.*, 118, 1, DOI 10.1002/jgrf.20100.
- Bear J. (1979) - *Hydraulics of Groundwater*. MacGraw-Hill, New York.
- Bell G.L (1968) - Piping in the Badlands of Dakota. *Proc. 6<sup>th</sup> Annual Engineering Geology and Soil Engineering Symposium, Boise, Idaho*, pp. 242-257.

- Bertagnini A., P. Landi, M. Rosi and A. Vigliargio (1998) - The Pomici di Base plinian eruption of Somma-Vesuvius. *Journal of Volcanology and Geothermal Research*, pp. 219-239.
- Berry L. (1970) - Some erosional features due to piping and sub-surface wash with special reference to the Sudan. *Geografiska Annaler*, 52A (2), pp. 113-119.
- Bartole R. (1984) - Tectonic structures of the Latian-Campanian shelf (Tyrrhenian Sea). *Boll. Ocean. Teor. Appl.*, 2, pp. 197-230.
- Betson R.P. (1964). What is watershed runoff?. *J. Geophys. Res.*, 69, pp. 1541-1552.
- Betson R.P., J.P. Marius and R.T. Joyce (1968) - Detection of saturated interflow in soils with piezometers. *Proc. Soil Sci. Soc. Am.*, 32(4), pp. 602-604.
- Betson R.P. and J.P. Marius (1969) - Sources areas of storm runoff. *Water Res. Res.*, 5, pp. 574-582.
- Bilotta E., L. Cascini, V. Foresta, and G. Sorbino (2005) - Geotechnical characterization of pyroclastic soils involved in huge flowslides. *Geotechnical and Geological Engineering* 23, pp. 365-402.
- Bodman C.B. and C.A. Coleman (1943) - Moisture and energy conditions during downward entry of water into soils. *Proc. Soil Sci. Soc. Am.*, 8, pp. 116-122.
- Bouwer H. (1986) - Intake rate: Cylinder infiltrometer. In A. Klute (ed.) *Methods of soil analysis. Part 1. SSSA, Madison, WI*, pp. 825-844.
- Brancaccio L., A. Cinque, F. Russo and D. Sgambati (2000) - Le frane del 5 – 6 maggio 1998 sul gruppo montuoso Pizzo D'Alvano (Campania): osservazioni geomorfologiche sulla loro distribuzione e sulla dinamica delle connesse colate. *Quaderni di Geologia Applicata*, 7-1, pp. 5-36.
- Brand E.W., J.Premchitt and H.B. Phillipson (1984) - Relationship between rainfall and landslides in Hong Kong. *Proceedings of the 4<sup>th</sup> International Symposium on Landslides*, 1, pp. 377-384.
- Brooks R.H. and A.T. Corey (1964) - Hydraulic properties of porous media. *Colorado State University, Hydrology Paper*, N° 3, March.
- Brunsen, D and J.B. Thornes (1979) - Landscape sensitivity and change. *Transactions of the Institute of British Geographers*. N.S.4: 463-484.
- Budetta P. and R. De Riso (2004) - The mobility of some debris flows in pyroclastic deposits of the northwestern Campanian region (southern Italy). *Bulletin of engineering geology and environment*, 63, pp. 293-302.
- BURC (2005) - Il Sistema di Allertamento Regionale per il rischio Idrogeologico e Idraulico ai fini di protezione civile. Ruoli e compiti delle strutture regionali di protezione civile nell'ambito delle procedure di previsione e prevenzione del rischio idrogeologico per il territorio regionale. *D.P.G.R. No 299 of June 30, 2005. Bollettino Ufficiale della Regione Campania, special number (Naples, August 1 2005)*,

ISSN1591-5417.

- Calver A., M. J. Kirkby and D. R. Weyman (1972) - Modelling hillslope and channel flow. In *Chorley R. J. (Ed.), Spatial Analysis in Geomorphology, Methuen, London, pp. 197-218.*
- Caine N., (1980) - The rainfall intensity-duration control of shallow landslides and debris flows. *Geografiska Annaler 62A, pp. 23-27.*
- Calcaterra D. and P. M. Guarino (1999) - Recent landslides in the urban area of Naples: the middle-eastern sector. In: *Proc. Conf. on "Geologia delle Grandi Aree Urbane", Bologna, Italy, November 4<sup>th</sup>-5<sup>th</sup> 1997, pp. 257-261 (in Italian).*
- Calcaterra D. and P. M. Guarino (1999) - Morphodynamics and recent landslides in the Neapolitan slopes (western sector). *Geologia Tecnica e Ambientale, 2/99, pp. 11-17 (in Italian).*
- Calcaterra D., M. Parise, B. Palma and L. Pelella (1999) - The May 5<sup>th</sup> 1998, landsliding event in Campania (southern Italy): inventory of slope movements in the Quindici area. In *Proc. Intern. Symp. on "Slope Stability Engineering", IS – Shikoku '99, Matsuyama, Japan, pp. 1361-1366.*
- Calcaterra D., M. Parise, B. Palma and L. Pelella (2000) - The influence of meteoric events in triggering shallow landslides in pyroclastic deposits of Campania, Italy. In: *Landslides in research, theory and practice, (Eds) Bromhead, E., Dixon, N., and Ibsen, M.L., Proc. 8th Int. Symp. on Landslides, Cardiff, UK, pp. 209-214.*
- Calcaterra D., R. de Riso, A. Evangelista, M.V. Nicotera, A. Santo, A.Scotto Di Santolo (2003) - Slope instabilities in the pyroclastic deposits of the Phlegraean district and the carbonate Apennine (Campania, Italy). In *Proc. International Workshop on Occurrence and Mechanisms of Flows in Natural Slopes and Earthfills, Iw-Flows2003, Sorrento (May 14<sup>th</sup>-16<sup>th</sup>, 2003).*
- Calcaterra D., M. Parise, B. Palma (2003) - Combining historical and geological data for the assessment of the landslide hazard: a case study from Campania, Italy. *Natural Hazards and Earth System Sciences, 3, pp. 3-16.*
- Calcaterra D. and A. Santo (2004) - The January 10, 1997 Pozzano landslide, Sorrento Peninsula, Italy. *Engineering Geology, 75, pp. 181-200.*
- Calcaterra D., D. Coppin, S. De Vita, M.A. Di Vito, G. Orsi, B. Palma and M. Parise (2007a) - Slope processes in weathered volcanoclastic deposits within the city of Naples: the Camaldoli Hill case. *Geomorphology, 87, pp. 132-157.*
- Campbell R.H. (1975) - Soil slips, debris flows, and rainstorms in the Santa Monica Mountains and vicinity, southern California. In: *US Geological Survey Professional Paper 851. Washington DC: U.S. Government Printing Office, 51 pp.*
- Cardinali M., M. Galli, F. Guzzetti, F. Ardizzone, P. Reichenbach and P. Bartoccini (2006) - Rainfall induced landslides in December 2004 in Southwestern Umbria, Central Italy. *Natural Hazard Earth System Sciences, 6, pp. 237-260.*

- Carrara A., B. D'Elia and E. Semenza (1985) - Classificazione e nomenclatura dei fenomeni franosi. *Geol. Appl. Idrogeol.*, 20, 223-243(in Italian).
- Carson M. A. and M.J. Kirkby (1972) - Hillslope Form and Process. *Cambridge University Press*, 475 pp.
- Casagrande A. (1971) - On liquefaction phenomena: report of a lecture. *Géotechnique*, 21, pp. 197-202.
- Cascini L. (2003) - La gestione scientifica dell'emergenza idrogeologica del maggio 1998. *Monografia, G.N.D.C.I., C.N.R. Edition. pp 376 (in Italian)*.
- Cascini L. (2004) - The Flowslides Of May 1998 In The Campania Region: The Scientific Emergency Management. *Rivista Italiana Di Geotecnica*, 2, pp. 11-44.
- Cascini L. and G. Sorbino (2004) - The contribution of soil suction measurements to the analysis of flowslide triggering. *Invited lecture, Proc. of the Int. workshop "Flows 2003-Occurrence and mechanisms of Flows in natural slopes and Earthfill"*, Sorrento, Pàtron Ed., pp. 77-86.
- Cascini L., S. Cuomo and D. Guida (2008) - Typical source areas of May 1998 flow-like mass movements in the Campania region, Southern Italy. *Engineering geology*, 96, pp. 107-125.
- Cascini L. S Cuomo, M. Pastor and G. Sorbino (2010) - Modeling of rainfall-induced shallow landslides of the Flow type. *Journal of Geotechnical and Geoenvironmental Engineering*, pp.85-98.
- Cascini L. G. Sorbino and S Cuomo (2014) - Seasonal effects of rainfall on the shallow pyroclastic deposits of the Campania region (southern Italy). *Landslides, Vol. 11, Issue 5, pp. 779-792, DOI 10.1007/s10346-013-0395-3*.
- Celico P. (1986) - Prospezioni idrogeologiche. *Liguori editore (In Italian)*.
- Celico P., F.M Guadagno and A. Vallario (1986) - Proposta di un modello interpretativo per lo studio delle frane nei terreni piroclastici. *Geologia Applicata e Idrogeologia*, 21, pp. 173-193 (in Italian).
- Celico P. and Guadagno F.M. (1998) - L'instabilità delle coltri piroclastiche delle dorsali carbonatiche in Campania: attuali conoscenze. *Quad. Geol. App.*, 5, pp. 129-188 (in Italian).
- Celico P., L. Esposito, V. Piscopo and S. Aquino (2000) - Problematiche idrogeologiche connesse con i fenomeni di instabilità delle coltri piroclastiche della dorsale del Pizzo D'Alvano (Campania). *Quad. Geol. App., Pitagora editrice*, 7(2), pp. 167-187 (in Italian).
- Celico P., P. De Vita, S. Fabbrocino, V. Piscopo, G. Galicchio and T. Gentile (2002) - Primi risultati dell'analisi dei debris flows nei versanti dei rilievi carbonatici perivesuviani. *Atti dei Convegni Lincei 181*, pp. 114-133 (in Italian).
- Chirico G.B., P. Claps, F. Rossi and P. Villani (2000) - Hydrologic conditions leading

- to debris-flow initiation in the Campanian volcanoclastic soil. Mediterranean Storms. *Proceedings of the EGS Plinius Conference*, pp. 473-484.
- Chleborad A.F. (2003) - Preliminary evaluation of a precipitation threshold for anticipating the occurrence of landslides in the Seattle, Washington, area. *U.S. Geological Survey Open-File Report 03-463*.
- Cinque A., Rolandi G. and Zamparelli V. (1985) - L'estensione dei depositi marini olocenici nei Campi Flegrei in relazione alla vulcano-tettonica. *Boll. Soc. Geol. Ital.*, 104(2), pp. 327-348.
- Cinque A., E. Patacca, P. Scandone and M Tozzi (1993) - Quaternary Kinematic evolution of the Southern Apennines. Relationship between surface geological features and deep lithospheric structures. *Annali di Geofisica*, vol. XXXVI, N.2, pp. 249-260.
- Cioni R., R. Santacroce and A. Sbrana (1999) - Pyroclastic deposits as a guide for reconstructing the multi-stage evolution of the Somma-Vesuvius caldera. *Bull. Volcanol.*, 60, pp. 207-222.
- Cole P.D. and C. Scarpati (2010) - The 1944 eruption of Vesuvius, Italy: combining contemporary accounts and field studies for a new volcanological reconstruction. *Geological Magazine*, 147 (3), pp. 391-415.
- Comegna L., E. Damiano, R. Greco, A. Guida, L. Olivares and L. Picarelli (2013) - Effects of the vegetation on the hydrological behavior of a loose pyroclastic deposit. *Procedia Environmental Sciences*, 19, pp. 922-931
- Corominas J. and J. Moya (1999) - Reconstructing recent landslide activity in relation to rainfall in the Llobregat River basin, Eastern Pyrenees, Spain. *Geomorphology*, 30, 1-2, pp. 79-93.
- Crosta G.B. and P. Frattini (2003) - Distributed modelling of shallow landslides triggered by intense rainfall. *Natural Hazards and Earth System Science*, 3, 1-2, pp. 81-93.
- Crosta G.B. and P. Dal Negro (2003) - Observations and modelling of soil slip-debris flow initiation processes in piroclastica deposits: The Sarno 1998 event. *Natural Hazards Earth Syst. Sci.*, 3, pp. 53-69.
- Crozier M.J. and R.J. Eyles (1980) - Assessing the probability of rapid mass movement. In: The New Zealand Institution of Engineers. *Proceedings 3<sup>rd</sup> Australia New Zealand Conference on Geomechanics*, New Zealand, Inst. Eng. Proc. Techn. Groups, 6, 2, pp. 47-2.51.
- Crozier M.J. (1997) - The climate-landslide couple: A southern hemisphere perspective. In: *Matthews J.A., D. Brunsten, B. Frenzel, B. Gläser and M.M. Weiß (eds.), Rapid Mass Movement as a Source of Climatic Evidence for the Holocene. Palaeoclimate Research*, Gustav Fischer Verlag, Stuttgart, 19, pp. 333-354.
- Crozier M.J. (1999) - Prediction of rainfall-triggered landslides: a test of the

- antecedent water status model. *Earth Surface Processes and Landforms*, 24, pp. 825-833.
- Cruden D.M. (1991) - A Simple Definition of a Landslide. *Bulletin of the International Association of Engineering Geology*, 43, pp. 27-29.
- Cruden D.M. and Varnes D.J. (1996) - Landslide types and processes. In: Turner A.K.; Shuster R.L. (Eds) *Landslides: Investigation and Mitigation. Transp. Res. Board, Spec. Rep. 247*, pp. 36-75.
- D'Argenio B., T.S. Pescatore and P. Scandone (1973) - Schema geologico dell'Appennino Meridionale. *Accad. Naz. Lincei Quad.*, 183, pp. 49-72.
- Davies TRH (1986) - Large debris flows: a macroviscous phenomena. *Acta Mechanica*, 63, pp. 161-178.
- Damiano E., L. Olivares and L. Picarelli (2012) - Steep-slope monitoring in unsaturated pyroclastic soils. *Engineering Geology*, 1-12, pp. 137-138.
- Deino A.L., G. Orsi, M. Piochi, S. de Vita (2004) - The age of the Neapolitan Yellow Tuff caldera-forming eruption (Campi Flegrei caldera - Italy) assessed by  $^{40}\text{Ar}/^{39}\text{Ar}$  dating method. *J. Volcanol. Geotherm. Res.* 133, pp. 157-170.
- De Vita P., P. Reichenbach, J.C. Bathurst, M. Borga, G.M. Crozier, T. Glade, F. Guzzetti, A. Hansen and J. Wasowski (1998) - Rainfall-triggered landslides: A reference list. *Environmental Geology*, 35, 2-3, pp. 219-233.
- De Vita P. (2000) - Fenomeni di instabilità delle coperture piroclastiche dei Monti Lattari, di Sarno e di Salerno (Campania) ed analisi degli eventi pluviometrici determinanti. *Quaderni di Geologia Applicata*, 7, pp. 213 – 235 (in Italian).
- De Vita P. and P. Piscopo (2002) - Influences of hydrological and hydrogeological conditions on debris flows in peri-vesuvian hillslopes. *Natural Hazards and Earth System Sciences*, 2, pp. 1-9.
- De Vita P., D. Agrello, F. Ambrosino and E. De Luzio (2003) - Characterisation of the hydrogeological surficial system pyroclastic soil-carbonate bedrock in the Sarno Mountain ridge. *Quaderni di Geologia Applicata*, Vol. 2, pp. 49-69, ISSN 1593-8433
- De Vita P., D. Agrello and F. Ambrosino (2006a) - Landslide Susceptibility assessment in ash-fall pyroclastic deposits surrounding mount Somma-Vesuvius. Application of geophysical surveys for soil thickness mapping. *Journal of Applied Geophysics*, 59, pp. 126-139.
- De Vita P., P. Celico, P. Siniscalchi and R. Panza (2006b) - Distribution, hydrogeological features and landslide hazard of pyroclastic soils on carbonate slopes in the area surrounding Mount Somma-Vesuvius (Italy). *Italian Journal of Engineering Geology and Environment*, 1, pp. 75-98.
- De Vita P. and M. Nappi (2013) - Regional distribution of ash-fall pyroclastic deposits in Campania (southern Italy) for landslide susceptibility assessment. In: *Landslide Science and Practice (Margottini C., P. Canuti and K. Sassa eds.)*, 3, Spatial Analysis

*and Modelling, Springer-Verlang, pp. 103-110, ISBN 978-3-642-31310-3.*

- De Vita P., E. Napolitano, J.W. Godt and R. Baum (2013) - Deterministic estimation of hydrological thresholds for shallow landslide initiation and slope stability models: case study from the Somma-Vesuvius area of southern Italy. *Landslides*, 10, pp. 713-728.
- De Vivo B., G. Rolandi, P.B. Gans, A. Calvert, W.A. Bohrson, F.J. Spera and A.E. Belkin (2001) - New constraints on the pyroclastic eruption history of the Campanian volcanic plain (Italy). *Mineral. Petrol.*, 73, pp. 47-65.
- Del Prete M, F.M. Guadagno and A.B. Hawkins (1998) - Preliminary report on the landslides of 5 May 1998, Campania, southern Italy. *Bull Eng Geol Environ*, 57, pp. 41-50.
- Di Crescenzo G. and A. Santo (2005) - Debris Slides-Rapid Earth Flow In The Carbonate Massifs Of The Campania Region (Southern Italy): Morphological And Morphometric Data For Evaluating Triggering Susceptibility. *Geomorphology*, 66, pp. 255-276.
- Dietrich W.E., C.J. Wilson and S.L. Reneau (1986) - Hollows, colluvium and landslides in soil-mantled landscapes. In *Hillslope Processes, edited by A.D. Abrahams*, pp. 361-388, Allen and Unwin, London.
- Di Filippo G., L. Lirer, S. Maraffi and M. Capuano (1991) - L'eruzione di Astroni nell'attività recente dei Campi Flegrei. *Boll. Sot. Geol. Ital.*, 110, pp. 309-331.
- Di Girolamo P., M. R. Ghiara, D. Stanzione, L. Lirer, R. Munno and G. Rolandi (1984) - Vulcanologia e petrologia dei Campi Flegrei. *Boll. Soc. Geol. It.* 103, pp. 349-413.
- Dunne T. and R. D. Black (1970a) - An experimental investigation of runoff production in permeable soil. *Water Res. Res.*, 6, pp. 478-490.
- Dunne T. and R. D. Black (1970b) - Partial area contribution to storm runoff in a small New England watershed. *Water Res. Res.*, 6, pp. 1296-1311.
- Eden W.J. and R.J. Mitchell (1970) - The mechanics of landslides in Leda Clay. *Canadian Geotech J*, 7, pp. 285-296.
- Esposito E., S. Porfido, C. Violante, C. Biscardini, F. Alaia, F. and G. Esposito (2004) - Water events and historical flood recurrences in the Vietri sul Mare coastal area (Costiera Amalfitana, southern Italy). *International Association of Hydrological Sciences (IAHS)*, 286, pp. 95-106.
- Evangelista A., M.V. Nicotera and A. Scotto di Santolo (2003) - Experimental on Theoretical Investigation on matric suction measurements in pyroclastic soils. *Proc. Int. Conf. on Fast Slope Movement-Prediction and Prevention for Risk Mitigation, Naples (May, 2003)*.
- Evangelista A. and A. Scotto di Santolo (2004) - Analysis and Field Monitoring of Slope Stability in Unsaturated Pyroclastic Soil Slopes in Napoli, Italy. *Conference proceedings of "Fifth International Conference on Case Histories in Geotechnical*

- Engineering*” (April 13<sup>th</sup>, 2004).
- Evangelista A., A. Scotto di Santolo and G. Lombardi (2007) - Previsione dell’innescio di fenomeni franosi nelle coltri piroclastiche della città di Napoli. *Conference proceedings of “XXIII Congresso Nazionale di Geotecnica, (May 16<sup>th</sup>-18<sup>th</sup>, 2007) (in Italian).*
- Fedele L., C. Scarpati, M. Lamphere, L. Melluso and V. Morra (2008) - The Breccia Museo formation, Campi Flegrei, southern Italy: geochronology, chemostratigraphy and relationship with the Campanian Ignimbrite eruption. *Bulletin of Volcanology* 70, pp. 1189-219.
- Fellenius W. (1927) - Erdstatische Berechnungen mit Reibung und Kohasion (Adha’sion) und unter Annahme kreiszylindrischer Gleitflächen. *Ernst and Sohn, Berlin.*
- Finetti I. and C. Morelli (1974) - Esplorazione sismica a riflessione dei Golfi di Napoli e Pozzuoli. *Boll. Geofis. Teor. Appl.*, 16(62-63), pp. 175-222.
- Fiorillo F. and R.C. Wilson (2004) - Rainfall induced debris flows in pyroclastic deposits, Campania (southern Italy). *Engineering Geology*, 75, pp. 263 - 289.
- Fisher R.V. and H-V. Schmincke (1984) - Pyroclastic rocks. *Springer-Verlang*, pp. 465.
- Fletcher J. E., K Harris, H.B. Peterson and Y.N. Chandler Y.N (1954) - Piping. *Trans. Am. Geophys. Union*, 35, pp. 258-262.
- Frattini P., G. B. Crosta, N. Fusi and P. Dal Negro (2004) - Shallow Landslides In Pyroclastic Soils: A Distributed Modeling Approach For Hazard Assessment. *Engineering Geology*, 73, pp. 277-295.
- Fredlund D.J., N.R. Morgenstern and R.A. Widger (1978) - The shear strength of unsaturated soils. *Canadian Geotechnical Journal*, 15 (3), pp. 313-321.
- Fredlund D.J. and H. Rahardjo (1993) - Soil mechanics for unsaturated soils. *Wiley, New York.*
- Freeze R.A. and J.A. Cherry (1979) - Groundwater. *Prentice-Hall Inc., Englewood Cliffs, New Jersey.*
- Fusco F., P. De Vita, E. Napolitano, V. Allocca and F. Manna (2013) - Monitoring the soil suction regime of landslide-prone ash-fall pyroclastic deposits covering slopes in the Sarno area (Campania - southern Italy). *Rend. Online Soc. Geol. It.*, 24, pp. 146-148.
- Fusco F. and De Vita P. (2015) - Hydrological behavior of ash-fall pyroclastic soil mantled slopes of the Sarno Mountains (Campania - southern Italy). *Rend. Online Soc. Geol. It.*, 35, pp. 148-151.
- Fusco F., R. Tufano, P. De Vita and D. Calcaterra (2016a) - Hydrological monitoring of landslide-prone soils covering Camaldoli Hill slopes (Napoli, Italy). *Abstract for the “88° Congr. Soc. Geol. Ita.”, Naples, Italy (September 7<sup>th</sup>-9<sup>th</sup>, 2016).*

- Fusco F., R.L. Baum, D. Calcaterra, P. De Vita and B.B. Mirus (2016b) - Local and distributed hydrological and slope stability modeling for assessing debris flow hazard along the Sarno Mountains (southern Italy). *Abstract for the "GSA Annual Meeting" Denver, Colorado, USA (September 25<sup>th</sup>-28<sup>th</sup>, 2016).*
- Fusco F., B.B. Mirus, R.L. Baum, P. De Vita, R. Tufano and D. Calcaterra (2016c) - Hydrological monitoring and numerical modelling of landslide-prone pyroclastic soils covering Camaldoli hill slopes (Naples, Italy). *Abstract for the "GSA Annual Meeting" Denver, Colorado, USA (September 25<sup>th</sup>-28<sup>th</sup>, 2016).*
- Gabet E.J., D.W. Burbank, J.K. Putkonen, B.A. Pratt-Sitaula and T. Oihala (2004) - Rainfall thresholds for landsliding in the Himalayas of Nepal. *Geomorphology*, 63, pp. 131-143.
- Gardner W.R. (1958) - Some steady-state solutions of the unsaturated moisture flow equation with application to evaporation from water table. *Soil Science*, 85, pp. 228-232.
- Glade T. and M. Crozier (1996) - Towards a national landslide information base for New Zealand. *New Zealand Geographer*, 52, 1, pp. 29-40.
- Glade T. (1998) - Establishing the frequency and magnitude of landslide-triggering rainstorm events in New Zealand. *Environmental Geology*, 35, 2-3, pp. 160-174.
- Godt J.W., R.L. Baum and A.F. Chleborad (2006) - Rainfall characteristics for shallow landsliding in Seattle, Washington, USA. *Earth Surface Processes and Landforms*, 31, 1, pp. 97-110.
- Godt J.W., W.H. Schulz, R.L. Baum and W.Z. Savage (2008) - Modeling rainfall conditions for shallow landsliding in Seattle, Washington. (In Baum R.L., J.W. Godt and L.M. Highland eds., *Landslides and Engineering Geology of the Seattle, Washington, Area: Geological Society of America Reviews in Engineering Geology*, v. XX, pp. 137-152, DOI: 10.1130/2008.4020(08).
- Govi M., G. Mortara and P. Sorzana (1985) - Eventi idrologici e frane. *Geologia Applicata Ingegneria* 20(2), pp. 359-375.
- Greco R., L. Comegna, E. Damiano, A. Guida, L. Olivares and L. Picarelli (2013) - Hydrological modelling of a slope covered with shallow pyroclastic deposits from field monitoring data. *Hydrology and Earth System Sciences*, 17, pp. 4001-4013.
- Guadagno F.M. (1991) - Debris Flow in the Campanian volcanoclastic soils (Southern Italy). *Proceedings International Conference on "Slope stability engineering developments and applications"*, Thomas Telford, London, pp. 125-130.
- Guadagno F.M. and P. Revellino (2005) - Debris avalanches and debris flows of the Campania Region (Southern Italy). In: *Debris-Flow Hazard and Related Phenomena*. Jacob M. and O. Hungr (eds.), Springer and Praxis editorials.
- Guadagno F.M., R. Forte, P. Revellino, F. Fiorillo and M. Focareta (2005) - Some aspects of the initiation of debris avalanches in the Campania Region: The role of

- morphological slope discontinuities and the development of failure. *Geomorphology*, 66, pp. 237-254.
- Guida D. (2003) - The role of the zero order basins in flowslide-debris flow occurrence and recurrence in Campania (Italy). *Proc. Int Conference on "fast slope Movements - Prediction and prevention for risk Mitigation"*, Pàtron Editore, Napoli, 1, pp. 255-262.
- Gurioli L., R. Cioni, A. Sbrana and E. Zanella (2002), Transport and deposition from pyroclastic flows over densely inhabited areas: Herculaneum (Italy). *Sedimentology*, 46, pp. 1-26.
- Guzzetti F., M. Cardinali, and P. Reichenbach (1994) - The AVI project: a bibliographical and archive inventory of landslides and floods in Italy. *Environ Manage*, 18, pp. 623-633.
- Guzzetti F., S. Peruccacci, M. Rossi and C.P. Stark (2007) - Rainfall thresholds for the initiation of landslides in central and southern Europe. *Meteorology and Atmospheric Physics*, 98, pp. 239-267.
- Guzzetti F., S. Peruccacci, M. Rossi and C.P. Stark (2008) -The rainfall intensity–duration control of shallow landslides and debris flows: an update. *Landslides* 5, 1, pp. 3-17.
- Haggett P. and R.J. Chorley (1969) - Network Analysis in Geography. *Arnold, London*, pp. 348.
- Haverkamp R. and M. Vauclin (1979) - A note on estimating finite difference interblock hydraulic conductivity values for transient unsaturated flow problems. *Water Resources Research*, Vol 15, 1, pp. 181-187.
- Heim A. (1932) - Bergsturz und Menschenleben. *Zurich, Fretz und Wasmuth*. (English translation by Skermer NA, 1989, *Landslides and human lives*. BiTech Publishers, Vancouver BC).
- Helvey J.D. and J.H. Patric (1965) - Canopy and litter interception of rainfall byhardwoods of Eastern United States. *Water Res. Res.*, 1(2), pp. 193-206.
- Hewlett J.D. (1961b) - Soil moisture as a source of base flow from steep mountain watersheds. *US Dept., Agric. Forest Ser., Southeastern Forest Experiment Station, Asheville, North Carolina, Station Paper No. 132*, pp. 11.
- Horton R.E. (1933) - The role of infiltration in the hydrological cycle. *Trans. Am. Geophys. Union*, 14, pp. 446-460.
- Horton R.E. (1937a) - Hydrological interrelation of water and soils. *Proc. Soil Sci. Soc. Am.*, 1, pp. 401-429.
- Hsieh P.A., W. Wingle and R.W. Healy (2000) - VS2DI: A Graphical Software Package for Simulating Fluid Flow and Solute or Energy Transport in Variably Saturated Porous Media. *U.S. Geological Survey, Water-Resources Investigations Report*, pp. 9-4130.

- Hungr O., S.G. Evans, M.J. Bovis and J.N. Hutchinson (2001) - A review of the classification of landslides of flow type. *Environmental and Engineering Geoscience*, 7, pp. 221-238.
- Hungr O, S. McDougall and M. Bovis (2005) Entrainment of material by Debris Flows. In: Jakob M, Hungr O (eds) *Debris flow hazards and related phenomena Chapter 7*. Springer, Heidelberg, pp. 135–158 (in association with Praxis Publishing Ltd).
- Hungr O., S. Leroueil and L. Picarelli (2014) - The Varnes classification of landslide types, an update. *Landslides*, DOI 10.1007/s10346-013-0436-y
- Hutchinson J.N. (1988) - General Report: Morphological and Geotechnical Parameters of Landslides in Relation to Geology and Hydrogeology. *Proceedings of 5<sup>th</sup> International Symposium on Landslides, Lausanne, 1*, pp. 3-35.
- Hutchinson J.N. and R.K. Bhandari (1971) - Undrained loading, a fundamental mechanism of mudflows and other mass movements. *Geotechnique*, 21, pp. 353-358.
- Ippolito F., F. Ortolani and M. Russo (1973) - Struttura marginale tirrenica dell' Appennino Campano: reinterpretazione di dati di antiche ricerche di idrocarburi. *Mem. Sot. Geol. Ital., XII*: pp. 227-250.
- Iverson R.M. (2000) - Landslide triggering by rain infiltration. *Water Resour Res* 36, pp. 1897- 1910, DOI 10.1029/2000WR900090.
- Jakob M. and O. Hungr (2005) - *Debris-flow Hazards and Related Phenomena*. Springer Verlag, pp. 739.
- Jamison V. C. and D.B. Peters (1967) - Slope length of claypan soil affects runoff. *Water Res. Res.*, 3, pp. 471-480.
- Janbu N. (1973) - Slope stability computations. In *embankement-Dam Engineering: Casagrande Volume*, edited by R. C. Hirschfeld and J. S. Poulos, pp. 47-86, John Wiley, Hoboken, N.J.
- Kim S.K., W.P. Hong and Y.M. Kim (1991) - Prediction of rainfall triggered landslides in Korea. In: *Landslides (Bell DH, ed)*, vol. 2. Rotterdam: A.A. Balkema, pp. 989-994.
- Kirkby M.J. and R.J. Chorley (1967) - Throughflow, overland flow and erosion. *Bull. Intern. Assoc. Sci. Hydrology*, 12, pp. 5-21.
- Kirkby M.J. (1969) - Infiltration, throughflow and overland flow. In *Chorley R. J. (Ed.) Water, Earth and Man*, Methuen, London, Ch. 5.1, pp. 215-227.
- Lacerda W.A. (2007) - Landslide initiation in saprolite and colluvium in southern Brazil: field and laboratory observations. *Geomorphology*, 87, pp. 104-119.
- Lappala E.G., R.W. Healy and E.P. Weeks (1987) - Documentation of computer program VS2D to solve the equations of fluid flow in variably saturated porous media. *U.S. Geological Survey, Water-Resources Investigations Report*, pp. 83-4099.

- Larsen M.C. and A. Simon (1993) - A rainfall intensity-duration threshold for landslides in a humid-tropical environment, Puerto Rico. *Geografiska Annaler*, 75A, pp. 13-23.
- Lefebvre G. (1995) - Collapse mechanisms and design considerations for some partly saturated and saturated soils. In: Derbyshire E. et al. (eds) *Genesis and properties of collapsible soils*. Kluwer Academic Publishers, pp. 361-374. Nelson J.D. and D.J. Miller (1992). *Expansive Soils*. John Wiley, NY.
- Lirer L., T. Pescatore, B. Booth and G.P.L. Walker (1973) - Two Plinian pumice fall deposits from Somma-Vesuvius, Italy. *Geol. Soc. Amer. Bull.*, 84, pp. 759-772.
- Loague K., C. S. Heppner, B. A. Ebel and J. E. VanderKwaak (2010) - The quixotic search for a comprehensive understanding of hydrologic response at the surface: Horton, Dunne, Dunton, and the role of concept-development simulation. *Hydrol. Process.*, 24: 2499–2505. doi:10.1002/hyp.7834.
- Lu N. and W.J. Likos (2004) - Rate of capillary rise in soils. *Journal of Geotechnical and Geoenvironmental engineering*, vol. 130 (6), pp. 646-655.
- Lu N., J.W. Godt and D.T. Wu (2010) - A closed-form equation for effective stress in unsaturated soil. *Water Resource Research*, 46, 5, pp. 1-14, W05515.
- Maass J.M., J.V. Vose, W.T. Swank and A. Martínez-Yrizar (1995) - Seasonal changes of leaf area index (LAI) in a tropical deciduous forest. *Forest Ecology and Management*, 74, pp. 171-180.
- Mele R. and S. Del Prete (1999) - Lo studio della franosità storica come utile strumento per la valutazione della pericolosità da frane. Un esempio nell'area di Gragnano (Campania). *Bull. of Soc. Geol. Italiana*, 118 (1), pp. 91-111.
- Melillo M., M.T. Brunetti, S. Peruccacci, S.L. Gariano and F. Guzzetti (2014) - An algorithm for the objective reconstruction of rainfall events responsible for landslides. *Landslides*, DOI 10.1007/s10346-014-0471-3.
- Musgrave G.W. and H.N. Holtan (1964) - Handbook of Applied Hydrology. *Chow, V., (Ed.), Ch. 12, McGraw-Hill, New York*.
- Napolitano E., De Vita P., F. Fusco, V. Allocca, F. Manna (2015) - Long-Term Hydrological Modelling of Pyroclastic Soil Mantled Slopes for Assessing Rainfall Thresholds Triggering Debris Flows: The Case of the Sarno Mountains (Campania-Southern Italy). In *Engineering Geology for Society and Territory (Lollino G. et al. Eds.)*, Vol. 2, pp. 1567-1570, DOI 10.1007/978-3-319-09057-3.
- Napolitano E., F. Fusco, R.L. Baum, J.W. Godt and De Vita P. (2015) - Effect of antecedent-hydrological conditions on rainfall triggering of debris flows in ash-fall pyroclastic-mantled slopes of Campania (southern Italy). *Landslides*, DOI 10.1007/s10346-015-0647-5.
- Napolitano E., F. Fusco and P. De Vita (2016) - Control of hydrological seasonal variability of ash-fall pyroclastic deposits on rainfall triggering debris flows in

- Campania (Southern Italy). *Proceedings of 4<sup>th</sup> Italian Symposium on Landslides, Naples (November 23<sup>th</sup>-25<sup>th</sup>, 2015), In Procedia Earth and Planetary Science.*
- Ng C.W.W. and Q. Shi (1998) - A numerical investigation of the stability of unsaturated soil slopes subjected to transient seepage. *Computer and Geotechnics*, 22(1) pp. 1-28.
- Nicotera P. and M. Civita, M. (1969) - Ricerche idrogeologiche per la realizzazione delle opere di presa delle sorgenti Mercato e Palazzo (Sarno). *Mem e Note Ist Geol Appl*, XI, pp. 7-64 (in Italian).
- Nikolopoulos E.I., S. Crema, L. Marchi, F. Marra, F. Guzzetti and M. Borga (2014) - Impact of uncertainty in rainfall estimation on the identification of rainfall thresholds for debris flow occurrence. *Geomorphology*, 221, pp. 286-297.
- Nutter W.L. (1969) - Management implication of subsurface stormflow and variable source concept. *Paper presented to the 1969 Annual Meeting of the Watershed Management Division, Society of American Foresters, October 13<sup>th</sup>-16<sup>th</sup>, Miami, Florida.*
- Öberg A.L. and G. Sällfors (1997) - Determination of shear strength parameters of unsaturated silts and sand based on the water retention curve. *Geotech. Test. J.*, 20, pp. 40-48.
- Orsi G., S. De Vita and M.A. Di Vito (1996) - The restless, resurgent Campi Flegrei nested caldera (Italy): constraints on its evolution and configuration. *J. Volcanol. Geotherm. Res.*, 74, pp. 179- 214.
- Papa M.N., V. Medina, E. Ciervo and A. Bateman (2013) - Derivation of critical rainfall thresholds for shallow landslides as a tool for debris flow early warning systems. *Hydrology and Earth System Sciences*, 17, pp. 4095-4107.
- Papa R., N. Pirone, M. Nicotera and G. Urciuoli. (2013) - Seasonal groundwater regime in an unsaturated pyroclastic slope. *Geotechnique*, 63, 5, pp. 420-426.
- Pappalardo L., L. Civetta, M. D'Antonio, A. Deino, M. Di Vito, G. Orsi, A. Carandente, S. De Vita, R. Isaia and M. Piochi (1999) - Chemical and Sr-isotopic evolution of the Phlegrean magmatic system before the Campanian Ignimbrite and the Neapolitan Yellow Tuff eruptions. *Journal of Volcanology and Geothermal Research* 91, pp. 141-66.
- Pasuto A. and S. Silvano (1998) - Rainfall as a triggering factor of shallow mass movements. A case study in the Dolomites. *Italy. Environ Geol* 35(2-3), pp. 184-189.
- Patacca E. and P. Scandone (2007) - Geology of the Southern Apennines. In: *Mazzotti, A., E. Patacca and P. Scandone (Eds.), "CROP-04", Special Issue, Italian Journal of Geosciences*, 7, pp. 75-119.
- Peres D.J. and A. Cancelliere (2014) - Derivation and evaluation of landslide-triggering thresholds by a Monte Carlo approach. *Hydrology and Earth System*

- Sciences*, 18, pp. 4913-4931.
- Perriello Zampelli S., E.B. Sessa and M. Cavallaro (2011) - Application of a GIS-aided method for the assessment of volcanoclastic soil sliding susceptibility to sample areas of Campania (Southern Italy). *Nat. Hazards*, DOI 10.1007/s11069-011-9807-7.
- Perrotta A. and C. Scarpati (2003) - Volume partition between the plinian and co-ignimbrite air fall deposits of the Campanian Ignimbrite eruption. *Mineral Petrol* 79, pp. 67-78.
- Peruccacci S., M.T. Brunetti, S. Luciani, C. Vennari and F. Guzzetti (2012) - Lithological and seasonal control on rainfall thresholds for the possible initiation of landslides in central Italy. *Geomorphology*, 139-140, pp. 79-90.
- Picarelli L., L. Olivares, L. Comegna and E. Damiano (2008) - Mechanical aspects of flow-like movements in granular and fine-grained soils. *Rock Mech. Rock Eng.*, 41(1), pp. 179-197.
- Pierson T.C. (1986) - Flow behavior of channelized debris flows, Mount St. Helens, Washington. In: *Abrahams AD (ed) Hillslope processes*. Allen and Unwin, Boston, pp. 269-296.
- Pierson T.C. and J.E. Costa (1987) - A rheologic classification of subaerial sediment - water flows. *Geological society of America Rev. Eng. Geol.* 7, pp. 1-12.
- Philip J.R. (1957-8) - The theory of infiltration. *Soil Sci.*, 83, pp. 345-357; pp. 543-448; 84, pp. 163-177; pp. 257-264; pp. 329-339; 85, pp. 278-286; pp. 333-337.
- Pyle D.M. (1989) - The thickness, volume and grain size of tephra fall deposits. *Bulletin of Volcanology*, 51(1), pp. 1-15.
- Ragan R.M. (1967) - Role of basin physiography on the runoff from small watershed. *Vermont Resources Research Center, Water Res. Res., Univ. Vermont, Burlington, Vermont, Report No. 17*, pp. 25.
- Ragan R.M. (1968) - An experimental investigation of partial area contributions. *Proceedings of the General Assembly, Internat. Assoc. Sci. Hydrology, Berne, Publication 76*, pp. 241-249.
- Rautiainen M., J. Heiskanen and N. Korhonen (2012) - Seasonal changes in canopy leaf area index and MODIS vegetation products for a boreal forest site in central Finland. *Boreal Environment Research*, 17, pp. 72-84.
- Revellino P., O. Hungr, Guadagno F.M. and S.G. Evans (2003) - Velocity and runout simulation of destructive debris flows and debris avalanches in pyroclastic deposits, Campania region, Italy. *Environmental Geology*, 45, pp. 295-311, DOI 10.1007/s00254-003-0885-z
- Richards L.A. (1931) - Capillary conduction of liquids through porous mediums. *J. Appl. Phys.*, 1, pp. 318-333, DOI 10.1063/1.1745010
- Rolandi G., A.M. Barrella and A. Borrelli (1993) - The 1631 Eruption of Vesuvius. *J.*

- Volcanol. Geotherm. Res.*, 58, pp. 183-201.
- Rolandi G., S. Maraffi, P. Petrosino and L. Lirer (1993a) - The Ottaviano eruption of Somma-Vesuvius (8000 y B.P.): a magmatic alternating fall and flow-forming eruption. *J. Volcanol. Geotherm. Res.*, 58, pp. 43-65.
- Rolandi G., G. Mastrolorenzo, A.M Barrella and A. Borrelli (1993b) - The Avellino plinian eruption of Somma-Vesuvius (3.76 kys B.P.): the progressive evolution from magmatic to hydromagmatic style. *J. Volcanol. Geotherm. Res.*, 58, pp. 67-88.
- Rolandi G., P. Petrosino and J. Mc Geehin (1998) - The interplinian activity at Somma-Vesuvius in the last 3500 years. *J. Volcanol. Geotherm. Res.*, 82, pp. 19-52.
- Rolandi G., F Bertolini, G. Cozzolino, N. Esposito and D. Sannino (2000) - Sull'origine delle coltri piroclastiche presenti sul versante occidentale del Pizzo d'Alvano (Sarno - Campania). *Quaderni Di Geologia Applicata*, 7-1, pp. 213-235 (in Italian).
- Rolandi G. (2001) - Il rischio vulcanico ed idraulico al Somma-Vesuvio. *Analisi e confronto - Interventi di ingegneria naturalistica nel Parco Nazionale del Vesuvio*, pp. 15-41.
- Rolandi G., R. Munno and I. Postiglione (2004) - The A.D. 472 Eruption Of The Somma Volcano. *J. Volcanol. Geotherm. Res.*, 129, pp. 291-319.
- Rolandi G, P. Petrosino and J. Mac Geehin (2006) - The Interplinian Activity at Somma-Vesuvius in the Last 3500 Years. *J. Volcanol. Geotherm. Res.*, 82, pp. 19-52.
- Rolandi G., A. Paone, M. Di Lascio and G. Stefani, (2007) - The 79 AD eruption of Somma: The relationship between the date of the eruption and the southeast tephra dispersion. *J. Volcanol. Geotherm. Res.*, 169, pp 87-98.
- Rosi M. and R. Santacroce (1984) - Volcanic hazard assessment in the Phlaegrean Fields: a contribution based on stratigraphic and historical data. *Bull. Volcanol.*, 47(2), pp. 359-370.
- Rosi M. and A. Sbrana (1987) - Phlegrean Fields. *CNR, Quad. Ric. Sci.*, 114, pp. 1-175.
- Rosi M., C. Principe and R. Vecci (1993) - The 1631 eruption of Vesuvius reconstructed from the review of chronicles and study of deposits. *J. Volcanol. Geotherm. Res.*, 58, pp. 151-182.
- Sassa K. (1985) - The mechanism of debris flow. *Proceedings of XI International Conference on Soil Mechanics and Foundation Engineering, San Francisco. Balkema, Rotterdam, the Netherlands*, pp.1173-1176.
- Sassa K. (1989) - Geotechnical classification of landslides. *Traduzione di Lesmo R. da Landslide News*, 3, *In Geologia Tecnica*, 4/90, Roma.
- Scarpati C., P. Cole and A. Perrotta (1993) - The Neapolitan Yellow Tuff-A large volume multiphase eruption from Campi Flegrei. Southern Italy. *Bull. Volcanol.*, 55,

pp. 343-356.

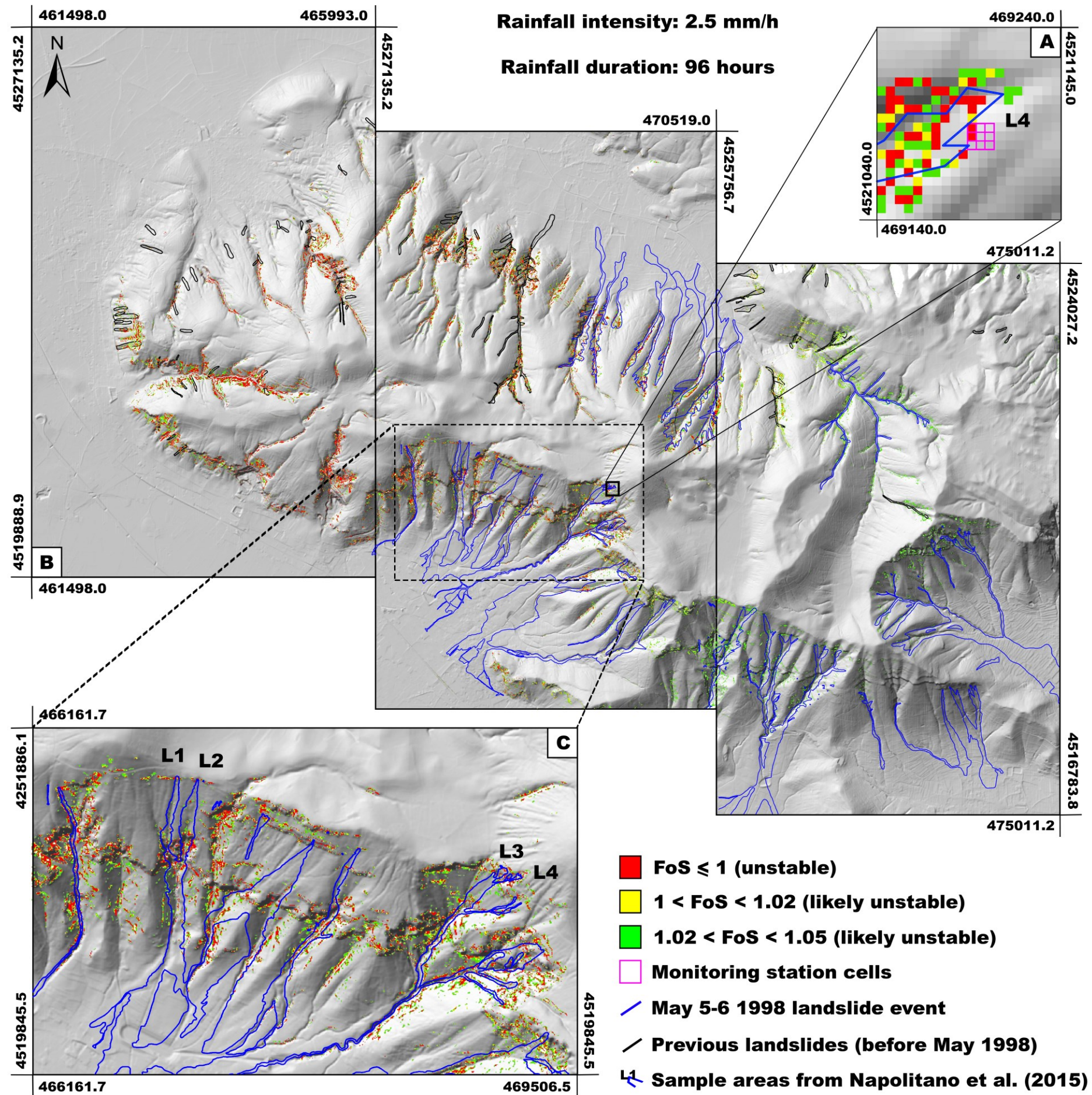
- Scarpati C., A. Perrotta, L. Lepore and A. Clvert (2013) - Eruptive history of Neapolitan Volcanoes: constraints from 40Ar-39Ar dating. *Geol. Mag.* 150 (3), pp. 412-425. DOI 10.1017/S0016756812000854.
- Scherillo A. and E. Franco (1960) - Rilevamento stratigrafico del territorio comunale di Napoli. *Boll. Sot. Nat. Napoli*, 69, pp. 255-262.
- Schmidt R. (1981) - Descriptive nomenclature and classification of pyroclastic deposits and fragments: recommendations of the I.U.G.S. *Subcommission on the Systematics of Igneous Rocks. Geology*, 9, pp. 41-43.
- Sherman L.K. (1944) - Infiltration on the physics of the soil moisture. *Trans. Am. Geophys. Union*, 25, pp. 57-65.
- Shoji S., R. Dahlgren and M. Nanzyo (1993) - Morphology of volcanic ash soils. In: *Volcanic Ash Soils, Elsevier*, pp. 7-35.
- Sigurdsson H., S. Carey, T. Cornell and T. Pescatore (1985) - The eruption of Vesuvius in A. D. 79. *National Geographic Research*, 1, pp. 3.
- Sirangelo B. and P. Versace (1992) - Modelli stocastici di precipitazione e soglie pluviometriche di innesco dei movimenti franosi. *Int. Proc. Of "XXIII Convegno idraulica e costruzioni idrauliche" (Firenze, August 31th - September 4th, 1992) III*, pp. 361-373.
- Skempton A.W. and J.N. Hutchinson (1969) - Stability of natural slopes and embankment foundations. In: *Proceedings, 7<sup>th</sup> International conference of soil mechanics and foundation engineering, Mexico, State of the Art volume*, pp. 291-340.
- Smith R.E. (1972) - The infiltration envelope: Results from a theoretical infiltrometer. *J. Hydrology*, 17, pp. 1-21.
- Sorbino G. (2005) - Numerical modelling of soil suction measurements in pyroclastic soils. In: *Tarantino Romero Cui (Ed.), Int. Symp. "Advanced experimental unsaturated soil mechanics"*. Taylor and Francis Group, London, pp. 541-547.
- Srivastava R. and T.-C.J. Yeh (1991) - Analytical solution for one-dimensional, transient infiltration toward the water table in homogeneous and layered soils. *Water Resources Research*, 27, pp. 753-762.
- Taylor D.W. (1948) - Fundamentals of soil mechanics. *Wiley, New, York*.
- Terlien, M.T.J. (1998) - The determination of statistical and deterministic hydrological landslide-triggering thresholds. *Environmental Geology*, 35, pp. 124-130.
- Terribile F., A. Basile, R. De Mascellis, A. Di Gennaro and S. Vingiani (2000) - I suoli delle aree di crisi di Quindici e Sarno: proprietà e comportamenti in relazione ai fenomeni franosi del 1998. *Quaderni di Geologia Applicata* 7 (1), pp. 60-79 (In Italian).

- Terzaghi K. (1943) - Theoretical soil mechanics. *Wiley, New York*
- Thornthwaite C.W. (1948) - An Approach toward a Rational Classification of Climate. *Geographical Review*, 38, pp. 55-94.
- Tranfaglia G. and G. Braca (2004) - Analisi idrologica e meteorologica dell'evento alluvionale del 25-26 ottobre 1954: confronto con le serie storiche e valutazione del periodo di ritorno di eventi analoghi. In *"Il nubifragio dell'ottobre 1954 a Vietri sul Mare. Costa di Amalfi, Salerno"* (E. Esposito, S. Porfido and C. Violante Eds.), n.2870, pp. 295-348.
- Tzukamoto Y. and H. Minematsu (1987) - Hydrogeomorphological characteristics of a zero-order basin. In proceeding, Symposium on Erosion and Sedimentation in the Pacific Rim. *IAHS Publ. 165*, pp 61-70.
- Tufano R, F. Fusco and P. De Vita (2016) - Spatial modeling of ash-fall pyroclastic deposits for the assessment of rainfall thresholds triggering debris flows in the Sarno and Lattari mountains (Campania, southern Italy). *Rend. Online Soc. Geol. It., Vol. 41*, pp. 210-213.
- TVA (Tennessee Valley Authority) (1965). Area-stream factor correlation. *Bull. Internat. Assoc. Sci. Hydrology*, 10(2), pp. 22-37.
- TVA (Tennessee Valley Authority) (1968) - The Upper Bear Creek Experimental Project 1965-67. *Knoxville, Tennessee*, pp. 49.
- Us Corps Of Engineers (1960) - The Unified Classification System. *Waterways Exp. Est.*
- USDA (2014) - Keys to soil taxonomy. *United States Department of Agriculture Natural Resources Conservation Service 12<sup>th</sup> edition*, pp. 372.
- Van Genuchten M.T. (1980) - A closed form equation for predicting the hydraulic conductivity of unsaturated soils. *Soil Science Society of America Journal*, 44, pp. 892-898.
- Vanapalli S., D. Fredlund, D.E. Pufahl and A.W. Clifton (1996) - Model for the prediction of shear strength with respect to soil suction. *Canadian Geotechnical Journal*, 33, pp. 379-392.
- Vanapalli S. and D. Fredlund (2000) - Comparison of different procedures to predict unsaturated soil shear strength. In: *Shackelford C., S.L. Houston and N.-Y. Chang (Eds) Advances in unsaturated geotechnics, Denver, Colorado, August 3<sup>th</sup> 2000. Geotechnical Special Publication 99. ASCE*, pp 195-209.
- Varnes D.J. (1978) - Slope movement Types and Processes. In *Special report 176: Landslides: Analysis and Control (R.L. Shuster and R.J.nKrizek, eds.)*, TRB, National Research Council, Washington, D.C., pp. 11-33.
- Vessia G., M. Parise, M.T. Brunetti, S. Peruccacci, M. Rossi, C. Vennari and F. Guzzetti (2014) - Automated reconstruction of rainfall events responsible for shallow landslides. *Natural Hazards Earth System Sciences*, 14, pp. 2399-2408.

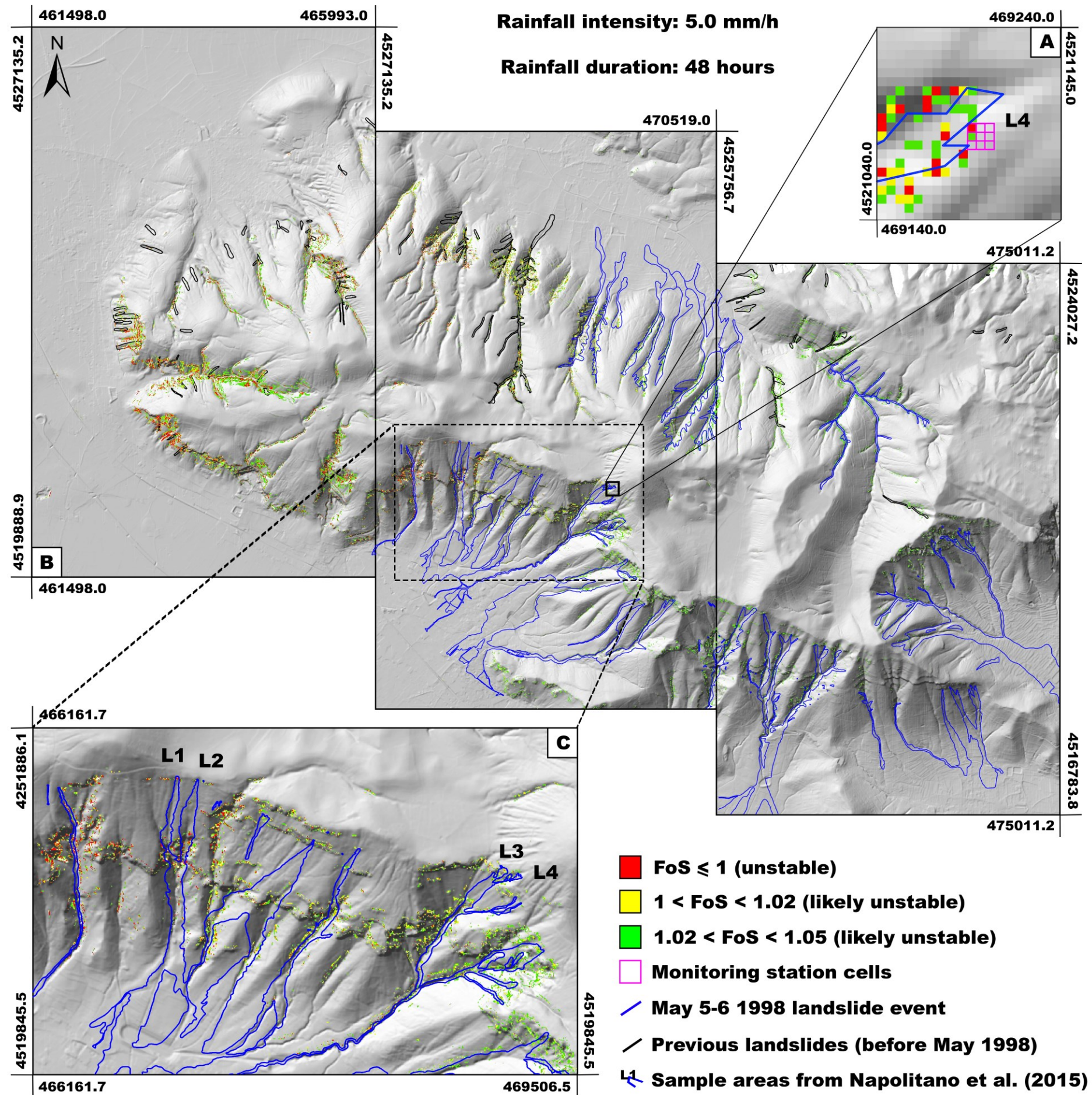
- Weyman D.R. (1970) - Throughflow on hillslope and its relation to the stream hydrograph. *Bull. Internat. Assoc. Sci. Hydrology*, 15(3), pp. 25-33.
- White I.D., D.N. Mottershead and J.J. Harrison (1996) - Environmental systems. 2<sup>nd</sup> ed. London. Chapman and Hall, pp. 616.
- Wieczorek G.F. (1987) - Effect of rainfall intensity and duration on debris flows in central Santa Cruz Mountains. In: *Debris flow-avalanches: process, recognition, and mitigation* (Costa J.E. and G.F. Wieczorek Eds.). Geological Society of America, *Reviews in Engineering Geology*, 7, pp. 93-104.
- Wieczorek G.F. and J. Sarmiento (1988) - Rainfall, piezometric levels, and debris flows near La Honda, California, in storms between 1975 and 1983. In: (Ellen, S.D. and G.F. Wieczorek Eds.). *Landslides, Floods and Marine Effects of the Storm of January 3-5, 1982, in the San Francisco Bay Region, California, U.S. Geological Survey Professional Paper, 1434*, pp. 43-62.
- Wieczorek G.F. (1996) - Landslide triggering mechanisms. In: *Landslides: investigation and mitigation* (Turner, A.K. and R.L.Schuster Eds). Washington DC. Transportation Research Board, National Research Council, special report, pp. 76-90.
- Wieczorek G.F. and T. Glade (2005) - Climatic factors influencing the occurrence of debris flows. In: Jakob M. and O. Hungr (eds.) - *Debris-flow Hazards and Related Phenomena*. Springer-Verlang, pp. 325-362.
- Wilson R.C. (1989) - Rainstorms, pore pressures, and debris flows: a theoretical framework. In: *Landslides in a semi-arid environment* (Morton D.M. and P.M. Sadler Eds.), California: Publications.
- WP/WLI (1993a) - A Suggested Method for Describing the activity of a Landslide. *Bulletin of the International Association of Engineering Geology*, 47, pp. 53-57.
- WP/WLI (1993b) - Multilingual landslide Glossary. Bi-Tech Publisher, Richmond, British Columbia, Canada, 59 pp.

## Attachments

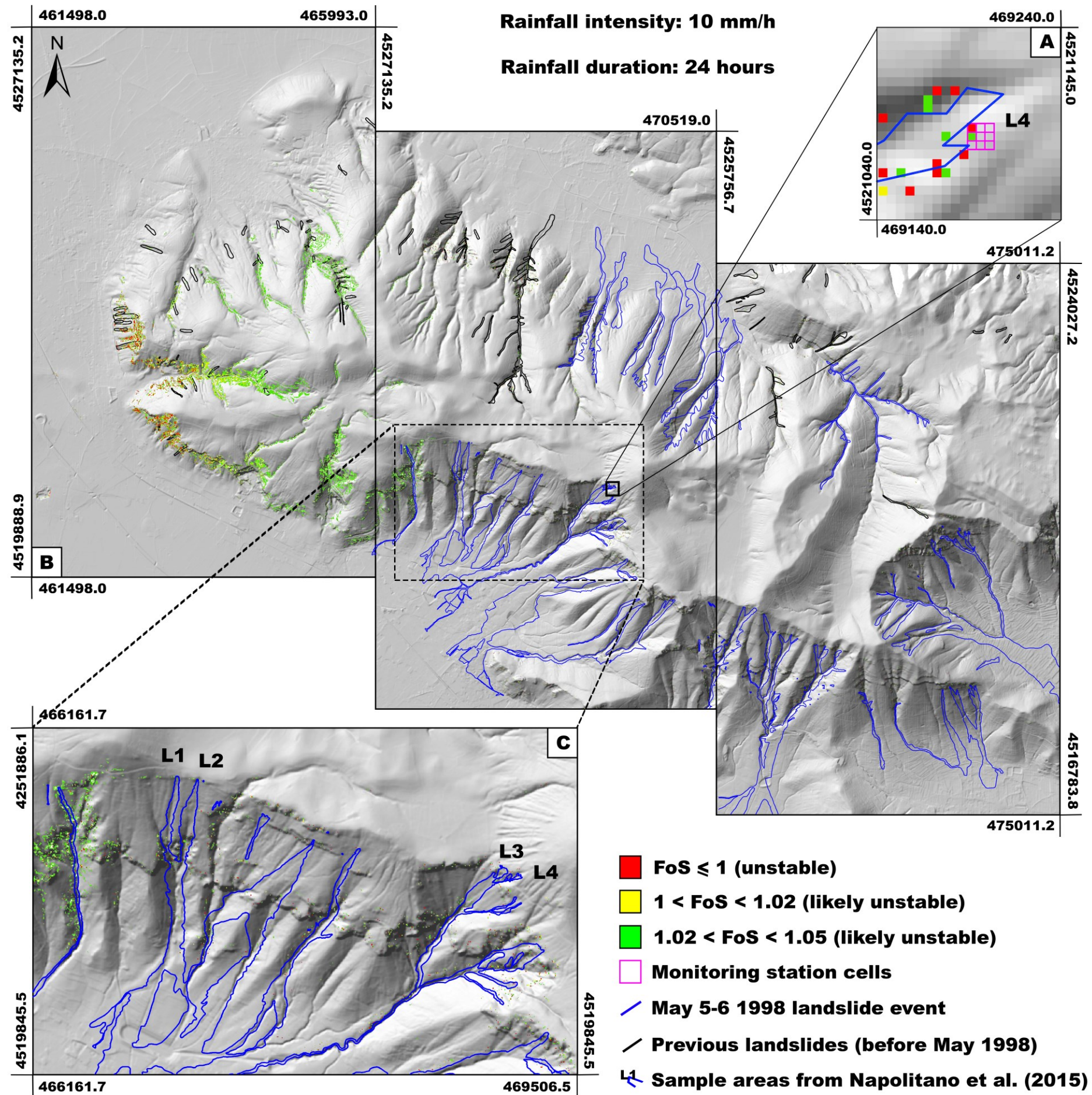
---



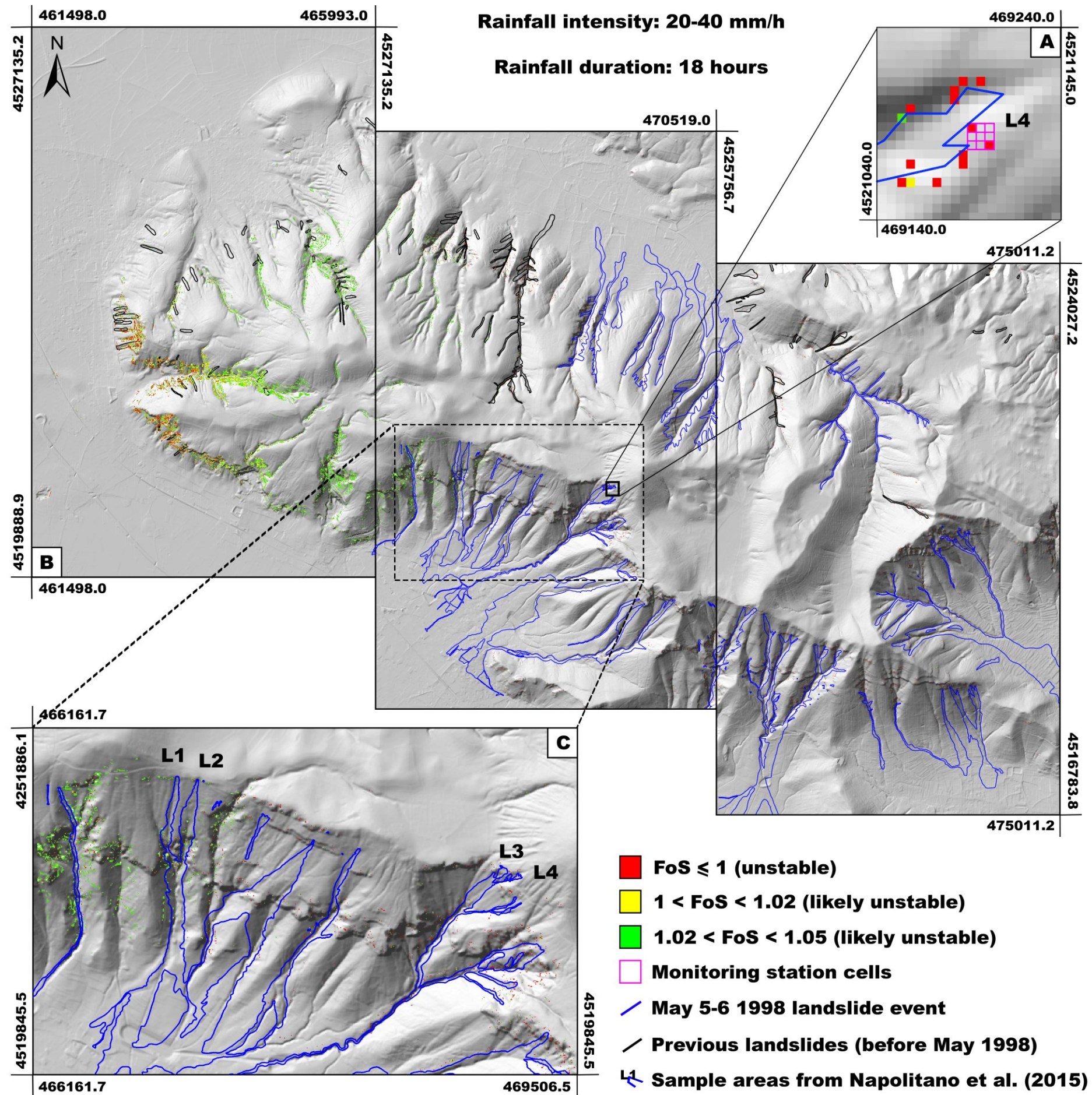
**Attachment 1.** Susceptibility maps at a distributed scale, for the whole area (A) and at local scale (B), resulting from a modeled constant rainfall intensity of 2.5 mm/h for 96 hours. Unstable and likely unstable cells were compared within sample areas (C) L1, L2, L3 (Napolitano et al., 2015), L4 and the entire Sarno Mountains landslide database containing the May 1998 Sarno landslide event. Monitoring station cells used for local scale modeling and L4 threshold definition are also shown (C).



**Attachment 2.** Susceptibility maps at a distributed scale, for the whole area (A) and at local scale (B), resulting from a modeled constant rainfall intensity of 5.0 mm/h for 48 hours. Unstable and likely unstable cells were compared within sample areas (C) L1, L2, L3 (Napolitano et al., 2015), L4 and the entire Sarno Mountains landslide database containing the May 1998 Sarno landslide event. Monitoring station cells used for local scale modeling and L4 threshold definition are also shown (C).



**Attachment 3.** Susceptibility maps at a distributed scale, for the whole area (A) and at local scale (B), resulting from a modeled constant rainfall intensity of 10.0 mm/h for 24 hours. Unstable and likely unstable cells were compared within sample areas (C) L1, L2, L3 (Napolitano et al., 2015), L4 and the entire Sarno Mountains landslide database containing the May 1998 Sarno landslide event. Monitoring station cells used for local scale modeling and L4 threshold definition are also shown (C).



**Attachment 4.** Susceptibility maps at a distributed scale, for the whole area (A) and at local scale (B), resulting from a modeled constant rainfall intensity of 20 and 40 mm/h for 18 hours. Unstable and likely unstable cells were compared within sample areas (C) L1, L2, L3 (Napolitano et al., 2015), L4 and the entire Sarno Mountains landslide database containing the May 1998 Sarno landslide event. Monitoring station cells used for local scale modeling and L4 threshold definition are also shown (C).